



University  
of Glasgow

Al-Sarraf, Ziad Shakeeb (2013) *A study of ultrasonic metal welding.*

PhD thesis

<http://theses.gla.ac.uk/4375/>

Copyright and moral rights for this thesis are retained by the author

A copy can be downloaded for personal non-commercial research or study, without prior permission or charge

This thesis cannot be reproduced or quoted extensively from without first obtaining permission in writing from the Author

The content must not be changed in any way or sold commercially in any format or medium without the formal permission of the Author

When referring to this work, full bibliographic details including the author, title, awarding institution and date of the thesis must be given

# **A STUDY OF ULTRASONIC METAL WELDING**

**Ziad Shakeeb Al-Sarraf**

A thesis for the degree of Doctor of Philosophy (PhD)

Submitted to the School of Engineering,  
College of Science and Engineering,  
University of Glasgow

April 2013



## DECLARATION

I declare that this thesis is a record of the original work carried out by myself under the supervision of Prof. Margaret Lucas in the School of Engineering at the University of Glasgow, United Kingdom, during the period of January 2009 to December 2012. The copyright of this thesis therefore belongs to the author under the terms of the United Kingdom Copyright acts. Due acknowledgement must always be made of the use of any material contained in, or derived from, this thesis. The thesis has not been presented elsewhere in consideration for a higher degree.

Signature \_\_\_\_\_

Printed name \_\_Mr. Ziad Shakeeb Al-Sarraf \_\_

Signature \_\_\_\_\_

Printed name \_Prof. Margaret Lucas \_\_\_\_\_



## **I. Abstract**

Ultrasonic metal welding (USMW) has received significant attention in the past few years, and has become more reliable and suitable for a wide range of applications. In recent years, the technique has been extensively used due to the advent of component miniaturisation and improvements in producing lightweight components. There are a number of advantages for USMW, including greater efficiency and speed, longer tool life, higher accuracy and no filler or flux needed to be used. Thus the technique can be viewed as being environmentally friendly. However, the technique is not inexpensive, primarily due to the high cost of welding tools. Therefore, the design and construction of a lateral-drive USMW system which is capable of joining thin metals is presented in this thesis. The fundamental aspect of this study is the design of an integrated spot welding horn, along with other welding components such as a stationary anvil, mounting holder, welding bed, as well as the relevant fixing tools and fixtures. High precision is required in the design of the components, and in particular the welding horn. Because the horn is responsible for transferring energy to the welding zone, specimens must be prevented from sliding during the joining process, and an appropriate clamping force must be applied which will ensure acceptable bonding. Many criteria have been examined to enhance the performance of a working horn. The horn excitation frequency has been matched to the transducer frequency, ensuring that the horn will be vibrated longitudinally close to 20 kHz, thereby allowing the tuned mode to be isolated from other non-tuned modes, which guarantees uniformity of the vibration amplitude at the horn working surface, high gain factor of 4.108, and the avoidance of any stress initiated at the points between connecting components. Examining of these criteria is essential in order to optimise the excitation of the horn and to transmit the energy with minimum dissipation. The analytical studies and the finite element (FE) modelling of the welding components were successfully simulated, from which the vibrational behaviour and dynamical characteristics of the system were precisely verified using experimental modal analysis (EMA). The welding stack (the horn connected to the transducer), welding components and fixtures were then set-up on the driving machine. The device was examined prior to welding to ensure the excitation at high vibration. Many tests were successfully conducted on the welding together of aluminium and copper in a number of different configurations using the ultrasonic metal spot welding system. Weld strength and quality were shown to depend on complex relations of process parameters such as clamping force, amplitude of vibration, welding time and input power. A series of weld combinations with different thicknesses and

variations in metal conditions were studied. The results of the lap tested specimens suggest that the bond strength is sensitive to the relationships between clamping force and vibration amplitude. Overall, the weld strength results suggest that the Al-Al welds are stronger and more consistent in terms of weldability than the Cu-Cu welds. In the welding of dissimilar metals, stronger welds are produced when the aluminium specimen is placed on top and in contact with the horn tip, rather than the copper. The thickness and surface condition of the metals such as hardness, surface roughness and oxides, are significantly affect the weld strength. In welding of Al-Cu or Cu-Al, an increase in energy and time was necessary to generate an acceptable bond. The use of stepped amplitude profiling results in a pronounced increase in the weld strength improves consistency and enhances weldability. However, horn tip/specimen adhesion and specimen marking did not occur under certain conditions. The results of the FE simulation and experimental tensile tests, for the load-displacement curves profiles, allow for good estimation of the maximum load and therefore weld strength. Weld quality of aluminium and copper specimens were observed through investigation of the deformed surfaces using Nomarsky optical microscopy and scanning electron microscopy (SEM). The results illustrate that good quality welds can be achieved by joining specimens, regardless of the surface condition of the metal. The SEM confirmed that no mixing occurred by melting or fusion between intimate surfaces, which indicates that USMW occurs due to adhesion and cohesion mechanisms. Furthermore, x-ray diffraction confirms the percentage of morphology between Al and Cu, which indicates that largest weld formations are prevalent for those specimens that are softer and lower in hardness and surface roughness, regardless of the type of tempering.

## II. Acknowledgments

First, I would like to express my gratitude to my God (**Allah**) for providing me the blessings to complete this thesis. Then, I would like to dedicate this work to the memory of my mum (**Walida**) who always was encouraging me whilst she was suffering from her disease. Then, I would like to thank my dad (**Shakeeb**) who is always encouraging me to complete this work. But I can not forget the great struggle of my lovely wife (**Joan**) who is beared high responsible to manage and control the life demands of our family and kids. Therefore, I really, appreciate her efforts with me to complete this work. So, I pleased to dedicate this work to my wife and to my two little angels (**Ward**) and (**Hamza**). Words alone cannot express what I owe them for their encouragement and patient love that inspired me to complete this work.

Special thanks to my ancle (**Atheel**) and to my mum in law (**Semaa**) whose gave me much more support to complete my study. I would like to thank my borthers (**Omar**) and (**Ahmed**) who's always encourage me to complete this work.

I would like to express my special thanks of gratitude to my supervisor, Professor **Margaret Lucas**, who gave me this great opportunity not only to support this work, but to discover the great features of high power ultrasonic welding technology. She continuously encouraged and supported me through my research programme and enabled me to know more and more about so many things.

The Iraqi Governments, for funding this research. Also, many thanks to the following colleagues, friends and family who's contributed their advice and support towards the development of this research. Staff at the School of Engineering, University of Glasgow, for their assistance, help and accommodating my demanding needs on resources throughout my studies.

The technical staffs, in particular Mr. Brian Robb and Mr. John Davidson and their colleagues, for their expertise, extensive help and assistance in the workshop and material lab and their patience and dedication to the challenging experimental testing configurations and testing techniques along three years, also Mr. Peter Chung for his efforts on using SEM. Thanks to All!

### III. Table of contents

DECLARATION .....	iii
I. Abstract.....	i
II. Acknowledgments .....	iii
III. Table of contents .....	iv
III. List of table captions .....	ix
V. List of figure captions .....	x
VI. List of symbols.....	xvii
VII. Abbreviations.....	xviii
Chapter 1 .....	1
1.1 Introduction .....	1
1.2 Outline of research .....	4
1.3 Historical background .....	7
1.4 Ultrasonic waves .....	8
1.5 Ultrasonic metal spot welding equipment.....	9
1.5.1 Wedge-reed ultrasonic spot welding system.....	10
1.5.2 Lateral-drive ultrasonic spot welding system .....	10
1.6 Principles of ultrasonic metal welding (USMW).....	11
1.7 Applications of ultrasonic metal welding (USMW) .....	14
1.8 Description of the research and key findings .....	15
Chapter 2 .....	17
Literature review .....	17
2.1 Introduction .....	17
2.2 Background of the design of ultrasonic tools.....	17
2.3 Research on solid-state bonding mechanisms.....	21

2.4 Process parameters in ultrasonic metal welding .....	24
2.5 Theory of USMW without melt or fusion.....	29
2.6 Temperature effects on the mechanisms of USMW .....	30
2.7 System parameters .....	31
2.7.1 Ultrasonic frequency .....	31
2.7.2 Vibration amplitude .....	32
2.7.3 Clamping force.....	32
2.7.4 Power, energy, & time .....	33
2.7.5 Materials.....	35
2.7.6 Specimen geometry.....	36
2.7.7 Tooling .....	36
2.8 Weldability.....	37
2.9 Summary .....	38
2.10 Aims and Objectives .....	39
Chapter 3 .....	41
Design of ultrasonic spot welding devices.....	41
3.1 Introduction.....	41
3.2 Design of ultrasonic devices .....	41
3.2.1 Equation of rod in longitudinal vibration.....	41
3.2.2 Analysis of the non-uniform geometry of the horn.....	44
3.3 Finite element analysis (FEA).....	48
3.4 Experimental modal analysis (EMA).....	49
3.4.1 Frequency response function (FRF).....	50
3.4.2 EMA measurement system .....	50
3.4.3 Vibrational signal processing.....	51
3.5 Design process for an ultrasonic spot welding system.....	52

3.6 Design of a spot welding horn .....	52
3.6.1 Stress analysis .....	58
3.6.2 Frequency separation .....	61
3.6.3 Amplitude uniformity .....	62
3.7 Manufacture of the spot welding horn .....	62
3.8 Validation between FEA and EMA .....	63
3.9 Design of welding components .....	66
3.10 Summary .....	68
Chapter 4 .....	70
Welding tests and metal investigations .....	70
4.1 Introduction .....	70
4.2 Selection of metal for ultrasonic spot welding .....	70
4.3 Tensile test machine set-up .....	72
4.4 Specimen configuration .....	73
4.4.1 Dog bone specimens .....	73
4.5 Extracting mechanical properties for aluminium and copper .....	74
4.6 Thickness of specimen .....	79
4.7 Width and length of specimen .....	79
4.8 Specimen roughness .....	80
4.9 Hardness test .....	82
4.10 Ultrasonic metal spot welding rig .....	83
4.11 Preparation of welding coupons .....	84
4.12 Experimental set-up of ultrasonic metal spot welding .....	85
4.13 Al-Al and Cu-Cu weld coupons .....	86
4.14 Al-Cu and Cu-Al weld coupons .....	89
4.15 The development of the weld .....	91

4.16 Ultrasonic spot welding for weld coupons of similar metals.....	93
4.16.1 0.1Al-0.1Al and 0.1Cu-0.1Cu weld coupons.....	93
4.16.2 0.3Al-0.3Al and 0.3Cu-0.3Cu weld coupons.....	95
4.16.3 0.5Al-0.5Al and 0.5Cu-0.5Cu weld coupons.....	96
4.17 Ultrasonic spot welding for weld coupons of dissimilar metals .....	96
4.17.1 0.1Al-0.1Cu and 0.1Cu-0.1Al weld coupons.....	97
4.17.2 0.3Al-0.3Cu and 0.3Cu-0.3Al weld coupons.....	98
4.17.3 0.5Al-0.5Cu and 0.5Cu-0.5Al weld coupons.....	99
4.18 Summary .....	100
Chapter 5 .....	101
Ultrasonic welding experiments and finite element simulation results .....	101
5.1 Introduction.....	101
5.2 Study of the influence of process parameters on weld strength.....	101
5.3 The influence of clamping force on weld strength.....	102
5.4 The influence of vibration amplitude on weld strength .....	107
5.5 The influence of ultrasonic power on weld strength.....	113
5.6 Amplitude profiling in USMW .....	116
5.7 The influence of amplitude profiling on weld strength.....	118
5.8 Extracting the curve for the joints of spot welding coupons.....	121
5.9 FE simulation of spot welding coupons .....	122
5.10 Summary .....	127
Chapter 6 .....	130
Weld quality .....	130
6.1 Introduction.....	130
6.2 Microscopic observation .....	130
6.3 The influence of clamping force on weld quality .....	134

6.4 The influence of vibration amplitude on weld quality .....	139
6.5 Scanning electron microscopy (SEM) investigations .....	145
6.6 Summary .....	153
Chapter 7 .....	155
Discussion, conclusions and suggestions for future work .....	155
7.1 Discussion .....	155
7.2 Conclusions .....	159
7.3 Future works .....	160
References .....	162
Appendix I: Publications.....	170

### III. List of table captions

Table 3-1 Material properties of steel horn.....	53
Table 3-2 Horn mode frequencies in the range (0-40 kHz) .....	64
Table 4-1 Metal thicknesses (Manufacturer's data).....	71
Table 4-2 Average tensile data for the aluminium dog bone configuration, (n=6).....	78
Table 4-3 Average tensile data for the copper dog bone configuration, (n=6).....	78
Table 4-4 Roughness results for the tested aluminium and copper with different thicknesses, n=5 for each metal thickness .....	81
Table 4-5 Hardness of aluminium and copper specimens of different thickness, .....	82
Table 4-6 Mechanical properties of aluminium and copper, (density and poisson's ratio from Goodfellow, data from tensile testing machine) .....	85
Table 4-7 Variable and constant parameters used for ultrasonic metal spot welding.....	86

## V. List of figure captions

Figure 1-1 Schematic of the ultrasonic bonding region [2] .....	1
Figure 1-2 Schematic of USMW system .....	2
Figure 1-3 Ultrasonic transducer.....	3
Figure 1-4 Ultrasonic modes [26] .....	8
Figure 1-5 Ultrasonic welding systems with transverse vibration pattern (a) Wedge-Reed and (b) Lateral-Drive.....	9
Figure 1-6 Schematic of ultrasonic welding processes [29] .....	12
Figure 2-1 Power vs. weld time for the ultrasonic welding [27] .....	34
Figure 2-2 Pressure variables [84] .....	34
Figure 2-3 Weldability of USMW chart [84].....	36
Figure 3-1 Model of a longitudinal bar .....	42
Figure 3-2 Different horn profiles, illustrating node positions, stress distributions and vibrational amplitudes [88] .....	45
Figure 3-3 Axisymmetric horn profile depicting stress distribution.....	46
Figure 3-4 Mode shape classification with contour of displacement for (a) 1 <sup>st</sup> Bending (b) 1 <sup>st</sup> torsional and (c) 1 <sup>st</sup> longitudinal modes of vibration of a rod .....	49
Figure 3-5 3D non-contact laser Doppler vibrometer with controller .....	50
Figure 3-6 Dimensions of the modelled spot welding horn.....	54
Figure 3-7 Horn welding tip model.....	55
Figure 3-8 Variation of resonance frequency for longitudinal mode versus radius of curvature ( $R$ ) for catenoidal horn profile .....	56
Figure 3-9 Variation of different mode horn resonance frequencies versus radius of curvature ( $R$ ) for catenoidal horn profile .....	56

Figure 3-10 Convergences of resonance frequencies for different numbers of elements in the FEA model .....	57
Figure 3-11 Normalised stress and displacement distribution along the horn length .....	58
Figure 3-12 Representation of the deformed (green) and undeformed (grey) mesh shape for the integrated ultrasonic spot welding horn excited at 20.81 kHz .....	59
Figure 3-13 Contour plots of the deformed shape for the spot welding horn at 20.81 kHz: (a) displacement along axial horn length and (b) von Mises stress along horn length .....	60
Figure 3-14 FE stress and displacement results for the tuned spot welding horn at 20.81 kHz .....	61
Figure 3-15 FEA normalised displacement of the horn tip versus radial distance of the horn surface when excited axially at 20.81 kHz.....	62
Figure 3-16 Manufactured spot metal welding horn.....	63
Figure 3-17 Schematic diagram of experimental modal analysis showing the various components and photographed of actual set-up .....	64
Figure 3-18 FRF measurements of the excited spot welding horn at 20 kHz.....	65
Figure 3-19 Validation of the modelling and manufactured ultrasonic spot metal welding horn using FEA and EMA for tuned horn at 20 kHz .....	66
Figure 3-20 Steel anvil machined knurl .....	67
Figure 3-21 Welding stack mounting holder connect with spot welding horn.....	68
Figure 4-1 Aluminium and copper specimens used in ultrasonic metal spot welding with thicknesses of 0.1, 0.3, and 0.5 mm .....	71
Figure 4-2 Universal test machine, Zwick/Roell z2.0.....	72
Figure 4-3 Extensometer set-up on universal test machine .....	73
Figure 4-4 Dog bone specimen dimensions for the tensile tests.....	74
Figure 4-5 Experimental tensile testing for aluminium and copper specimens with variable thicknesses of 0.1, 0.3 and 0.5 using an extensometer.....	75

Figure 4-6 Typical stress-strain diagram with 0.2% offset method.....	76
Figure 4-7 Typical tensile test data for aluminium and copper specimens at 0.1, 0.3 and 0.5 mm thickness.....	77
Figure 4-8 Geometry of the overlapped welding specimen showing the adding of dummies layers to ensure alignment of the specimen during mechanical testing.....	80
Figure 4-9 Dektak model-6M instrument for measuring specimen surface roughness [119] .....	80
Figure 4-10 Scan roughness profile automatically measured with step detection software [28] .....	81
Figure 4-11 Micro hardness testing instrument .....	82
Figure 4-12 Ultrasonic metal spot welding rig as set-up in the Zwick/Roell test machine .....	83
Figure 4-13 Knurled horn and anvil surfaces with alignment fixture.....	84
Figure 4-14 Ultrasonic welding coupons of similar metals: (a)- Al-Al and (b)- Cu-Cu with different welding conditions: clamping force 100-500 N, vibration amplitude 42 $\mu\text{m}$ , welding time 1-3 sec .....	88
Figure 4-15 Ultrasonic welding coupons of dissimilar metals: (a) Al-Cu and (b) Cu-Al with different welding conditions: clamping force 100-500 N, vibration amplitude 42 $\mu\text{m}$ , welding time 1-3 sec .....	90
Figure 4-16 Set-up of the complete USMW system.....	91
Figure 4-17 Set-up of the welded specimens on the Zwick/Roell tensile test machine.....	92
Figure 4-18 Set-up the extensometer in tensile test machine.....	93
Figure 4-19 Tensile-shear testing of the welded coupons for aluminium and copper metals at thicknesses of 0.1 mm .....	94
Figure 4-20 Tensile-shear test of the welded coupons for aluminium and copper metals at thicknesses of 0.3 mm .....	95

Figure 4-21 Tensile-shear test of the welded coupons for aluminium and copper metals at thicknesses of 0.5 mm .....	96
Figure 4-22 Tensile-shear test of the welded coupons for aluminium and copper metals at thicknesses of 0.1 mm .....	97
Figure 4-23 Tensile-shear test of the welded coupons for aluminium and copper metals at thicknesses 0.1 mm .....	98
Figure 4-24 Tensile-shear test of the welded weld coupons for aluminium and copper metals at thicknesses of 0.1 mm.....	99
Figure 5-1 Welding strength vs. clamping force, joining similar metals, for amplitudes of 17 $\mu\text{m}$ , 30 $\mu\text{m}$ and 42 $\mu\text{m}$ .....	103
Figure 5-2 Welding strength vs. clamping force, joining dissimilar metals, for amplitudes of 17 $\mu\text{m}$ , 30 $\mu\text{m}$ and 42 $\mu\text{m}$ .....	107
Figure 5-3 Welding strength vs. vibration amplitude, joining similar metals, for clamping forces of 100 N, 300 N and 500 N, and for amplitudes of 17 $\mu\text{m}$ , 30 $\mu\text{m}$ and 42 $\mu\text{m}$ .....	110
Figure 5-4 Welding strength vs. vibration amplitude, joining dissimilar metals, for clamping forces of 100 N, 300 N and 500 N, and for amplitudes of 17 $\mu\text{m}$ , 30 $\mu\text{m}$ and 42 $\mu\text{m}$ .....	112
Figure 5-5 Welding power vs. clamping force for the joining of similar metals, for amplitudes of 17 $\mu\text{m}$ , 30 $\mu\text{m}$ and 42 $\mu\text{m}$ .....	114
Figure 5-6 Welding power vs. clamping force for the joining of dissimilar metals, for amplitudes of 17 $\mu\text{m}$ , 30 $\mu\text{m}$ and 42 $\mu\text{m}$ .....	115
Figure 5-7 Schematic of amplitude profiling showing a curves and amplitude profile, stepped amplitude profile (green) and profile amplitude ramp (red) [5] .....	117

Figure 5-8 Welding Strength vs. clamping force for comparison between constant and amplitudes profiling in the welding of similar metals, for 17 $\mu\text{m}$ , 42 $\mu\text{m}$ constant and dropping 42-17 $\mu\text{m}$ .....	119
Figure 5-9 Welding Strength vs. clamping force for comparison between constant and amplitudes profiling in the welding of dissimilar metals, for 17 $\mu\text{m}$ , 42 $\mu\text{m}$ constant and dropping 42-17 $\mu\text{m}$ .....	121
Figure 5-10 Lap shear spot welding model geometry and boundary conditions .....	123
Figure 5-11 Mesh shapes for lap-shear spot welding test coupons: (a) undeformed (b) deformed (c) contours of stress and displacement .....	124
Figure 5-12 Comparison between experimental and FE results of lap shear spot welding test performed in a weld joint of aluminium and copper, thickness 0.1 mm .....	125
Figure 5-13 Comparison between experimental and FE results of lap shear spot welding test performed in a weld joint of aluminium and copper, thickness 0.3 mm .....	126
Figure 5-14 Comparison between experimental and FE results of lap shear spot welding test performed in a weld joint of aluminium and copper, thickness 0.5 mm .....	126
Figure 6-1 Nikon Nomarsky optical microscope .....	131
Figure 6-2 Peeled specimens of similar metals, (a) Al-Al debonded specimens and (b) Cu-Cu debonded specimens .....	132
Figure 6-3 Peeled specimens of dissimilar metals, (a) Al-Cu and (b) Cu-Al .....	133
Figure 6-4 Photographs of peeled aluminium upper specimens, with double tipped arrows show direction of ultrasonic vibration, scale bar of 500 $\mu\text{m}$ , red dashed circle show weld area, amplitude of 42 $\mu\text{m}$ and thickness: (a) 0.1 mm, annealed (b) 0.5 mm, half-hard .....	134
Figure 6-5 Photographs of peeled copper upper specimens, with double tipped arrows show direction of ultrasonic vibration, scale bar of 500 $\mu\text{m}$ , red dashed circle show weld area, amplitude of 42 $\mu\text{m}$ and thickness: (a) 0.1 mm, annealed (b) 0.5 mm, half-hard .....	135

Figure 6-6 Photographs of peeled Al-Cu specimens, with double tipped arrows show direction of ultrasonic vibration, scale bar of 500  $\mu\text{m}$ , red dashed circle show weld area, amplitude of 42  $\mu\text{m}$  and thickness of 0.1 mm: (a) annealed aluminium (b) annealed copper .....138

Figure 6-7 Photographs of peeled Al-Cu specimens, with double tipped arrows show direction of ultrasonic vibration, scale bar of 500  $\mu\text{m}$ , red dashed circle show weld area, amplitude of 42  $\mu\text{m}$  and thickness of 0.5 mm: (a) half-hard aluminium (b) half-hard copper .....138

Figure 6-8 Photographs of peeled aluminium specimens, with double tipped arrows show direction of ultrasonic vibration, scale bar of 500  $\mu\text{m}$ , red dashed circle show weld area, clamping force of 500 N and thickness: (a) 0.1 mm, annealed (b) 0.5 mm, half-hard .....140

Figure 6-9 Photographs of peeled copper specimens, with double tipped arrows show direction of ultrasonic vibration, scale bar of 500  $\mu\text{m}$ , red dashed circle show weld area, clamping force of 500 N and thickness: (a) 0.1 mm, annealed (b) 0.5 mm, half-hard .....142

Figure 6-10 Photographs of peeled Al-Cu specimens, with double tipped arrows show direction of ultrasonic vibration, scale bar of 500  $\mu\text{m}$ , red dashed circle show weld area, clamping force of 500 N and thickness of 0.1 mm annealed: (a) aluminium (b) copper...144

Figure 6-11 Photographs of peeled Al-Cu specimens, with double tipped arrows show direction of ultrasonic vibration, scale bar of 500  $\mu\text{m}$ , red dashed circle show weld area, clamping force of 500 N and thickness of 0.5 mm half-hard: (a) aluminium (b) copper ..144

Figure 6-12 Scanning electron microscopy (SEM).....145

Figure 6-13 SEM images of Al-Cu specimens, magnified at 50 x, thickness: (a) 0.1 mm annealed, (b) 0.5 mm half-hard. the lower image shows the mating surface to the upper image .....146

Figure 6-14 Anaglyph z-position images of Al-Cu specimens, magnified at 50x, thickness: (a) 0.1 mm annealed, (b) 0.5 mm half-hard, showing the same specimens as in Figure 6-13 .....	147
Figure 6-15 Deformation of (Al-Cu), clamping force 500 N, amplitude 42 $\mu\text{m}$ , length of the path 4 mm, (a) 0.1 mm annealed, (b) 0.5 mm half-hard .....	149
Figure 6-16 SEM images of (Al-Cu) specimens, magnified at 50 x, clamping force 500 N, amplitude 42 $\mu\text{m}$ , (a) 0.1 mm annealed, (b) 0.5 mm half-hard. Regions 1-4 show the regions examined by SEM in Figures 6-17 and 6-18.....	149
Figure 6-17 SEM EDAX images of 0.1 mm annealed surfaces for Al-surface-1 (a) and Cu- surfaces-2 (b), show as regions 1 and 2 in Figure 6-16 .....	151
Figure 6-18 SEM EDAX images of 0.5 mm half-hard surfaces for Al-surface-3 (c) and Cu- surfaces (d), show as regions 3 and 4 in Figure 6-16.....	152

## VI. List of symbols

$\mu m$	Amplitude of vibration.
$d$	Average length of the diagonal of the indenter in mm.
$R_a$	Average roughness.
$L_1$	Body length.
$S$	Cross-sectional area.
$A_o$	Cross-sectional area of the specimen.
$\rho$	Density.
$u$	Displacement.
$\epsilon_{Eng}$	Engineering strain.
$\sigma_{Eng}$	Engineering Stress.
$F$	Force.
$\omega$	Frequency.
$HV$	Hardness number.
$D_1$	Horn input diameter.
$D_2$	Horn output diameter.
$R$	Horn profile.
$l$	Length.
$n$	Mode order.
$f_n$	Natural frequency.
$x$	Position.
$\nu$	Poisson's ratio.
$L_2$	Shaft length.
$\epsilon$	Strain.
$\sigma$	Stress.
$t$	Time.
$W$	Ultrasonic power.
$c$	Velocity of the stress wave.
$\lambda$	Wave length.
$E$	Young's modulus of elasticity.

## VII. Abbreviations

ASTM	American Society of Testing and Materials.
CAM	Computer Aided Manufacture.
CNC	Computer Numerical Control.
DEM	Digital Elevation Model.
DFT	Digital Fourier Transform.
EDAX	Energy Dispersive x-Ray Analyser.
EMA	Experimental Modal Analysis.
FFT	Fast Fourier Transform.
FEA	Finite Element Analysis.
FEM	Finite Element Modelling.
FSW	Friction Stir Welding.
FRF	Frequency Response Function.
SEM	Scanning Electron Microscopy.
UTS	Ultimate Tensile Strength.
USMW	Ultrasonic Metal Welding.





## Chapter 1

### 1.1 Introduction

Ultrasonic metal welding (USMW) was invented over 60 years ago and has since been used to weld several types of metals and their alloys. USMW involves a solid-state joining process in which metals are fastened together through the application of pressure combined with localized high frequency shear vibrations at the welding zone. The action of high frequency relative motion between the metals locally softens the overlap zone of the specimens to be welded, forming a solid-state weld because of the progressive shearing and deformation between surface asperities which disperses oxides and contaminants through a high frequency, scrubbing motion. This increases the area of pure metal contact between the adjacent surfaces, in which the metal atoms are forced together to create a strong weld, as shown in Figure 1-1 [1-3]. Welding is defined as a localised coalescence of metals or non-metals produced by either heating of the materials to a suitable temperature with or without the application of pressure, or by the application of pressure alone, with or without the use of filler metal [4]. Studies state that the ultrasonic welding of metals consists of complex processes such as plastic deformation, work hardening, breaking of contaminant films, crack formation and propagation, fracture, generation of heating by friction and plastic deformation, re-crystallisation and inter-diffusion [5]. In addition, slip and plastic deformation are the two different mechanisms which control the nature of the solid-state bond in ultrasonic welding.

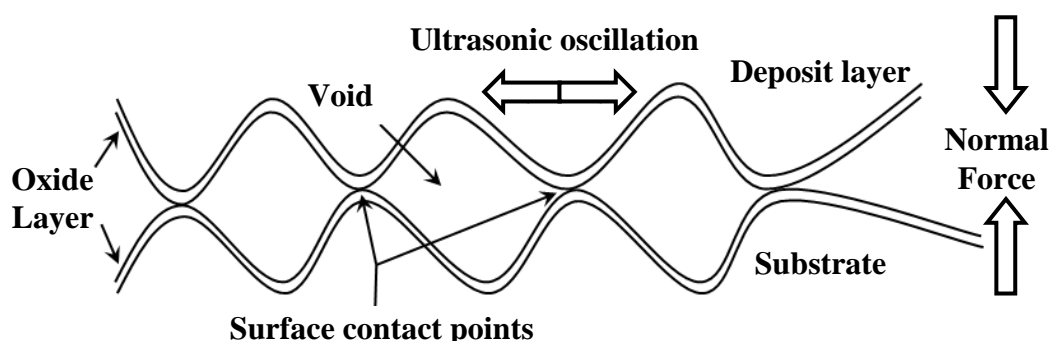


Figure 1-1 Schematic of the ultrasonic bonding region [2]

Recently, USMW has become a very popular technology for overcoming many of the joining difficulties in the welding of similar and dissimilar metals, including plates, sheets, foils, wires and ribbons, as well as many types of assembly which can be supported on an

anvil [6]. Moreover, the process can be applied successfully for joining various metal workpieces or bonding a metalized substrate, ceramic or glass using metal. Also, the process is suited to the application of welding thicker gauges, due to its capacity for higher power systems. In addition, the USMW process is considered to be more efficient than other conventional processes such as resistance welding in consuming a minimal amount of energy [7, 8]. The USMW process is more reliable and applicable in certain cases with respect to the other modern processes such as friction stir welding (FSW), because the energy generated from the process is concentrated at the weld line compared to the top surface in FSW. Although USMW and FSW are similar with the advantages of solid-state friction welding, the welding cycle in USMW is very short compared to FSW, and the join produced has good mechanical properties with less damage around the welding area [9-11]. Generally, the application of USMW depends on which way the two specimens are joined, using a combination of normal and shear forces. Friction also has an important role in creating a scrubbing effect between the mating surfaces during the supply of vibration, whilst the static force is applied normally to enhance the welding effect [12]. While the USMW technique is applied extensively to join metals, the widest current uses are typically for various alloys of copper, aluminium, gold, silver, magnesium and related softer metal alloys [13]. Therefore, it is likely that the technique has a promising future for improving the joining of lightweight components in applications as diverse as electronics, automotive, medical devices, aerospace and also increasingly in the sustainable energy industry in the manufacture of products such as solar absorbers [14, 15]. The set-up of an USMW system is illustrated in Figure 1-2. From the figure it can be seen that the system components consist of ultrasonic generator, transducer, booster and a horn, in addition to other welding components such as a rigid anvil, fixing tools and fixtures.

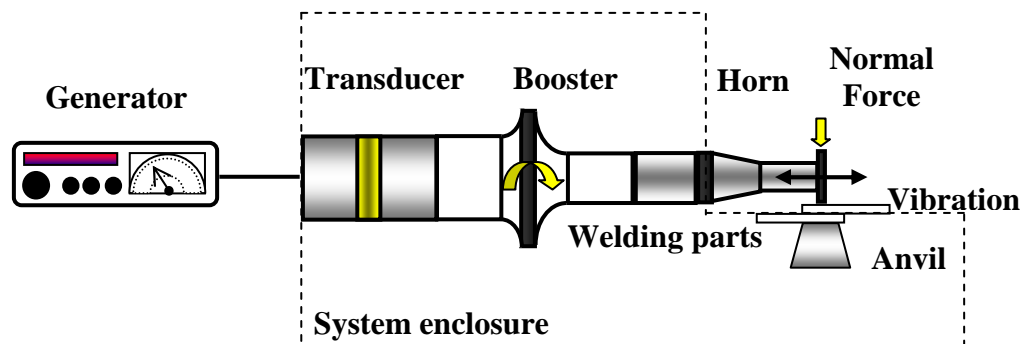


Figure 1-2 Schematic of USMW system

For most commercial welding systems, the maximum efficiency can be obtained in the resonant condition of the system. Commonly, the line voltage of the electrical power is converted into high frequency power, which can then be used for a wide range of metal welding applications using a frequency between 15-70 kHz, or above 100 kHz in the case of micro-bonding. 20 kHz is usually the most popular frequency in USMW. The electrical energy is supplied by a generator. The transducer (Figure 1-3) converts electrical energy into mechanical energy at the same frequency, through the use of a number of piezoceramic disks, but with a low amplitude resulting at the transducer working surface, typically in the range between 10-30  $\mu\text{m}$  [1]. Most welding systems will then adopt the use of a booster which controls the vibration amplitude, and can serve as a mounting for the entire stack. However, this can lead to an increase in the heating between connecting parts as well as resulting in a high stress at the joining points. The horn is considered as a tool in the welding system which has the ability to transmit ultrasonic energy from the transducer to the welding specimens and also to clamp the upper part of the substrate during the welding process. The low amplitude generated from the transducer is then amplified by the booster and the horn and the amplitude varies depending on the design of welding tools and the capacity of the generator.

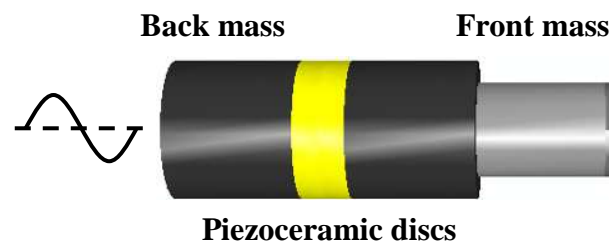


Figure 1-3 Ultrasonic transducer

The welding frequency is specified according to the application. At specific frequency, higher amplitude at the horn working surface can result in higher power dissipation. In ultrasonic welding, the machine is usually set by a certain mode. For example welding by time (an open-loop process) operates on the assumption that the fixed time results in a fixed amount of energy delivered to the joint and that the sonic wave remains independent of the energy. Welding by energy (a closed-loop process) is the second mode of operation. The generator will measure the amount of power drawn and integrate it over time using

feedback control. When appropriate, the delivery of the ultrasonic energy is stopped by the generator whilst the energy is dissipated. The third welding mode involves welding by distance or post-height, and allows joining by a specific weld depth. The ultrasonic generator will continue delivering energy to the parts being welded until the preset displacement between welding tool and surface metal is reached [5, 16].

In general, ultrasonic welding has two main applications, namely ultrasonic metal welding and ultrasonic plastic welding. It is well known that the ultrasonic welding process for metals is distinct from the process used in plastic welding. The main difference is that in metal welding, the ultrasonic vibration is moving parallel to the plane surface of the specimens being welded. In plastic welding, the vibrations are perpendicular to the surfaces. Another reason is that the nature of the bond in metal welding is represented by a solid-state, which means that no melt or fusion is required between adjacent specimens, whereas in plastic welding, the process directly depends on the melting of adjacent specimens. Nevertheless, most components of an ultrasonic system such as generators, transducers and welding horns are similar for the two systems. Although the ultrasonic welding technique has developed since 1950, and a great number of publications have been issued to study the variables in different welds, it is acknowledged that a large number of these studies are focused on ultrasonic plastic welding, and that ultrasonic metal welding is less understood. Therefore, to understand the mechanism of the USMW process, the ultrasonic components and the effects of different related parameters were investigated. This was achieved through the design of an ultrasonic system suitable for metal welding.

## **1.2 Outline of research**

In this research, four parts were considered to address the lack of understanding of the issues surrounding USMW, and for investigation of the metal behaviour during the welding of similar and dissimilar thin metals. The first part relates to the design and manufacture of the ultrasonic welding system which is capable of joining thin gauges such as light plates, sheets and foils. The model of the welding horn was developed based on the enhancement of the vibrational and dynamic characteristics. The FE analysis package Abaqus was used to develop the final configuration of the welding horn. Many attempts to resolve criteria that influenced the performance of the horn were performed using FE simulation, which included the matching of the horn excitation frequency to the operating frequency, ensuring the horn vibrated longitudinally at the operating frequency, isolation

of the tuning mode from other non-tuned modes, ensuring uniformity of the vibration velocity at the horn working surface, high gain factor and the avoidance of stress at connecting components. The reason for performing these analyses is to ensure that the horn is excited at the desired vibration mode and ensure the maximum transfer of ultrasonic energy to the weld specimens. Modal analysis and harmonic analysis were used to examine the natural frequencies and mode shapes of the tuned welding horn. In this study, a lateral-drive system is selected as the type of ultrasonic welding configuration, and is shown in Figure 1-2. This system has been chosen to investigate ultrasonic spot welding. In order to guarantee the successful welding together of any metals, careful design of components and fixtures is required. The horn is tuned longitudinally at the ultrasonic operating frequency, in this case 20.81 kHz. This operating frequency should be matched with the specific frequency of the transducer. Any minor change or inaccurate calculation which is made when designing a horn may lead to a shift in the operating frequency of a few hundred hertz from the excitation frequency. This deviation in frequency affects the dynamic and vibration characteristics of the tuned horn, which can then lower the vibration amplitude, affecting the weld strength and lowering the quality of the weld.

The second part of the work discusses the design and manufacture of the other welding components such as a rigid anvil, welding stack holder, rigid bed, fixing tools and fixtures. FE analysis with Abaqus is again used to develop the geometries of the welding components with respect to the size and dimensions of the welding stack and to the thickness and dimensions of the metals to be welded. Many studies use conventional welding machine to produce welds and study the effects on several variations of weldment. These studies are focused on the change or modification in the welding tip and fixing tools. However, these machines are usually limited in terms of delivering energy and in the control of process parameters. Therefore, this study aims to design and construct a welding machine suitable for joining thin metals and conduct studies on several parameters that influence the strength and quality of the welds. The welding rig is set-up and mounted on a driving machine (Universal test machine) through connecting the welding stack with the mounting holder. The vibration response of the welding stack is examined after connecting it to the driving machine to avoid damping effects and shifting frequency that can result in a drop in the ultrasonic amplification of the exciting components. The unique axial motion of the welding stack by driving machine, allows good control of applying load, as using 2 kN machine load cell. The ultrasonic generator is used to control the energy delivered to

the weld, In addition, the welding cycle of each test is specified from the preset of the machine program. Therefore in this research, the design of the welding system allows to produce welds in a different manner, which is capable to control system parameters, and study the strength and quality of joining metals, which can be limited by conventional welding machines. In addition, the welding system has the ability to improve the weld, enhance weld strength and increase consistency through the control of system and ultrasonic parameters, which are not available in most welding machines.

The third part of the research is concerned with studying welding conditions through investigation of the process and metal parameters, and their effect on weld strength and weld quality. Aluminium and copper have been selected for these welding studies, for which four different weld coupons are studied, comprising Al-Al, Cu-Cu, Al-Cu and Cu-Al. The weld coupons are selected from sheets with thicknesses of 0.1, 0.3 and 0.5 mm, for annealed and half-hard metals conditions. Experiments are conducted in order to study the influence of the process parameters (clamping force, amplitude of vibration, welding time and ultrasonic power) on the weld strength. The enhancement of the weld strength is dependent on the energy supplied to the deforming area and the relationships between welding parameters. The operation is rapid, as the time duration for welding is usually one second. A tensile shear test is employed to examine the weld strength through study of the relationships between the joint strength and the different process parameters. Amplitude profiling is an approach that has recently been applied in the field of USMW to increase the weld strength, enhance the joint and reduce specimen marks. This thesis also discusses the matching of the amplitude to the various weld phases through the optimisation of the weld cycle to increase the weldability of joined metals with respect to those produced at constant amplitude.

The fourth part of the research investigates the weld quality of the joined metals. The investigation begins with an examination of the factors which influence the quality of the weld by the analysis of the deforming surfaces. Optical microscopic examinations are performed to analyse the different parameters of the weld through the extraction of details about the morphology of the welding area. Investigations using scanning electron microscopy, SEM, show how the deposition percentage of the welded specimens is particularly sensitive to the metal surface conditions, such as hardness and surface roughness, which strongly affects the quality of the weld. The weld quality is also

influenced by the clamping force and the vibration amplitude of the welding tip. Higher weld quality is obtained through an appreciation of the best combination of different process parameters for the specific metal joining configuration.

The objectives of this study were to design an ultrasonic metal spot welding system suitable for joining thin metals, and which is able to investigate the behaviour of joints during different welding conditions, especially focusing on the influence of clamping force, constant amplitude and amplitude profiling to enhance the weld strength and improve weld quality. Good weld strength and quality depends on the accurate design of tools to ensure high energy is imparted to the deforming region, but the weldability of metals also depends on the relationships between process and metal parameters and the capacity of the ultrasonic generator.

### **1.3 Historical background**

The issue on the welding by mechanical vibration was reported by Willrich in 1950 who obtained cold weld at the region of resistance welding through apply low frequency vibration to the tool that designed for this purpose. Similar results were recorded in research conducted in the United States. The USMW technique was first demonstrated at early 1950s [1]. Research at that time revealed that producing a weld was occasionally accomplished by ultrasonic means. Leading from this, in 1953 the first report concerning the application of the ultrasonic energy to cold welding appeared [17, 18]. The practical application for welding by ultrasonics was then better defined. However, the first research investigation aimed at developing the USMW technique was not proposed until the 1960s because the patent at that time did not acknowledge that the existing machines would be able to make a metallurgical bond and create a forming state without the need to heat or melt the metal through the use of any flux or agent filler material [19]. The USMW technique then continued to develop to include a wide range of applications for structural components during the 1960s. After that, the technique was used to cover many fields in automotive engineering and manufacturing processes. In 1969 the first assembly of a car was achieved by using USMW. Since the USMW technique has been used widely in a multitude of fields [20, 21]. Now, many industrial sectors are benefitting from using USMW in some capacity, such as in the automotive, manufacturing, electrical and electronics, aeronautical and aerospace industries.

## 1.4 Ultrasonic waves

Ultrasonics is defined as the use of ultrasound and the generation of acoustic waves. The mechanical waves are generated according to the oscillation transmitted through solids or liquids, and characterised by parameters of frequency, amplitude and wave speed. For frequency, the human ear can typically detect sound between 20 Hz and 20 kHz, which is the range called audio [22]. If sound is transmitted below the audible range of hearing, then it is called infrasound, and when the transmission is above the audible range it is described as ultrasound [23, 24]. Sound is transmitted through a medium by oscillation of molecules through the direction of wave travelling. The range of low and high power ultrasonics is varied from 20 kHz to 2 MHz [25]. Ultrasonic waves can travel easily in any media, solid or fluid, which causes the medium to exhibit an oscillation in a characteristic shape of motion called a mode. A normal mode of vibration is a pattern of motion in which all parts of the medium move sinusoidally with the same frequency. In any vibrational system, the frequencies of the normal mode are referred to as the natural frequencies or resonant frequencies. In general, three common modes can be observed in ultrasonics, classified as axial (longitudinal), torsional, and flexural (transverse) modes, as seen in Figure 1-4.

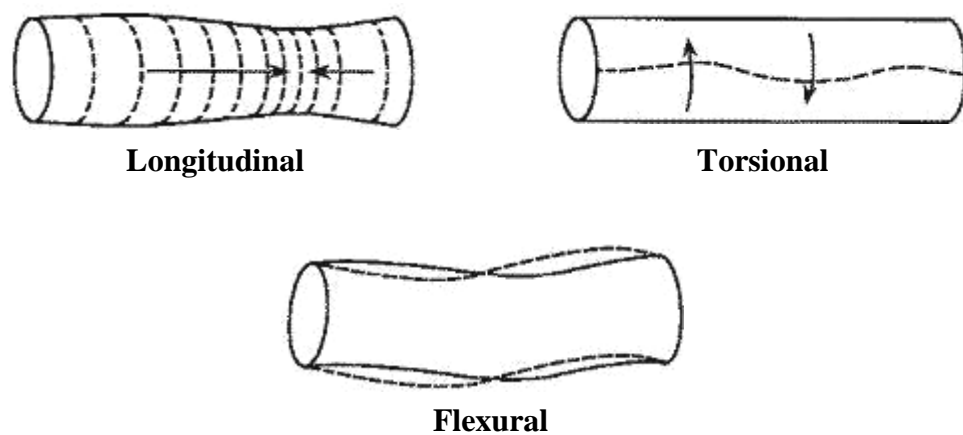


Figure 1-4 Ultrasonic modes [26]

In the longitudinal mode, the direction of displacement of medium particles from their positions of equilibrium coincides with the propagation direction of the wave. Mechanical longitudinal waves can also be referred to as compression waves. The torsional mode represents the oscillatory angular motion, which causes twisting of the system. In the flexural mode, particle displacement is perpendicular to the propagation direction of the wave.

## 1.5 Ultrasonic metal spot welding equipment

In ultrasonic welding, there are several variations of the process which can be adopted, based on the type of the weld, geometry, and the metals to be joined. The ultrasonic welding of metals is then obtained using transverse ultrasonic vibrations to create a scrubbing action between the specimens. Several variations of ultrasonic welding exist, for example, seam, line, spot, torsion, and ring. This research will be focused on ultrasonic metal spot welding, which is perhaps the most common approach in the application of automobile part manufacture and also used in many industrial assembly lines. Moreover, this kind of weld is typically used when bonding particular types of sheet metal, because the bonding zone covers only a small area of the sample, typically up to around  $40 \text{ mm}^2$  [14]. In general, two configurations of ultrasonic metal welding systems can be used to spot weld metal substrates together, namely a wedge-reed system or a lateral-drive system, as shown in Figure 1-5. Although these systems are different in shape and application, the vibrational mechanisms at the deforming area are the same [27]. The components of the two systems are discussed briefly as follows:

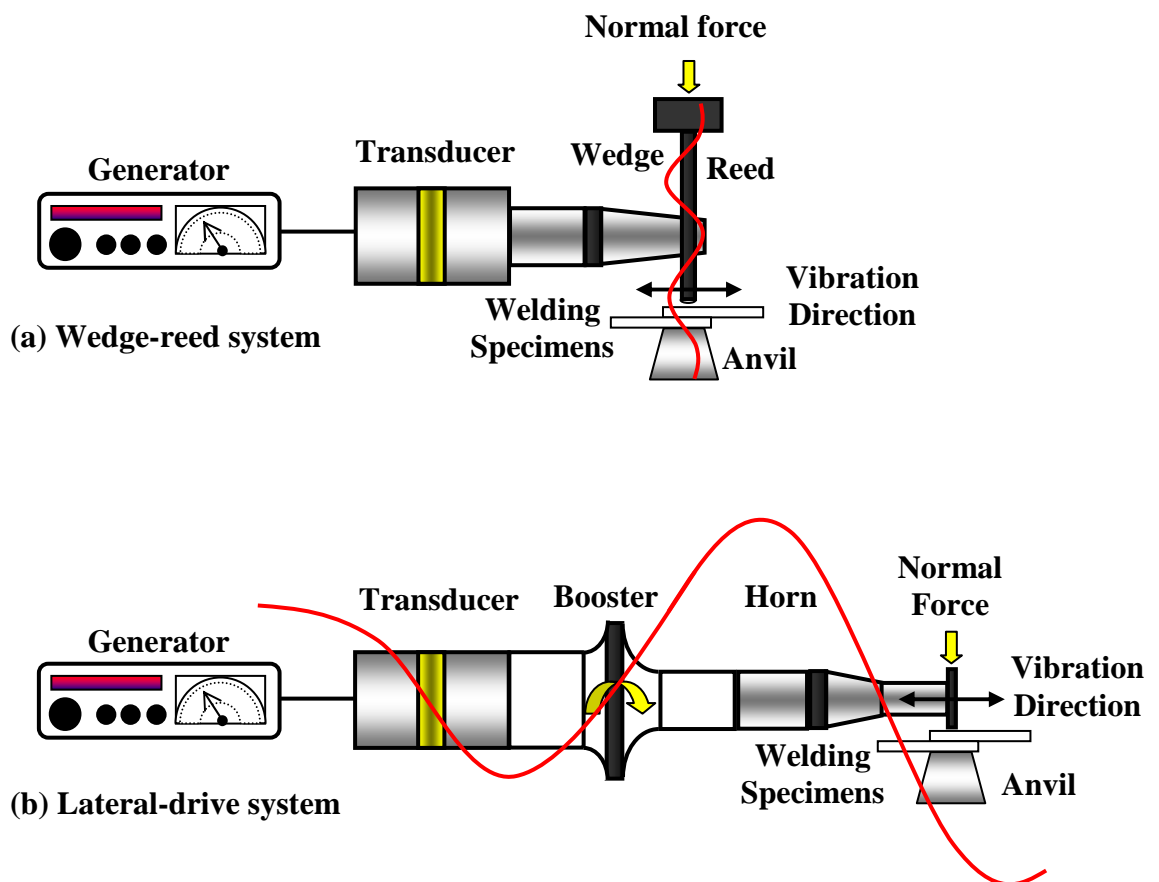


Figure 1-5 Ultrasonic welding systems with transverse vibration pattern (a) Wedge-Reed and (b) Lateral-Drive

### **1.5.1 Wedge-reed ultrasonic spot welding system**

In the wedge-reed system shown in Figure 1-5 (a), the components are the generator, transducer, and wedge and reed series of components, used to produce and transmit the ultrasonic vibration energy and transfer it to the specimens that are clamped between the horn tip and the anvil. The normal force is applied using either a pneumatic, hydraulic or electrical device that can easily control the upwards and downwards movement of welding horn. During operation, the vibration amplitude may vary according to the tool design and power setting for a given application. Normally, the amplitude is in the range of 10 to 100 microns peak-peak. The magnitudes of the normal force fall between a few Newtons to several kilo-Newtons [28]. It is necessary to mention here that the ‘wedge’ amplifies the vibration amplitude that is imparted through the reed, to the welding tip. Welding or brazing is usually used to connect the wedge to the vertical reed to prevent any losses of the transferred vibration energy to the welding region. While the reed is vibrating in the bending mode, an oscillation motion is created. In some cases for the wedge-reed system, it is preferable to design the anvil as a vibrating member resonating out-of-phase, to increase the motion across the specimens [1]. In fact, this may increase the capability of this type of welding system to bond traditionally unsuitable or higher-strength alloys. In wedge-reed system, as the transducer is directly brazed to the reed and the latter is directly touch to the welds through welding tip. Thus the transducer is only capable of driving the welding tip and has inability to control weld parameters, as no resistance is directly received by it.

### **1.5.2 Lateral-drive ultrasonic spot welding system**

For this type of ultrasonic weld, the system consists of a transducer, booster and a horn with a welding tip, as seen in Figure 1-5 (b). The term, ‘welding stack’ is sometimes used to refer to the horn and booster which is connected together to the transducer. In a similar manner to the wedge-reed system, the transducer produces a vibration of the piezoelectric disks. The booster increases the transducer amplitude depending on the gain value, serves as a mounting for the welding stack, and also acts as a clamp of the joint specimens. The welding horn can further increase the vibration amplitude at the welding area. In this type of welding system, the horn is mounted parallel to the vibration direction of the exciting

tool. Therefore, the ultrasonic energy is transferred to the specimens in a transverse manner. The specimens, usually two thin sheets or foils of the selected metals, are situated in a lap joint configuration. The specimens to be welded are firmly clamped between the welding horn tip and the stationary anvil, where the upper specimen is gripped against the knurled pattern on the horn tip surface. Likewise, the lower specimen is gripped against the knurled surface anvil. The ultrasonic vibration of the welding horn is in the parallel direction to the specimen surface, creating a scrubbing motion at intimate surfaces. This leads to a relative friction motion at the mating specimens, causing shear, deformation, and a flattening of the surface asperities and then subsequent weld formation. Generally, lateral-drive and wedge-reed welding systems are similar in terms of the vibration phenomena which are exhibited, such as, transverse, linear and resonant at the specific operating frequency. The vibration is similar between them however, the way in which the vibrations are produced are different. The two systems are influenced the welding zone in the same way, through a solid-state mechanism that occurred at the interface, without the need to melt or fuse of the substrate metal. This work depends on design a configuration of lateral-drive system, which is suitable for joining thin gauges.

In this work a welding system which has a configuration of a lateral-drive system is selected to allow for study of the factors that influence the performance of the working horn. These factors cannot be readily studied with a wedge-reed system, as the horn is not in direct with the weld specimen. Furthermore, the lateral-drive system can allow for measurement of process parameters, such as clamping force and vibration amplitude, more accurately than the wedge-reed system, because these parameters can be measured at the transducer for a lateral-drive system but not for a wedge-reed system. This helps to relate the weld strength of the joined metals to the different welding conditions. In addition, this study investigates the welding of thin metal specimens, which require high vibration amplitude with low applied force and this can best be obtained from the lateral-drive system.

## **1.6 Principles of ultrasonic metal welding (USMW)**

Since most studies predominantly focus on ultrasonic plastic welding and its applications, the principles of USMW and its range of applications remain not fully understood. To understand USMW, it is preferable to start with the principle of the technique, including any variations or differences from other processes used in conventional welding systems.

The principle of the welding operation occurs from creating an oscillating shear force at the interface between the mating surfaces, to disperse oxides, voids, liquids and contaminants, and offer new contact at many points. During the supply of vibration at a local area, the resultant oscillation causes an increase in diffusion across the interface, resulting in a weld similar to that produced by diffusion welding [29]. At the bonding area, dynamic shear stresses are generated due to the combined influence of static load and ultrasonic vibration. The effects of interfacial slip and plastic deformation will increase the temperature of the scrubbing area, which itself is always lower than the melting point of base metal. The properties of the joining metals can influence the temperature at the interface between the two surfaces, which means that the temperature can be higher for those metals with a low thermal conductivity such as steel, than for other types of metals which have high thermal conductivity such as aluminium and copper. For that reason, the ultrasonic technique consumes less power when it is applied to the welding of higher thermal conductivity metal, compared to other processes such as resistance welding. Figure 1-6 shows the phases of the welding process [29, 30].

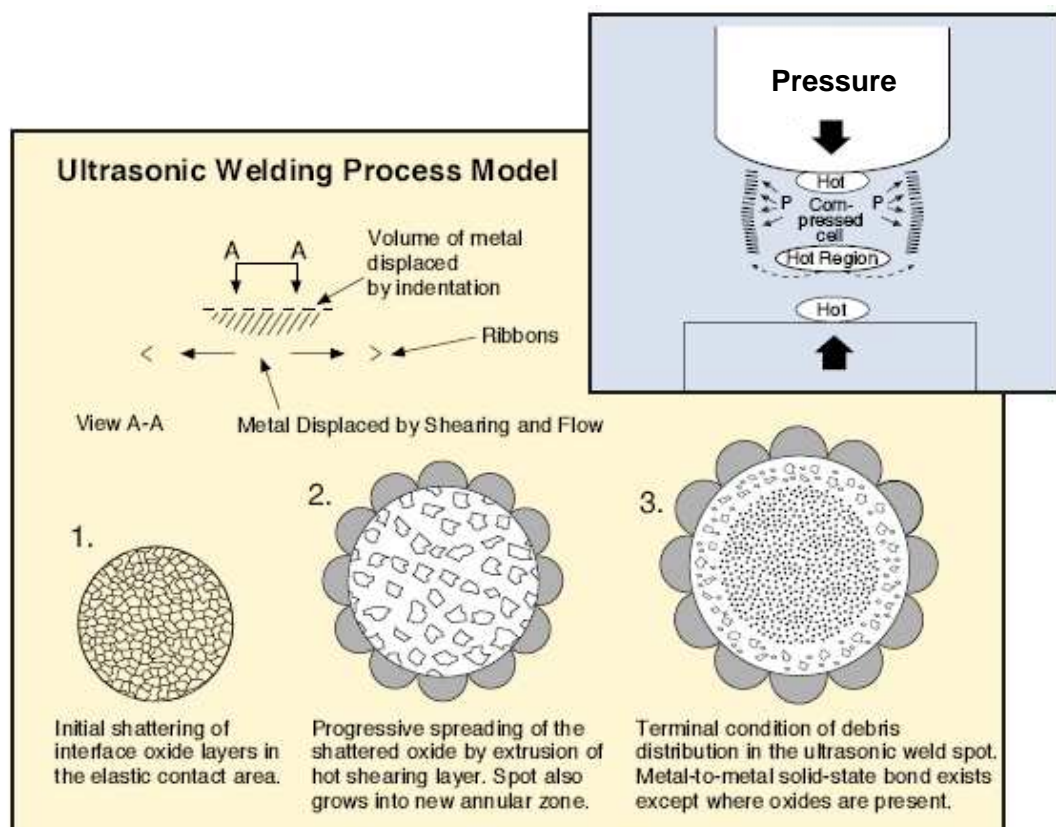


Figure 1-6 Schematic of ultrasonic welding processes [29]

The welding operation means that the system is vibrated in a transverse manner. As mentioned above, the wedge-reed system and lateral-drive system are both developed to enhance the transverse vibration. In the wedge-reed system, the transducer resonates axially and produces vibration in the direction towards the wedge. This vibration amplitude is relatively small in comparison with the amplitude of the tool. The vibration passed along the reed is a bending (flexural) mode, which means that the motion in the transverse mode is similar to the vibration as seen in Figure 1-5 (a). In the lateral-drive system, the booster serves the same function as the wedge and also fixes the welding stack through a mounting parallel to the vibration direction of the tuned horn. Ultrasonic energy is transferred to the specimens by a welding tip which vibrates transversely through contact with the upper specimen surface, as shown in Figure 1-5 (b). The selection of the type of weld system will depend on certain parameters, such as the required vibration amplitude, clamping force, vibration energy and the specimen thickness to be welded. However, the properties of the deformed area are similar to those for parent metals. In the wedge-reed system, a weld is produced using low vibration amplitude with a high clamping force, which results in high energy transferral to the welding zone. In the lateral-drive system, high amplitude and low clamping force are required to produce a weld. However, this type of welding process is only suitable for joining thin sheets, foils, and fine wires. The reason is to avoid the increase of any bending stresses due to a load increase, which if exceeded, leads to early fatigue failure. Ultrasonic metal welding systems can be used successfully in different welding applications, such as continuous seam welding which is used for joining specimens through the integration of a rotating disc operating as the horn tip. Continuous welding is easily obtainable by this type of welding process due to the passing of the welded specimens between the vibration of the rotating disk and the fixed anvil, or the welded specimens could also be moved between the tip and a counter-rotating anvil. The mechanism of applying the force in this process is similar to spot welding. In continuous welding, the bonding area may be produced in the manner of overlapping seam welds, and welding foils can be produced by this type of welding [6]. Ring welding, often called torsion welding produces closed-loop joints which are usually circular but may have different shape, such as square, rectangular or oval. The horn tip is hollow and is set parallel to the weld interface and it is vibrated parallel to the surface of the welding specimens. At least two transducers are required to produce this type of weld with sufficient power [1]. Line welding is another process in which the specimens to be welded are firmly clamped between the stationary anvil, while the horn tip is moved linearly and

oscillated parallel to the plane of the weld interface, and perpendicular to the direction of the applied load and welding line. This type of welding produces a linear weld[6], and is suitable for thin metals [29].

In USMW, more than one parameter can affect the nature of the weld, and these parameters are classified into two groups: process parameters and metal parameters. Process parameters consist of static load (clamping force), amplitude of vibration, welding time, resonance frequency and electric power. Metal parameters include the features of the specimens being welded, such as hardness, surface roughness, oxides and contaminants [27, 28, 31]. The control of parameters is not easy due to complex setting between process and metal parameters. In USMW, the thickness of the specimen being joined can affect the nature of the weld. Therefore, for a given thickness, if the amount of total force is small, the weld produced is not good due to the low stresses at the interface, since the stress is proportional to the applied force. By increasing the thickness of the welded specimens, excessive deformation can be imparted at the top surface. The size of the weld tip also influences the weld as it is related to the specimen thickness and contact stresses. As the thickness of the specimen increases so must the weld tip size in order to maintain the stress level at the interface. However, this causes an increase in the force in the specimens, which requires more power to maintain the welding process. A higher welding force may also suppress the velocity of the welding tip, resulting in lower amplitude. Unfortunately, no schedules are available to help analyse the issues behind weld tip size, specimen thickness and weldability of the specimens [1]. The period of time for the weld cycle varies with the thickness of the specimens, composition of the metal to be welded and the capacity of the generator [29].

### **1.7 Applications of ultrasonic metal welding (USMW)**

Applications of USMW are found to be extensive in many fields and industries such as electrical/electronic appliances, packaging, automotive and medical instruments. Recently, the technique has been adopted due to the demand for sustainable energy products such as those that are welded for solar absorber panels, whilst the technique has also been used more efficiently to weld equipment for aeronautical and aerospace fields. USMW is widely used for joining metals, and the process can be used to weld in any environment such as in water or in a vacuum [14, 32]. In general, the process is extensively used with ductile metals and their alloys, due to requiring moderate power to produce a weld. Harder or

refractory metals are more difficult to weld by ultrasonic methods, as those types require more power to obtain a weld. Currently, USMW technique is used for alloys of aluminium, copper, magnesium, titanium, nickel, silver and gold. As mentioned in section 1.6, the process of ultrasonic metal welding is different between lateral-drive and wedge-reed configurations due to the variations in the direction of ultrasonic vibration, range of applied clamping force, and the magnitude of vibration amplitude, as well as the thickness of the specimens being welded. Thicker metals and their alloys are welded by a wedge-reed system, because a high amount of energy is required to join larger thicknesses of welded specimens, whilst, electrical cables, wire harnesses, splicers, sheet metals, foils, ribbons, meshes and wires can be successfully joined to thin sheets or tubes by using lateral-drive system.

## **1.8 Description of the research and key findings**

This research provides details of the design, characterisation and testing of a lateral-drive ultrasonic metal spot welding system. The welding machine is capable of joining relatively thin metals, such as sheets, plates, foils and wires. The ultrasonic spot welding horn is modelled and fabricated with sufficient precision, not only for producing good welds but also to enable the examination of many issues encountered in the design of ultrasonic tools. These issues have largely received less attention in the literature in recent years, but are important to understand, as they have a direct effect on the performance of the working horn. For example, matching the horn excitation frequency to the operating frequency of the transducer ensures that the horn will be vibrated longitudinally very close to the operating frequency, allowing a separation of the longitudinal frequency mode through the isolation of the tuning mode from other non-tuned modes, which guarantees uniformity of the vibration amplitude at the horn working surface, high gain factor and the avoidance of stress which may initiate at the points between connecting components. The proper design of the exciting horn is essential to ensure transmission of ultrasonic energy to the weld specimens with minimum dissipation. The welding stack (the horn connected with the transducer) is mounted on a driving (universal-test) machine, allowing the control of the range of forces that are recommended for joining different thicknesses.

The vibration amplitudes are provided by the regulation of the ultrasonic energy that is delivered to the welding stack. In this work, the force and vibration levels which are utilised assist in overcoming the limitations which are identified in many studies in the

literature, in which conventional ultrasonic machines are commonly used. In this research, it is shown how the ultrasonic welding machine is capable of controlling system parameters, which in turn provides a good degree of weldability for a range of different welding conditions. This allows the weld strength and quality to be examined through the dependencies of process parameters such as clamping force, amplitude of vibration, welding time and input power, and also metal parameters such as thickness, hardness and surface roughness. In addition, the machine enables the USMW of thin gauges, and produces good-quality joints through an increase in both the weld strength and weld quality, and a reduction of weld defects.

## **Chapter 2**

### **Literature review**

#### **2.1 Introduction**

This chapter reviews the developments which have occurred in the design of ultrasonic tools (horns) and discusses various tool profiles which are commonly used in the transfer of ultrasonic energy to welding specimens. Furthermore, studies relating to the USMW technique and the associated critical operating parameters are reviewed, which explain the mechanisms behind the solid-state bonding process for different welding applications. The unique features of USMW are also explained, by an analysis of the different stages of the welding process. In addition, it is explained the theory of USMW without melt or fusion, and how other characteristics are observable, such as low levels of heat generation during scrubbing motions which can occur in certain USMW procedures. Studies utilising different welding configurations are reviewed, and also for the welding of other metal configurations, such as thin sheets, foils and wires. In this chapter, a brief discussion of system parameters, as relevant to this study, is appropriate, as these parameters are dependent on one another, and the relationship of these parameters depends on the specific welding system.

#### **2.2 Background of the design of ultrasonic tools**

The first observation of electrical-mechanical conversion in certain types of crystal was discovered by Pierre Curie and Jacques Curie [33]. This discovery resulted in successful implementation of the piezoelectric effect in ultrasonics, where it is now utilised in many ultrasonic devices. In the subsequent years, studies into ultrasonics continued, and scientists such as Paul Langevin worked in the field of acoustics to enhance the intensity of acoustic power in order to develop high-power acoustic capability. The ability to produce high acoustic intensities meant that the design of ultrasonic tools suitable for higher-power applications was possible [34, 35]. The theory of the solid horn as a concentrator (also called resonator) of elastic energy or as an impedance transformer was established in order to develop acoustics research. Pierce [36] used tapered solid couplers to investigate the transfer of acoustic energy along the taper. The analysis of the tapered solid horn was

studied by Mason, who successfully adapted the theory of the horn for the compressive wave in air to the compressive elastic waves in a solid medium. High power ultrasonic systems were produced as a result of the discovery of piezoelectric materials [37]. In just one decade, Mason designed his ultrasonic horn which could be driven by a high power generator. Merkulov in the Soviet Union analysed ultrasonic concentrators, and derived the equations to compute the resonant dimensions of horns and extract the gain coefficient. The analysis was based on selecting the optimal variable cross-section of the rod to excite the longitudinal vibration mode. The study also reviewed several horn profiles such as exponential, conical and catenoidal. The reason for studying these profiles was to extract the highest gain at the horn. The largest gain is produced by the catenoidal shape [38]. Other studies focused on different horn profiles, such as the solid conical horn presented by Ensminger, who conducted his study on finding particle velocity, particle velocity amplification, stresses, length, and mechanical impedance of sections of solid cones. This research was based on an assumption that the steel horn was designed to be half-wave length and tuned at 20 kHz, for which the gain was recorded at 4.61, similar to the gain value that was calculated by Merkulov [39]. Different types of metals were selected for tuning the horn, such as in the study conducted by Neppiras, who investigated the excitation of tuned horns. The author's results suggest that good acoustic quality can be produced from a horn that is made from titanium, as this metal has lower internal losses and a high stress threshold [40]. Belford [41] studied the design of solid stepped horns through the analysis of the horn dimensions. The results that were extracted from mathematical analysis showed that sufficient gain could be achieved from the stepped horn compared to the exponential or even the catenoidal horn.

Amza and Drimer [42] analytically determined the effect of concentrator mass on the operation of the vibration modes. The study was carried out on exponential, conical and catenoidal concentrators. The study concluded that the catenoidal profile of the concentrator offer high gain. Various studies were performed on the design of ultrasonic horns used for ultrasonic machining, such as the study published by Satyanarayana et al [43], which discussed different horn profiles such as exponential, conical and stepped. The study involved the calculation of resonance length, gain, stress and displacement. The study concluded that the exponential horn can produce sufficient gain compared to the other horn profiles. A recent study on the design and simulation of a stepped horn by Nanu et al[44], showed how an ultrasonic horn was used to aid electro-discharge machining. The

study, which was supported by FEA, involved the measurement of resonance frequency and amplitude at points located on the horn surface. Shu et al explored the analysis and design of a horn used for embedding or encapsulating a metal into joined specimens [45]. The FE software code ANSYS was employed to specify the geometry and dimensions of the horn and also to compare the numerical results with experimental results. The simulation reduced the trial-and-error time for machining and also enabled the modification of horn dimensions.

Derks [31] explored the design of welding devices through using FEA to develop and optimise the shape of an ultrasonic resonator, and subsequently excited the mode of vibration of two profiles, namely cylindrical and rectangular resonators. The study focuses on the problems that are often met with resonator design which is used for welding, such as poor energy transmission to the weld, short tool life and noise during excitation of tools. The study demonstrated the design of ultrasonic resonator with a wide output cross-sections of such a complexity that creating an ultrasonic resonator. In addition, the author attempt to excite longitudinal modes of vibration in cylindrical and rectangular dimension perpendicular to the longitudinal axis was greater than a quarter wavelength [25]. A high power ultrasonic transducers was designed by Muhlen [46] whose design was based on the use of piezoelectric rings to produce high power. The author stated that the design of a slender horn must be avoided if possible, due to the excitation of lateral modes of vibration that could lead to component damage during operation. Commonly, the FE method can be used to accurately design ultrasonic horns. The method is widely used for many different shapes, including circular and rectangular. Adachi et al [47] presented a modal vibration analysis of rectangular ultrasonic welding horns. This was achieved by setting the length of the horn to the half-wavelength of longitudinal vibration at 20 kHz. A number of slits were added to reduce the effect of Poisson's ratio, to ensure a uniform amplitude distribution at the horn working surface. The study found that the natural frequency of longitudinal mode is determined by the values of the column width, slit width and bridge thickness. Furthermore, the study concluded that the effect of varying the column width at both ends of the tools is shown to be negligible small.

O'Shea [48] modelled a high-power ultrasonic horn to study the influence of mode shapes and frequencies. The model suggests that the horn should ideally be excited at a purely axial mode with uniform vibration amplitude at the horn working surface. The results of

the modelled horn investigation proved that the effect of design factors such as slot length, slot width and the number of slots control the mode shapes and the frequency separation. The numerical results correlated with the experiments. Woo et al [49] conducted a theoretical study of an acoustic horn which was excited by high ultrasonic power. The optimal dimensions of the horn were investigated in order to achieve high vibration. This was accomplished using the FE analysis code ANSYS. Another study of high power ultrasound used in ultrasonic cutting and welding of thermoplastic textures was presented by Silva [50]. The FE analysis was used to predict the vibration amplitude for the wide blade horn through simulation. It confirmed that the electrical impedance was reduced due to the increase in the number of piezoceramic discs. However, the vibration amplitude was observed to be non-uniform along the horn working surface. An analytical study was performed by Amza [51] in order to design an ultrasonic booster for the ultrasonic welding device. The ANSYS model extracts the system modes and frequency of the exciting device.

The proper design of high-power ultrasonic tools and horns has become very important in many fields, especially after the discovery of piezoelectric materials. The majority of the literature has focused on the design of tools with different profiles, such as tapered, conical, rectangular, step and catenoidal, in order to investigate the transferral of high acoustic power with high gain. Furthermore, most of this research has attempted to study the dimensions of the tools in order to enhance system modes and frequency of excitation. Most researchers generally agree that the catenoidal tool profile is the optimal choice, as it is capable of providing high gain compared to other tool profiles. Studies in the literature also show that the type of metal which is used in the design of these tools is critical for ensuring good acoustic quality. For example, Titanium has a low internal stress compared to steel, and so would be the favoured choice. However, steel possesses a good level of wear resistance. Other studies examine the resonance frequencies and vibration modes of exciting tools, based on analysis of different parameters such as shape, length and mass, as well as the slot length, slot width and the number of slots, which themselves can control mode shapes and frequency separation. Although previous studies have attempted to investigate these criteria in the design of ultrasonic tools, it is clear that there is still a general lack of understanding, as the research was conducted on designs without attaching any mass, which can significantly influence the resonance frequencies and system modes. In addition, the frequency separation has not received in-depth study or analysis, despite

the fact that it can affect the level of tool excitation and the tool gain. The stress in the ultrasonic tools is another critical criterion which has not previously received much attention. It is an important factor to consider, because the increase in stress can lead to the development of heat between connecting components, subsequently resulting in losses in the transfer power as heat dissipation, affecting the performance of the exciting tool. In the literature, most of the resonance frequency and mode shape studies on these tool designs are purely numerically-derived, and have not yet been precisely correlated with experimental modal analysis.

In this work, an integrated ultrasonic metal welding horn has been designed which is capable of joining thin metals. A catenoidal horn profile was selected as this can provide greater amplitude with lower stress. The horn with proper gain was attached to the transducer with an integrated welding tip specially designed for spot welding. A flange coupling was also attached to the body of the horn, showing zero displacement at the nodal plane during horn excitation. The FEM code Abaqus was used to identify the vibration characteristics of the horn, such as resonance frequency and vibration modes, to ensure that the horn is tuned longitudinally with a good separation of the excited mode from other non-tuned modes. Finally, numerical results were correlated with experimental modal analysis.

### **2.3 Research on solid-state bonding mechanisms**

Generally, USMW is considered as a solid-state bonding process in which the bond is viewed as the strongest of the welded specimens [52]. The welding process comprises simple mechanism of bonding, in which the surfaces to be welded slide in contact with each other under the effect of an applied compressive force. The influence of high ultrasonic shear vibration combined with the compressive force results in a bond due to the increase in both slip and plastic deformation. However, the forming area could be initiated not only by sliding and plastic deformation, but also by a break in the thin film at intimate surfaces. Other ways in which this forming area could be created are by work hardening, crack propagation, generation of heat by friction, re-crystallisation and diffusion [52, 53]. The USMW process is considered to be comparable to other welding processes such as friction welding and pressure welding, in which the solid-state bond can be generated by heating without fusion or by mechanical force alone, due to the intense plastic deformation at the welding zone. A solid-state bonding approach was described by Tylecote [54], which

summarised that the formation of a solid-state bond is dependent on the conditions at the intimate surfaces, such as the collapse of surface asperities, and the removal or dispersion of oxides [27]. Many studies explore the joint formation in USMW. These studies vary in terms of the explanations they offer regarding the morphology of the welding area relative to heating, friction, or diffusion welding. Due to the combination of normal and shear forces, the relative motion between intimate surfaces begins to remove and clean asperities, which creates microwelds at many points between the adjacent surfaces. From the increase in the shear and normal forces, the bonding area starts to increase through a spreading of the microwelds. The area of microwelds is reinforced and increased by a growing level of friction between intimate surfaces. Welds are complete when the power received by deforming area of intimate surfaces is sufficient. Chang and Frisch [55] studied the bonding mechanism for welding a sphere to a plate. The way in which the study was conducted was based on the oscillation of two contact surfaces of elastic spheres, developed by Mindlin. The experimental study of welding aluminium with copper predicts an expression for the coefficient of friction between contact surfaces. The study showed that the optimum welding condition can be achieved by maximising the slip area and resulting in high deformation at the area of contact surfaces. Heymann et al [56] used a spherical horn in a number of experiments to study the effect of surface preparation in the joining of samples prior to welding. They observed that a strong weld can be identified from using degreased samples. In addition, they noted that the level of adhesion of the horn to the sample increased with sample cleanliness. Harthorn [17] conducted a study on the comparison between USMW with high and low frequencies of ultrasonic (20 kHz) and subsonic (30 Hz) values for the welding of aluminium. After many trials, it was found that the nature of the welds remained unchanged, even after the trials were repeated. Also, it was indicated that the phenomena of diffusion and re-crystallisation do not play an important role when welding with a low frequency because the temperature does not exceed room temperature. Harthorn summarised that the interfacial layer in the ultrasonically welded metal is plastically deformed. Antonevich [53] referred to the basic principles of USMW. He studied the relationships between weld strength and process variables such as clamping force, weld time and tool velocity for a copper sphere welded to a copper plate. He showed that there is a minimum vibration between intimate surfaces is necessary for welding. Also, the author confirmed that the process revealed the frictional phenomena of galling and seizing under the influence of the clamping force. Neppiras [40] investigated an USMW technique for coupling shear vibration with specimens. The study

expanded the knowledge of joining metals by ultrasonic shear welding. Welds were produced under compression and tangential vibration. The study concluded that fretting and adhesion can occur within a micro-slip region, resulting in a rapid temperature rise. However, there is no possibility of melting at this point. Also, it was found by experiment that it can take only tenths of a second to produce a satisfactory weld. In addition, the weldability, which means the ability of metal to be welded, can be affected by pressure, which when a limit is exceeded, can result in a drop in the weld strength due to the fact that the higher load can reduce the vibration at the welding region. With the assumption that bonding using ultrasonics causes interatomic diffusion at the weld interface, Okada et al [57] presented work on mechanisms of USMW based on microscopic observation, x-ray diffraction, temperature measurement of joined specimens, and microanalysis by x-ray. The experimental work was performed using an ultrasonic spot welding machine to produce a weld, after which an examination of the temperature rise at the cross-section area of the bond using an alumel-chromel thermocouple. The result showed that the weld strength was influenced by the condition for the age-hardenable alloy. Another study on diffusion, was published by Hazlett et al[58], concluded that the mechanism of bond formation in USMW is by metallic adhesion, as the diffusion occurs due to a high level of mixing at the interface. However, this diffusion gradually decreases when the weld has relatively high bond strength. Prangnell and Bakavos [7] reported on the mechanism of joint formation using high power ultrasonic metal spot welding to join aluminium sheets. The investigation was performed using x-ray tomography and high resolution scanning electron microscopy, to characterise the stages of weld formation and microstructure evolution. The study concludes that high power ultrasonics is a promising, energy-efficient, alternative solid-state joining technique, but that strong welds can only be produced once a critical threshold welding energy is exceeded.

One conclusion which can be drawn from the literature is that the competence of USMW governs the quality of the resultant solid-state bond, which is generated by heating, friction, re-crystallisation and interatomic diffusion at the weld interface. A number of studies have shown that the level of adhesion at contact surfaces was dependent on sample cleanliness, where grease or contamination of the specimens can result in low weld strength, since a part of the ultrasonic power is consumed by the removal of surface impurities. It is clear that the effect of high ultrasonic shear vibration combined with the clamping force on the effectiveness of USMW has received less attention. Although a

number of specimen deformation studies have been performed using USMW, they have traditionally adopted the wedge-reed system, which requires a high clamping force with low amplitude. However, in the current work, the USMW has been used to study the relationships between process parameters such as clamping force and vibration amplitude, welding power and welding time, and metal parameters such as thickness, hardness and surface roughness, on a solid-state diffusion bond. In recent times, x-ray and scanning electron microscopy has been considered to be an efficient technique for investigating the mechanism of solid-state bonding, by analysing the deformation of joined surfaces. However, these techniques have been found to result in less attention being made to the weld mechanism. This study used optical observation and scanning electron microscopy to study the mechanism of solid-state bonding and compare the weld quality of metals under a variety of process and metal parameter conditions.

## **2.4 Process parameters in ultrasonic metal welding**

In order to review the current knowledge in the area of USMW, it is important to have an appreciation of the configurations of the lateral-drive system compared to the wedge-reed system, as the two configurations are different with respect to the application of clamping force and vibration amplitude. However, both welding configurations share the solid-state mechanism. Many studies have been performed using different welding conditions, and which have varied the control of different system parameters such as the clamping force, amplitude of vibration, welding time and ultrasonic power, as well as metal thickness and material surface conditions. These studies, in addition to those concerned with microwelding, were carried out in the joining of similar and dissimilar metals such as thin sheets, wires, foils and substrate layers.

In USMW, the relationships between process and metal parameters are complicated and not easy to control, because any change in the parameters can affect the strength and quality of the joining specimens. Derks [59] summarised a study on ultrasonic bond quality for wire deformation. The analysis of the bond quality was carried out for different magnitudes of vibration amplitude. Derks divided the parameters that influenced the bond quality into two groups, one called ‘machine parameters’, such as clamping force, vibration amplitude, time and temperature, and the other called ‘system parameters’, such as the ultrasonic horn, tool material, geometry and stiffness of the product clamping. It was concluded that the shifting of amplitude is strongly affected by not only the length of the

horn but also the impedance matching. Elangovan et al [60] performed a study on welding copper to copper using a USMW machine. The study is based on Taguchi's method for optimising process parameters such as welding pressure, welding time and vibration amplitude, in order to enhance weld strength. The analysis of variance was employed to study the influence of different process parameters on weld strength. The study concluded that the relationships between both weld pressure and amplitude, and also weld pressure and time, are more significant in order to properly predict weld strength than the relationship between weld time and amplitude. The author [61] developed an effective methodology to optimise the welding conditions and maximise joint strength. The study which was conducted was based on using a response surface methodology and a genetic algorithm in the welding of aluminium specimens. The authors inferred that the weld strength significantly decreases with an increase of pressure, because high pressure can reduce relative motion between surfaces and hence reduce the area of contact. Also, the vibration amplitude was increased and altered the weld strength. In general, an increase in amplitude means that there is a consequential increase in contact between surfaces. Moreover, the author used the Taguchi Method to optimise welding parameters for joining similar metals such as Al-Al, and also for dissimilar metals, such as welding copper to brass. The results of optimising ultrasonic parameters showed agreement in temperature and stress between FE modelling and experimental work of ultrasonic welding [62, 63].

Matsuoka [64] offered a description of an experimental study of the ultrasonic welding of metals. The experiments were conducted to join aluminium and copper together. The results summarised that the proper selection of process parameters, such as welding pressure, amplitude of vibration and welding duration, has to be made for every welding condition [65, 66]. Imai et al [67] reported on an experimental study on the optimisation of ultrasonic welding of an aluminium alloy onto three other aluminium alloys. In the study, a welding machine with 1200 W and a nominal frequency of 15 kHz was employed to produce the welds. The author investigated how oxide films and organic coatings can be separated from the bonding area by the influence of ultrasonic shear vibration. Another study was published by the authors [32], describing the welding of aluminium and copper alloys. The experiments were carried out using two different environmental conditions, where one was in air and the other underwater. The reason for selecting different environments was to investigate the joining of metals together and to study the solid-state bonding mechanism of the weld in different environments. The results showed that the

welding process underwater required more time and a large welding pressure compared to the welding process in air.

Kodama [68] presented a comparative study of the welding of softer metals such as aluminium, copper, brass and gold. The study investigated factors that influence the bonding, such as the coefficient of friction, frequency effects, specimen dimensions, surface roughness, contamination, the anvil which is used and the specimen overlap. The results of welding wires by ultrasonic means showed that the weld strength can be influenced by these factors. For example, the coefficient of friction can be influenced by joining thick plates, because slippage can occur between the spherical surface tool tip and the specimen which possibly incurs a detrimental effect on bonding. When welding a thin wire, the amplitude of vibration can be reduced by the increase of the frequency in order to achieve high strength for a small deformation. Long or wide specimens can also affect the weld strength, because the vibrations from the specimen propagate, and reflected waves return in anti-phase. It is also known that surface roughness and contaminations influence joint strength, as a proportion of ultrasonic power is consumed to remove impurities and asperities of the intimate surfaces prior to welding. Daniels [9] studied a number of variables which are involved in USMW such as pressure, power and time. A number of measurements were carried out on aluminium and copper to study the welding conditions. The author confirmed that both metal to metal and metal to non-metal welds can be made. The study showed that the thickness of the welded metal was found to be proportional to the electric power and clamping force required. Hulst [69] described the physical nature of ultrasonic welding and investigated the influence of the process on weld quality. The study analysed the process parameters such as vibration amplitude, clamping force and weld interval in relation to the weld strength. The results were extracted from the welding of 80  $\mu\text{m}$  copper wire. The authors depended on using the deformed width of the wire as a guide to weld quality. They concluded that the clamping force must be sufficiently high to prevent sliding between the horn and the upper specimen. Furthermore, selection of the clamping force is necessary to provide good contact between the specimens, and to ensure the transmission of ultrasonic energy sufficiently to the welded area. Watanabe et al [70] studied the welding of dissimilar metals, by investigating the welding of aluminium to copper and also aluminium to austenitic stainless steel. The purpose of the study was to analyse the effects of metal surface conditions such as hardness and surface roughness on the strength of the joined metals. They summarised that the surface roughness of harder

metals such as copper strongly affects the bond strength, by producing a weak joint compared with softer metals such as aluminium. Also, harder metal requires more energy to permit diffusion and allow for welding than softer metal.

The effectiveness of using insert metals for achieving stronger joints was investigated by Watanabe et al [71]. The study involved using an insert metal to join a mild steel sheet and an aluminium alloy sheet to enable the examination of joint strength and the study of the variability of welding parameters such as clamping force and welding time on weld strength. The results have indicated that excessive clamping force leads to a reduction of the frictional motion at the interface which then reduces the strength. However, excessive welding time can cause cracks to initiate in the welded specimens. Bloss and Graff [72] evaluated the weldability of advanced alloys such as stainless steel, titanium and nickel-based alloys. The experiments, which were carried out using a 3.6 kW commercial ultrasonic spot welder machine at 20 kHz, were conducted to study the welding energy versus tensile strength. The results emphasise that the weldability was significantly influenced by the yield strength and the hardness of the oxide layer, meaning that the Ti alloy exhibits excellent joinability for ultrasonic welding due to its thin oxide layer which is easily removed by ultrasonic oscillations, whilst nickel-based alloys were found to be more difficult to weld due to the hard oxide layer, which requires more energy to remove.

Wright et al [73] studied the effects of thickness on combinations of aluminium sheets with thicknesses varying from 1.2 mm to 2.5 mm. The authors explained that no variation in weld strength can be observed by placing the thicker specimen near to the side of the welding tip, and the process parameter setting has proven to be much more significant in determining the strength of the weld. Their study was carried out using a wedge-reed welding machine. Annoni and Carboni [74] described their experimental study of the performance of high power USMW used to examine weld strength. A 3.0 kW lateral-drive welding machine was employed to join together 1.2 mm-thick aluminium AA 6022-T4 specimens. A study of the tensile-shear strengths of spot welded lap joints was carried out to provide statistical analysis of welding formations. The results indicated that a high weld strength can be obtained using a high vibration horn amplitude. However, it was found that other process parameters such as clamping force and time have a low influence on weld strength. Studies of the ultrasonic welding of dissimilar metals were presented by Zhu et al [75]. The welds were produced from joining a 6061 aluminium alloy sheet to a Ti6Al4V

titanium sheet. The investigation analysed the mechanical properties and the diffusion of welded sheets, and also the weldability between dissimilar sheets for various welding pressures and welding times, where diffusion at the weld interface was observed. Kim et al [76] conducted a study of the problems of weld quality which arise from the use of conventional welding methods. The investigation was carried out using ultrasonic metal spot welding for joining copper to nickel plated copper sheets. The load and failure type of the T-peel test were examined, for which the tests were conducted using a factorial experimental design according to the varying welding pressures and times. A tensile machine was used to evaluate the quality of the bond and identify the weldability of the peeled tests. The results were used to determine both optimal process parameters and the weld quality range for the T-peel test.

An approach recently developed in USMW to increase the weld strength and combat a number of common issues in the field, such as tool/specimen adhesion and specimen marking, is called amplitude stepping or amplitude profiling. Baboi and Grewell [77] demonstrated the use of amplitude stepping in the ultrasonic welding of aluminium. Amplitude profiling welding begins with the setting of the higher amplitude value, where the weld interface requires higher velocities for surface scrubbing to be effective, thereby creating a solid-state weld at the intimate specimen surfaces. The amplitude is then dropped to a lower point, to reduce frictional heating and softening of the specimen, reducing shear as the weld forms and thus minimising damage. A series of experiments were carried out to improve welding strength using the stepped amplitude approach, the results of which were then compared with a constant amplitude result. It was observed that high strength can be produced by the stepped amplitude method, because when the metal begins to soften at the first stage, a reduction in the amplitude is required to enhance the strength and reduce the tool/specimen adhesion as well as specimen marking. However, the authors performed another study that used buffer sheets to reduce the sticking of specimens with the welding tool and minimise specimen marks. The experiments showed that placing buffer sheets of zinc or copper between the horn tip surface and the upper surface prior to the ultrasonic welding of aluminium can help to reduce sticking and marking with a slight increase in strength [78]. It should be mentioned that there is a significant difference between the welding of metal plates and welding wires. In the case of welding plates, the weld takes place depending on the internal or sublayer deformation due to the interface sliding, whereas when bonding a wire to a substrate, no relative motion can be observed

between them, resulting in less internal deformation at the contact area [58, 79]. Thus, a lower heat generation is located at the interface and the wire is squeezed over the substrate with a significant amount of deformation. Most details of bonding wires are described by Joshi [28].

In conclusion, the above results show that the studies on process and metal parameters in USMW are different and dependent on the drive system used, being either wedge-reed or lateral drive, in applying normal and oscillatory forces. It was seen that a large proportion of the literature focuses on the relationship between process parameters such as clamping force, vibration amplitude, welding time and welding power, and metal parameters such as thickness, hardness and surface roughness. A large number of these studies examine the weld strength by considering either one or two parameters as constant, for example welding force and vibration amplitude. However, a suitable result could be obtained by studying the weld strength and weld quality under a variety of clamping forces and vibration amplitudes. A number of studies were carried out on joining similar and dissimilar metals by USMW. They showed that the metal parameters can influence the weld strength and weld quality. For example, an increase in hardness and surface roughness can affect the bonding strength, but the majority of these investigations did not consider the influence of specimen thicknesses on weld strength to any great extent. Furthermore, other studies suggest that the sheet thickness has no effect on the resultant weld strength, especially when the upper specimen is in contact with the welding tip, whereas weld strength can be significantly affected by a relationship between process parameters. A study involving different metal thicknesses could provide a better indication of the effect of a change of weld strength and weld quality in relation to the process parameters. The current work reported in this thesis was performed using a stepped amplitude, which is a process parameter which can be used to improve weld strength and weld quality, to join similar and dissimilar metals of a variety of thicknesses. The application of a stepped-amplitude has been previously confined to only a small number of studies which were performed on the welding of identical aluminium specimens.

## **2.5 Theory of USMW without melt or fusion**

Ultrasonic metal welding is one of the most popular welding techniques, and depends on a form of solid-state bonding. The nature of the solid-state can be characterised in three stages, based on a brief study by Wodara [80]. The first stage of solid-state begins with the

applied normal force which removes any asperities and brings the surfaces of the specimens to be joined into close contact. A number of reviews focus on the nature of the metallic contact at the joint interface under the influence of an applied force, where most specimens are still covered by impurities, oxide layers or voids that are dispersed after the creation of plastic deformation. The nature of the van der Waals force transition between close contact surfaces is identical when joining similar metals, because there is no difference in hardness. Conversely, there is often difficulty with contact encountered at the joining surfaces when bonding dissimilar metals due to the hardness at the facing surfaces having a different value, resulting in the deformation being higher for softer metals than harder metals. Thus, metallic contact can take place by electron exchange at intimate surfaces. In the second stage of solid-state bonding, chemical or dislocation action takes place, by activated atoms on joint surfaces [5]. De Vries showed that the chemical bonds start to form at a distance of 4 to 5 Å between metal atoms of the joined surfaces. After intermetallic bonding takes place, the third stage of solid-state bonding is followed by a joint formation between specimens at the welding region. At the interface, grains are destroyed by the effects of plastic deformation, whilst the effect of elastic deformation exists and leads to a relaxation in the residual stresses, of which the latter is altered by an increase in temperature. However, the ultrasonic vibrations raise the values of these stresses. The reason for the observed relaxation is related to the change in the atomic structure of the metal involved in the process, and in addition to the relaxation, recrystallisation and diffusion also occur. The diffusion process results in an increase in strength of the joint formation, although it has little effect on the deformation area between intimate surfaces because of the short welding cycle [28, 29].

## **2.6 Temperature effects on the mechanisms of USMW**

In USMW, solid-state bonding can take place as a result of heat generation, where temperature is raised locally by the influence of friction and plastic deformation. As a result of the supply of high shear vibration between the interfaces of the specimens, the temperature starts to rise at the initial stage of the welding process, which can then stay constant or even drop, depending on the ultrasonic parameters and metal properties. In USMW systems, the temperature released from the deformation area is low relative to the melting temperature of the base metal, for which the maximum welding temperature can vary from 30-50 % of the absolute melting temperature of the base metal [81]. Other studies suggest that the temperature produced as a result of the USMW process can vary

between 60-80 % of the base metal [28]. Most studies that involve measuring temperature in USMW use thermocouples or an infrared camera to record the temperature. It is noticed that the temperature increase in the welding area is dependent on the ultrasonic energy that is delivered to the weld zone. Melting and fusion are required in plastic welding, but they are not in metal welding. For that reason the temperature factor was excluded from this study.

## **2.7 System parameters**

There are many parameters that can influence the behaviour and operation of USMW systems, such as ultrasonic frequency, amplitude of vibration, clamping force, welding power, ultrasonic energy, and welding time. These parameters can be classified as process parameters. There are other parameters relating to the nature of metal to be welded, which can be classified as metal parameters. They include sample cleanliness from oxides and contaminants, hardness, surface roughness, specimen dimensions, and the effects of the tool fixtures. A brief discussion of the system parameters is important in this study, as the relationships between them can affect the nature of the weld strength and weld quality. Ensuring and maintaining a high level of control of these parameters and variables remains a major challenge for industry and manufacturing.

### **2.7.1 Ultrasonic frequency**

In ultrasonic systems, the transducer is designed so that it is tuned at a specific frequency. Most ultrasonic welding equipment uses frequencies in the range of 15 to 300 kHz. In metal welding systems, the frequency range is between 20 to 40 kHz. The most common frequency is 20 kHz [14], as used in this work. In other welding systems, such as in microwelds, the frequency can be a much higher value, such as 60 to 120 kHz [27]. The generator is the device that can control the frequency of oscillation, which remains constant during welding. The dimensions and types of the metals used in an ultrasonic assembly are selected to enable the system to be tuned at the operating frequency. However, any changes in the welding system might lead to a shift in frequency, for example due to system heating, variation in clamping force, or wear effects on tools. These variations can also significantly affect the vibration amplitude of the exciting tool. Taking these variations into account, systems must then compensate to allow welding to be performed at the operating frequency. In fact, there is a noticeable difference in the operating frequency for different ultrasonic welding systems. In a wedge-reed system, the

power is directly transmitted to the reed and cannot be directly monitored by the transducer. Whilst in a lateral-drive, the system allows accurate control of parameters at the weld zone. From a practical perspective, modern power controllers with automatic integrated feedback circuitry are more effective in compensating for the shifting of the frequency and operate by tracking the driving frequency of the transducer to keep the system in a resonant state [27, 82]. From the review of these different welding systems and configurations, it was judged that to allow accurate control of welding parameters, a lateral-drive system would be more reliable compared to a wedge-reed system. Also, because this study discusses the welding of thin metals, it was decided that a lateral-drive system configuration should be adopted for ultrasonic metal spot welding.

### **2.7.2 Vibration amplitude**

In this study, vibration amplitude is considered to be one of the most significant parameters which can influence the strength and quality of a weld. It is related to the power of the system. In ultrasonic tools, the amplitude describes the amount of axial expansion and contraction of excitation [83], and is characterised by small vibrations in the order of 10-50  $\mu\text{m}$  peak-to-peak at the weld [1]. In the lateral-drive system, the operator can control the value of amplitude by increasing or decreasing it through the modification of the current passing through the transducer. For example, the system can be set to any specific value of amplitude which results in the supply of the correct amount of power. The condition is different in wedge-reed systems, as the operator cannot control the amplitude, because the transmission of the ultrasonic oscillation occurs at the reed. In addition, the wedge-reed system usually requires low amplitudes to allow high energy transferral to the welding zone. Therefore, low amplitude is recommended in wedge-reed systems due to the requirement of high force [29, 72]. In this work, the amplitude range was to be varied from 17  $\mu\text{m}$  up to 42  $\mu\text{m}$ , according to the specification of used ultrasonic generator.

### **2.7.3 Clamping force**

Clamping force, or static normal load, is other system parameter of USMW. The effect of clamping force is important in a solid-state bonding mechanism [28]. In USMW systems, the force is usually applied by pneumatic or hydraulic systems which are confined between the horn tip and the fixed anvil. The required magnitude of the force is strongly dependent on the type of metals used, thicknesses of the specimens to be joined and the weld area. In USMW, the range of applied clamping force is from several tens of Newtons to thousands

of Newtons [1]. The lateral-drive system requires a low clamping force with high amplitude to produce the weld, whilst high force with low amplitude is recommended in a wedge-reed system [29]. Care must be taken when selecting the force value, because excessive force can cause sample deformation and the dissipation of more energy, however insufficient force can lead to slip of the horn tip over the contact surface or sticking occurring between the horn and the upper specimen. This can result in an increase in the temperature of the weld and can occasionally cause damage to the horn. In this work, the force was specified to address the requirements of joining thin metals and reach values up to 1 kN.

#### **2.7.4 Power, energy, & time**

Power, energy, and time are listed as separate system parameters; a mode of ‘weld to energy’ is often used to control weld quality by compensating for the variation of joining specimens [84]. For each weld cycle, these parameters are firmly related to each other [1]. When starting the welding process, the electrical power is transferred across the transducer to the welding specimens. This occurs during the welding cycle. The relationship between the power supply and welding time varies and can be affected by the type of metal to be welded, the geometry, and the surface finish. Also, the power can be influenced due to changes in vibration amplitude and clamping force. Figure 2-1 illustrates the basic power curve which is a common characteristic during USMW. The area under the power curve is the energy delivered during the welding time [27].

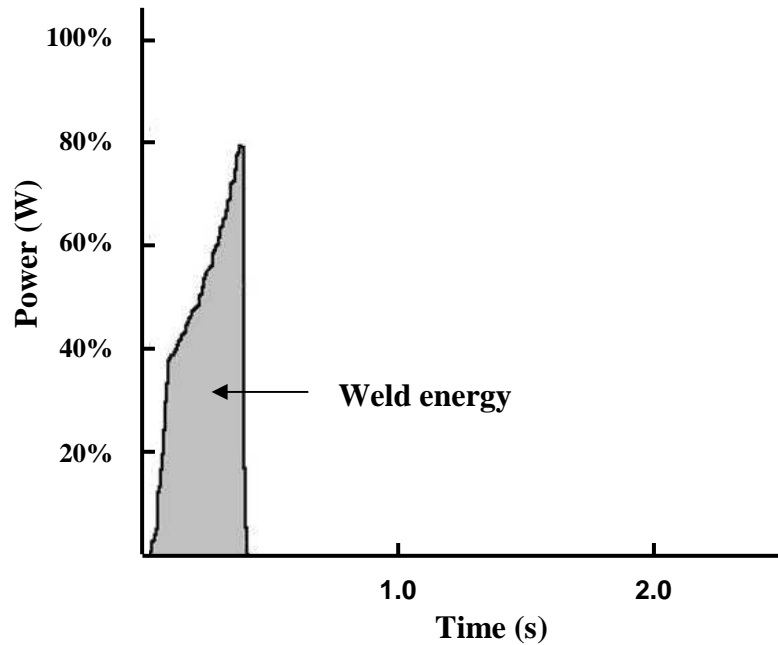


Figure 2-1 Power vs. weld time for the ultrasonic welding [27]

Generally, USMW systems require a minimum amount of electrical power to maintain the motion (vibration) of the welding stack at a zero-loading condition. The value of power is directly proportional to the mechanical load [84]. Therefore, an increase in pressure and maintenance of other parameters can increase the mechanical load or force applied in the welding process. This subsequently raises the power level. Therefore, less time is required to deliver the same amount of energy, as shown in Figure 2-2.

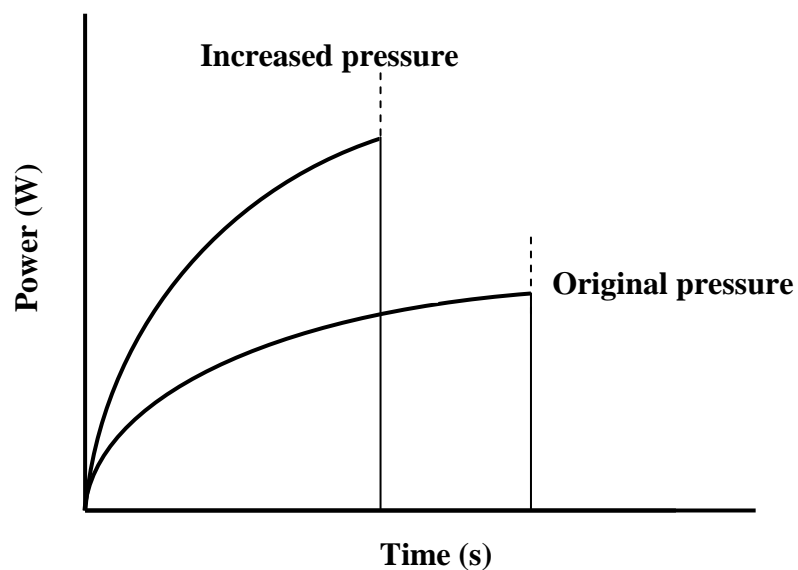


Figure 2-2 Pressure variables [84]

Some of the modern USMW systems utilise closed-loop feedback to allow for monitoring time during the motion of the welding stack. Therefore, the welding cycle is completed when the process reaches the desired level of energy. In most USMW systems, there is evidence that the setting of power, energy and time as independent is not reliable. Thus, a better approach would be to set just one of them to reach the level of the weld, and leave the others dependent. Many factors can affect the actual power that is delivered to the welding zone, such as the electrical-mechanical conversion characteristics of the piezoelectric material, the interface losses in transducer-horn systems, the amount of power dissipated by ultrasonic tools and material assembly [1]. Welding time is usually determined from levels of both welding power and energy, and can be represented as a dependent or independent variable according to the system used. Ultrasonic welding is unique in that the process is complete within approximately one second or sometimes less. However, welding time can exceed one second in some cases relative to the specification of the weld specimen, but this can create problems such as poor surface appearance, internal heating, and internal cracks [6]. Typical ultrasonic welds can be obtained by joining softer metals such as aluminium and copper alloy sheets, with a time-duration of up to one second.

### **2.7.5 Materials**

USMW allows similar and dissimilar metals to be joined. The key considerations of the metals that are used in USMW are Young's modulus, hardness, and yield strength [1]. The welding of metals is now becoming one of the common applications of power ultrasonics [27]. Dukane company published a weldability chart used for metals and their alloys in USMW [85], as shown in Figure 2-3. The chart classifies the metals and their alloys into three categories: high-quality welds with symbols of a circular shape, medium-quality welds with symbols of a triangle shape, whereas the space indicates either not suitable for welding or have not yet been identified from the weldability. The chart information depends on data from a variety of different experiments, and sources.

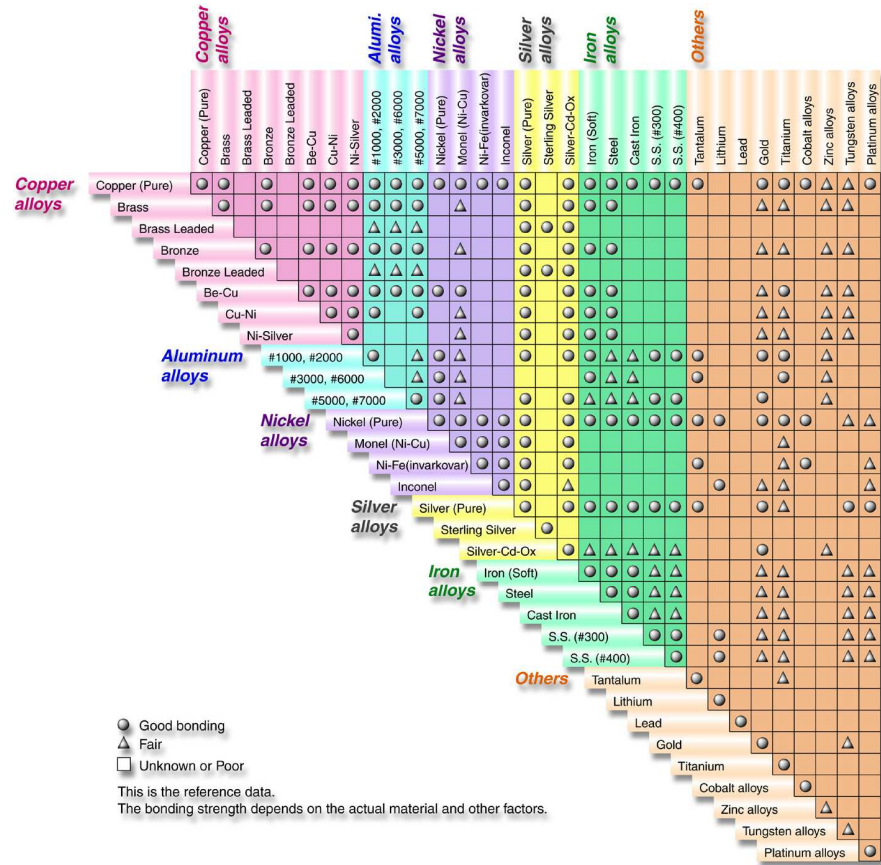


Figure 2-3 Weldability of USMW chart [84]

### 2.7.6 Specimen geometry

The shape and dimensions of the specimens that are used in USMW is also important and can affect the strength and quality of the weld. Thickness is considered as the dominant factor, which means that thinner specimens can be welded with a lower power compared to thicker specimens, on the condition that the duration of the welding cycle is constant. Furthermore, if the specimen placed on top near to the welding tip is relatively thick, then more power and high clamping force are required. In USMW systems, particularly spot welding, the specimens are placed in an overlapped shape parallel to the direction of vibration [1, 14, 27]. In this work, the geometry of used specimens was selected relative to the dimension of horn tip.

### 2.7.7 Tooling

Tooling can be defined as the components of the ultrasonic system that consist of the welding horn, in particular the horn tip that makes contact with the upper specimen, and

the stationary anvil that holds the lower specimen. Power transmission and static forces applied to the welded specimens are usually passed through tooling. The tools must be sufficiently strong in order to transmit the required level of power and force through multiple welding cycles. High-quality welding results in part from tooling with high hardness to avoid deformation and high toughness to prevent fractures [27]. In USMW systems, the amount of heat generated in the tooling is low compared to the melting temperature of the base metal. The deformation area also does not melt, however the weld can 'glow' and may be red-hot during the welding cycle when the joining of high strength metals is being undertaken [27]. This glow in the weld is unacceptable and may increase the likelihood of the welding tools sticking to the specimens being welded, and can leave an undesirable mark on the specimen surface. Most ultrasonic welding systems use a detachable horn tip, and replaceable or stationary anvils. However in other systems, the tools are machined as integrated components with knurled flat surfaces to avoid slippage and increased roughness for improving grip during the welding process. However, welding tips can take different surface profiles such as rounded, spherical or convex curvature to alter the stress pattern [1, 14]. In this work, the horn tip surface has machined knurled flat.

## **2.8 Weldability**

The weldability, also known as joinability[86], is defined as the ability of the metal to be welded. Another definition of weldability is based on the American Welding Society, AWS, [6], which defines weldability as "the capacity of a metal or combination of metals to be welded under fabrication conditions into a specific, suitably designed structure, and to perform satisfactorily in the intended service." Over the years, most metals and their combinations have been investigated for their ultrasonic weldability and are classified in the weldability chart shown in Figure 2-3. The weldability is used as a criterion to determine the suitability of the welding process and can be used to compare weld quality between metals. However, it cannot be determined if the metal to be welded is suitable for intended service. Good weldability of the metal means that it is easy to meet the requirements of the welding process. Most standards define the weldability qualitatively, comprising the metallurgical compatibility of the metal or alloy with the specific welding process to be used and the ability to weld with metals. This is in agreement with the opinion of Bloss, who evaluates the weldability using welding standards and testing procedures, such as the production of sound welds with tensile strengths close to the base metal, the improvement and identification of repeatable welding under similar welding

conditions, and the use of the same setting of the welding tools to obtain a high-quality weld without leaving any excessive indication of tool sticking or wear [27]. Finally, a weld with a crack-free deformed area can be attributed to good weldability [16].

## 2.9 Summary

The use of the superimposed ultrasonic technique in the metal welding process was invented over 60 years ago. Since then, the improvements and developments made to ultrasonic tools have been widespread due to the increase in the demand for USMW. Many studies and research reports focus on the fact that welding horns provide more than one function, such as the transfer and delivery of energy to the welding area, and also the clamping of the upper specimen during the welding process. These studies utilise different shapes and profiles depending on the type of welding application, and the literature typically focuses only on the investigation of the resonance frequency and vibration amplitude at the horn working surface, whilst other criteria such as modal frequency separation, amplitude uniformity of horn working surface, stress and also gain factor have received less attention. Therefore, a study of horn design criteria is provided in this thesis, and addresses issues which have not been dealt with in depth in the literature, such as the addition of mass to the horn, in the form of an integrated horn tip and flange coupling, which will result in a shift of resonance frequency, an influence on the vibration modes, a reduction of amplitude and a lower gain.

The most significant finding from the study of USMW was that to enhance weld strength and improve weld quality, the accurate design of welding components, the transfer of high ultrasonic energy with low dissipation to the specimens being welded, ensuring proper relations between process and metal parameters, and sufficient capacity of ultrasonic generator are required. It has been shown in this chapter that although many studies in the literature do attempt to explain the influence of process parameters such as clamping force, amplitude of vibration, welding time and welding power on the tensile shear strength of welded specimens, they are normally only concerned with the welding of wires or foils, which is significantly different from welding sheet metal. The studies in the literature have claimed that the strength of the weld is significantly affected by the increase or decrease of the magnitudes of certain process parameters. However, most of these studies analyse welds of constant thickness, with very little evidence provided on the variation of welding strength with different thicknesses, especially when the thickness of the upper specimen in

contact with the horn tip is increased. In addition, the proportion of ultrasonic energy that is delivered to the welding horn has also received less attention, because the effect of metal parameters such as hardness or surface roughness have not been accurately investigated in the literature. Studies of the influence of vibration amplitude on weld strength have been conducted in the literature, however most are dependent on the use of stepped amplitude to enhance the strength and quality of the welds, through the setting of different amplitudes of the horn, and are also reliant on relationships between other ultrasonic and metal parameters. All of this influences the weldability of joints, and can eventually lead to the creation of cracks. For that reason, a few studies have focused on using stepped amplitudes to enhance the weld strength and reduce the sticking of specimens, but these studies have not validated the influence of the stepped amplitude on the weldability of the metals, as the method is restricted to the joining of aluminium with constant thickness. The present study benefits from the stepped amplitude to enhance the strength of the joints by conducting experiments using different thicknesses of similar and dissimilar metals. Additionally, it is not possible to compare directly the results reported in the literature, since many of those sets of results were obtained using different welding machines, such as wedge-reed, lateral-drive or magnetostrictive transducer-based machines instead of piezoelectric transducer-based systems. The literature studies also used different metals or different specimen dimensions. In this thesis, a parameterised approach is taken to the study of USMW to allow the influence of parameters on weld strength and quality to be directly compared.

## **2.10 Aims and Objectives**

The aims of this study are the design, characterisation and manufacture of an integrated lateral-drive ultrasonic metal spot welding system, which is capable of joining thin metals. The system is created to overcome many of the issues encountered in previous studies, which have normally depended on using commercial welding machines, and to study many of the criteria that reduced the efficiency of transferring ultrasonic energy to the welding area. The present work has many objectives concerned with controlling process parameters, and allows for the studying of weld strength and weld quality of joined metals, and for study of the relationships between process parameters through focusing on the clamping force, amplitude of vibration, welding power and welding time, and examining the weldability under different metal conditions and for variable specimen thicknesses. A further objective is to enhance the joinability between metals through improved weld strength and increase in consistency of the weld, as well as the ability to reduce specimen

adhesion to the welding horn tip and specimens marking. Finally, the main objective of the study is to provide a foundation for an effective tool design to enable a high level of performance which can result in the successful welding together of thin metals.

## Chapter 3

### Design of ultrasonic spot welding devices

#### 3.1 Introduction

In recent years, there has been an increasing focus on the design, testing, and characterisation of USMW components. FE software is now able to solve complex problems in less time and consequently with less expense. In this chapter, the design and characterisation of spot welding components and fixtures will be discussed. The aim of this work is to show how the welding components can be properly designed, accurately manufactured, tested and corrected in order to be able to achieve satisfactory ultrasonic energy, used effectively to improve welding. Therefore, it is desirable to give a brief description of each part of the welding component assembly, called the welding stack, which will be used in the USMW system. The design of the mounting holder, their fixing parts and the stationary anvil are also discussed. Finite element analysis (FEA) has also been adopted in order to allow a comparison with experimental modal analysis (EMA) to be made, in order to improve the performance of welding devices.

#### 3.2 Design of ultrasonic devices

Industry more commonly utilises high power ultrasonics in their manufacturing processes and tools are normally required to be tuned to a specific operating frequency. The derivation of the general equation of motion of a simplified component is the first step in developing an FE model.

##### 3.2.1 Equation of rod in longitudinal vibration

When a uniform slender rod is excited along the length axis, longitudinal vibration occurs. Therefore, a straight rod with a length  $l$  and a cross-section area  $S$ , has a longitudinal displacement given by  $u$ . The basic assumptions are that the rod is isotropic, uniform and in a free-free boundary condition. The governing equation of the rod can be derived by considering that  $x$  refers to a point location along the section of the rod and  $t$  is the time, whilst the rod has a small element  $dx$ , which is subjected to an applied force  $F$ , a

displacement  $u$  and a change in displacement  $u + \frac{\partial u}{\partial x} dx$ . The length of the element  $dx$  is increased to  $\frac{\partial u}{\partial x} dx$  and the strain in the material of the elongated element is  $\frac{\partial u}{\partial x}$  as shown in Figure 3-1.

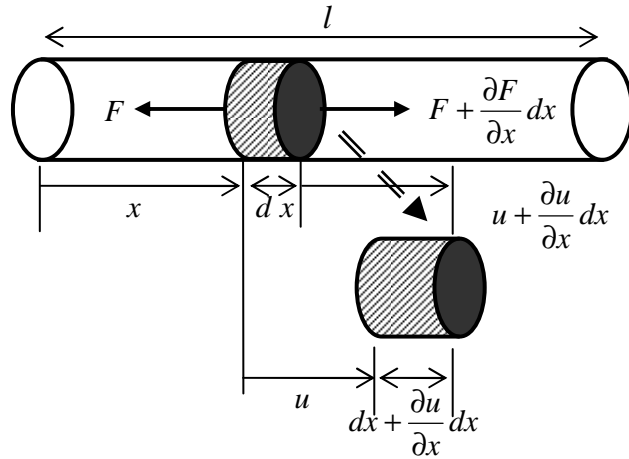


Figure 3-1 Model of a longitudinal bar

For an elastic material, we know that  $\sigma = E \varepsilon$ , where the  $\sigma$  is the stress in the element,  $\varepsilon$  is the strain and  $E$  is the Young's modulus. The strain  $\varepsilon$  can be given by:

$$\varepsilon = \frac{u + \frac{\partial u}{\partial x} dx - u}{dx} = \frac{\partial u}{\partial x} = \frac{F}{ES} \quad (3.1)$$

where  $S$  is the cross-sectional area, and  $F$  is the applied force.

By applying Newton's second law to the equilibrium condition of force on a rod towards longitudinal displacement  $u$ , the equation of motion becomes:-

$$\sum F = m \frac{\partial^2 u}{\partial t^2} \quad \text{where } \frac{\partial^2 u}{\partial t^2} \text{ is the acceleration} \quad (3.2)$$

$$F = \sigma S = ES \frac{\partial u}{\partial x} \quad (3.3)$$

$$F + \frac{\partial F}{\partial x} dx - F = \rho S dx \frac{\partial^2 u}{\partial t^2} \quad (3.4)$$

Where  $\rho$  is the density.

Substitution Equation (3.4) in Equation (3.1):

$$ES \frac{\partial^2 u}{\partial x^2} = \rho S dx \frac{\partial^2 u}{\partial t^2} \quad (3.5)$$

$$E \left( \frac{\partial^2 u}{\partial x^2} \right) = \rho \frac{\partial^2 u}{\partial t^2} \quad (3.6)$$

The equation can be rewritten as follows:-

Or:

$$c^2 \frac{\partial^2 u}{\partial x^2} = \frac{\partial^2 u}{\partial t^2} \quad (3.7)$$

where  $c = \sqrt{\frac{E}{\rho}}$  and is the velocity of the stress wave in the rod. The one-dimensional propagation of the longitudinal elastic wave in the rod can be analysed by the equation (3.7), which is usually called the wave equation. The solving of partial differential equations (3.7) can be performed by separation of variables as shown below:

$$u(x, t) = U(x)Y(t) \quad (3.8)$$

Substituting (3.8) in (3.7):

$$\frac{1}{U} \frac{d^2 U}{dx^2} = \frac{1}{c^2} \frac{1}{Y} \frac{d^2 Y}{dt^2} \quad (3.9)$$

In Equation (3.9) the left hand side is independent of  $x$  whereas the right hand side is independent of  $t$ . The derivation can then be simplified further:

$$\frac{d^2 U}{dx^2} + \left( \frac{\omega}{c} \right)^2 U = 0 \quad (3.10)$$

$$\frac{d^2 Y}{dt^2} + (\omega)^2 Y = 0 \quad (3.11)$$

The general solution can take the form:

$$U(x) = A \sin \frac{\omega}{c} x + B \cos \frac{\omega}{c} x \quad \text{and} \quad Y(t) = C \sin \omega t + D \cos \omega t \quad (3.12)$$

$A, B, C$  and  $D$ , are the constants of the Equation (3.12). The general solution becomes:

$$u(x, t) = \left( A \sin \frac{\omega}{c} x + B \cos \frac{\omega}{c} x \right) (C \sin \omega t + D \cos \omega t) \quad (3.13)$$

From this, and on the assumption that the rod is free-free, the natural frequency is found to be:

$$f_n = \frac{n}{2l} \sqrt{\frac{E}{\rho}} \quad (3.14)$$

Where  $n$  is the mode order and  $l$  is the tuned length. It can be seen from Equation (3.14) that the length and the material properties  $E$  and  $\rho$  are the properties on which the natural frequency is dependent.

### 3.2.2 Analysis of the non-uniform geometry of the horn

In ultrasonic welding, different horns can give different vibration amplitudes, depending on the non-uniformity of the horn design which boosts the vibration amplitude supplied by the transducer. The shape and style of the welding horn can be designed to satisfy a range of applications and process requirements. Modifying the cross-sectional area between the input and output surfaces of the horn leads to a change in vibration amplitude depending on the nature of the alteration. This ratio in vibration amplitude between the horn surfaces is referred to as gain. Horns can have many different profiles, such as uniform, conical, exponential, catenoidal and stepped. The gain of the horn is calculated from the profile [87], and some different horn gain profiles are shown in Figure 3-2.

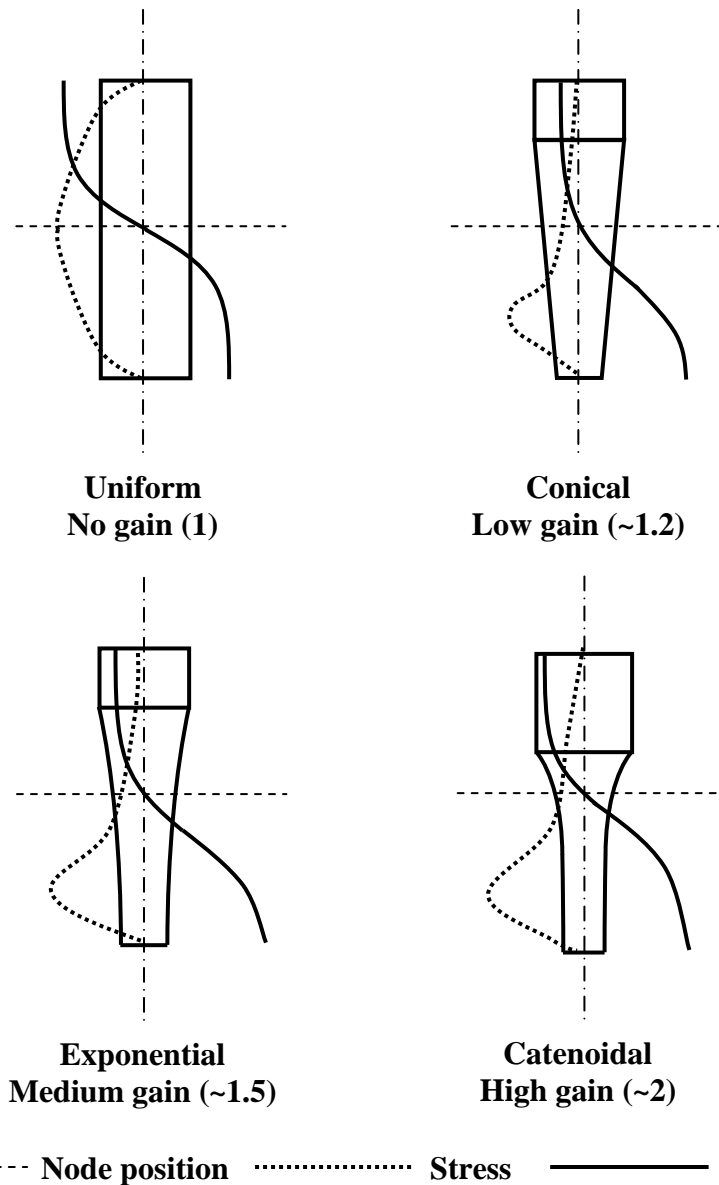


Figure 3-2 Different horn profiles, illustrating node positions, stress distributions and vibrational amplitudes [88]

To understand the difference between the horn profiles shown in Figure 3-2, it is necessary to derive their equations, starting from the concept of longitudinal vibration theory derived by Merkulov [88]. An axisymmetric profile is used to analyse the equations of horn profiles, starting from the assumption that the stress waves remain in plane and that the non-uniform cross-section of the profile produces amplitude gain towards the smaller face [25]. The horn profile is shown in Figure 3-3.

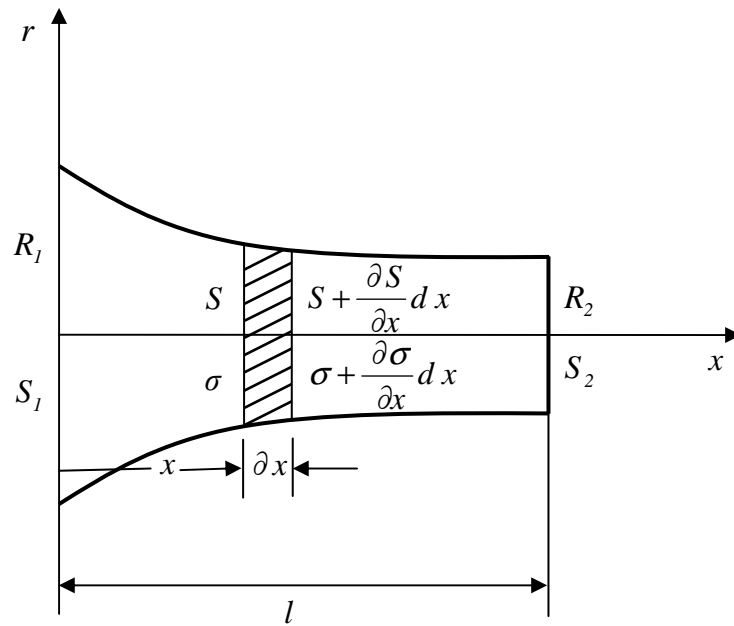


Figure 3-3 Axisymmetric horn profile depicting stress distribution

On the assumption that the lateral out-of-plane stresses are considered negligible, the equation of motion for a small element of the axisymmetric profile with input cross-section area  $S_1$  and radius  $R_1$ , and output cross-section area  $S_2$  and radius  $R_2$ , can be determined through the application of Newton's second law.

$$\sum F = m \frac{\partial^2 u}{\partial t^2} \quad (3.15)$$

where  $F$  is the force,  $m$  the mass and  $\frac{\partial^2 u}{\partial t^2}$  is the acceleration. The equation of the horn element can be expressed as shown in Equation (3.16):

$$\left( S + \frac{\partial S}{\partial x} dx \right) dx + \left( S - \left( S + \frac{\partial S}{\partial x} dx \right) \right) dx = S dx \quad (3.16)$$

Stress is defined as  $\sigma = \frac{F}{S} \Rightarrow F = \sigma S$  where  $\sigma$  is the stress in the bar,  $F$  is the force and  $S$  is the cross-sectional area. Simplifying Equation (3.16) gives

$$\sigma S + \frac{\partial S}{\partial x} \sigma dx + \frac{\partial \sigma}{\partial x} S dx - \sigma S = 0 \quad (3.17)$$

Substituting Equation (3.16) and Equation (3.17) in Newton's law gives the equation of motion of the tapered bar as described by Merkulov [89], as:

$$\rho S \partial x \frac{\partial^2 u}{\partial t^2} = \frac{\partial \sigma}{\partial x} S dx + \frac{\partial S}{\partial x} \sigma dx \quad (3.18)$$

The following equations of motion were derived by Merkulov [38] who obtained the resonant length for several horn profiles, shown in Figure 3-2. The corresponding equations to calculate the resonant length,  $l$ , of these horn profiles are shown below.

$$l = \frac{\lambda (k_l)}{2 \pi} \quad (3.19)$$

For a conical profile

Where,  $k = \frac{\omega}{c}$  and  $(k_l)$  are equation roots.

For an exponential profile

$$l = \frac{\lambda}{2} \sqrt{\frac{(n\pi)^2 + \ln^2\left(\frac{R_1}{R_2}\right)}{\pi^2}} \quad (3.20)$$

Where,  $n = 1, 2, 3, \dots$  and  $\lambda = \frac{c}{f}$ .

For an catenoidal profile

$$l = \frac{\lambda}{2} \sqrt{\frac{\left(\sqrt{k^2 - \gamma^2}\right)^2 + \left(\cos^{-1}\left(\frac{R_1}{R_2}\right)\right)^2}{\pi^2}} \quad (3.21)$$

where  $\gamma = \frac{1}{l} \cos^{-1} \frac{R_1}{R_2}$ , selecting which horn profile to use normally depends on the application and vibration amplitude requirement, and is a compromise between the

component integrity and the gain [25]. From all horn profiles shown in Figure 3-2, the catenoidal horns can offer high gain compared with the other horn profiles such as conical and exponential horns [90]. Although high amplification can be obtained from the horn, stress can be responsible for inducing fatigue failure [91]. FE analysis has become suitable method of dealing with the design and modelling of ultrasonic components.

### **3.3 Finite element analysis (FEA)**

Finite element analysis (FEA) is one of several numerical methods that can be used to provide solutions for most complex problems. Ultrasonic technology is a field that has benefitted from using FEA to determine the vibrational characteristics of the modelled tools and their assemblies prior to work [90]. FEM has been developed with high precision, and consist of a computer model of structure or design that is analysed for specific results. The FEM works on modelling the structure using a mesh of elements connected together using nodes. The structure have elements with either simple or complex material properties and loading conditions can be simulated on the nodes or elements of the mesh and a verify of analytical results can be determined depending on the type of analysis requested by the user [92]. In FEM, a variety of mesh techniques exist to mesh models of different topology. In this study, the meshing technique is free meshing which are used to simplify complex profile shapes and allow the FE software to generate a high quality mesh. The FEA software Abaqus [93] has been adopted for all simulations. A mesh convergence study was conducted to develop a reliable and accurate FE model. The modal frequencies were extracted for different mesh densities, and a combination of static and dynamic loading was used to calculate the natural frequencies and mode shapes. In general, ultrasonic tools such as horn employ one mode of vibration which can be bending (F), torsional (T) or longitudinal (L) mode as shown in Figure 3-4, were extracted from FE simulation of rod with a uniform cross-section area. The FEA shows an accurate prediction of the longitudinal mode frequency that occurs at 20 kHz, proving that Equation (3.14) can be effectively applied to provide a good estimation for the tuned length.

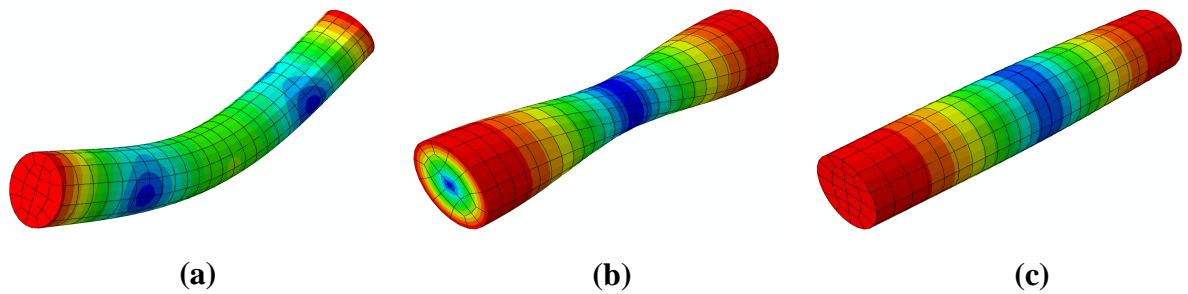


Figure 3-4 Mode shape classification with contour of displacement for (a) 1<sup>st</sup> Bending (b) 1<sup>st</sup> torsional and (c) 1<sup>st</sup> longitudinal modes of vibration of a rod

In Abaqus, the vibrational analysis of the system can be performed in two steps. The frequency step is first applied to calculate the natural frequencies and corresponding mode shapes of the model [93]. Secondly, a steady-state dynamic step is used, which predicts the vibration amplitude and phase of the modelled system as well as the stress and strain for the applied loading conditions [25]. In this study, a frequency convergence study is conducted for the welding horn to investigate the accuracy of modelling results, which the mesh density of the modelled horn is outlined in the forthcoming sections.

### 3.4 Experimental modal analysis (EMA)

Experimental modal analysis (EMA) is a technique which can be used to determine the modal parameters of natural frequencies, damping factors and mode shapes of a linear, time-invariant structure using a set of frequency response measurements extracted from an excited structure [94]. In the 1960s, the advent of digital computing and the development of the Fast Fourier Transform (FFT) opened a wide range of opportunities to employ EMA in different applications. Normally, FEA is used as a numerical technique to calculate the modal parameters, but the validation of FE simulations can be obtained using EMA. The EMA works when energy supplied to the structure with known of frequency content. The response spectra of the resonance system can be clearly amplified. The transfer function or frequency response function (FRF) can then be obtained by the analysis of the response and force spectra. In this work EMA is used to predict the modal parameters for the ultrasonic spot welding horn.

### 3.4.1 Frequency response function (FRF)

The frequency response function (FRF) represents the output to input ratio of a structure. The FRF can be used to characterise the dynamic properties of a mechanical system such as natural frequencies and mode shapes. The output response of the structure is measured in terms of displacement, velocity or acceleration, and is captured in the time domain but it is converted to the frequency domain through using a Fast Fourier Transformation algorithm (FFT). Complex functions of transformation contain real and imaginary components, or magnitude and phase, to describe the response of the structure [95].

### 3.4.2 EMA measurement system

For the EMA, the testing equipment consists of a function generator that produces a random excitation signal [96], an amplifier, which amplifies the signal from the function generator, a transducer which transforms the amplifier electrical signal into mechanical vibrational motion by means of the piezoceramic discs, and a structure such as an ultrasonic welding horn which is excited by the vibration of transducer. The vibrational response of the testing structure can be measured by using a 3D non-contact laser Doppler vibrometer, shown in Figure 3-5, where a signal is transmitted and received using a laser beam from a single point on a vibrating structure surface.



Figure 3-5 3D non-contact laser Doppler vibrometer with controller

Data are captured by data acquisition system and model analysis software, and then interpret the experimental data using FFT analysis respectively. A laser Doppler vibrometer is an optical device that is able to detect the instantaneous velocity of a surface

of a structure. The device works upon two principles, the Doppler shift and optical interferometry. The measurements are obtained by focusing a direct laser beam at a target on the structure and measuring of Doppler shifted wavelength of the reflected beam by means of using interferometry. Accurate test is obtained by a direct line of sight to the target point on the surface of testing structure. The Doppler shift describes how the frequency of the wave will change when the source of wave is translated relative to the observer. There is slight difference between the wavelengths of reflected light from the wavelength of the incident light. If moving towards the incident light the wavelength begin to decreases as the distance is shorter and vice versa. By knowing the wavelength of the incident light, the velocity of the structure can then be determined from the change in the wavelength of the light. But within the high frequency of the light beam, direct demodulate is not possible and the detection of difference between two superimposed wavelength is obtained by using optical interferometry [25, 90].

### **3.4.3 Vibrational signal processing**

The response of different points located on the surface of a structure can be measured through the use of a spectrum analyser. The FRF is computed by the Fast Fourier Transform which converts the signal measurements in the time domain to the frequency domain using digital Fourier transform (DFT) analysis. A form of the FFT algorithm was developed by Cooley and Tukey in 1960s [97]. Inaccurate results can be produced using DFT analysis by aliasing, which is a problem which results from too slow a sample rate, as a discretisation of the continuous time history is misinterpreted. Also, the spectrum measurements by DFT can be distorted if the high frequency signals are misinterpreted as low frequency signals. Anti-aliasing filters can be used to solve the aliasing problem, where the time signal is subjected to a low-pass filter. Leakage is a problem where a sample of the signal which is taken from finite length of the time history coupled with the periodicity, is also represented as a problem. The periodicity principle considers all signals to be periodic, but this is not the case with random excitation signals. Minimising these problems can be addressed by changing the duration of the measurement period, using zero padding where zeros are added to the end of measured sample, or windowing technique such as rectangular, hanning, hamming and exponential is used on the time domain signal prior to analysis of the Fourier transforms [98]. In this work, the measurements of FRFs were applied to the manufactured welding horn, using both high-pass filter and hanning window to minimise the leakage and aliasing. The results of EMA are improved by

collecting responses during the analysis for each measurement point and the averaging the FRF results to reduce the noise content and to improve final FRF.

### **3.5 Design process for an ultrasonic spot welding system**

This study describes the modelling, design and fabrication of an ultrasonic spot metal welding system which can be used to join similar and dissimilar metals. The design of the ultrasonic spot welding system matches in configuration to the lateral-drive system, which is suitable for joining thin metals. Design and modelling is needed to develop a welding system that is composed of a welding horn, stationary anvil, rigid bed, mounting holder and fixtures. The welding horn is the principal component used in an USMW system to transfer ultrasonic energy to the welding zone [99, 100]. The horn is fixed to the upper surface of the top specimen, whilst the lower specimen is fixed to the anvil. Ultrasonic welding components are required to build a welding system that result in high weld strength and quality. FEA has been used to predict the dynamic properties of welding components. In addition, validation of the modelling of the welding components is carried out using EMA. Finally, the designed components were manufactured.

### **3.6 Design of a spot welding horn**

In the USMW system design, the welding horn transmits vibrational energy to the welding area. Consequently, the horn must be designed and tuned at very close to the operating frequency of the transducer, which for this study is 20.81 kHz longitudinal. To ensure a desirable welding horn performance, it is important to isolate the longitudinal mode frequency from other vibration modes. In addition, the vibration amplitude at the horn working surface must be sufficient to match the amplitude requirement of welding metals. Examining of surface uniformity is also required in the design of a horn due to its influence on weld quality. Uniformity can be defined as the ration of minimum/maximum amplitude of the horn working surface. Another consideration in the horn design which must be taken into account is the high stress at the nodal plane. The first step in the development of this welding system is the design and fabrication of the welding horn. The shape and size of the horn are restricted by the spot welding configuration. AISI 1030 carbon steel was selected as the horn material due to its high wear resistance, which is desirable for USMW [101]. The basic physical and mechanical properties for AISI 1030 carbon steel are tabulated in Table 3-1 [102].

Table 3-1 Material properties of steel horn

AISI 1030 Carbon steel	
Density	7850 kg/m <sup>3</sup>
Hardness (Vicker's)	188
Ultimate tensile strength	550 MPa
Yield tensile strength	345 MPa
Elongation at break	32.0%
Young's Modulus	210 GPa
Poisson's ratio	0.30
Shear Modulus	80.0 MPa
Bulk Modulus	140 GPa

The horn was designed as a half-wavelength to match the working frequency of the ultrasonic transducer. The design of the welding horn was performed by using FEA to predict natural frequency, mode shape, vibration amplitude and stress. The successful analysis of these criteria can result in the welding horn vibrating with the desired amplitude and frequency. The wavelength of the steel horn is calculated from Equation (3.14), which the length of the horn is considered to be equal to the half-wavelength. The horn profile is modelled and fabricated to match the requirement of the spot welding process. All dimensions of the horn are numerically determined by using Abaqus software, including the horn input diameter  $D_1$  which was found to be 34 mm and matches to the output diameter of the transducer. The horn output diameter  $D_2$  is 16 mm, the body length  $L_1$  is 67.14 mm and the shaft length  $L_2$  is 61.26 mm, the catenoidal horn profile  $R$  is 10 mm. The half wave-length, which is equal to the total horn length, is 128.4 mm. The horn is equipped with an integral flange coupling which is fixed at the nodal plane. The benefit from designing a flange is to mount a welding stack (a horn connected with a transducer) and to be able to apply a static force perpendicular to the specimens. The flange is machined from AISI 1030 carbon steel where its dimensions were defined by using Abaqus. The FE simulation was used to optimise the flange thickness to be 5 mm and flange diameter as 50 mm to shift a high stress toward the nodal plane. The welding tip is also designed as an integral part to assist in eliminating stress concentration. Figure 3-6 shows the integrated spot welding horn design.

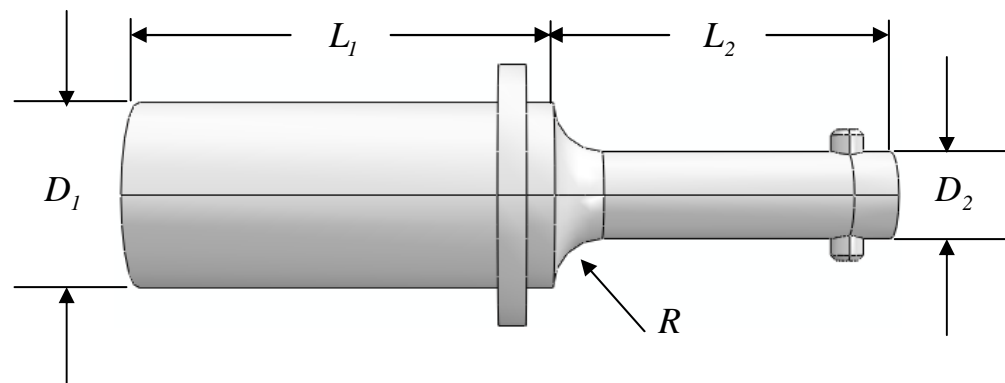


Figure 3-6 Dimensions of the modelled spot welding horn

In ultrasonic welding, a welding tip may be attached to the horn to increase the intensity of ultrasonic energy input at the welding zone and to reduce the slippage through contact surfaces between the upper specimen and horn tip. A weld tip is usually a replaceable or interchangeable part that is tightened onto another component such as a horn, or is machined as an integral part of a solid horn. In most cases, the use of detachable tips is common in ultrasonic welding, especially in industry. Although the welding tip and anvil contact surfaces are usually designed as flat surfaces, the welding tip can be designed with either a convex or cylindrical shape to help eliminate contact stresses [103]. Generally, most welding tips are made from titanium or hardened steel to perform spot welding. The tip surface can be machined with either knurled patterns or surface roughened to avoid unacceptable slippage during welding. In this study, a flat welding tip protrusion was designed as an integral horn tip to achieve the conditions of spot welding and to ensure sufficient energy is transferred to the welding zone. The welding tip was machined from the same horn material, AISI 1030 carbon steel, and hardened to 55-60 RC by quenching from 1100°C. This helps to avoid wear between the horn tip and the specimen upper surface, and also prevents any horn material precipitating on the surface of the welded metal during high excitation. The edge of the welding tip was rounded to reduce the stress developed during excitation. The dimensions of the welding tip were selected to match the dimensions of the horn. Figure 3-7 illustrates the welding tip design which was used for the ultrasonic spot welding horn.

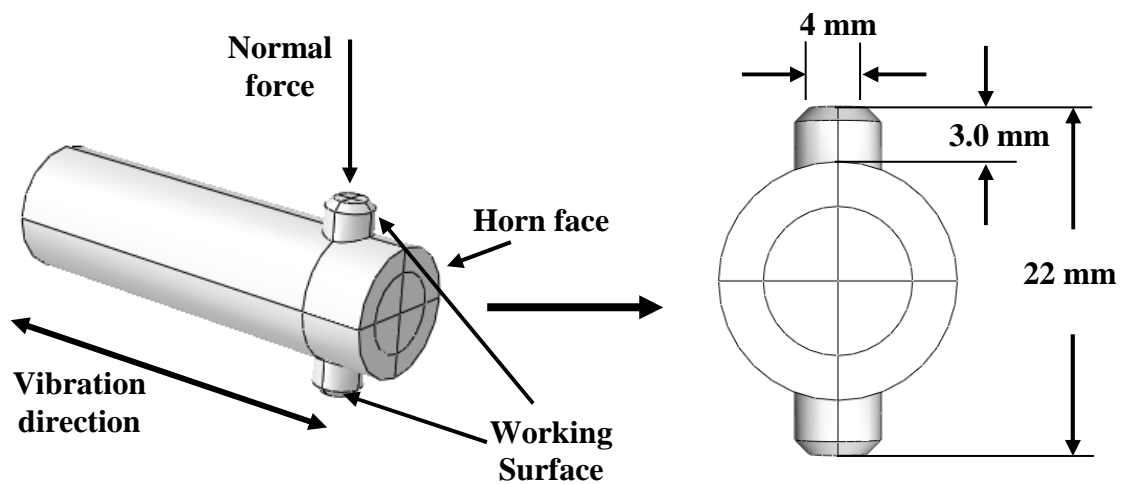


Figure 3-7 Horn welding tip model

The horn tip surface was machined as a knurl pattern in order to be able to effectively engage the specimens and to prevent them from slipping during the welding process. The dimensions of the knurls are usually small compared to the area of the tip. The knurl dimensions were set from evidence that the knurl width of the horn must be much less than the width/depth dimensions of the horn, and that the knurl depth is small compared with the size of a horn face [28]. The knurled dimensions were determined with reference to a 4 mm diameter flat horn face. The width of the knurl tip has a value of 0.02 mm and the knurl depth has a value of 0.05 mm. Abaqus was used to determine the position of the welding tip, because adding the tip means an increased mass of the welding horn which leads to a shift the horn resonance frequency. Another concern in designing a horn is the catenoidal horn profile  $R$  shown in Figure 3-6, which is designed to minimise the stress generated in the stepped part of the horn. Numerical data were extracted from the simulation to match the value of catenoidal horn profile  $R$  to the resonance frequency of modelled horn, 20.81 kHz as shown in Figure 3-8. In addition, the variation of resonance frequencies with change in catenoidal horn profile  $R$ -values, was extracted from FE modelled horn as shown in Figure 3-9. The solutions show that the FEA is effectively used to predict the variation of frequencies, which provides confidence in the modelling approach for the determination of frequencies and mode shapes.

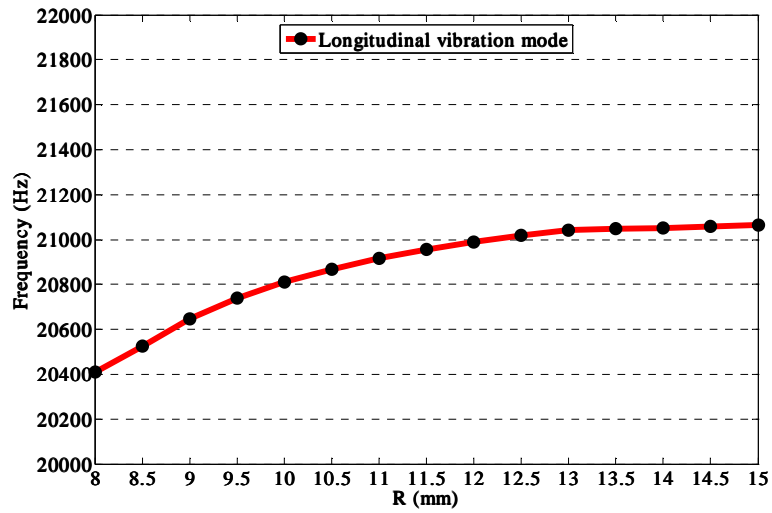


Figure 3-8 Variation of resonance frequency for longitudinal mode versus radius of curvature ( $R$ ) for catenoidal horn profile

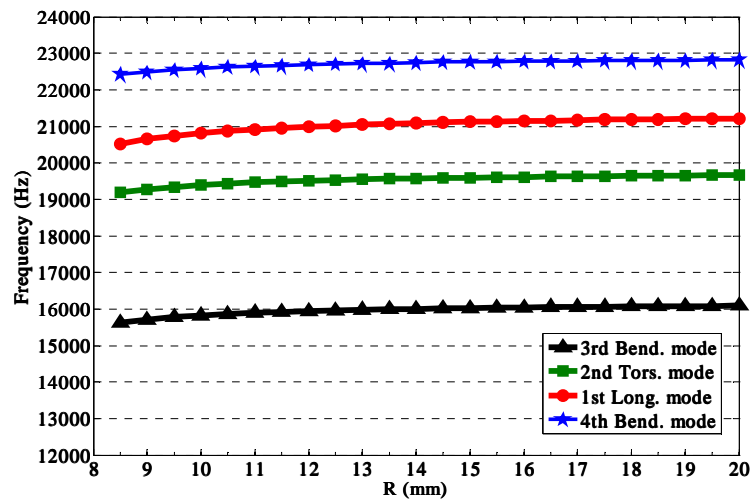


Figure 3-9 Variation of different mode horn resonance frequencies versus radius of curvature ( $R$ ) for catenoidal horn profile

Figure 3-10 shows the frequency convergence for a modelling of an integrated spot welding horn, which the desired longitudinal mode and the surrounding flexural and torsional modes are calculated using Abaqus, for different number of elements and the results are plotted in Figure 3-10 (a), (b) and (c).

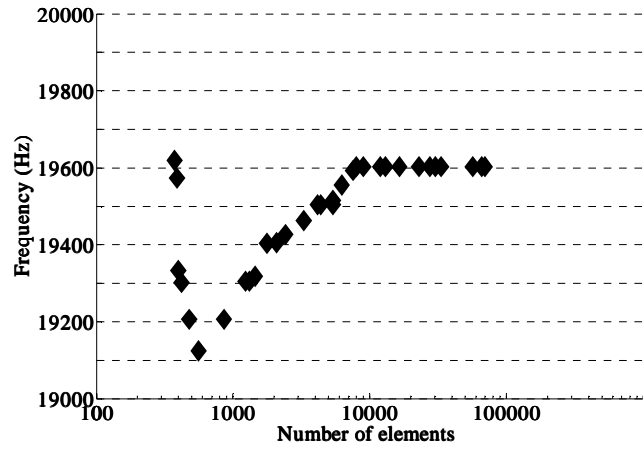
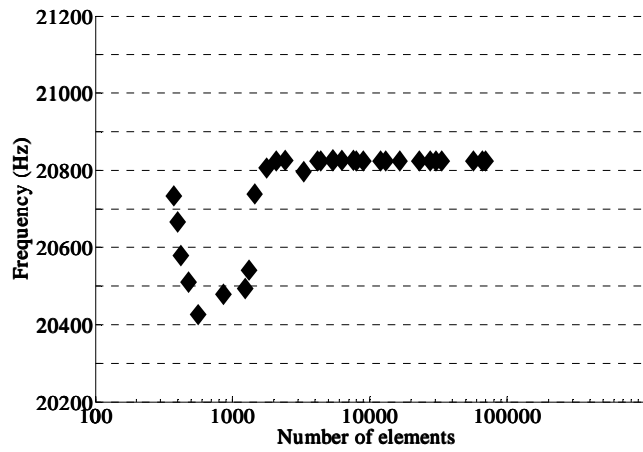
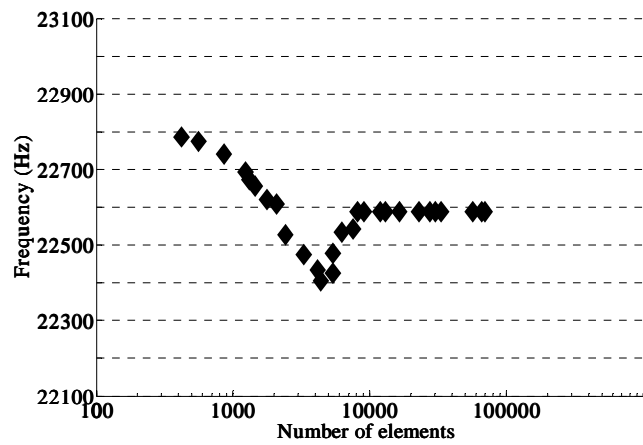
(a) 2<sup>nd</sup> torsional mode(b) 1<sup>st</sup> longitudinal mode(c) 3<sup>rd</sup> flexural mode

Figure 3-10 Convergences of resonance frequencies for different numbers of elements in the FEA model

It can be seen that the torsional and flexural modes converge on common frequencies when the number of elements in the model reaches 8000, whereas the longitudinal mode converges at 6000 elements. The results show that the convergence of the tuned mode (the 1<sup>st</sup> longitudinal mode) can be obtained for a lower number of elements compared to the other non-tuned modes, such as the 3<sup>rd</sup> flexural and the 2<sup>nd</sup> torsional modes. It can be observed from the results that divergence for a low number of elements occurs, due to the curvature of the catenoidal profile. However, the solution proves that the FE package Abaqus is sufficiently more accurate for solving the problems of frequency domain for components using both types of elements, thus providing confidence in the determination of natural frequencies and mode shapes.

### 3.6.1 Stress analysis

The spot welding horn was designed as an integrated tool with both a welding tip and flange coupling. Therefore analysis of the stress is required to avoid any damage or fatigue failure that could occur during operation. FE analysis can be used to predict stress and displacement of the horn. Care must be taken when machining the horn because any damage or poor finishing will lead to raised stresses. Figure 3-11 shows the normalised stress distribution and vibrational displacement of the half-wavelength horn tuned at 20.81 kHz. The results were predicted from Abaqus simulation with a frequency step using either the Lanczos or subspace steps eigensolver to extract natural frequencies for a frequency range up to 40 kHz.

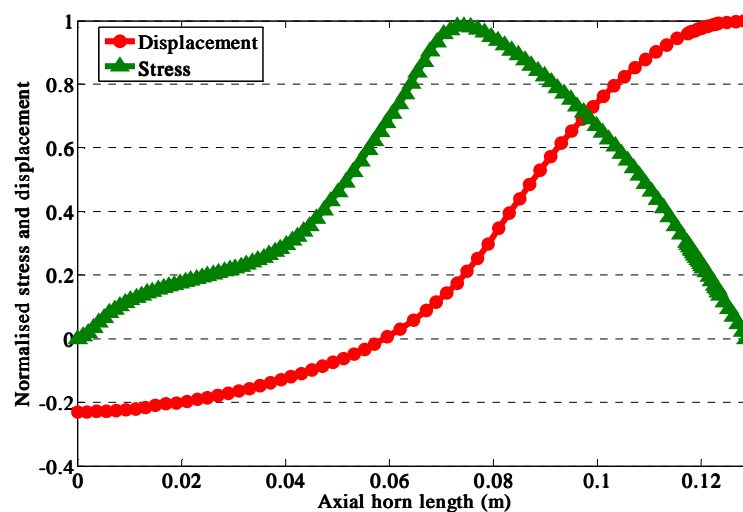


Figure 3-11 Normalised stress and displacement distribution along the horn length

In the modelling procedure, a steady-state dynamics direct step was included after the frequency step to predict amplitude and phase of the horn under predefined loading of a harmonic excitation for a specified frequency. The natural frequencies and mode shapes of the horn can be calculated by the frequency step, whilst the stress and displacement amplitude for a given loading condition can be predicted by steady-state dynamics direct step. After the application of the loading condition to the longitudinal mode of vibration, the stress of the horn can be analysed using von Mises criteria [104]. Figure 3-12 depicts the undeformed and deformed horn, excited in the longitudinal mode at 20.81 kHz.

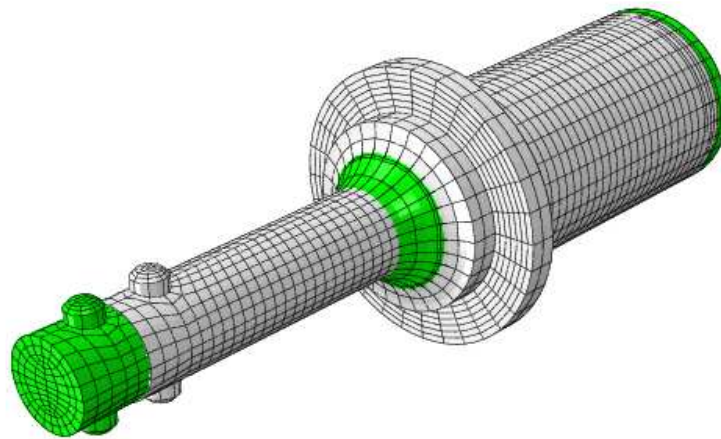


Figure 3-12 Representation of the deformed (green) and undeformed (grey) mesh shape for the integrated ultrasonic spot welding horn excited at 20.81 kHz

The operating principle for a periodic function usually depends on using a sine wave with set amplitude of transducer at 5  $\mu\text{m}$ . The results of the FE-simulation and a pictorial representation of the stress distributions are displayed in Figure 3-13.

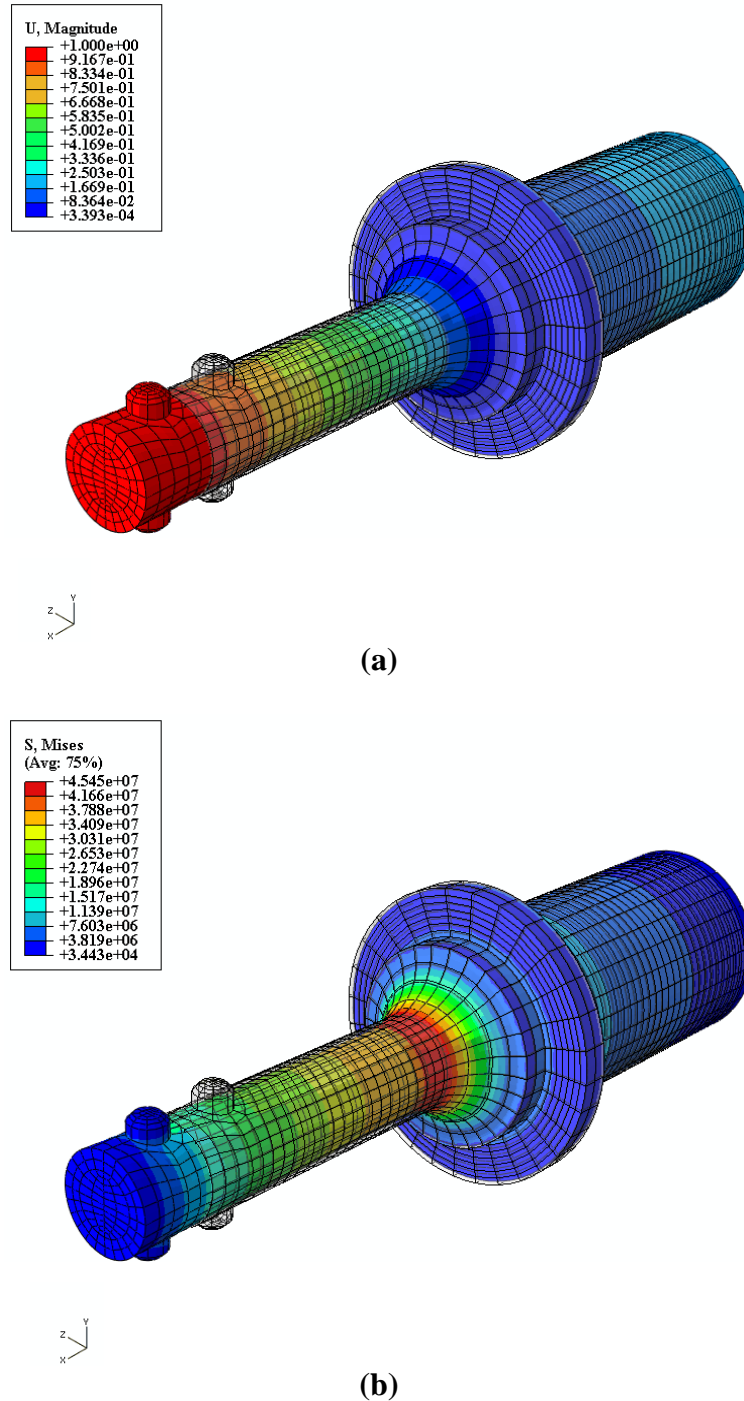


Figure 3-13 Contour plots of the deformed shape for the spot welding horn at 20.81 kHz: (a) displacement along axial horn length and (b) von Mises stress along horn length

These contour plots for the spot welding horn indicate the location of maximum stress at the nodal plane and measurement of vibration amplitude at the horn tip. The nodal plane and von Mises stress distribution of the tuned horn along the longitudinal direction can be clearly observed in Figure 3-14. Results were obtained from the FE analysis on the condition that the horn movement is only in the direction of longitudinal vibration. By

exciting the horn with 20.81 kHz from the ultrasonic transducer, and by setting the output amplitude of transducer at 5  $\mu\text{m}$ , as the applied loading conditions to the horn, the calculated maximum Mises-stress was 45.4 MPa and was located at a distance 80 mm from the horn input diameter. The peak value of stress is located close to the nodal plane which the latter was measured at 60 mm from the input diameter of the horn. In this study, the maximum stress of the horn design is significantly lower than the yield strength of the AISI 1030 carbon steel, which it is safe to assume from the FEA that the ultrasonic welding horn operate within safe operating regime in terms of stress levels.

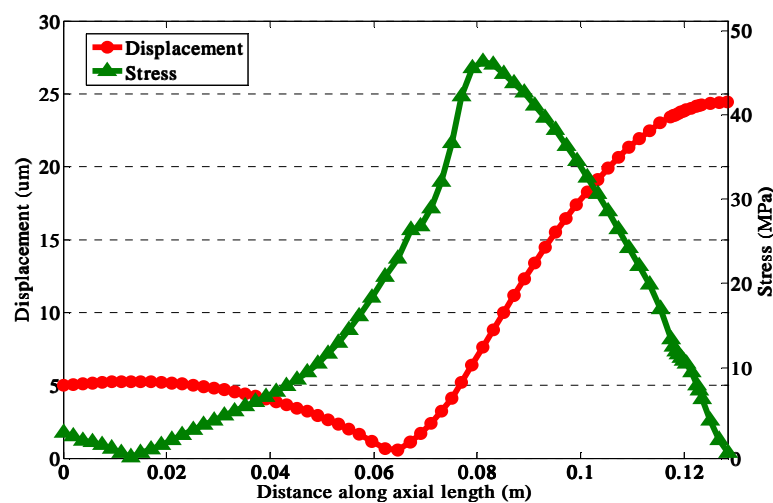


Figure 3-14 FE stress and displacement results for the tuned spot welding horn at 20.81 kHz

### 3.6.2 Frequency separation

Modal frequency separation of the spot welding horn response is very important in examining the performance of the horn. For this, the spread between the tuned and non-tuned modal frequencies of the exciting horn must be measured. The advantage for maximising the horn modal frequencies is to avoid any coupling of the resonant frequency. The horn design for ultrasonic metal welding requires a pure longitudinal vibration mode with a good separation from bending and torsional modes to avoid any distortion in horn movement or reduction in horn gain [48, 105, 106]. Improving the frequency separation for the integrated spot welding horn is not easy due to the inclusion of additional masses to the horn, namely the horn tips and flange coupling, and any change in size or dimensions of these masses may lead to a reduction in the separation between vibration modes. FE analysis can be used to estimate the separation of welding horn frequencies. Previous

studies suggest that a frequency separation greater than 1 kHz around the longitudinal mode must be obtained in order to operate the tool effectively with high gain [105, 107]. The horn longitudinal mode was determined to be 20.81 kHz, whereas other modes around the longitudinal mode are recorded at a frequency separation of 1.779 kHz from the flexural mode and 1.211 kHz from the torsional mode, and further from other modes.

### 3.6.3 Amplitude uniformity

Horn amplitude uniformity is defined as the relation in terms of response between the minimum and maximum amplitude at the horn working surface [106]. In USMW, the quality of joining metals can be affected by the amplitude uniformity of the horn working surface. In this work, FE simulations predict good estimation to the amplitude uniformity of the horn tip working surface, which is about 99 %, because the horn tip has a small flat diameter of 4 mm. Figure 3-15 shows the normalised uniformity displacement of the horn tip working surface (Figure 3-7).

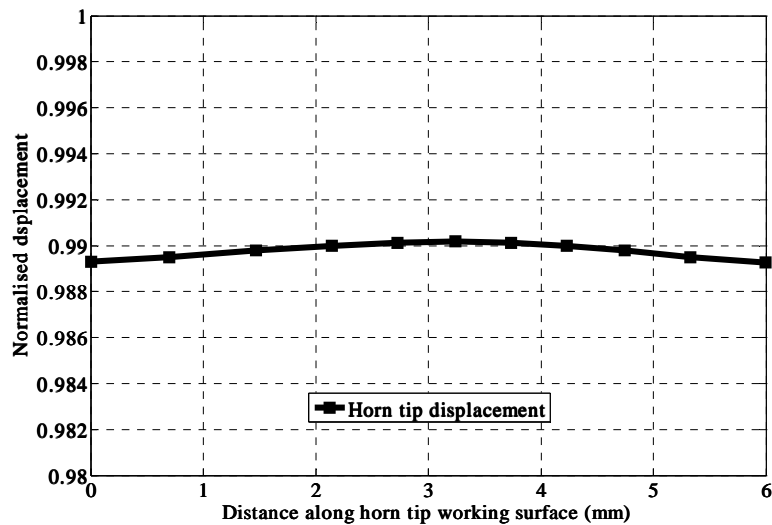


Figure 3-15 FEA normalised displacement of the horn tip versus radial distance of the horn surface when excited axially at 20.81 kHz

## 3.7 Manufacture of the spot welding horn

The spot welding horn was fabricated using the computer aided manufacturing (CAM) technique, where four axes of the intelligent computer numerically controlled (CNC) machine were configured to create a horn. Figure 3-16 depicts the manufactured 20.81 kHz

ultrasonic spot metal welding horn with the required size and dimensions, which is suitable for welding different metals.



Figure 3-16 Manufactured spot metal welding horn

### 3.8 Validation between FEA and EMA

Finite element analysis of the spot welding horn was carried out to predict the natural frequencies and vibrational mode shapes of the horn. EMA is then required to validate the results found from modelling. Experimental analysis was conducted on the horn connected to the transducer, by creating a grid of measurement points on the horn. The set-up of the equipment used in the EMA for the ultrasonic spot welding horn connected with transducer can be seen in Figure 3-17. The experimental testing equipment used in this study consists of a Signal Calc ACE data unit, an amplifier, a 3D laser Doppler vibrometer (Polytec, 3D CLV-3D) with signal processing unit and computer, and a dynamic signal analyser using Signal Calc ACE data acquisition software. The horn was then connected to an ultrasonic transducer by means of a stud which was designed for this purpose. The tuned horn was excited with a broadband signal between 0 and 40 kHz, created by a function generator which is built into the data acquisition hardware. The sample rate, 204.8 kHz, and resolution, 1.56 Hz, of the data acquisition hardware are applied within the 0-40 kHz range [108]. The amplifier boosts the signal provided by the function generator. The electrical signal of the amplifier was converted to mechanical vibration by the ultrasonic transducer, thus exciting the horn. Measurement of the velocities over the whole grid of points on the horn surface was performed using 3D LDV. The time domain data was recorded and transformed to the frequency domain using a FFT. The measurements of modal parameters such as resonance frequencies and mode shapes of the ultrasonic welding horn could then be measured using ME'Scope VES modal analysis software.

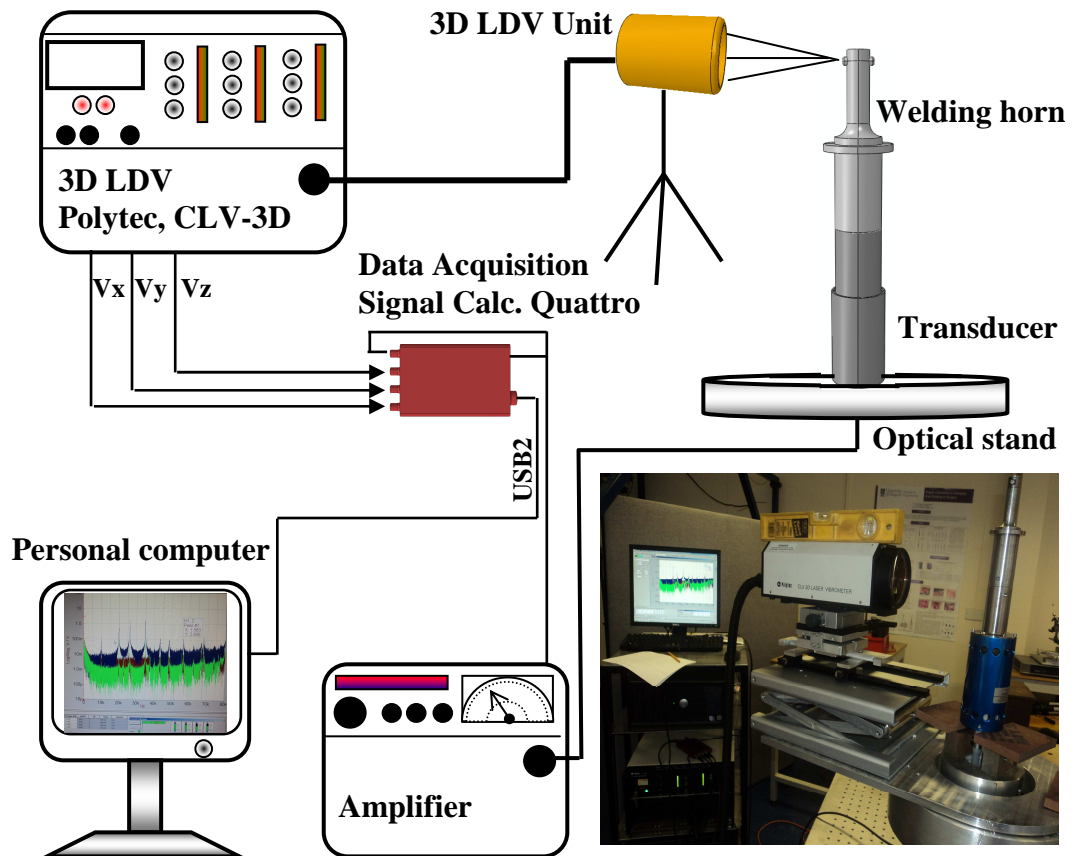


Figure 3-17 Schematic diagram of experimental modal analysis showing the various components and photographed of actual set-up

In Figure 3-18, the spectrum shows a good separation between natural frequencies, and the value of the longitudinal mode (L) is clearly identified. Other modes such as torsional (T) mode and bending or flexural (F) mode show an acceptable comparison with those predicted from the FEA. Agreement between the FEA and EMA data for the excited horn at an operating frequency of 20 kHz is within 3.68 % of all natural frequencies up to 40 kHz, as tabulated in Table 3-2. It can be observed that the 2<sup>nd</sup> torsional mode is difficult to recognise in the EMA, because it was thought that this mode is merged due to connecting the horn with the transducer, which is not considered in the initial calculation.

Table 3-2 Horn mode frequencies in the range (0-40 kHz)

Mode	FEA	EMA	Error %
1 <sup>st</sup> T	13190	13692	-3.66
2 <sup>nd</sup> F	15821	15740	0.51
2 <sup>nd</sup> T	19600	-	-
1 <sup>st</sup> L	20811	20770	-0.19
3 <sup>rd</sup> F	22590	23454	-3.68

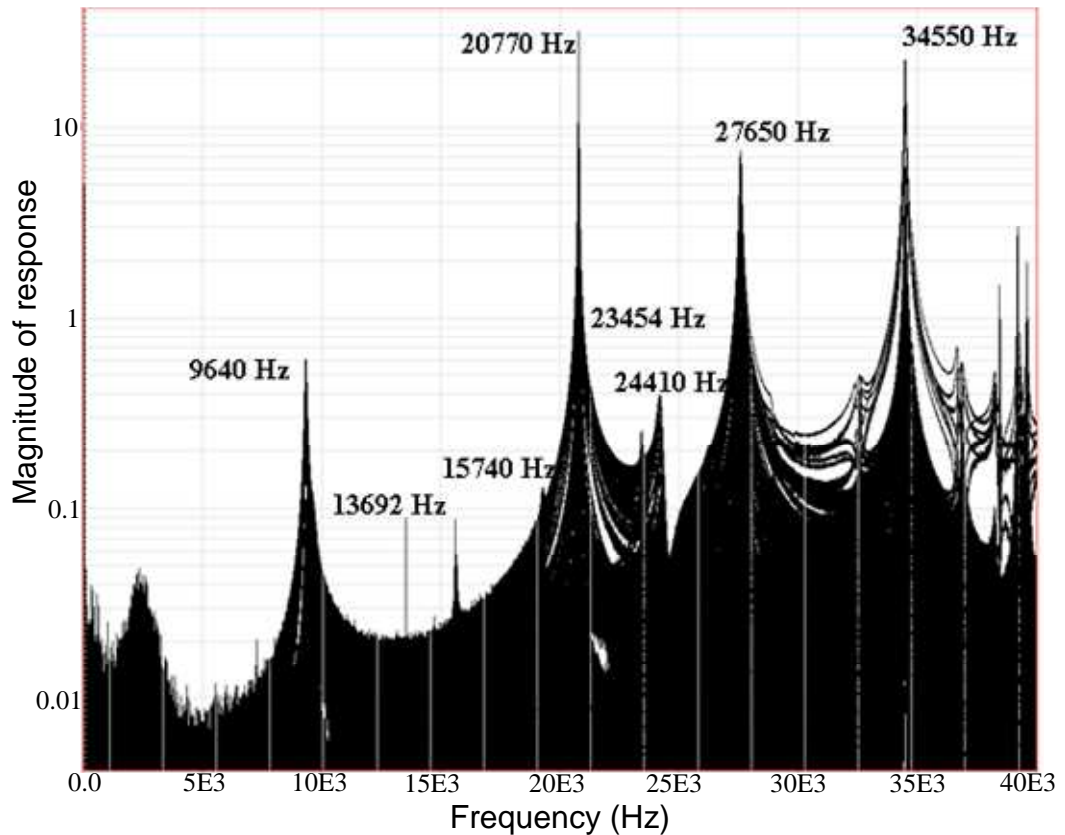


Figure 3-18 FRF measurements of the excited spot welding horn at 20 kHz

The welding horn exhibits responses in several modes, however a torsional mode, bending mode and longitudinal mode for the comparison between FEA and EMA are shown in Figure 3-19. Another criterion in the design of a horn is the vibration amplitude, the amplitude can be defined as the peak-to-peak displacement of the horn at its working face [77]. In USMW, the amplitudes vary from 10 to 50 or 60 microns at the weld [14]. In some welding systems, the amplitude is a dependent variable, where it is related to the power applied to the system. In other systems, the amplitude is an independent variable capable of being set and controlled at the power supply through a feedback control system. In this work, an integrated horn with the additional masses such as welding tip and flange coupling was designed to provide high gain at the welding tip surface, where the gain factor is defined as the ratio of the output surface to input surface amplitude of the horn [109]. In this study, the horn gain was 4.108.

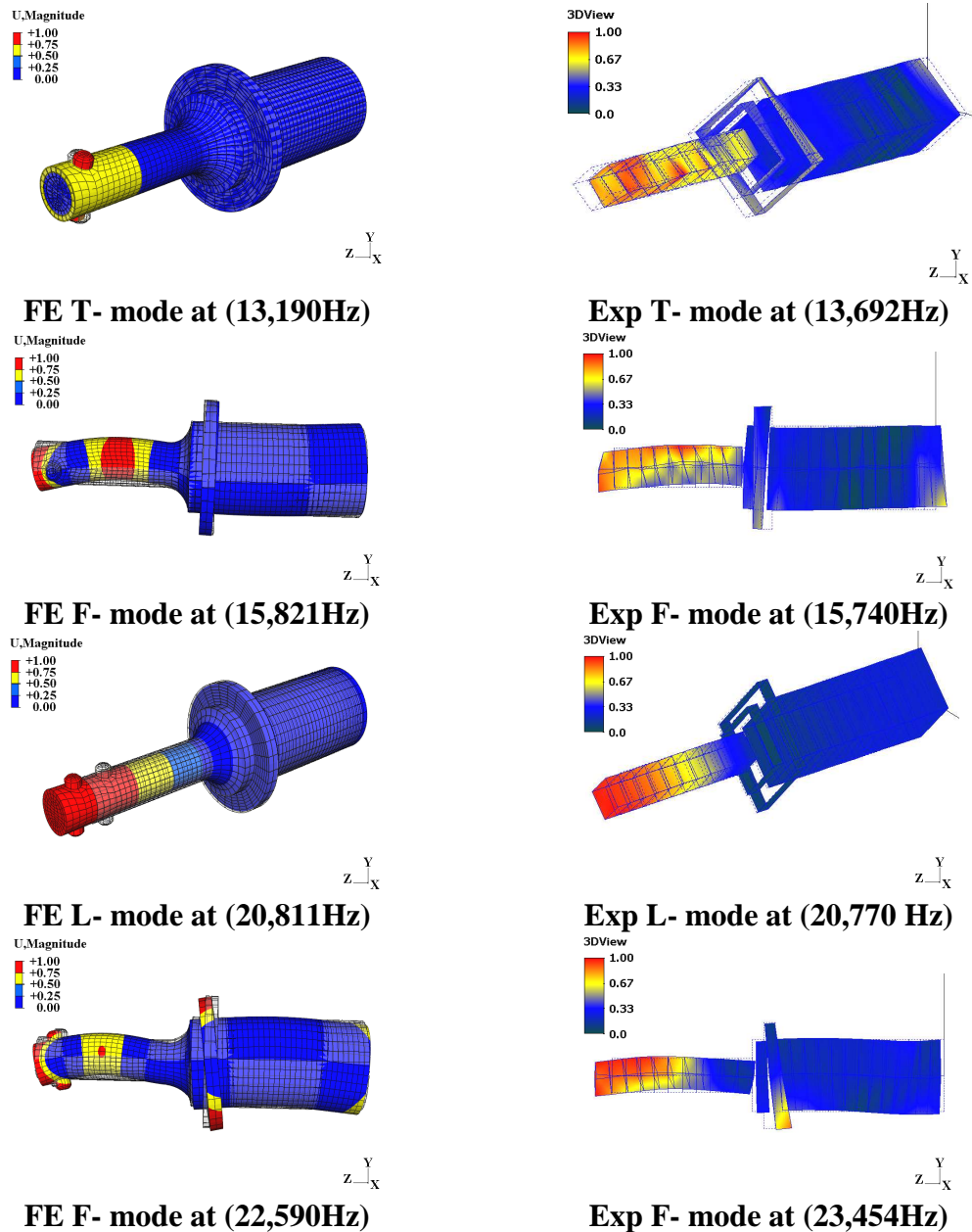


Figure 3-19 Validation of the modelling and manufactured ultrasonic spot metal welding horn using FEA and EMA for tuned horn at 20 kHz

### 3.9 Design of welding components

In USMW, the selection of the components, such as the anvil, is dependent on the nature of the welding system. Normally, anvils are designed to align and hold welded specimens. Types of anvils which are used in ultrasonic welding include rigid (stationary) anvils and counter resonant anvils [28]. The rigid anvil is made from steel or aluminium and is normally used in ultrasonic spot welding [99]. This type is mostly involved in USMW. The

second type of anvil is used to vibrate out of phase with the horn vibration such as in a wedge-reed system. Flattened knurled surfaces are usually used in the design of anvils to match the tip surface of the welding tool and to avoid slipping between the specimens and the welding tool during the process. This study involved the design and manufacture of an anvil which is suitable for USMW, which the size and dimensions of the anvil are selected according to the dimensions of welding specimens. The anvil material was made from AISI 1030 carbon steel and the surface area is (50 x 50 mm). Figure 3-20 shows the manufactured stationary anvil with knurled surface.

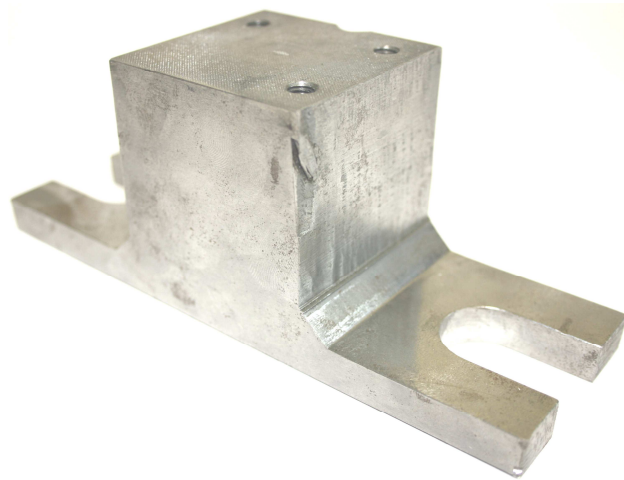


Figure 3-20 Steel anvil machined knurl

The spot welding horn was connected with the ultrasonic transducer by means of a stud made for this purpose, and the welding stack was mounted on the driving machine (tensile-test machine) through a specially designed mounting holder (Figure. 3-21). Care must be taken when designing a holder, because any inaccuracy in the design can result in losses and unwanted absorption of power, damping and a decrease in the horn response. The rigid holder was securely clamped to the welding stack at the nodal plane which is located at the flange coupling on the horn. Thin rubber was used around the flange circumference to ensure a full insulation of touch the horn with the mounting holder.

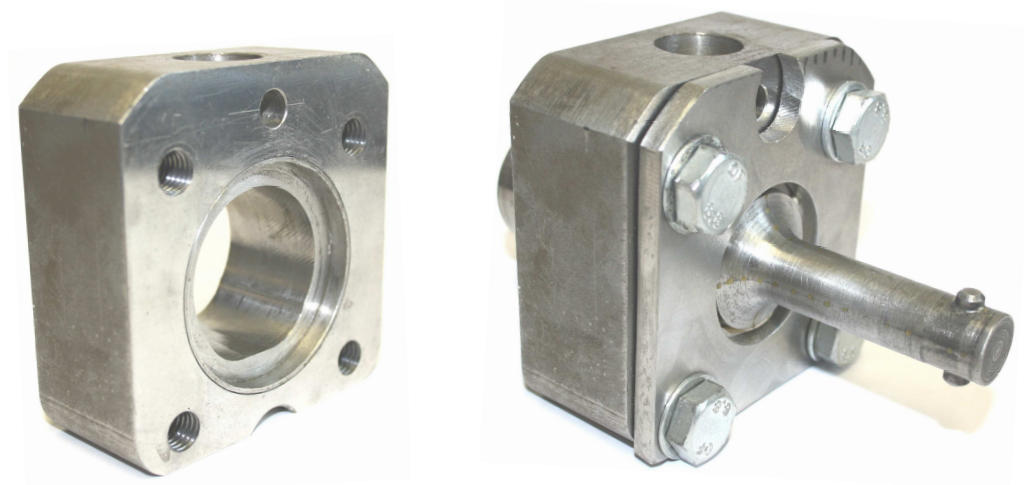


Figure 3-21 Welding stack mounting holder connect with spot welding horn

Prior to the set-up of the welding machine, the vibrational characteristics and frequency response of the welding stack were determined by using a 3D laser Doppler vibrometer. The frequency response was collected for different conditions, first when the horn was connected with the transducer alone, and then when the welding stack was connected to the mounting holder, to observe the variation in the response. From knowing that the gain of the horn is 4.108 and the transducer excitation amplitude is  $5 \mu\text{m}$ , the response for the welding stack at the horn tip was found to equal  $20.35 \mu\text{m}$ , whereas the response for the connected welding stack with the mounting holder was found to be  $20.15 \mu\text{m}$ . This confirmed the accuracy and isolation of the connected excited components from the rigid assembly. For the entire welding system, a rigid bed and other fixing tools were designed to fix the components in place for welding.

### 3.10 Summary

A lateral-drive ultrasonic metal spot welding system has been introduced and described in terms of the system components, and by including FE simulation as part of the design process. Based on the assumption of longitudinal vibration of a uniform rod, the calculation of the half-wave length for the tuned horn was discussed, and the modelling of the steel horn was completed by using FEA. The horn modal frequencies and associated mode shapes were then confirmed using EMA. The flange coupling allows for providing a nodal mounting in order to connect the welding stack to the driving machine (tensile-test machine). Many criteria were examined in the design of the horn such as exciting at the operating frequency of 20.81 kHz, stress distribution, vibration amplification, frequency

separation, amplitude uniformity and gain factor. The performance of the horn was modelled by tuning the horn at the longitudinal mode. The location of high stress, gain and welding tip amplitude were determined by driving the transducer at amplitude of 5 microns in the longitudinal mode. Von Mises stresses were calculated to characterise the stress in the horn, which was found to be lower than the yield point of the steel, whilst the local stresses around welding tip were recorded very low values. The position of the highest stress was located close towards the nodal plane. Frequency separation of the horn was affected by the horn catenoidal profile, flange coupling on the horn and the location of the welding tip. FEA and EMA show good agreement of vibration modes around the tuned longitudinal mode of the horn with at least 1.211 kHz from the torsional mode and 1.779 kHz from the flexural mode, which is acceptable in ultrasonic welding. The catenoidal profile of the integrated horn provides a gain of 4.108. The ultrasonic horn has been measured and calculated as having longitudinal mode of vibration at 20.77 kHz. Welding components were also designed, such as a rigid anvil, mounting holder, rigid bed and fixing tools. Geometries of the welding components were specified to the size and dimensions of the welding stack and to the thickness and dimension of the metal to be welded. Examining the output response of the welding stack connected to the holder is required prior to welding to check the damping during the process, loss of power, shift in frequency and a drop in vibration amplitude.

## **Chapter 4**

### **Welding tests and metal investigations**

#### **4.1 Introduction**

This chapter discusses the welding test procedure and the investigation of the metals that are used in ultrasonic metal spot welding. Firstly, the mechanical properties of the selected metals must be extracted. Aluminium and copper are the two types of metals used in USMW, but the technique can be easily applied to other metals. The properties of each metal are obtained using a universal testing machine to determine the Young's modulus, yield tensile strength, ultimate tensile strength and elongation after test completion. The dimensions and thickness of the specimens were prepared according to the standard required for the welding of thin specimens. The hardness and surface roughness were investigated as they affect weld strength and quality. The ultrasonic metal spot welding system was mounted on a tensile test machine in order to conduct the welding experiments, where a large number of similar and dissimilar specimen configurations were successfully welded under different conditions. In this chapter, the weld development for different configurations of Al-Al, Cu-Cu, Al-Cu and Cu-Al will briefly be discussed. The process and metal parameters were specified and set depending on a range of assumptions, including the conditions of the lateral-drive welding system required to bond thin gauges. Tensile shear tests of fully-formed welds were performed for a number of weld configurations containing aluminium and copper specimens. The tensile test machine was then used to drive configurations with specimens of a range of thicknesses including 0.1, 0.3 and 0.5 mm to failure. These configurations were composed of both similar and dissimilar metals. The strengths of the welded specimens were investigated by varying the applied parameters such as clamping force, amplitude of vibration, welding power and welding time.

#### **4.2 Selection of metal for ultrasonic spot welding**

This study explores the USMW of aluminium and copper. Specimens with thicknesses of 0.1, 0.3, and 0.5 mm were used, as shown in Figure 4-1. In general these softer metals are widely used in ultrasonic welding due to their high thermal conductivity, which enhances

the diffusion of atoms between intimate surfaces [110]. It is also advantageous to weld by ultrasonic means rather than fusion welding, because the latter requires more energy and is more time-consuming [14]. A lateral-drive ultrasonic welding system has been designed to join similar and dissimilar metals and to study system and metal parameters which influence weld strength and weld quality. In this study, metals used for welding were supplied by Goodfellow [111]. The properties are varied in temper-state between annealed and half-hard. Table 4-1 details the metals used for different thicknesses of aluminium and copper.

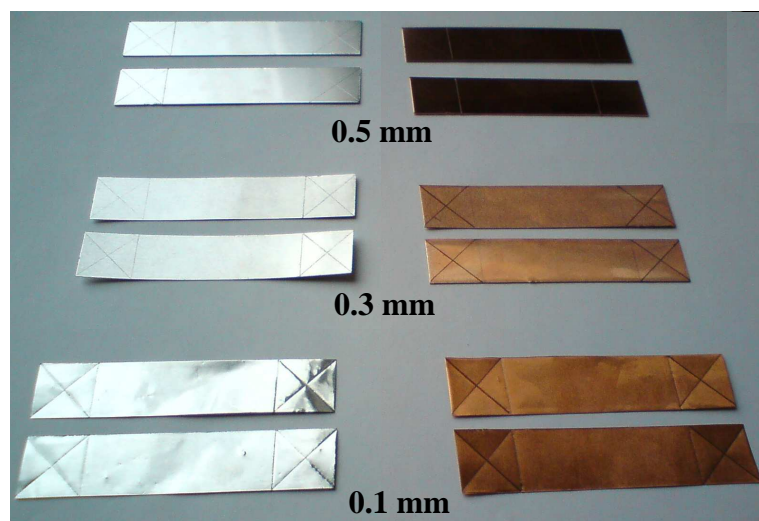


Figure 4-1 Aluminium and copper specimens used in ultrasonic metal spot welding with thicknesses of 0.1, 0.3, and 0.5 mm

Table 4-1 Metal thicknesses (Manufacturer's data)

Material	Thickness	Purity	Temper
Foil	(mm)	(%)	-
Al	0.1	99.0	Annealed
Cu	0.1	99.9	Annealed
Al	0.3	99.0	Half-hard
Cu	0.3	99.9	Annealed
Al	0.5	99.0	Half-hard
Cu	0.5	99.9	Half-hard

### 4.3 Tensile test machine set-up

A tensile test is a method used to determine the behaviour of materials under a uniaxial loading condition provided by a universal testing machine [112]. The calibrated testing machine, Zwick/Roell Z2.0, is set up to determine the mechanical properties for all types of aluminium and copper metals used in this study, as shown in Figure 4-2.

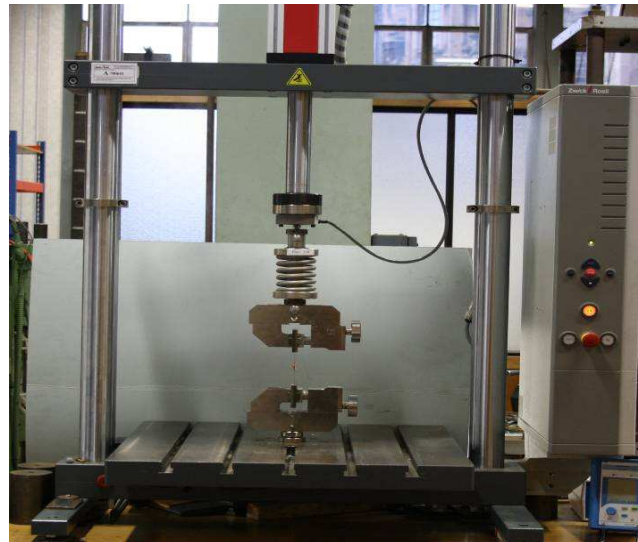


Figure 4-2 Universal test machine, Zwick/Roell z2.0

Metal characterisation results are extracted from many tests performed with the uniaxial tensile test machine. Specimens with specified dimensions are mounted on the 2-kN load cell tensile machine, which records the tensile load and elongation (displacement) of the pulled specimen. The end-result is a load-displacement diagram. The process can yield highly accurate results, especially for measuring stress. However, for strain the relative stiffness of the test machine and samples lead to errors, therefore strain was measured using an extensometer. An extensometer is a device used with a universal testing machine to measure the actual extension of a specimen or component when the external load is applied in tension or compression. According to the British Standard 3846, an extensometer is defined as ‘a device comprising measuring and recording or indicating equipment used for determining extension and hence strain.’ [113]. In this study, a calibration extensometer (model 3543-025M-050-LTv) is used to measure extension, from which the data were recorded and stored within machine software [114]. Figure 4-3 shows the extensometer set-up on the tensile test machine.

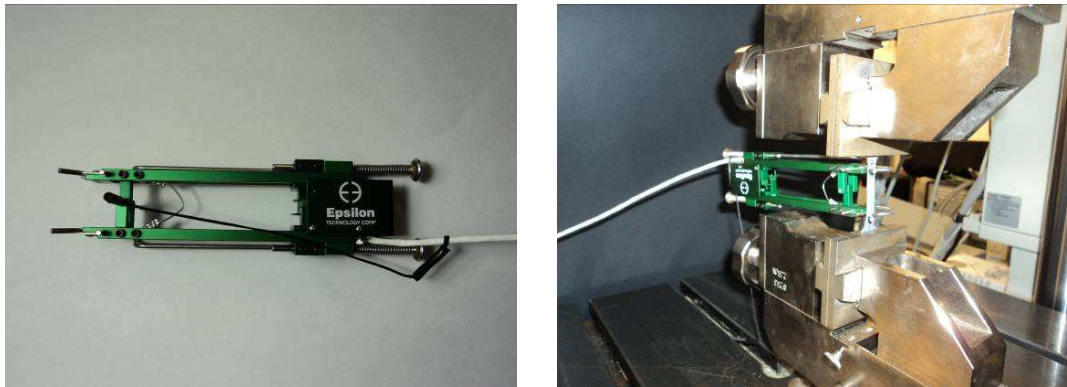


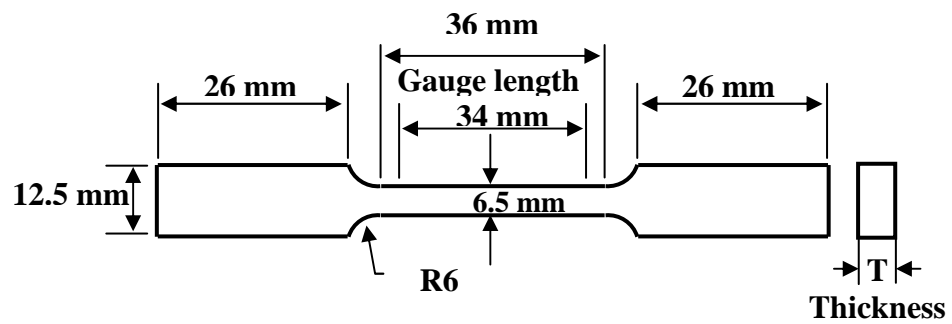
Figure 4-3 Extensometer set-up on universal test machine

## 4.4 Specimen configuration

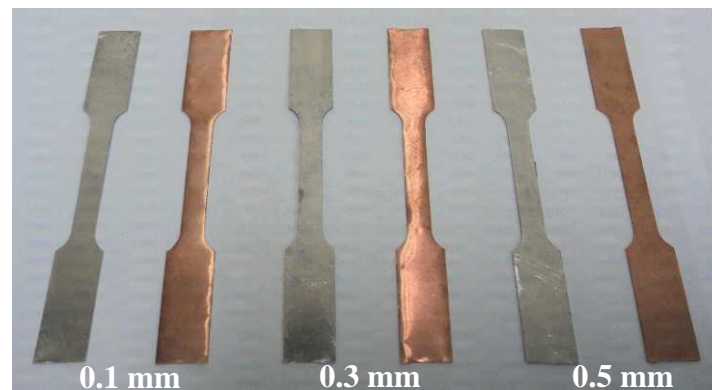
All specimens used in ultrasonic spot welding testing are characterised by their mechanical properties. The specimens are prepared according to the specifications provided by ASTM E8M Standard and British Standard 546 [115-117]. The specimens were cut and prepared to have a dog bone shape, based on standardised tensile testing. The metal is carefully cut without leaving any grooves, notches, burrs, gouges, rough edge surfaces or overheating that may affect the surface finish of the specimen [118]. The aluminium and copper dog bone specimens were arranged in the tensile machine for testing.

### 4.4.1 Dog bone specimens

Specimens used for the metal characterisation tests were prepared according to the rules obtained from standard test methods for the tension testing of metallic metals, which is an ASTM E8M Standard. The gauge length used for the test is 34 mm, with 26 mm of grip section at each side. The thickness of the specimens varies from 0.1, 0.3 and 0.5 mm for aluminium and copper, which are the same thicknesses for the specimens used to prepare spot welding specimens. The width of the specimen is 6.5 mm, whilst the overall length is 100 mm. The transition radius is located between the grip sections and the gauge length with value up to 6.0 mm, whereas the length of the reduced section is not less than 36 mm. Three specimens are prepared of each metal type for testing speeds of 14 mm/min, 7 mm/min, and 2 mm/min. The strain rate is set according to standard test methods for tension testing of metallic materials (ASTM E8M standard). The details and dimensions of the prepared specimen are shown in Figure 4-4.



(a) Schematic of the test specimen, dog bone (ASTM, E8M Standard)

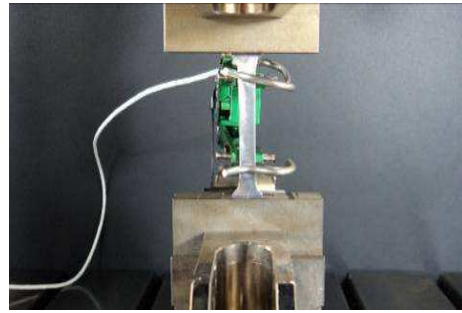


(b) Prepared tensile test specimens for selected metals with thicknesses of 0.1, 0.3 and 0.5 mm

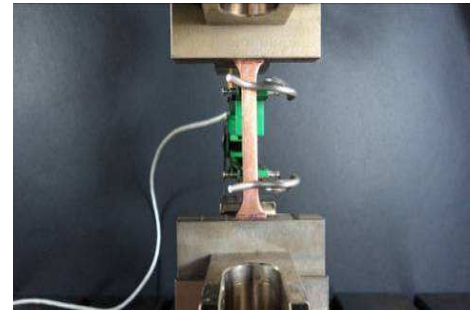
Figure 4-4 Dog bone specimen dimensions for the tensile tests

#### 4.5 Extracting mechanical properties for aluminium and copper

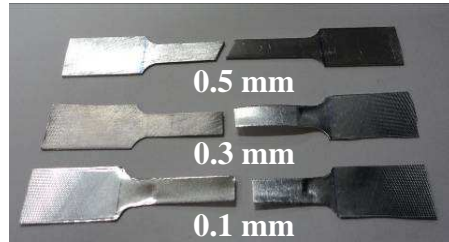
The aluminium and copper specimens are tested on a uniaxial testing machine to extract their mechanical properties. The testing is carried out for each metal by performing extensometer measurements on the machine as shown in Figure 4-5. In the experiments, each test is repeated six times for each configuration and for every testing speed (2 mm/min, 7 mm/min and 14 mm/min). As shown in Figure 4-5, the extensometer has two arms which are aligned to markings on the specimen. As the specimen is loaded in tension, it displays the change in displacement being measured due to the deformation of the specimen. The extensometer recorded the data and transferred it to the machine controller, where the relationship between load and displacement was processed by the machine software.



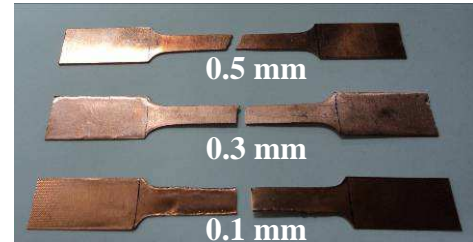
Extensometer set-up on Al-specimen



Extensometer set-up on Cu-specimen



Fractured aluminium specimens



Fractured copper specimens

Figure 4-5 Experimental tensile testing for aluminium and copper specimens with variable thicknesses of 0.1, 0.3 and 0.5 using an extensometer

A load-versus-displacement curve is the immediate result of such a test. The mechanical properties of the metals are obtained from a stress-strain diagram. Average load displacement data recorded from the uniaxial tensile tests is converted into engineering strain and engineering stress by using Equation (4.1) and Equation (4.2) as shown below. The reason for converting this data is to identify elastic-plastic behaviour of the metal and to determine the mechanical properties such as yield stress, UTS and break stress [25]. Furthermore, the data is required in order to define material properties in FE simulation of the spot welded specimens (explained in Chapter 5). A typical stress-strain diagram for a metal under tensile load is shown in Figure 4-6.

$$\epsilon_{Eng} = \Delta L / L \quad 4.1$$

$$\sigma_{Eng} = F / A_o \quad 4.2$$

where  $\Delta L$  is the absolute deformation of the specimen,  $L$  is the initial gauge length of the specimen,  $F$  is the applied load and  $A_o$  is the cross-sectional area of the specimen.

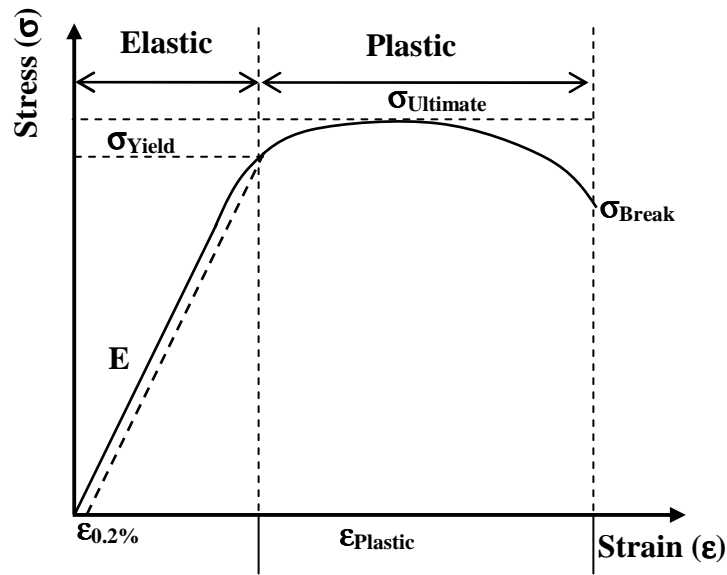


Figure 4-6 Typical stress-strain diagram with 0.2% offset method

The results were produced from the tensile testing of the specimens of aluminium and copper. Most specimens fractured around the centre of the deformed specimen. Figure 4-7 shows the typical values of engineering stress and engineering strain which are plotted for specimens of aluminium and copper with different thicknesses of 0.1, 0.3 and 0.5 mm and for testing speeds of 2 mm/min, 7 mm/min and 14 mm/min. The Young's modulus of the aluminium and copper metals was determined by using a 0.2 % offset method (Figure 4-6) to estimate the linear portion of the curve up to the estimated yield point. Ultimate tensile stress, UTS, is determined from the highest stress value on the stress-strain diagram. The average for Young's modulus, yield stress and UTS for the aluminium and copper specimen metals for a range of thicknesses are tabulated in Table 4-2 and Table 4-3. The tables compare the data extracted from the extensometer measurements for every testing speed. The extracted mechanical properties for all specimens of aluminium and copper can then be used in FE modelling in order to numerically study the behaviour of welded specimens and to compare the weld strength of the joined metals with respect to yield and ultimate stress magnitudes for each tensile test specimen.

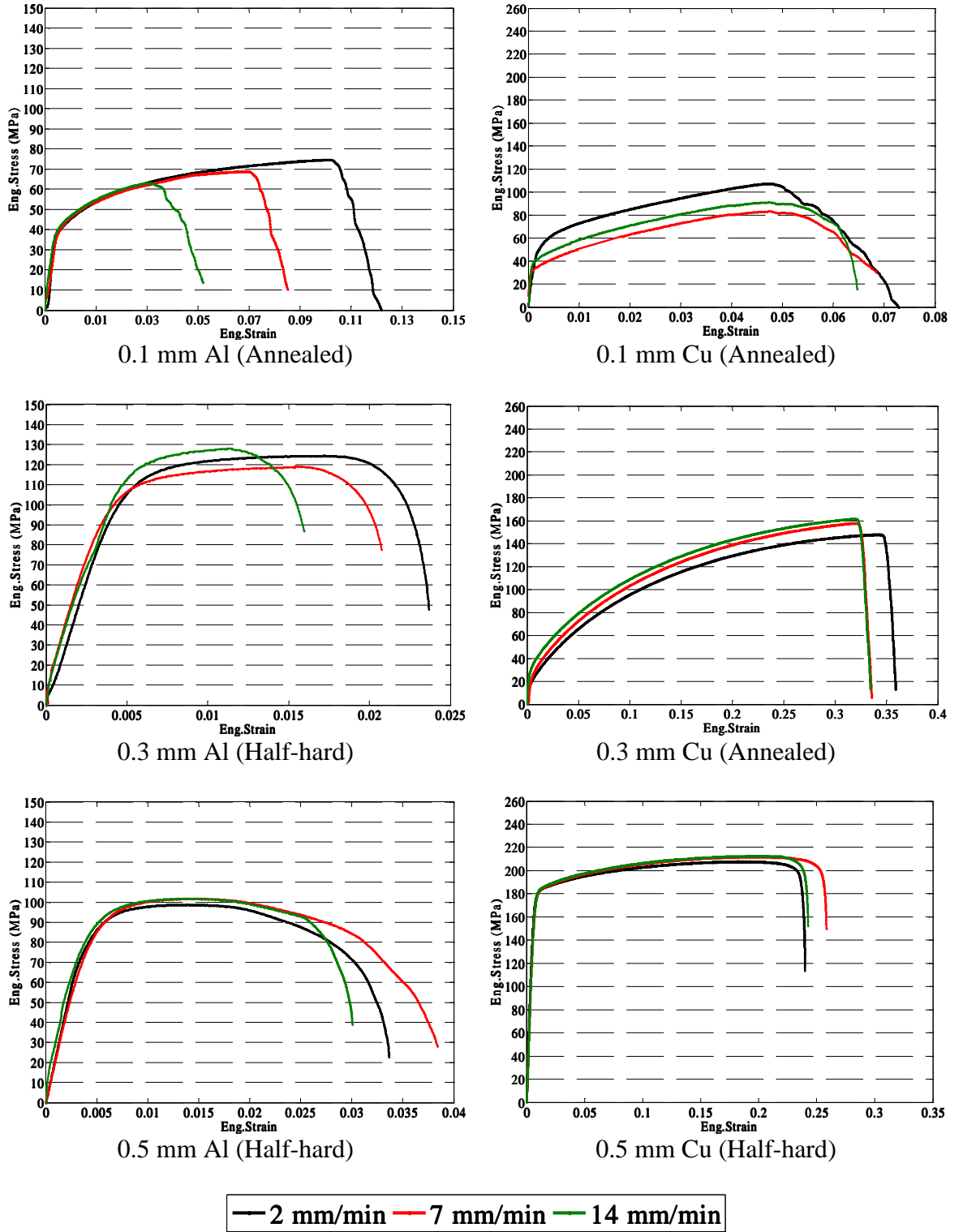


Figure 4-7 Typical tensile test data for aluminium and copper specimens at 0.1, 0.3 and 0.5 mm thickness

Table 4-2 Average tensile data for the aluminium dog bone configuration, (n=6)

Material Specimen		Thickness (0.1 mm)		
Method of Test		Extensometer		
Test Speed (mm/min)	2	7	14	
Young's Modulus E (GPa)	69.8	70.0	70.5	
Yield Stress (MPa)	55.0	56.5	56.8	
UTS (MPa)	63.1	68.7	74.9	

Material Specimen		Thickness (0.3 mm)		
Method of Test		Extensometer		
Test Speed (mm/min)	2	7	14	
Young's Modulus E (GPa)	69.5	69.6	70.2	
Yield Stress (MPa)	108.4	113.3	119.4	
UTS (MPa)	118.9	124.1	128.0	

Material Specimen		Thickness (0.5 mm)		
Method of Test		Extensometer		
Test Speed (mm/min)	2	7	14	
Young's Modulus E (GPa)	69.5	70	70.8	
Yield Stress (MPa)	89.3	90.5	93.0	
UTS (MPa)	97.3	107.1	108.3	

Table 4-3 Average tensile data for the copper dog bone configuration, (n=6)

Material Specimen		Thickness (0.1 mm)		
Method of Test		Extensometer		
Test Speed (mm/min)	2	7	14	
Young's Modulus E (GPa)	119.2	120	123.3	
Yield Stress (MPa)	37.1	44.0	57.3	
UTS (MPa)	81.8	91.1	107.2	

Material Specimen		Thickness (0.3 mm)		
Method of Test		Extensometer		
Test Speed (mm/min)	2	7	14	
Young's Modulus E (GPa)	120.0	120.0	121.4	
Yield Stress (MPa)	68.3	69.3	106.6	
UTS (MPa)	82.3	90.8	107.0	

Material Specimen		Thickness (0.5 mm)		
Method of Test		Extensometer		
Test Speed (mm/min)	2	7	14	
Young's Modulus E (GPa)	120.0	120.3	120.6	
Yield Stress (MPa)	169.2	171.3	172.4	
UTS (MPa)	208.1	212.6	212.7	

#### **4.6 Thickness of specimen**

Ultrasonic welding relies on the generation of relative motion of the specimens at the interface, where the energy delivered from the ultrasonic generator is directed into the upper specimen and propagates through to the welding zone, whilst part of the energy is lost due to friction at intimate surfaces, resulting in the dissipation of heat. In this work, different thicknesses of 0.1, 0.3 and 0.5 mm for the aluminium and copper metal were selected. The reasons for choosing these thicknesses are related to the amount of delivering power from generator, up to 1 kW, and the requirements of the lateral-drive welding system, which is capable of welding thin components. Furthermore, the process is fast, being around 1 second in duration, and the amount of energy that is delivered is not enough to weld thicker metals. However, increasing the welding time can lead to the creation of cracks which affects both weld strength and quality. Most studies focused on ultrasonic welding place a thin specimen in the vicinity of the welding tool to ensure that high ultrasonic energy is imparted to the welding area. These studies confirm that the thickness of the upper specimen is more significant than the thickness of the lower specimen which has less impact on energy consumption. This work has aimed to use similar thicknesses for all welding tests.

#### **4.7 Width and length of specimen**

The dimensions of the specimens that are used in ultrasonic metal spot welding are prepared according to the specifications provided by ASTM Standard and British Standard, and relative to the diameter of the horn tip, which is 4 mm. The dimension of the specimen length, which was specified according to specimen width and welding area, is 50 mm, whilst the width is 10 mm. The overlapped area is  $10 \times 10 \text{ mm}^2$ , where the welding area matches the diameter of the horn tip. Long or wide specimens that are used in USMW can sometimes make welding difficult, because the vibrations from the specimen propagate and the reflected waves are returned in anti-phase [68]. Figure 4-8 shows the geometry of the overlapped specimen position used in the ultrasonic metal spot welding tests.

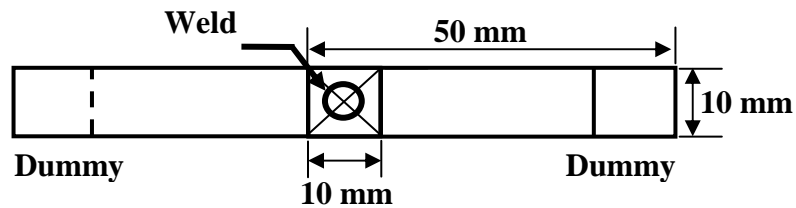


Figure 4-8 Geometry of the overlapped welding specimen showing the adding of dummies layers to ensure alignment of the specimen during mechanical testing

#### 4.8 Specimen roughness

The surface roughness of both the aluminium and the copper specimens in this study are measured with a Veeco Dektak surface profiler Model 6M, because the roughness is considered as one of the critical parameters that affects the weld strength [70]. The calibrated instrument is capable of measuring a variety of substrates through indication of the average roughness,  $R_a$ . The Dektak instrument utilises a diamond tipped stylus to measure features with an x-y precision stage which is moved over the specimen under the stylus. The vertical displacement of the stylus is converted into an electrical signal corresponding to the dimensions of the test specimen, and then converted into a digital format which can be displayed on a screen. Figure 4-9 shows the roughness instrument used in this study.



Figure 4-9 Dektak model-6M instrument for measuring specimen surface roughness [119]

The roughness of the test specimens is measured by determining the arithmetic height of roughness irregularities that are measured from the mean line within the evaluation length, which is 2 mm [28]. In the experiments, each test is repeated 5 times for each configuration and for every metal thickness. It is calculated with the Equation (4.3). Figure 4-10 shows how to determine the roughness average. The results of the roughness for aluminium and copper specimens with thicknesses of 0.1, 0.3 and 0.5 mm, are tabulated in Table 4-4.

$$R_a = \frac{1}{L} \int_0^L |y| dx \quad 4.3$$

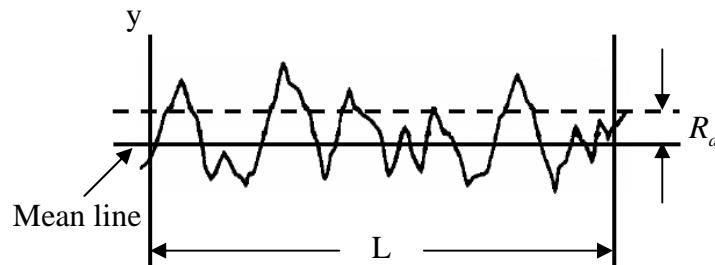


Figure 4-10 Scan roughness profile automatically measured with step detection software [28]

Table 4-4 Roughness results for the tested aluminium and copper with different thicknesses, n=5 for each metal thickness

Material	Aluminium			Copper		
Thickness (mm)	0.1	0.3	0.5	0.1	0.3	0.5
Roughness, $R_a$ ( $\mu\text{m}$ )	0.5	1.5	3.2	0.6	1.3	3.3

It can clearly be seen that the roughness values of the selected metals vary relative to the temper condition of the metal. Half-hard specimens show higher roughness magnitudes compared with the annealed specimens, as shown in Table 4-4. If the surface roughness of the specimen being welded is too low, then the welding area cannot be developed due to high glide between specimens, whereas if the surface roughness is too high, hot spots may occur.

## 4.9 Hardness test

Specimens were measured to determine hardness using a calibrated Wilson-Wolpert Micro Vickers 401 HVA, as shown in Figure 4-11.



Figure 4-11 Micro hardness testing instrument

The Vickers test machine uses a diamond indenter in the shape of a square-base pyramid, which applies a 1 kN load pressed into a test metal. The Vickers hardness number, HV, is determined by Equation (4.4). The total range of hardness for metals is typically from HV100 to HV1000 [120]. In the experiments, each test is repeated 5 times for each configuration and for every metal thickness. The measured values for hardness are tabulated in Table 4-5.

$$HV = 1.8544 \cdot F / d^2 \quad 4.4$$

$F$  is the force in kN and  $d$  is the average length of the diagonal of the indenter in mm .

Table 4-5 Hardness of aluminium and copper specimens of different thickness, n=5 for each metal thickness

Material	Aluminium			Copper		
Thickness (mm)	0.1	0.3	0.5	0.1	0.3	0.5
Hardness number, HV	273 ± 40	544 ± 70	676 ± 70	517 ± 70	563 ± 80	863 ± 20

In Table 4-5, it can be seen that copper has higher hardness than aluminium. In welding, the hardness is a weldability indicator, meaning that an increase in hardness will lower the weldability of the metal [17], because harder metals require more energy to generate welds than softer metals.

#### 4.10 Ultrasonic metal spot welding rig

The ultrasonic metal spot welding rig is shown in Figure 4-12. The welding system is composed of ultrasonic generator, ultrasonic transducer, spot welding horn, stationary anvil, mounting holder, fixing tools and fixtures. The Sonic System generator (Model L-500) supply the power to the transducer which is used to convert the electrical signal into mechanical vibration represented at the output working surface of the transducer. The transducer is excited with operating frequency of 20 kHz. The L-500 ultrasonic generator which is used in the welding tests operates at a constant current and maintains a pre-set amplitude. The L-500 ultrasonic generator delivers the required voltage to maintain the current, from which a maximum amplitude of 12  $\mu\text{m}$  peak-to-peak can be produced with a current of 620 mA, whilst the voltage across the transducer can vary from 100V when unloaded to 1000V when loaded. The total acoustic power drawn by the transducer is read by the wattmeter which is located on the front panel of generator. The amplitude can be checked on the amplitude response meter.

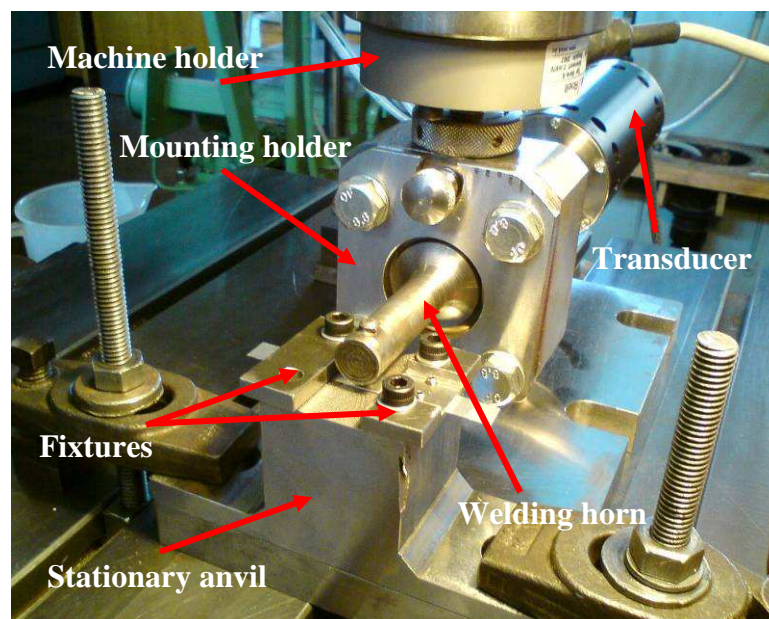


Figure 4-12 Ultrasonic metal spot welding rig as set-up in the Zwick/Roell test machine

In the current project, the ultrasonic spot welding horn was securely connected to the transducer, the tensile test machine Zwick/Roell is employed to fix the welding stack securely by holding it at the nodal plane. A mounting holder was designed for this purpose. The benefit of using the tensile test machine is to control the applied load over the welded specimens, and to allow a wide range of testing loads by using a large capacity 2 kN load cell which is sufficient for joining thin metals, as well as to provide stability to the affixed stationary anvil and fixtures on the high rigidity machine bed. The machine software records the results of the welding tests. The specimens are supported between the horn tip and the stationary anvil, where the knurled surface of the horn tip touches the upper specimen during the weld, whilst the lower specimen is held up by a knurled stationary anvil. This produces relative motion between the intimate surfaces to improve bonding. To ensure weld alignment, specimens must be held in a fixture to maintain pressure between them. Rigid fixtures which are used in all welding trials are made from stainless steel. Knurled surfaces for the horn and anvil with the alignment fixture are shown in Figure 4-13.

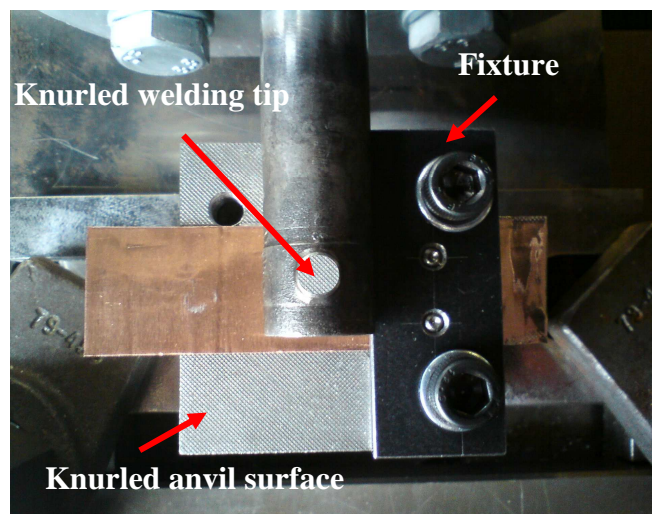


Figure 4-13 Knurled horn and anvil surfaces with alignment fixture

#### 4.11 Preparation of welding coupons

Many weld configurations were produced in this work in order to obtain quality welds and study the impact of various process parameter settings on weld strength and quality using different specimen thicknesses. For the welding of similar metals, these configurations were arranged as aluminium-aluminium, Al-Al, and copper-copper, Cu-Cu, whereas in the welding of dissimilar metals, they were arranged as Al-Cu (meaning Al over Cu) and Cu-

Al (Cu over Al). The specimens were also subjected to different heat treatments, such as annealing and half-hard tempering. The mechanical properties of the aluminium and copper that are used in this study are obtained from the calculations of Table 4-2 and Table 4-3, which the data are located within the range of metal properties that obtained from Goodfellow. The data are tabulated in Table 4-6.

Table 4-6 Mechanical properties of aluminium and copper, (density and poisson's ratio from Goodfellow, data from tensile testing machine)

Material Specimen (Aluminium)			
Temper	<u>Annealed</u>	<u>Half-hard</u>	<u>Half-hard</u>
Thickness, mm	0.1	0.3	0.5
Density, kg/m <sup>3</sup>	2700	2700	2700
Poisson's ratio	0.345	0.345	0.345
Modulus of elasticity, GPa	70.1	69.8	70.0
Yield strength, MPa	56.1	113.7	90.9
Ultimate tensile strength, UTS, MPa	68.9	123.7	104.2
Material Specimen (Copper)			
Temper	<u>Annealed</u>	<u>Annealed</u>	<u>Half-hard</u>
Thickness, mm	0.1	0.3	0.5
Density, kg/m <sup>3</sup>	8960	8960	8960
Poisson's ratio	0.343	0.343	0.343
Modulus of elasticity, GPa	120.8	120.4	120.3
Yield strength, MPa	46.1	81.4	170.9
Ultimate tensile strength, UTS, MPa	93.4	93.4	211.1

#### 4.12 Experimental set-up of ultrasonic metal spot welding

Prior to welding, the tensile test machine Zwick/Roell was pre-set to record the data of clamping force and welding time. The value of clamping force must remain constant during the whole welding process. The range of the weld time was set by the program of the tensile machine. Ultrasonic parameters such as the supplied power and vibration amplitude were also set prior to welding. Different values of vibration amplitude were set by controlling the ultrasonic generator. The maximum value of the amplitude which was recorded at the working surface of the transducer was 12  $\mu\text{m}$ . This value of amplitude is not sufficient to produce weld. The gain 4.108, of the designed welding horn provides sufficient amplitude magnification for successful welding. The specimens were cut and

placed in an overlap position to achieve the condition of spot welding. The knurled horn tip was clamped to the upper specimen whilst the lower specimen was held by the knurled surface of the stationary anvil. All specimens were welded with no prior surface treatments such as removing grease or lubricant. The test of each weld coupon was repeated to ensure confidence of the welding process. Many tests were repeated by application of the same welding conditions. Variable and constant parameters that are used in the ultrasonic spot welding processes are tabulated in Table 4-7.

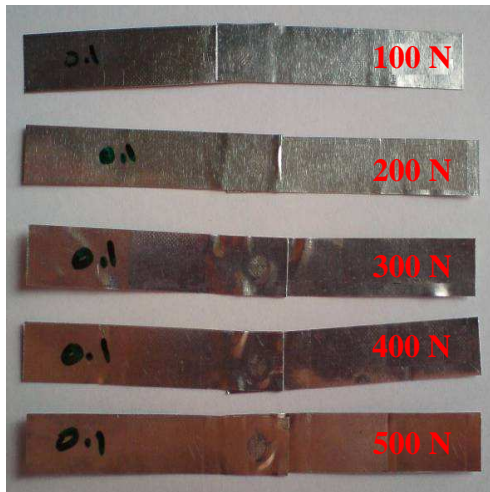
Table 4-7 Variable and constant parameters used for ultrasonic metal spot welding

Variable parameter	Value	Constant parameter	Value
Ultrasonic power, W	100-1000	Specimen dimension, mm	50 x 10
Clamping force, N	10-1000	Welding time, sec	1.0-3.0
Metal thickness, mm	0.1, 0.3, 0.5		
Amplitude of vibration, $\mu\text{m}$	17-42		

#### 4.13 Al-Al and Cu-Cu weld coupons

The first set of experimental tests involved the welding of similar metals in the arrangements of Al-Al and Cu-Cu. Most studies recommend that the thin specimen is placed nearer to the welding tip to allow a high amount of ultrasonic energy to be transferred to the welding zone, whilst the thicker specimen is placed near the anvil where the power consumption has little effect [9, 121]. In this study, all weld coupons were produced from joining specimens with the same thickness. The amount of ultrasonic energy passed to the specimens being welded is proportional to the clamping force, amplitude of vibration and welding time. Therefore, to weld the specimens together, a certain amount of ultrasonic energy is necessary. This will depend on the assembly of the components and the capacity of the ultrasonic transducer. Insufficient power can produce weak welds due to inadequate growth of the deformed area, however excessive power can result in a severely deformed weld, where the damage can be observed on the surface of the joined specimens after debonding. This can lead to a deterioration of the weld strength and the introduction of cracks in the formed weld [122]. The clamping force must be sufficiently high to prevent sliding between the horn tip and the upper specimen, especially for high horn amplitude. If the clamping force is too high, then the friction generated between specimens is increased. This can then affect the relative motion at intimate

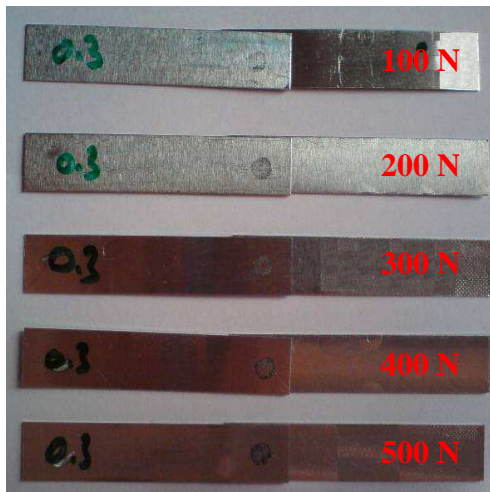
surfaces, whilst if the clamping force is too low, then the contact area between the surfaces is not sufficient to produce a proper weld. The magnitude of amplitude of the horn tip is related to the increased voltage of the generator. As the voltage is changed, the amplitude is also changed. If the amplitude is low, then the weld produced is insufficient, because low amplitude with low clamping force means that a longer time is required to achieve a good weld, due to the difficulty of removing the oxide film from the surface. However if the amplitude is very high, then the specimen may not be held correctly in position. Furthermore, excessive amplitude may lead to the production of specimen marking and sticking of the surface of the upper specimen with the horn tip [5]. The ultrasonic welding technique allows easy joining in a sufficient time, usually 1 second. However, the increased or decreased time required can affect the quality and strength of the weld [67]. Prolonged welding time causes fatigue damage, whilst insufficient time can result in incomplete welds. In the experiments, the welding time was mostly set to 1 second however different tests were carried out by extending the welding time to 2 or 3 seconds, to allow more energy transferred to the welding zone, especially when welding the thicker weld coupons. Figure 4-14 (a) and (b) shows the welded coupons for the welding of similar metals, Al-Al and Cu-Cu, for different sets of welding conditions. The welding parameters have to be carefully controlled, where suitable settings can be determined from the welding tests, and can be identified through the examination of weld strength.



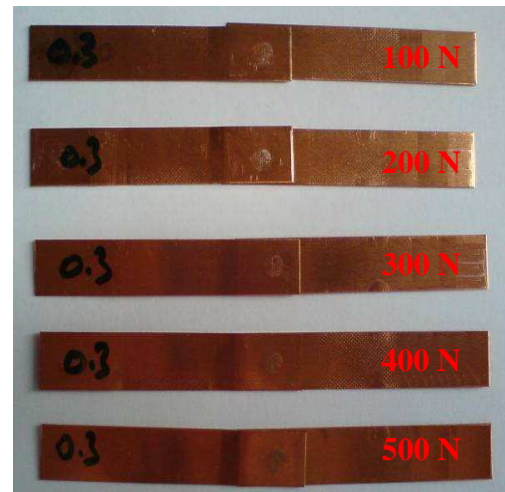
Al-Al specimens, thickness 0.1 mm



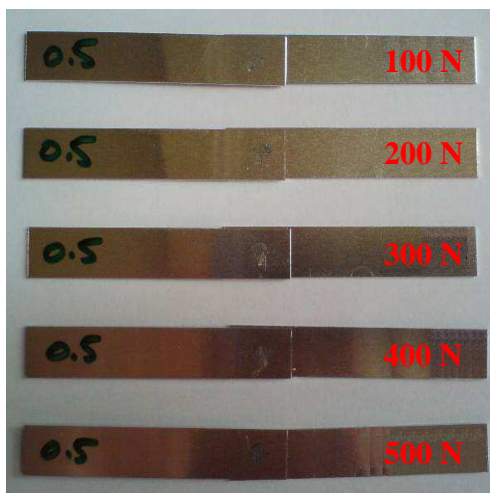
Cu-Cu specimens, thickness 0.1 mm



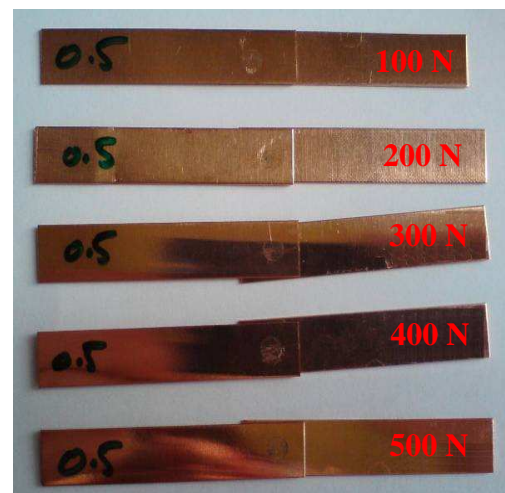
Al-Al specimens, thickness 0.3 mm



Cu-Cu specimens, thickness 0.3 mm



Al-Al specimens, thickness 0.5 mm



Cu-Cu specimens, thickness 0.5 mm

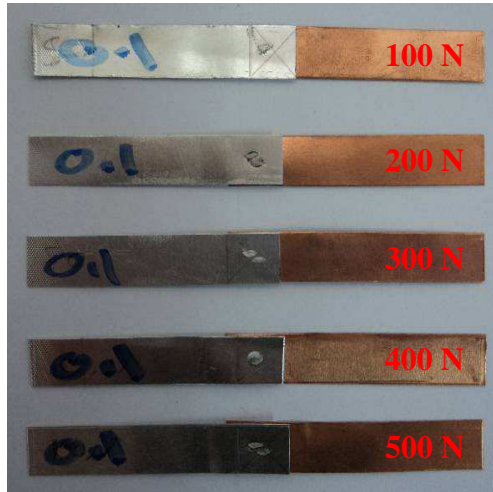
(a)

(b)

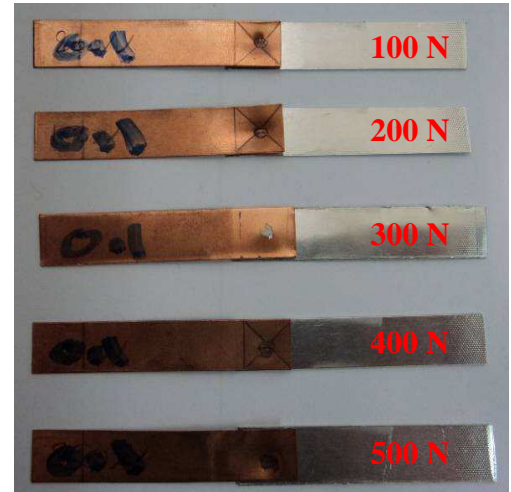
Figure 4-14 Ultrasonic welding coupons of similar metals: (a)- Al-Al and (b)- Cu-Cu with different welding conditions: clamping force 100-500 N, vibration amplitude 42  $\mu$ m, welding time 1-3 sec

#### **4.14 Al-Cu and Cu-Al weld coupons**

The second set of tests was carried out on the joining of dissimilar metals in Al-Cu and Cu-Al arrangements. In the experiments, the first arrangement of the welded coupons to be tested was the Al-Cu configuration. The aluminium was situated so that it touched the horn tip surface, whilst the copper was placed underneath over the stationary anvil. A further welding procedure was conducted by placing the copper specimen touching with the horn tip surface, and the aluminium placed on the anvil, to obtain a Cu-Al configuration. It was found that in general, the energy consumption depended on the properties and thickness of the specimen which was placed in touch with the horn tip. Several factors were found to affect the power consumption, such as metal thermal conductivity, thickness and metal surface conditions, for example hardness and surface roughness. In the experiments, it was observed that the control of process parameters was critical for high-quality welding of Al-Cu and Cu-Al. Good welds were obtained from the joining of the dissimilar metals, however higher weldability was observed when the aluminium was placed as the upper specimen. Generally, it was shown that obtaining a good weld depends on the proper control between the clamping force, amplitude of vibration, power supply and welding time. In addition, the influence of the thickness, hardness and metal surface roughness can significantly change the weldability of the metals. Figure 4-15 (a) and (b) shows the welded coupons for the welding of dissimilar metals Al-Cu and Cu-Al, under different sets of welding conditions.



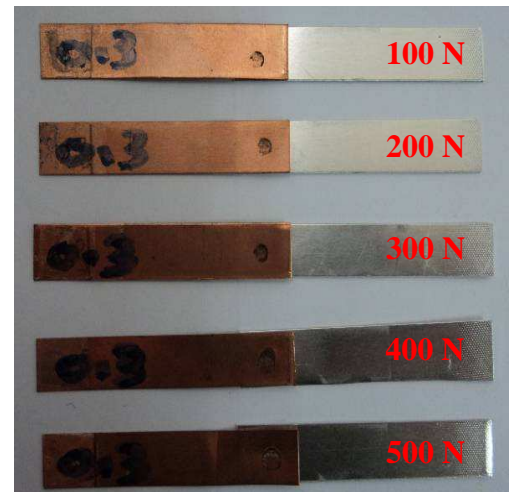
Al-Cu specimens, thickness 0.1 mm



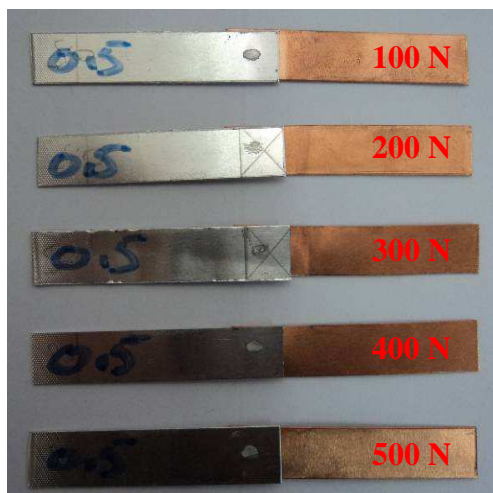
Cu-Al specimens, thickness 0.1 mm



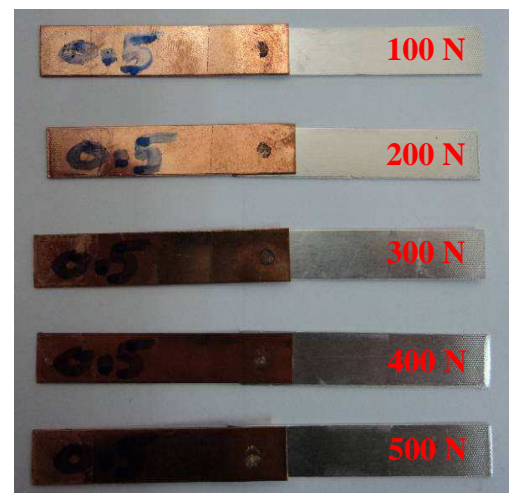
Al-Cu specimens, thickness 0.3 mm



Cu-Al specimens, thickness 0.3 mm



Al-Cu specimens, thickness 0.5 mm



Cu-Al specimens, thickness 0.5 mm

(a)

(b)

Figure 4-15 Ultrasonic welding coupons of dissimilar metals: (a) Al-Cu and (b) Cu-Al with different welding conditions: clamping force 100-500 N, vibration amplitude 42  $\mu\text{m}$ , welding time 1-3 sec

#### 4.15 The development of the weld

A lateral-drive ultrasonic configuration system was designed for the welding of thin metals, which was capable of studying the effects of varying process and metal parameters on weld strength and quality. The tensile machine program and ultrasonic generator were set to control the process parameters. Figure 4-16 illustrates the set-up of the complete ultrasonic metal spot welding system.

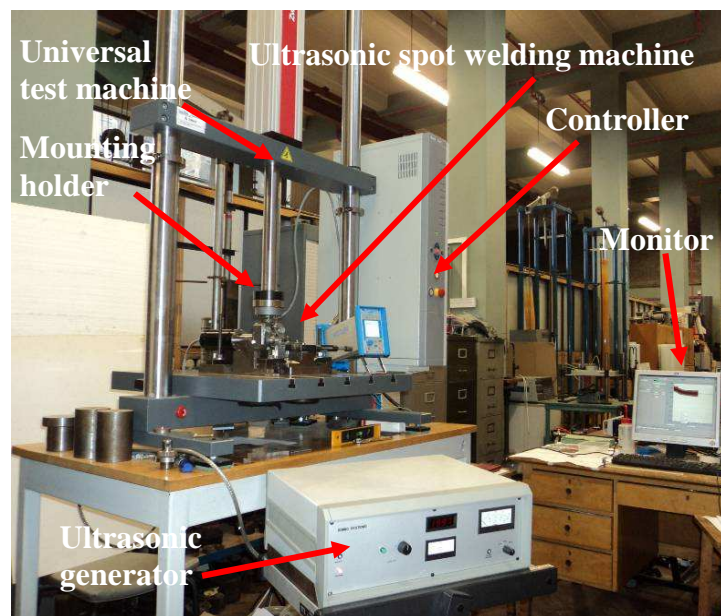


Figure 4-16 Set-up of the complete USMW system

The metals were chosen to be welded together in different arrangements, such as Al-Al, Cu-Cu, Al-Cu and Cu-Al. A number of the specimens were also subjected to different heat treatments, and so a proportion of the specimen configurations were annealed and the others were in the half-hard temper condition. The mechanical properties of the materials in these conditions are tabulated in section 4.11. The relationships between the process and metal parameters with respect to the thickness and type of metals affect the weldability of joined specimens. The term ‘good’ weld is defined as when the two specimens are welded together, with no indication of failure detected on the edge of the welding area, and where the welded specimens are fixed together such that a relatively high force would be required to prise them apart. However, a ‘bad’ weld is usually referred to as a weak bonded joint, which can be easily fractured with a relatively low force [87]. Again, a uniaxial tensile test machine was adopted to examine the strength of the joint in terms of weld strength, which

was obtained from knowledge of the value of maximum force. If separation of the joined specimens can be obtained from the force acting normal to the weld interface, then the breaking force is called the tensile weld strength, and at the same time, the shear weld strength can be determined by measuring the shear force acting parallel to the weld interface [55]. In this study, the strength of the welded specimens was evaluated using the Zwick/Roell test machine. The test consisted of pulling the overlap-welded specimen in tension by the two machine-arm grips as seen in Figure 4-17. The lower arm is normally fixed whilst the upper arm is moved at a cross-head speed of 0.1 mm/min.

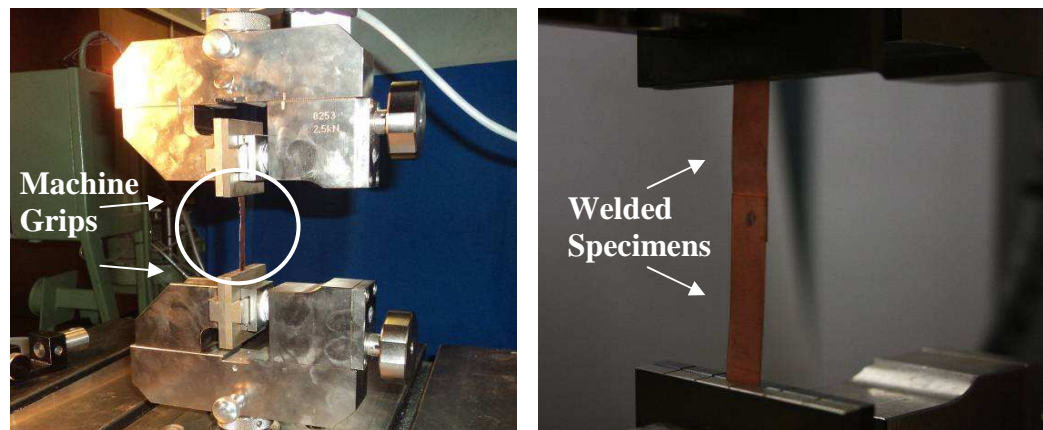


Figure 4-17 Set-up of the welded specimens on the Zwick/Roell tensile test machine

The yield strength, ultimate strength and fracture, whether by shearing of the welded specimens or by a tearing of the parent metal, were all recorded by machine software. The most commonly monitored variable in tensile testing is the peak load (maximum force), which is measured by the machine load cell. However, an accurate measurement of the displacement at the peak load (maximum displacement) must also be monitored and can be extracted through extensometry measurements. The extensometer set-up is shown in Figure 4-18. Lap-shear specimens are ideal in the study of the shear strength of welded joints, and the studies of the weld strength for weld coupons of similar and dissimilar metals with thicknesses of 0.1, 0.3 and 0.5 mm are outlined in the forthcoming sections.

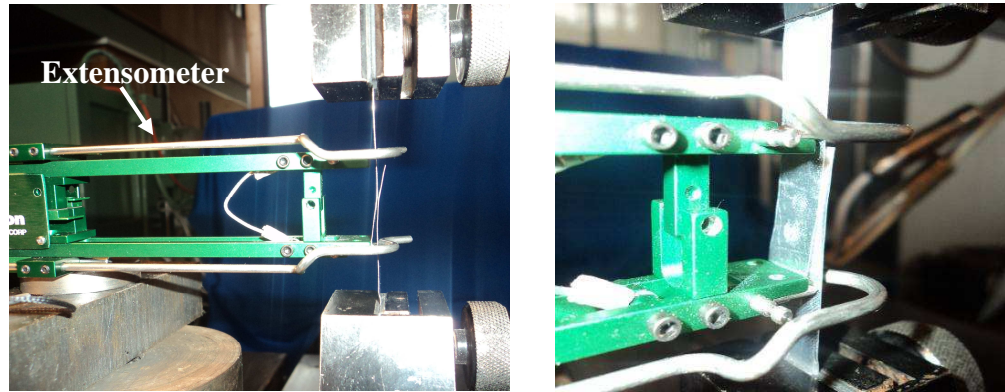


Figure 4-18 Set-up the extensometer in tensile test machine

#### 4.16 Ultrasonic spot welding for weld coupons of similar metals

The first sets of experiments were conducted to weld the coupons of Al-Al and Cu-Cu, where three different thicknesses of each metal, consisting of 0.1, 0.3 and 0.5 mm thick specimens pass. The ultrasonic spot welding process was applied for different sets of parameters. The complete process time was set to be 1 second for the majority of the tests, and was controlled by the machine software. Further tests were performed with a complete process time of up to 2 or 3 seconds, especially for joining metals of greater thickness. Welding time was set by machine software to allow the clamping force to be applied within a short period time, 1 second. The clamping force was specified according to the capacity of the machine load cell, and varied from 10 N up to 1 kN. Different power inputs were also applied through using regulator which allows changing the voltage supplied to the generator across the constant current, resulting in different magnitudes of vibration amplitude, ranging from 17  $\mu\text{m}$  to 42  $\mu\text{m}$ . The power drawn from the welding stack is recorded from the wattmeter of the ultrasonic generator. In the experiments, the amplitude must remain unchanged during the whole test. Many tests were conducted to obtain good quality welds using different thicknesses of aluminium and copper specimens. The welded specimens were debonded using a tensile test machine to determine the joint strength of each test.

##### 4.16.1 0.1Al-0.1Al and 0.1Cu-0.1Cu weld coupons

In this study, the data of maximum load which are obtained from the tensile testing of all combinations can be considered to the indication of weld strength. The lap-shear test,

considered as a destructive test, was used to debond the welded specimens in a tensile test machine until the weld spot or the specimens failed, and the maximum value of the load was measured in order to obtain the weld strength. Figure 4-19 shows the tensile shear test of the welded coupons of 0.1Al-0.1Al and 0.1Cu-0.1Cu. Different configurations and settings of process parameters produced welds with different strengths. In general, the 0.1 mm thick specimens tore rather than debonded. The maximum load magnitudes were determined from the average values of three tensile tests, which were extracted for each setting of clamping force and vibration amplitude, with a welding time equal to 1 second.

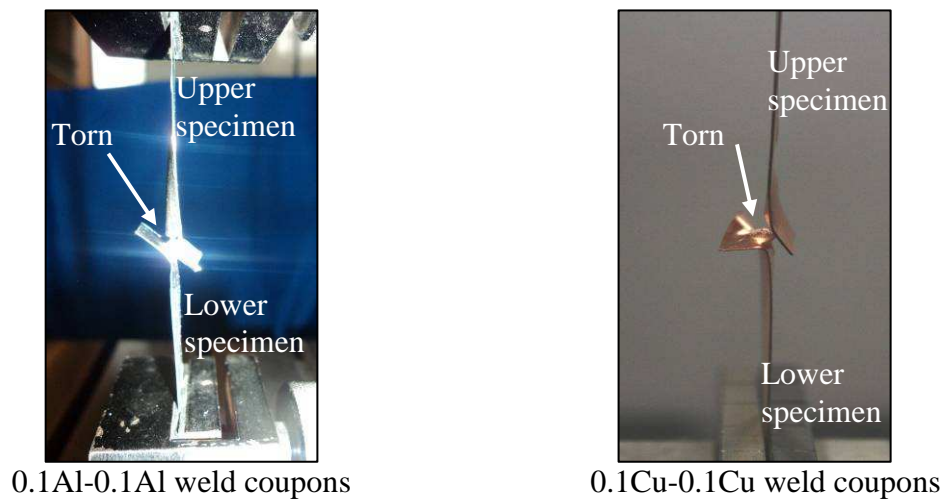


Figure 4-19 Tensile-shear testing of the welded coupons for aluminium and copper metals at thicknesses of 0.1 mm

Higher values of maximum load were obtained from debonding the Al-Al joined specimens compared to the Cu-Cu specimens. This shows that the values of welding strength were influenced by the selection of process parameters with respect to the thickness and metal surface conditions, such as hardness and surface roughness. It should be noted that both aluminium and copper specimens were 'annealed'. It was seen from the experiments that the strength of the weld increased with increased applied force and vibration amplitude but, in some cases, the tensile test for these bonded specimens resulted in tearing around the weld area rather than a debonding separation of the lower and upper specimen.

#### 4.16.2 0.3Al-0.3Al and 0.3Cu-0.3Cu weld coupons

The strengths of the weld coupons of 0.3Al-0.3Al and 0.3Cu-0.3Cu were determined by analysing the debonding between the joined specimens. The lap-shear test was run until either the spot weld or the joined specimens were failed. Then the peak value of the pulling load were recorded which indicated the maximum weld strength. Figure 4-20 illustrates the tensile shear test of the welded coupons of 0.3Al-0.3Al and 0.3Cu-0.3Cu. The tests were conducted on welds of similar metals under different configurations of ultrasonic parameters, of which the average values of maximum load were obtained. The magnitudes of the maximum load were determined from the average values of three tensile tests which were extracted from joining specimens at each clamping force setting and vibration amplitude level and ensuring that the duration of the processes do not exceed 1 second. Again, higher weld strengths were recorded for the debonded Al-Al specimens compared with the Cu-Cu specimens. Generally, the energy consumed is higher with the thicker or harder metals compared with thinner metals [9]. Therefore, more energy was consumed with the half-hard aluminium relative to the annealed copper in spite of their similar thicknesses. During experiments, tearing of the upper specimen was identified for both welded coupons of aluminium and copper, where the weld had involved a high applied force and high vibration amplitude.

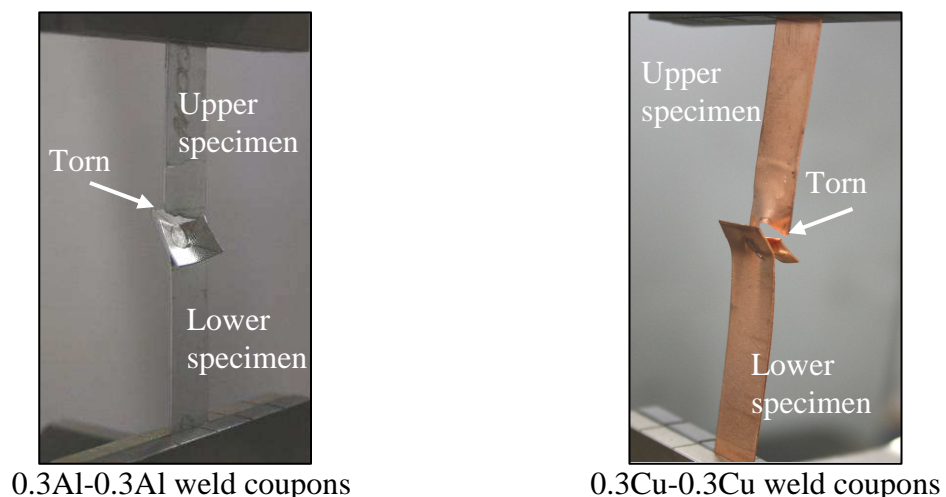


Figure 4-20 Tensile-shear test of the welded coupons for aluminium and copper metals at thicknesses of 0.3 mm

### 4.16.3 0.5Al-0.5Al and 0.5Cu-0.5Cu weld coupons

The same procedure for extracting weld strength was applied in the debonding of the weld coupons of 0.5Al-0.5Al and 0.5Cu-0.5Cu, as shown in Figure 4-21. Again, the maximum load data was obtained from the average magnitudes of three tensile tests which were conducted on specimens which were joined for each clamping force setting and vibration amplitude level. It was clear that the thickness, hardness and surface roughness are the predominant factors governing the required amount of consumed power at the weld zone. Furthermore, the 'half-hard' condition of both the aluminium and copper metals influences the amount of energy transferred to the welding area. It was noted here that the specimens were debonded after completing the test but the whole welded associated with the lower and upper specimen remained stuck to the lower specimen. Furthermore, the specimens of the two metals show no indication of tearing of the parent metal. this is indicative of a good weld but not necessarily a strong weld.

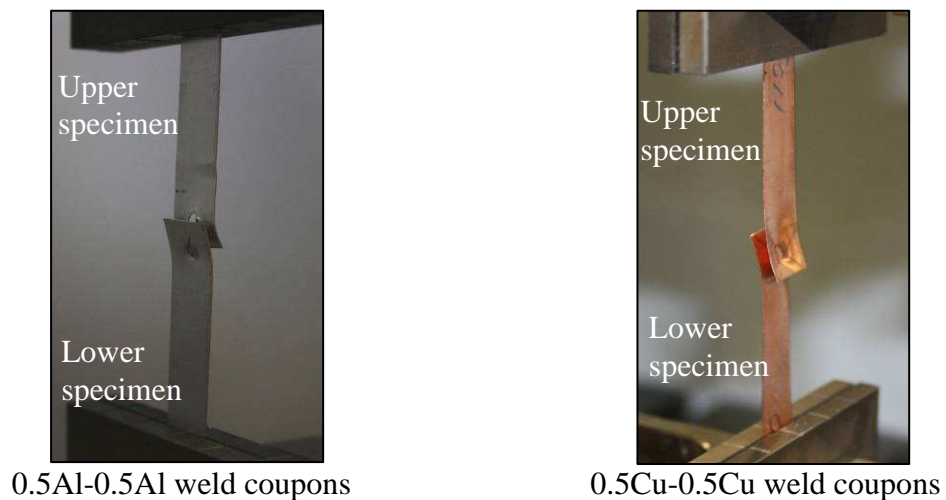


Figure 4-21 Tensile-shear test of the welded coupons for aluminium and copper metals at thicknesses of 0.5 mm

### 4.17 Ultrasonic spot welding for weld coupons of dissimilar metals

The second set of experiments which were conducted involved the weld coupons of Al-Cu and Cu-Al, and again three different thicknesses of each metal were considered, comprising 0.1, 0.3 and 0.5 mm, with each weld coupons consisting of equal joining metal

specimen thicknesses. As in welding of similar metals, the welds were generated for different process parameter configurations, and the time for the welding process was set at 1 second, with the exception for the relatively large thickness of 0.5 mm. The time for this thickness is increased to enable the delivery of more energy to the joining area. The clamping force range was controlled by the machine load cell, and set to vary from 10 N up to 1 kN. During welding, the amplitude of the horn tip must be constant. When welding dissimilar metals, it is important to determine which joining metal is placed in contact with the horn tip rather than underneath, as many studies show that the placement of the softer metal in contact with the horn tip can increase the energy transmission to the welding area, which results in greater weld strength[27, 70].

#### 4.17.1 0.1Al-0.1Cu and 0.1Cu-0.1Al weld coupons

The lap-shear test was carried out in order to examine the weld strengths of the weld coupons of 0.1Al-0.1Cu and 0.1Cu-0.1Al. Details from this tensile test are shown in Figure 4-22. Many tensile tests were undertaken to examine the strength of the welded joint, and the results were extracted from the joining specimens with different process parameter settings. The average values were determined from three repeat tests. It was seen from the images of Figure 4-22, that the specimens were debonded after completing the test with no tearing of the deformed surfaces. This indicates that dissimilar metals require more power and time to provide a strong weld.

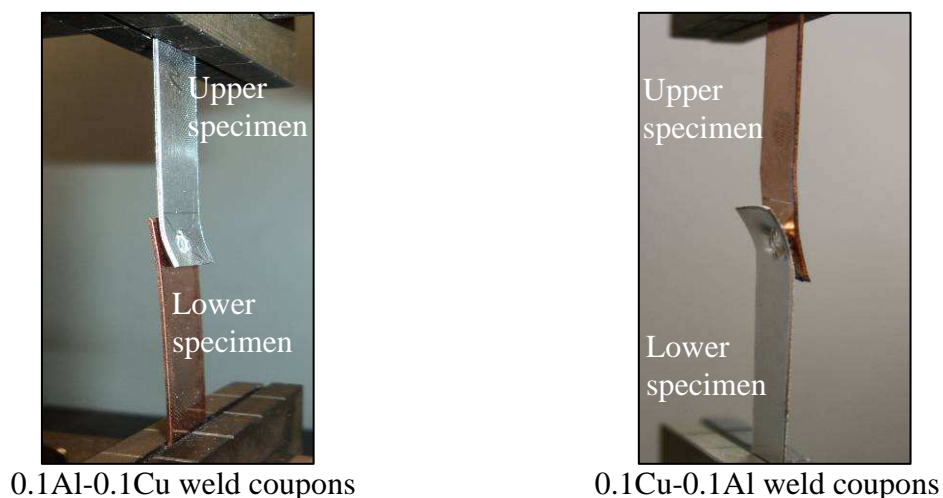


Figure 4-22 Tensile-shear test of the welded coupons for aluminium and copper metals at thicknesses of 0.1 mm

#### 4.17.2 0.3Al-0.3Cu and 0.3Cu-0.3Al weld coupons

The welding experiments for the weld coupons of 0.3Al-0.3Cu and 0.3Cu-0.3Al were carried out for different process parameter settings. Figure 4-23 illustrates the tensile shear test of weld coupons of 0.3Al-0.3Cu and 0.3Cu-0.3Al. The magnitudes of the maximum load were extracted from the average values found from three tensile tests which were conducted on the specimens which were joined at each clamping force setting and vibration amplitude level. Again, higher weld strengths were recorded for the debonded Al-Cu compared to the debonded Cu-Al specimens, as the amount of ultrasonic energy delivered to the welding area varied depending on the thickness and metal surface conditions. In Figure 4-23, the images show that the debonded of joined specimens show slight bend of the overlapped areas with no indications of the dislocation to the deformed areas. Generally, the amount of energy consumed is higher with thicker or harder materials compared to thinner metals [9]. Therefore, more power was consumed by ‘half-hard’ aluminium than ‘annealed’ copper. However excessive energy can deteriorate the weld integrity through fatigue initiation at the welding area or shearing of the formed weld, resulting in lower bond strength.

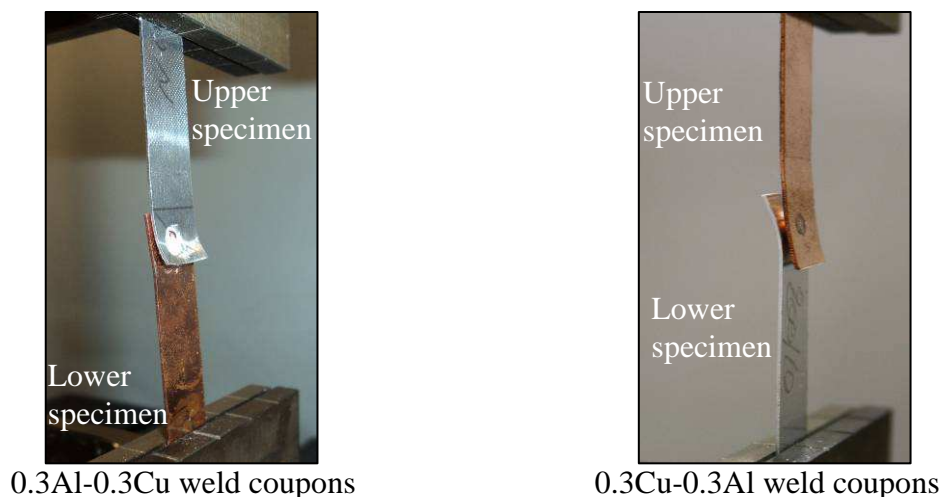
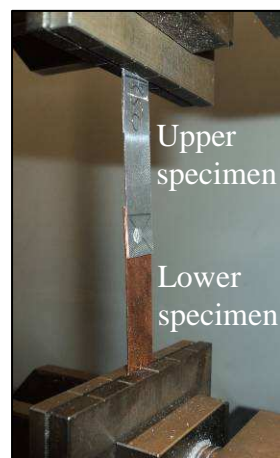


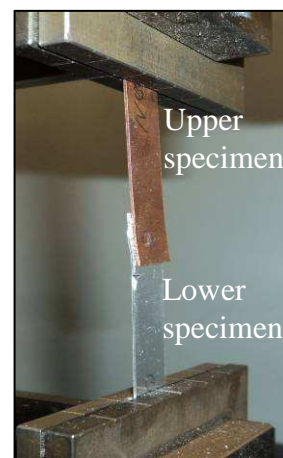
Figure 4-23 Tensile-shear test of the welded coupons for aluminium and copper metals at thicknesses 0.1 mm

### 4.17.3 0.5Al-0.5Cu and 0.5Cu-0.5Al weld coupons

In this part of the experiments, the thickness of the joint significantly affects the weld strength, as the two metals which are used are both in the ‘half-hard’ material condition. The first set of tests was carried out by placing the aluminium specimen in contact with the horn tip, whilst the copper specimen was situated underneath over the fixed anvil. The experiments were repeated but with a change in applied clamping force, amplitude of vibration, welding power and welding time for each test. The maximum load was measured using tensile testing. In the second part of the experiments, the welds were produced making the specimen in contact with the horn tip to be copper. Similar welding conditions were applied to produce a high-quality joint, but the debonded specimens’ exhibit variations in terms of maximum load. There are many ways in which the weld strength can be influenced, such as insufficient welding time or applying too low a value of clamping force. In addition, if the hardness and surface roughness of the upper metal are too high, then this can lead to an increase in energy dissipation which results in an improper weld. Figure 4-24 shows the tensile shear test of the weld coupons of 0.5Al-0.5Cu and 0.5Cu-0.5Al for different parameter configurations. The average values are determined from three tests for each weld. The thicker specimens with different hardness and surface roughness result in welds with relatively low strength, as part of energy was dissipated. This leads to debonding of the overlap areas with no indication of specimen bending and no observing of torn surfaces.



0.5Al-0.5Cu weld coupons



0.5Cu-0.5Al weld coupons

Figure 4-24 Tensile-shear test of the welded weld coupons for aluminium and copper metals at thicknesses of 0.1 mm

## 4.18 Summary

Investigations of the aluminium and copper metals that are used in ultrasonic metal spot welding tests have been carried out. All metals were cut and prepared according to the standard test procedure for the ultrasonic spot welding of thin specimens, and material specifications were defined according to international standards. The mechanical properties of the aluminium and copper were investigated using uniaxial tensile testing with extensometry over a range of crosshead velocities. The mechanical properties of each metal were determined using conventional stress-strain relations to extract the Young's modulus, yield strength and ultimate tensile strength, and each test was repeated for three different thicknesses of 0.1, 0.3 and 0.5 mm with different metal tempering. Hardness and specimen roughness were investigated for the different thicknesses, as these parameters can affect the weldability of the joined metals. The ultrasonic spot welding system was mounted on the tensile test machine so that a series of experiments on the welding of aluminium and copper metals by the control of different process and metal parameters could be conducted. Many tests were performed on the welding of similar and dissimilar welding configurations, such as Al-Al, Cu-Cu, Al-Cu and Cu-Al, to allow the study of strength and quality for a range of welding conditions. Good welds were obtained for tests involving constant parameters. The weldability of the specimens to be joined varied depending on the clamping force, amplitude of vibration, welding power and welding time settings. In addition, the studies on the properties of the welded specimens such as thickness, hardness, surface roughness and oxides have shown that they affect the ability to weld, and the relation between process parameters and metal parameters with respect to the specimen thicknesses shows that the weldability of the joined metals was affected, due to the influence on weld strength and the quality of the weld. Further discussion on the relationships between process parameters such as clamping force, amplitude of vibration, welding time and power supply is included in Chapter 5.

## **Chapter 5**

### **Ultrasonic welding experiments and finite element simulation results**

#### **5.1 Introduction**

This chapter presents the welding analysis and the experimental results which were obtained from the ultrasonic metal spot welding tests. The experimental results of each welding process are discussed for weld configurations of Al-Al, Cu-Cu, Al-Cu and Cu-Al, for specimen thicknesses of including 0.1, 0.3 and 0.5 mm. The strengths of the welded specimens were investigated by varying the parameters of clamping force, amplitude of vibration, welding power and welding time. In addition, the influence of metal conditions and surface properties was studied by investigating the effect of metal hardness and also metal surface condition such as surface roughness and oxides which affect the specimens. The temper states of the selected aluminium and copper were either annealed or half-hard for the range of specimens used in the weld tests. Ensuring matches of process parameters coupled with the relevant specimen thickness can result in a high weld strength and good weld quality. In this research, an approach was used to solve issues that are often encountered when using this technique, such as horn/specimen adhesion, specimen marking and the ability to enhance weld strength through using stepped amplitude profiling. Also, the mechanical properties of aluminium and copper which were outlined in Chapter 4 were used in the FE model of the joined specimens. The load-displacement curves were simulated to predict the maximum force of the debonded specimens and to correlate the results with the results of the load-displacement curves which were obtained experimentally.

#### **5.2 Study of the influence of process parameters on weld strength**

In USMW, the matching between process parameters is not simple due to complex relations between them, which influence the performance and subsequent results of the ultrasonic welding process [27, 68, 122]. In this research, it was decided to focus on the clamping force and amplitude of vibration as the two main parameters in order to study their influence on weld strength and quality of weld. Also, previous studies have set these

parameters as constant values in examining welds. All of the experiments detailed in this study were conducted on weld coupons, using three different thicknesses.

### **5.3 The influence of clamping force on weld strength**

In USMW systems, the force is usually produced hydraulically or pneumatically, or by any electromechanical system [29, 53]. However, in this study, the clamping force was applied through the uniaxial movement of the upper arm of the testing machine. During welding, the force must remain constant and act at a right angle to the plane surface of the welded specimens. The clamping force is considered to be one of the most effective means of controlling the weld strength. The machine software was set to control the applied force. After weld completion, the welding coupons were debonded by the tensile test machine then the weld strength of debonded specimens was determined from the ultimate load. Figures 5-1 and 5-2 show the variations of the weld strength against clamping force, in the joining of similar and dissimilar weld coupons of aluminium and copper metals for thicknesses of 0.1, 0.3 and 0.5 mm. The average magnitude of maximum load was determined and plotted as a function of clamping force, in increments of 50 N, for amplitudes range of 17, 30 and 42  $\mu\text{m}$ , and a constant welding time of 1 second. The double error bars in the charts represent one standard deviation of the three tests for each selected parameter. From the analysis of the debonded specimens, it was observed that the weld strength increases with clamping force, reaching a peak at a certain value of clamping force. The weld strength then decreases after this point. It is known that imparting an excessive clamping force results in high friction generation and therefore a suppression of the relative motion between intimate surfaces, resulting in a reduction in weld strength [71]. In addition, an increase in vibration amplitude also raises the welding strength. Increased amplitude means that there is a consequential increase in the scrubbing motion between metallic surfaces, which leads to better bonding and in turn raises the weld strength.

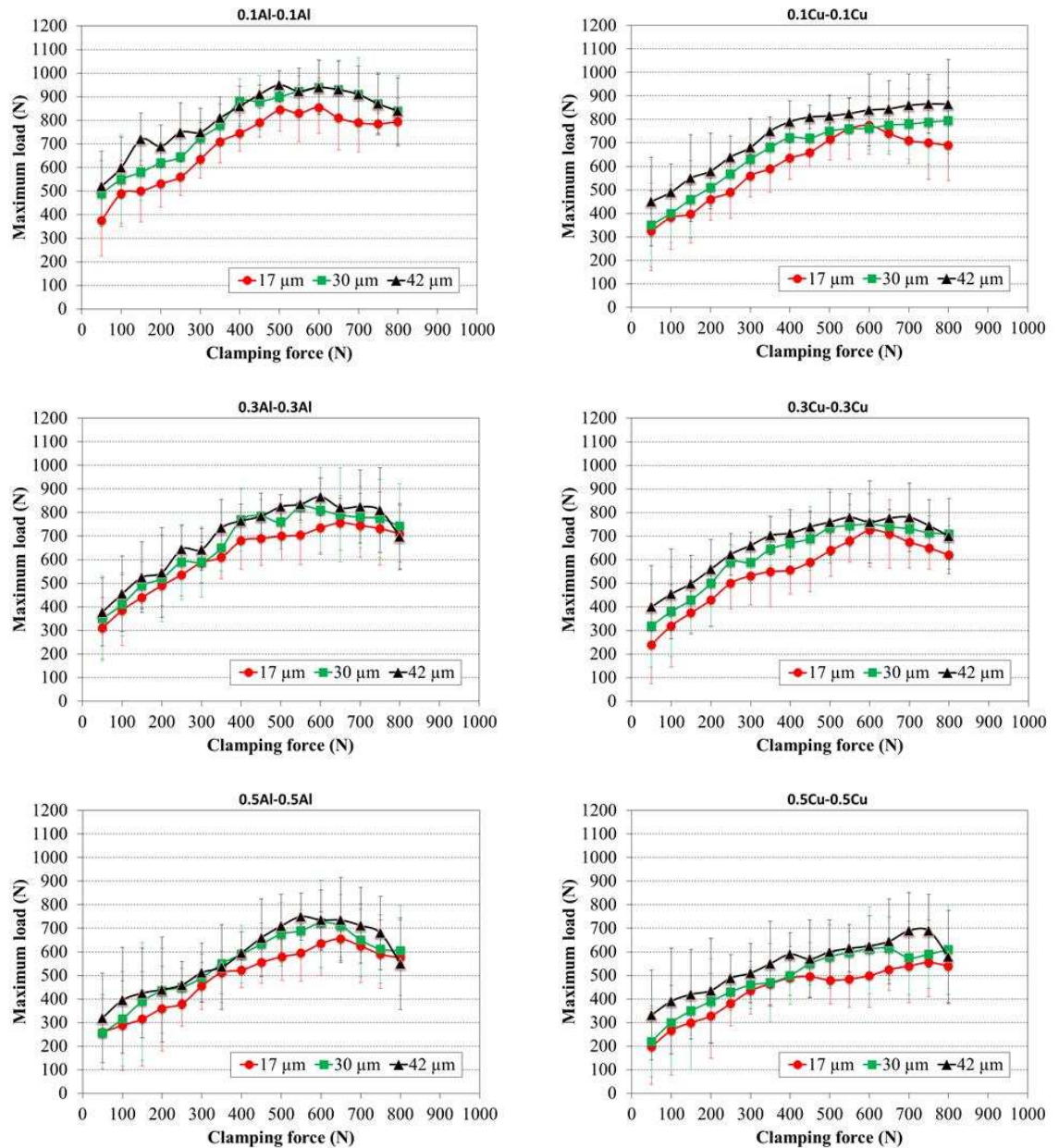


Figure 5-1 Welding strength vs. clamping force, joining similar metals, for amplitudes of 17 μm, 30 μm and 42 μm

It can be seen from Figure 5-1 that higher value of weld strength for the weld coupons of 0.1Al-0.1Al was recorded at 855 N after the clamping force fixed at 600 N, for amplitude of 17 μm. This value can be elevated by increasing the horn amplitude to magnitudes such as 30 μm or 42 μm, resulting in higher weld strengths of around 940 N and 950 N, at clamping force magnitudes of 600 N and 500 N respectively. The welding coupons of 0.1Cu-0.1Cu exhibited slightly lower weld strength. There is a difference in thermal conductivity between aluminium ( $237 \text{ Wm}^{-1}\text{k}^{-1}$ ) and copper ( $401 \text{ Wm}^{-1}\text{k}^{-1}$ ), the reason for

the lower strength is also related to the dissipation of ultrasonic energy due to the influence of hardness and surface roughness of the copper specimen, although the aluminium and copper metals of 0.1 mm specimen thicknesses are annealed (see Table 4-1). For welding coupons of 0.3Al-0.3Al and 0.3Cu-0.3Cu, the overall weld strength shows increases due to an increase in the force, up to certain point then the strength begin to lower. However, the variations between the 0.3Al-0.3Al and 0.3Cu-0.3Cu are smaller, and can be attributed to a difference in metal conditions, in that the aluminium is half-hard and the copper is annealed (see Table 4-1). Furthermore, a relatively high standard deviation was evident in the joining of 0.3Cu-0.3Cu compared to 0.3Al-0.3Al and on a number of occasions horn tip/specimen adhesion and specimen marking were observed with welding the higher vibration amplitude of 42  $\mu\text{m}$ . In the case of welding coupons of 0.5Al-0.5Al and 0.5Cu-0.5Cu, the determined data of weld strength suggested a drop relative to previous thicknesses. The increased thickness, as well as the hardness and roughness, meant that more energy was required to produce the weld, as the oxide still not completely removed between intimate surfaces. However, a prolonged welding time could lead to initiate fatigue damage or cracks [55]. Also, excessive welding time can affect the existing molecular bond in the welded area, because continuous of the scrubbing motion will begin to dislocate the bonding that formed [61, 63]. The weld strength was compromised when this thickness level was tested, especially for the welding coupons of 0.5Cu-0.5Cu, because the energy received by the weld was insufficient due to either the limitation of the generator (of up to 1 kW), the short welding cycle of 1 second or due to the severity of the oxide for the half-hard copper surface.

It is clear that the weld strength of the dissimilar metal is similar to the weld strength of the consisting of similar metals, in spite of the variation in determining data. The same welding conditions were applied when welding aluminium and copper with thicknesses of 0.1, 0.3 and 0.5 mm. Two sets of experiments were carried out on the welding of Al-Cu and Cu-Al weld coupons. Starting from the welding coupons of 0.1Al-0.1Cu and 0.1Cu-0.1Al, by continuously incrementally increasing the clamping force but keeping the welding time constant, it can be observed that the weld strength begins to increase up to 845 N at 17  $\mu\text{m}$  and with clamping force of 550 N, but after that the strength dropped to the value slightly below of 500 N. The overall strengths exhibited higher values when the ultrasonic energy was increased, and in particular the horn amplitude increase. For this condition, the strength was calculated to be around 870 N and 890 N at the two amplitude

settings 30  $\mu\text{m}$  and 42  $\mu\text{m}$  respectively, which the values were indicated at clamping force of 500 N. It is very important to consider which metal constituent of the joint must be placed on top [70], because this can effect on the amount of consumed energy at the welding area, since the surface condition of the metal is a factor which influences the energy consumed. Higher values of weld strengths were obtained when the aluminium specimen was situated on top, touching the horn tip, rather than underneath. This was confirmed with few studies which have revealed that the joint strength can be increased between 2-5 % when aluminium is situated near to the horn tip, rather than underneath [70]. Conversely, the strength of welding coupons of 0.1Cu-0.1Al exhibited low values relative to the strength was indicated from 0.1Al-0.1Cu. When welding the coupons of 0.3Al-0.3Cu and 0.3Cu-0.3Al, the debonded specimens exhibited a resistance to bonding due to the increase in thickness, because more energy was required to produce the weld within a short time. Higher standard deviations were indicated for those experiments which placed aluminium specimens at the horn tip. This was expected, because the aluminium used was configured as half-hard metal, where the hardness and surface roughness significantly influences the energy transferred to the welding area, which then results in low of the deformation, compared with the annealed copper. However, the overall strength shows higher values when joining aluminium to copper rather than joining copper to aluminium, due to the increase in vibration amplitude. For example, at a vibration amplitude of 17  $\mu\text{m}$  and relatively clamping force of 500 N, the weld strength which is measured is high for 0.3Al-0.3Cu, compared to higher strength of 0.3Cu-0.3Al, that is indicated low under the same value of clamping force.

In the welding coupons of 0.5Al-0.5Cu and 0.5Cu-0.5Al, there was some difficulty in joining the two specimens together, because the specimen thicknesses restricted the energy transferred to the deformation area, and also because there was a similarity in metal surface conditions of the aluminium and copper (half-hard), with their differences being their hardness and surface roughness. The weld strength begins to gradually increase due to the increase in clamping force, where higher weld strength magnitudes were recorded after an increase in both the clamping force (incremental) and amplitude. For example, at a vibration amplitude of 17  $\mu\text{m}$  and relatively low clamping force (below 150 N), the weld strength which is measured is low, and it is simple to break apart the welded specimens, indicating that this type of weld is of poor quality and can be referred to as a 'bad weld'. However, increase energy with a corresponding decrease in force can result in a degree of

slip between the horn tip and weld specimen, and this is obviously undesirable. Conversely, an increase in the horn velocity can impart an alteration in the resultant weld strength for high vibration amplitudes, such as 42  $\mu\text{m}$ . However, the resultant welds leads to an increase in standard deviation and leaves significant marks on the surface of the weld. Although high force was required to avoid slipping between the horn tip and work specimen, sticking can become more prevalent at higher clamping forces, particularly when clamping force exceeds 600 N, when the observed weld strength for constant amplitude becomes progressively lower.

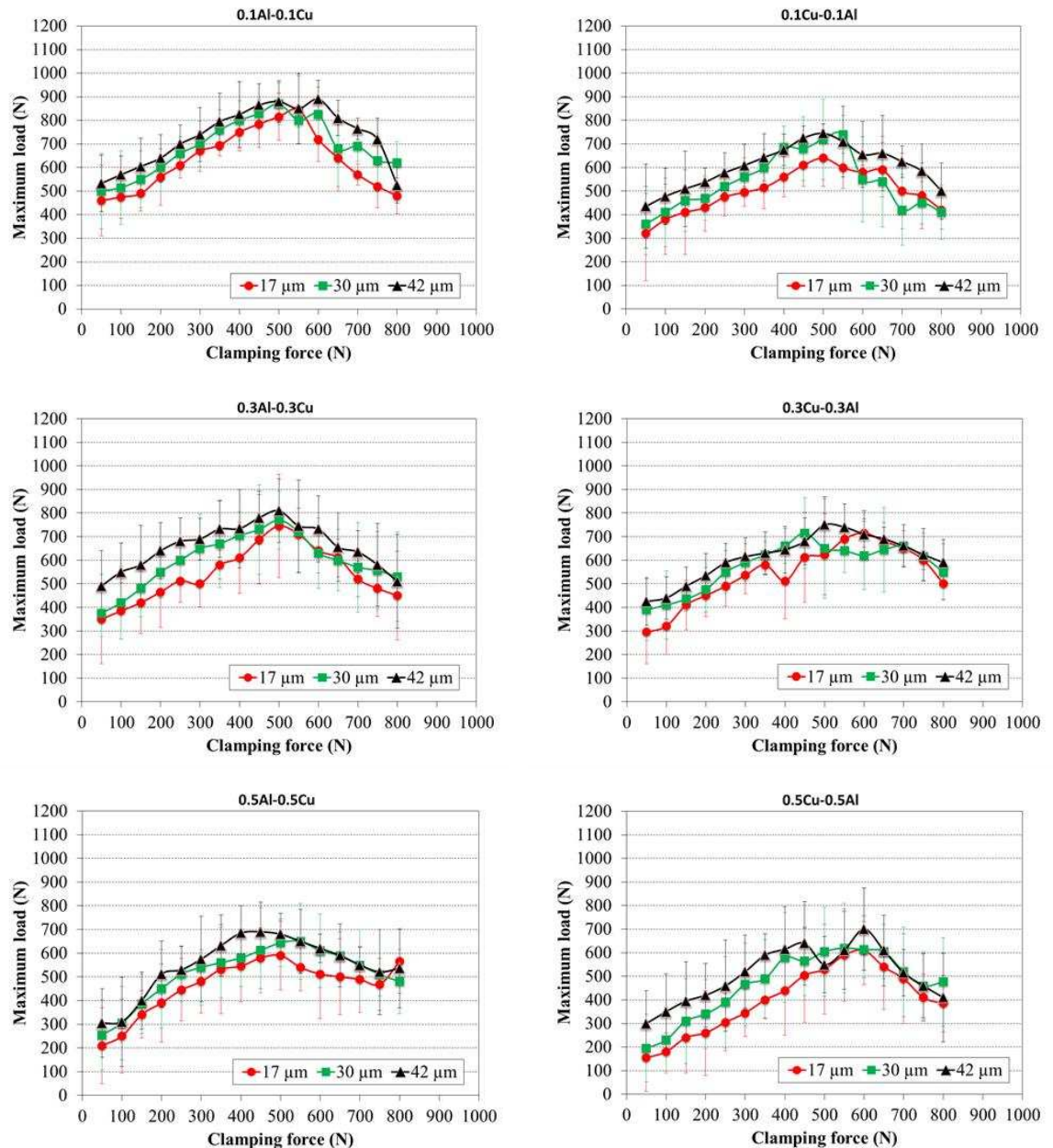


Figure 5-2 Welding strength vs. clamping force, joining dissimilar metals, for amplitudes of 17  $\mu\text{m}$ , 30  $\mu\text{m}$  and 42  $\mu\text{m}$

#### 5.4 The influence of vibration amplitude on weld strength

In this work, the horn was excited with three different setting such as 17, 30 and 42  $\mu\text{m}$ . Figures 5-3 depicts the weld strength versus vibration amplitude for the welds of similar metals for both aluminium and copper, with thicknesses of 0.1, 0.3 and 0.5 mm. The figure for each weld coupons were determined by forcing the joints to failure by means of a tensile shear test using a tensile test machine. All of the joints which were tested were subjected to clamping force magnitudes of 100, 300 to 500 N, and each test was completed

with a welding time of up to 1 second. From the first tests of the 0.1Al-0.1Al weld coupons, it was noticed that the weld strength begins to increase due to the increase in clamping force, whilst both vibration amplitude 17  $\mu\text{m}$  and welding time 1 second are kept unchanged. The raise in vibration amplitude seems to be effective on the weldability of the welded specimens, because increase amplitude results in an increase in the level of scrubbing motion between intimate surfaces. For example, this difference is observable by comparing the results for 30  $\mu\text{m}$  amplitude to the results at amplitude of 42  $\mu\text{m}$ . This was expected because an increase in amplitude can cause higher deformation between metallic surfaces, which leads to an increase the distribution of the weld and maximise the joint quality. Similar effects of the increased of vibration amplitude on weld strength were observed for the welding of the 0.1Cu-0.1Cu weld coupons. However, the extracted data shows that the welded joint has a low strength compared to the 0.1Al-0.1Al welded joint, even when the amplitude is raised to 30  $\mu\text{m}$  or 42  $\mu\text{m}$ . The metal surface conditions of the copper significantly influenced the weld strength, and had more of an effect on the joint than the aluminium surface conditions. The aluminium and copper for this type of thickness were used from annealed metals.

For the weld coupons of 0.3Al-0.3Al and 0.3Cu-0.3Cu, the weld strength was influenced by the increase in the thickness of the specimens, as well as the hardness and surface roughness of the metals. In addition to the metal conditions, the aluminium specimens were in the half-hard condition, whilst the copper specimens were in the annealed condition. As before, the tests were performed using three amplitude settings, comprising 17, 30 and 42  $\mu\text{m}$ . The weld strength begins to rise due to force increase, on the assumption that the vibration amplitude and welding time remains constant. The results exhibit much variation between aluminium and copper data. It was also observed that the energy transferred to the welding area was significantly absorbed by the individual specimens. The percentage of consumed energy varied according to the specimen thickness and metal condition, as well as the duration of the welding cycle. Higher amplitudes offer higher weld strengths for both 0.3Al-0.3Al and 0.3Cu-0.3Cu weld coupons, however, in this range of thickness the weldability of the copper specimens exhibited an increase in strength. This confirmed that the type of temper metal could influence the bond. For the welding of 0.5Al-0.5Al and 0.5Cu-0.5Cu weld coupons, the weld strength slightly dropped compared to the welding of both 0.1 mm and 0.3 mm thicknesses. The energy dissipated increased due the increase in thickness, and also due to the influence of half-hard

condition. Again, the weld strength is greater due to the increase in vibration amplitude, especially at 42  $\mu\text{m}$ , but it is noticeable that the strength remains lower for the welding coupons of Cu-Cu specimens. It was clarified that there is some difficulty with the joint of specimens of 0.5 mm thickness, particularly when the vibration velocity become too high, such as at 42  $\mu\text{m}$  amplitude, because the high scrubbing motion will impair the weld strength and can occasionally lead to an incomplete weld.

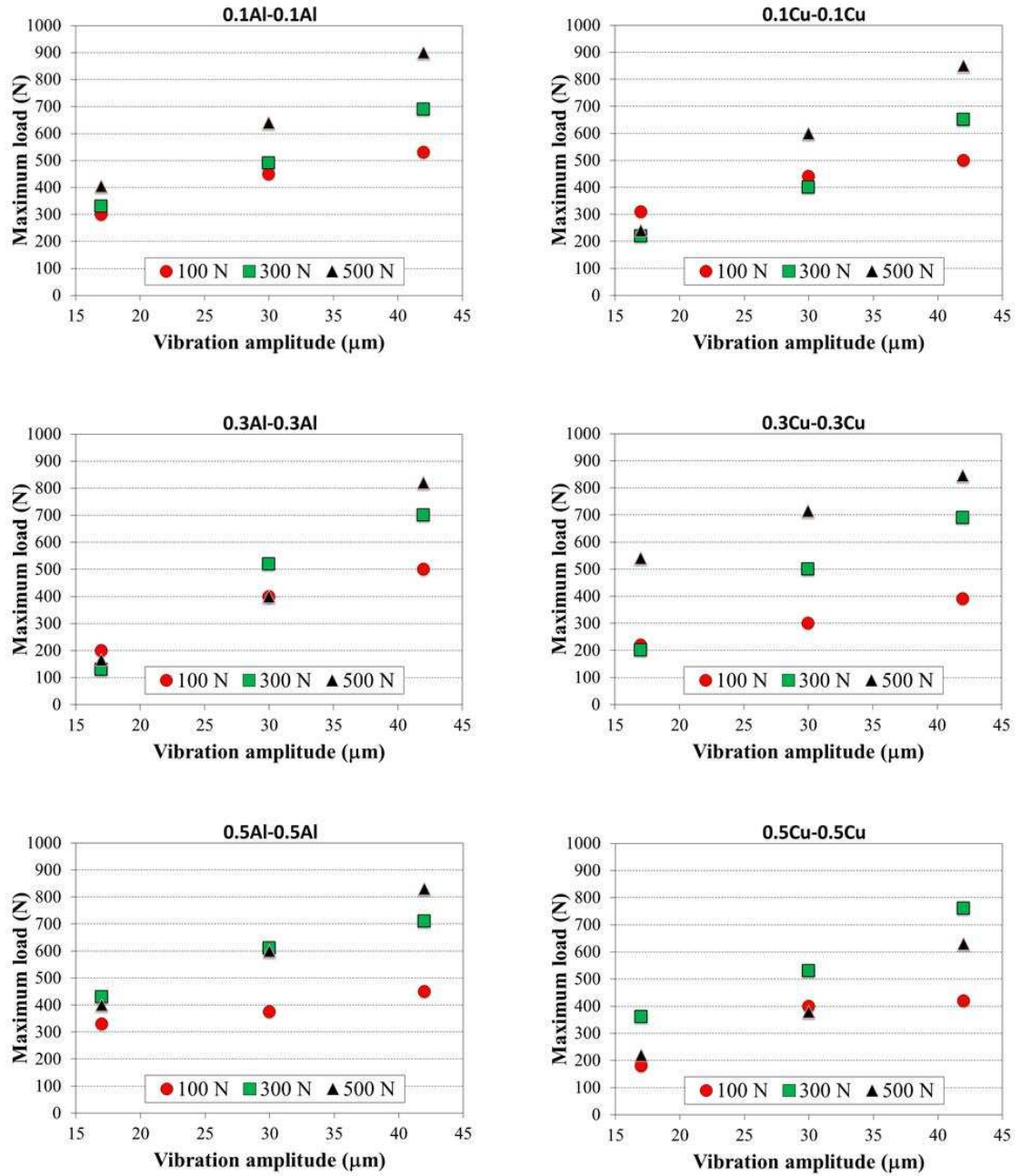


Figure 5-3 Welding strength vs. vibration amplitude, joining similar metals, for clamping forces of 100 N, 300 N and 500 N, and for amplitudes of 17 μm, 30 μm and 42 μm

Figures 5-4 depicts the weld strength versus vibration amplitude for all tensile shear tests conducted on joined dissimilar metals. The figure for the debonded specimens were obtained from weld coupons of 0.1Al-0.1Cu show that the strength was increased by a constant increment of clamping force between 100 N, 300 N and 500 N, with a vibration amplitude of 17 μm and a welding time of 1 second, and high strength was clearly identified due to a raise in amplitude. It was observed that the 0.1Cu-0.1Al weld coupons,

which was also subjected to three different vibration amplitudes of 17, 30 and 42  $\mu\text{m}$ , exhibited lower strength, indicated by tensile testing. This is because part of the energy that is transferred to the welding area was dissipated by copper. The energy dissipated relates to the surface properties of the metal, such as hardness and roughness, as well as the condition of the tempered metals. For the 0.3Al-0.3Cu and 0.3Cu-0.3Al weld coupons, the data of the weld strength appear to be related to the increase in horn amplitude. However, this relation does not seem uniform, as the aluminium and copper were in different metal conditions, being half-hard and annealed respectively. It can then be concluded that the soft surface of the annealed copper specimen can allow good bondability rather than the hard surface of aluminium. This agreed with the assumption that the softening of the metals occurs not only due to the raise in temperature at the deformation area, but also because of the preferential absorption of acoustic energy at the metal atoms dislocations [74].

For the tensile shear tests of 0.5Al-0.5Cu and 0.5Cu-0.5Al debonded weld coupons, it was observed that the welding strength depended on the vibration amplitude. Again, the strength data for each test were collected by varied the clamping force between 100 N, 300 N and 500 N. During the experiments, it was expected that the weld strength would be lower than the strength of thinner joining specimens. This is another reason that aluminium and copper were used in the half-hard condition, which leads to a decrease in strength, on the condition that the welding is performed within 1 second. In general, the overall weld strength begins to increase due to the increase in the horn amplitude, however higher strengths were observed at 42  $\mu\text{m}$ . It is important to state that the weldability of joined metals decreases as the mass or thickness of the specimens in contact with the horn tip increase [40]. This thickness constraint can eliminate the effects of ultrasonic welding compared to other conventional welds. However, employing the generator at high capacity can reduce this limitation, and enable thicker specimens to be welded. However, the relationships between clamping force and amplitude of vibration must be properly matched, because a low clamping force is not sufficient to produce a weld, whilst very high force can suppress the relative motion between the intimate surfaces. The increase in horn excitation can lead to a rise in amplitude, but it can be difficult to support specimens in the same position when a very high amplitude is used. However, if the horn confers low amplitude to the subject metal, then the removal of the oxide layer may not be uniform, resulting in lower strength. It should be stated that in most operations, obtaining a quality

weld depends on supplying a sufficient level of energy with a short duration ultrasound pulse. Excessive energy can sometimes lead to specimen sticking to the horn tip, or in other cases the joined metals may be vulnerable to fatigue fractures.

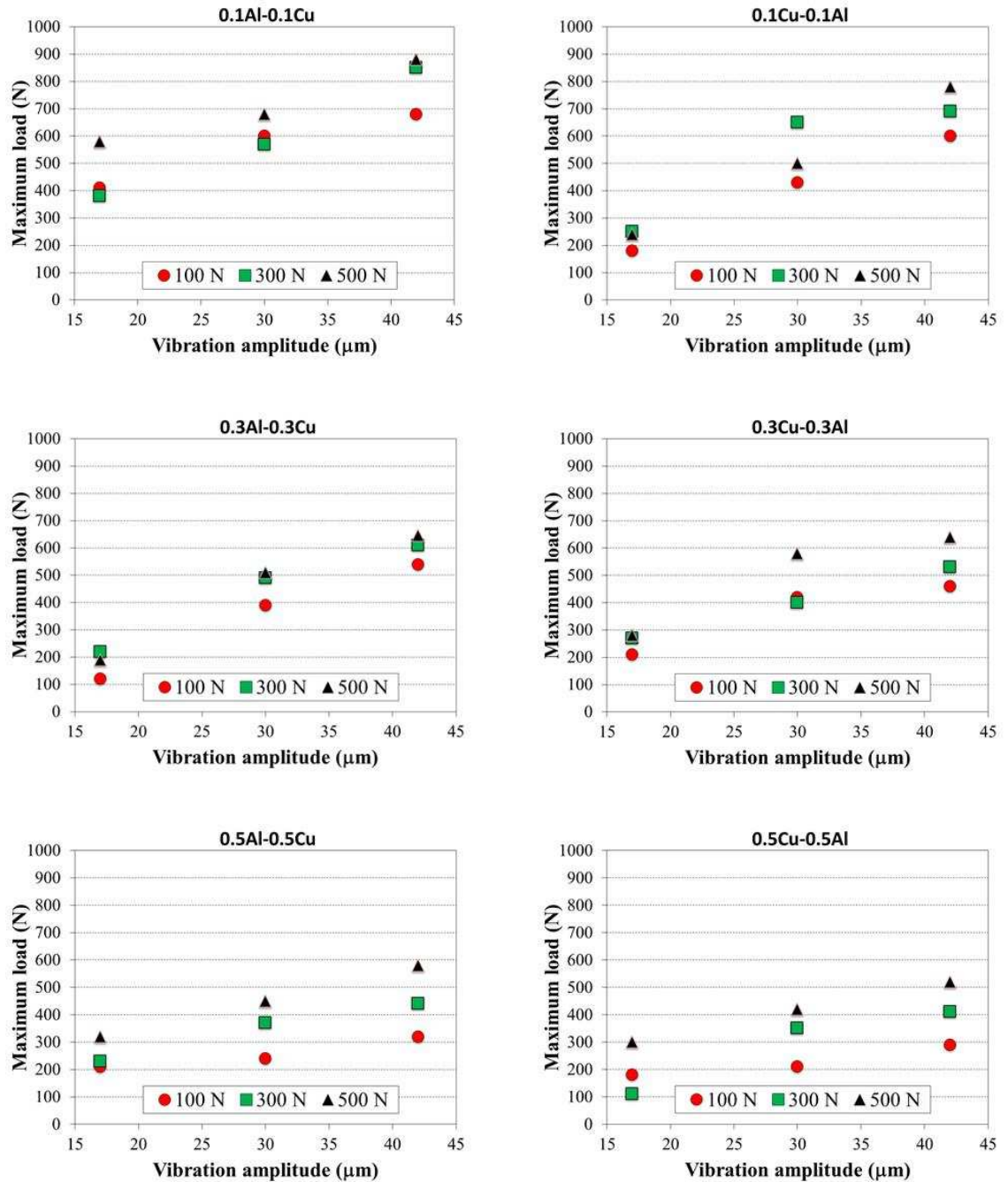


Figure 5-4 Welding strength vs. vibration amplitude, joining dissimilar metals, for clamping forces of 100 N, 300 N and 500 N, and for amplitudes of 17 μm, 30 μm and 42 μm

## 5.5 The influence of ultrasonic power on weld strength

In this section, the influence of the ultrasonic power on the weld strength for given quantities of clamping force and vibration amplitude will be explored. The power values were drawn from the ultrasonic generator, through reading the wattmeter which is located in the front panel of generator. Figure 5-5 shows the variations in welding power across the range of clamping forces which were applied to the system for both Al-Al and Cu-Cu weld coupons, with specimens of thicknesses comprising 0.1, 0.3 and 0.5 mm. The power was recorded relative to the increase in clamping force, whilst other parameters such as vibration amplitude, 17  $\mu\text{m}$ , and welding time, 1 second, remained constant. In the experiments, the average welding power was determined by three welds for each clamping force setting, with the range indicated in the graphs comprising double-error bars representing one standard deviation for each parameter set. It was noticed from collecting data, that more power is consumed by the deformation area when increase in vibration amplitude (for example at 30  $\mu\text{m}$  instead of 17  $\mu\text{m}$ ), and that higher power values were recorded at higher amplitude (42  $\mu\text{m}$ ). When comparing 0.1Al-0.1Al and 0.1Cu-0.1Cu, the former have low level of drawn power under the same welding conditions. The variation in reading power values becomes significant when different properties of aluminium and copper, such as hardness and surface roughness, are encountered. This is in spite of the fact that the two metals are both temper-annealed.

For the 0.3Al-0.3Al and 0.3Cu-0.3Cu weld coupons, the reading of power values was elevated due to increase in thickness of the joined metals, as similar welding conditions were applied on aluminium and copper specimens. However, the copper specimens consumed a lower quantity of acoustic power, because the copper was in an annealed condition, different from the aluminium which was half-hard. The standard deviations and the range and variation of recorded power values were determined for three welding tests, conducted for each clamping force setting. Higher standard deviations were recorded in comparison with the previous thickness 0.1 mm, specifically when the amplitude value was increased, for example to 42  $\mu\text{m}$ . In the welding case of 0.5Al-0.5Al and 0.5Cu-0.5Cu weld coupons. More energy was required to compensate for the thickness of the welding tests, especially when the horn was tuned at 42  $\mu\text{m}$ . However, excessive power with excessive clamping force was not possible due to the limitations of the lateral-drive welding system. Also, the ultrasonic power must not be too high or too low, as very high power can lead to the initiation of dynamic interfacial compressive stresses that can

damage the welds, whilst too low a power can result in very weak welds [9]. The standard deviations of the power curves at a thickness of 0.5 mm were derived from three welding tests conducted for each clamping force. The resultant error bars showed a high level of fluctuation of the power supplied for both aluminium and copper.

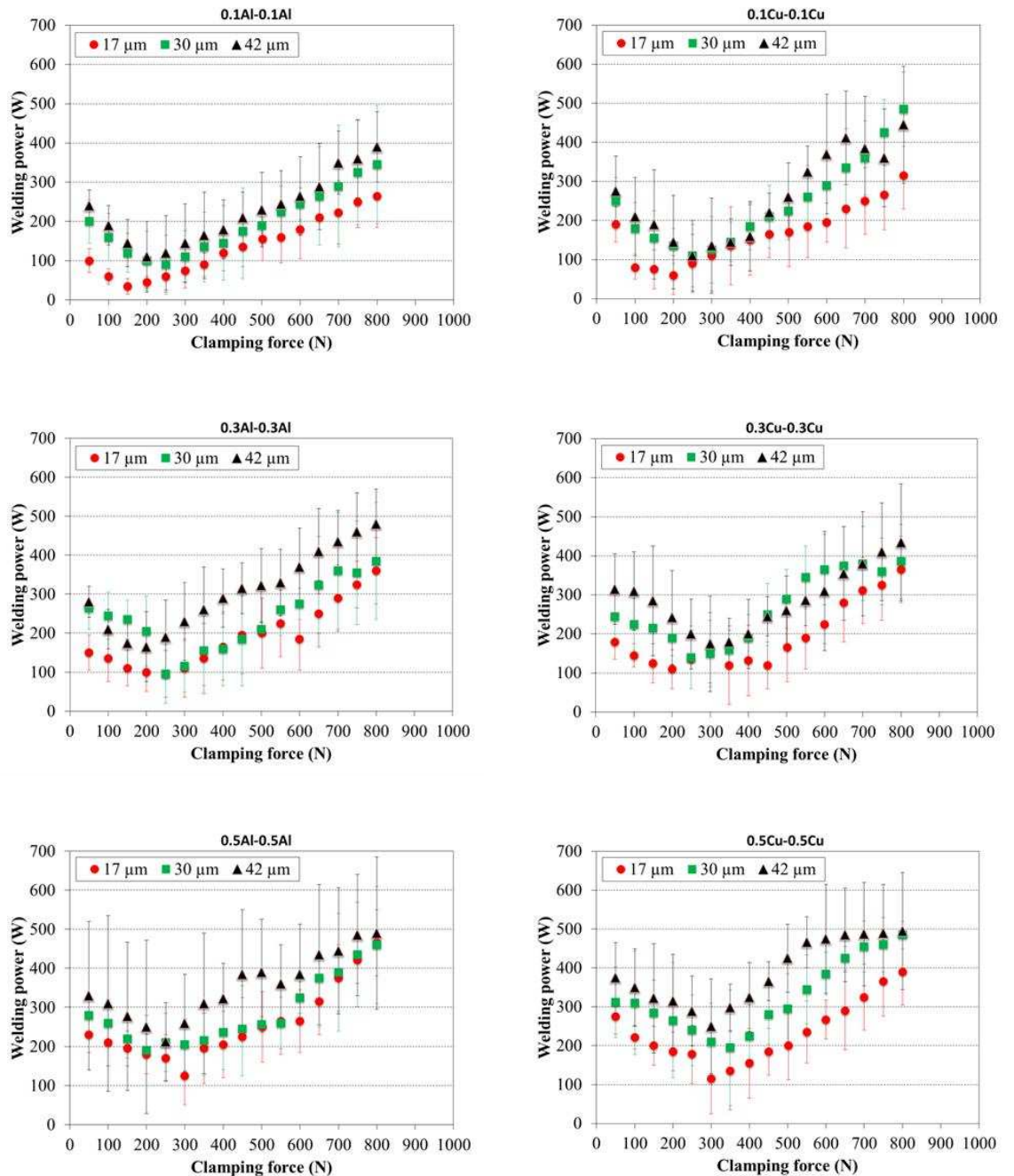


Figure 5-5 Welding power vs. clamping force for the joining of similar metals, for amplitudes of 17 μm, 30 μm and 42 μm

It was expected during tests that high fluctuation levels could be related to many reasons such as, specimen thickness, surface conditions of metals and the type of tempering metals, as the aluminium and copper were used from half-hard. Figure 5-6 shows the variations in ultrasonic power as the clamping force is incrementally increased for Al-Cu and Cu-Al weld coupons.

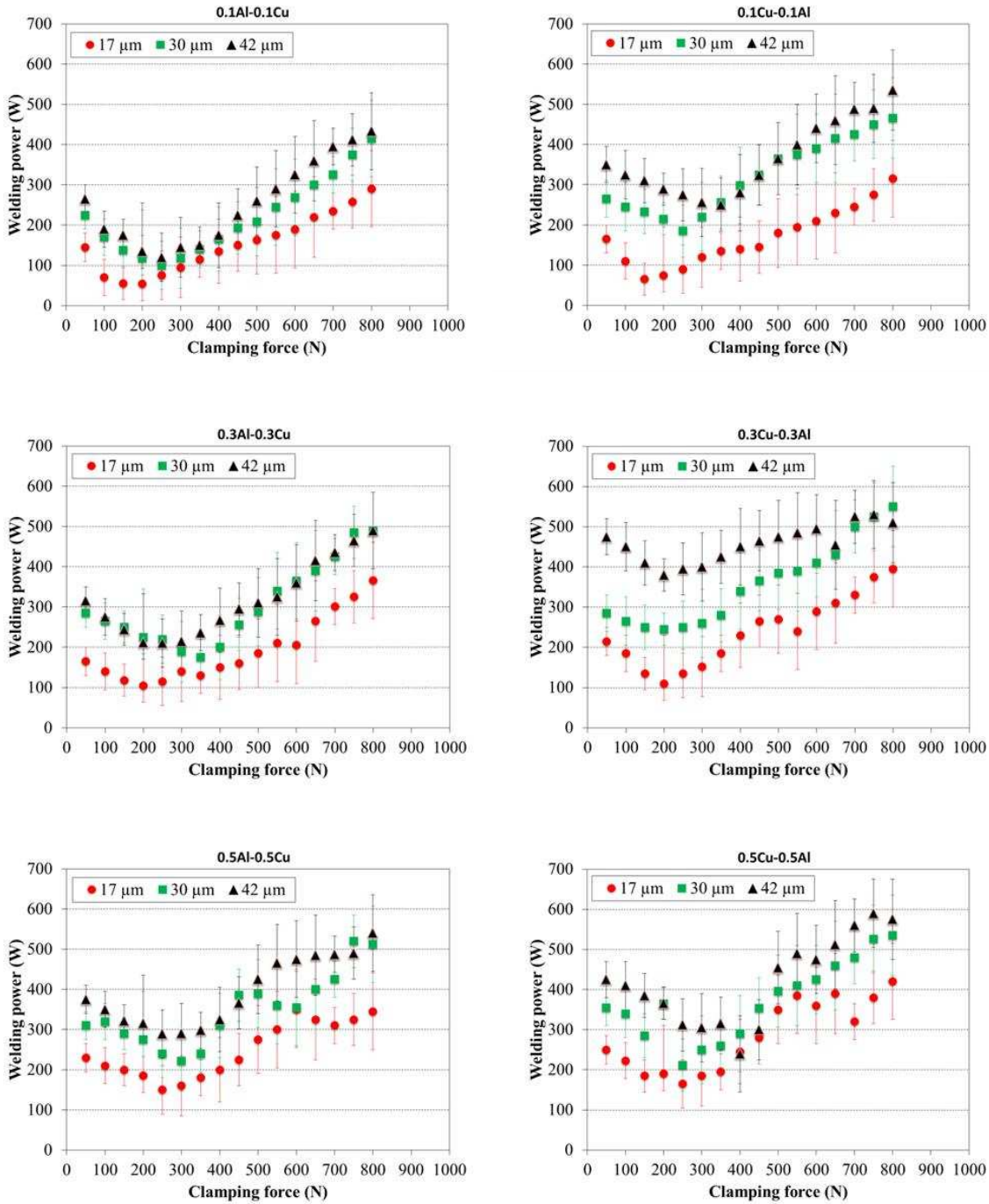


Figure 5-6 Welding power vs. clamping force for the joining of dissimilar metals, for amplitudes of 17 μm, 30 μm and 42 μm

The power drawn from the generator to the welding zone was gradually increased with a rise in clamping force, whilst the overall power consumption were changed with the increase in horn amplitude, specifically at both 30 and 42  $\mu\text{m}$ . Relating to the condition that more energy is required by harder metals than softer metals, the welding of 0.1Cu-0.1Al required more energy than the welding of 0.1Al-0.1Cu, which higher values of drawn power were recorded at high force. Higher power values were recorded with increasing the thickness of the joint such as in joining 0.3Al-0.3Cu and 0.3Cu-0.3Al, and more progressively in joining 0.5Al-0.5Cu and 0.5Cu-0.5Al. For that reason, the weld with no hardness variation can be more suitable in providing adequate bond strength, and can eliminate the deterioration of strength that occurs as a result of excessive power [55]. It was observed that when the amplitude of the horn becomes high (30 or 42  $\mu\text{m}$ ) the drawn power indicated high standard deviations, for the thicknesses of 0.1 mm and 0.3 mm and more significantly indicated with the thickness of 0.5 mm, because the aluminium and copper were different in tempering conditions and have strong oxide, especially for those specimen having half-hard condition, which recommended more energy to remove the oxide. Also, the copper specimens have high roughness, relative to the aluminium. Therefore, more power was drawn by the 0.5Cu-0.5Al weld coupons.

## **5.6 Amplitude profiling in USMW**

Most welding systems operate with pre-selected constant amplitude [123], applied during the whole welding process. However, variations in the amplitude of the vibrating tool can occur due to the influence of load stiffness, as no system can be considered to be infinitely rigid [77, 124]. In general, there were several issues encountered with this USMW technique such as tool/specimen adherence, specimen marking and less consistency in the generation of adequate weld strength. Recently, a number of studies have shown that the control of ultrasonic welding by adopting amplitude profiling can be advantageous for weld enhancement. There are a number of studies which outlined the amplitude profiling procedure in the literature, and these studies have involved the application of amplitude profiling for the welding of aluminium [5, 77].

Two different amplitude settings are used in the amplitude profiling, compared to the constant amplitude that is used in conventional welding processes. Figure 5-7 summarises the procedure the implementation of amplitude profiling. The first setting is denoted by the symbol 'A', whilst the second setting is referred to by symbol 'B'. The trigger between the

transitions of the amplitude settings, between A and B, can usually be made by control of the time, energy level or power value parameters. For the current work, the control of power was selected as the trigger between amplitude A and amplitude B as the variation in amplitude is proportional to the change of input power to the transducer. Amplitude profiling welding begins with the setting of the higher amplitude value 'A', where the weld interface requires higher velocities for surface scrubbing to be effective, thereby creating a solid-state weld at the intimate specimen surfaces. The amplitude is then dropped at point 'B' to reduce frictional heating and softening of the specimen, reducing shear as the weld forms and thus minimising damage.

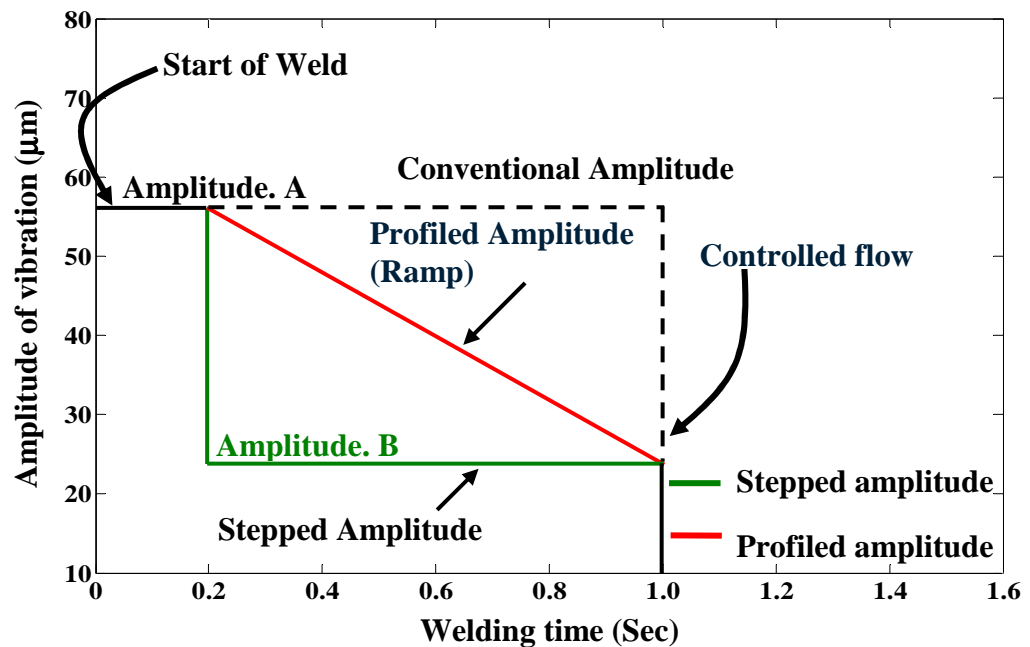


Figure 5-7 Schematic of amplitude profiling showing a curves and amplitude profile, stepped amplitude profile (green) and profile amplitude ramp (red) [5]

In this research, the setting of amplitude profiling was adopted in the welding of similar and dissimilar metals by ultrasonic spot welding. This approach has been implemented for two reasons. The first is that it helps to reduce sticking between the joining specimens and the welding tip. It is hoped that lower marking and a consequential increase in weld strength consistency will result. The second reason relates to the application of amplitude profiling on tests using different metals, because it has been shown that previous studies generally only use amplitude profiling in the welding of aluminium.

## 5.7 The influence of amplitude profiling on weld strength

The amplitude profiling was applied to investigate the weld strength. Figure 5-8 shows the resulting variations in weld strength as the clamping force is incrementally increased for weld coupons of similar aluminium and copper specimens at thicknesses of 0.1, 0.3 and 0.5 mm. A series of experiments were conducted using constant amplitudes of 17 and 42  $\mu\text{m}$  respectively. The switch from high amplitude to low amplitude took from 1 to 2 second to complete and was implemented by a change in input power to the transducer. Tensile testing was then conducted to debond the welded specimens and to extract the peak strength for each weld test performed with both constant and profiling amplitude inputs. It can be seen from both 0.1Al-0.1Al and 0.1Cu-0.1Cu weld coupons that the weld strength is increased using amplitude profiling compared to the constant amplitude approach which has previously been used. Higher strength was recorded at 550 N of clamping force, being observed to be approximately 1000 N, whilst the overall strength exhibited is higher for Al-Al welding. Furthermore, it was predicted that the strong weld that can be produced by amplitude profiling promotes high stiffness, and this correlates with the previous studies that carried out on welding aluminium. However, the amplitude profiling resulted in slightly lower weld strength, whilst the average value for each test was determined from three tensile tests at each clamping force and vibration amplitude setting, for the usual welding duration from 1 to 2 second. For the 0.3Al-0.3Al and 0.3Cu-0.3Cu weld coupons, the weld strength was lower due to the increase in thickness of the joined specimens. The amplitude profiling indicated a maximum weld strength reaching approximately 900 N, and located at clamping force of 450 N, whilst a welding strength of around 800 N was attained for the 0.3Cu-0.3Cu weld coupons. It was noticed that metal conditions influenced the weld strength, as the aluminium, half-hard, and copper, annealed were used as the subject specimens in these tests. Furthermore, higher constant amplitude, in this case 42  $\mu\text{m}$ , resulted in a higher standard deviation found in the joining of 0.3Cu-0.3Cu compared to 0.3Al-0.3Al. Despite the fact that the standard deviation was clearly lower for the amplitude profiling tests for the aluminium and copper specimens, sticking and specimen marking are not prevented from occurring, particularly for higher clamping forces.

A lowering of strength was observed to coincide with an increase in the thickness of welded specimens, such as for both 0.5Al-0.5Al and 0.5Cu-0.5Cu weld coupons. The half-hard property of aluminium and copper for a thickness of 0.5 mm led to a reduction in weld strength. It was expected from tests, that the energy transferred to the welding area

was not entirely sufficient to remove the oxide especially for those specimens are welded from half-hard metal condition, which influenced on weld strength. Unfortunately, the capacity of the generator (in this case up to 1 kW) imposes this limitation. However, matching between setting of process parameters and energy delivered to the weld, can improve joint strength, decrease marking and low the ability of the horn tip and specimens to properly adhere.

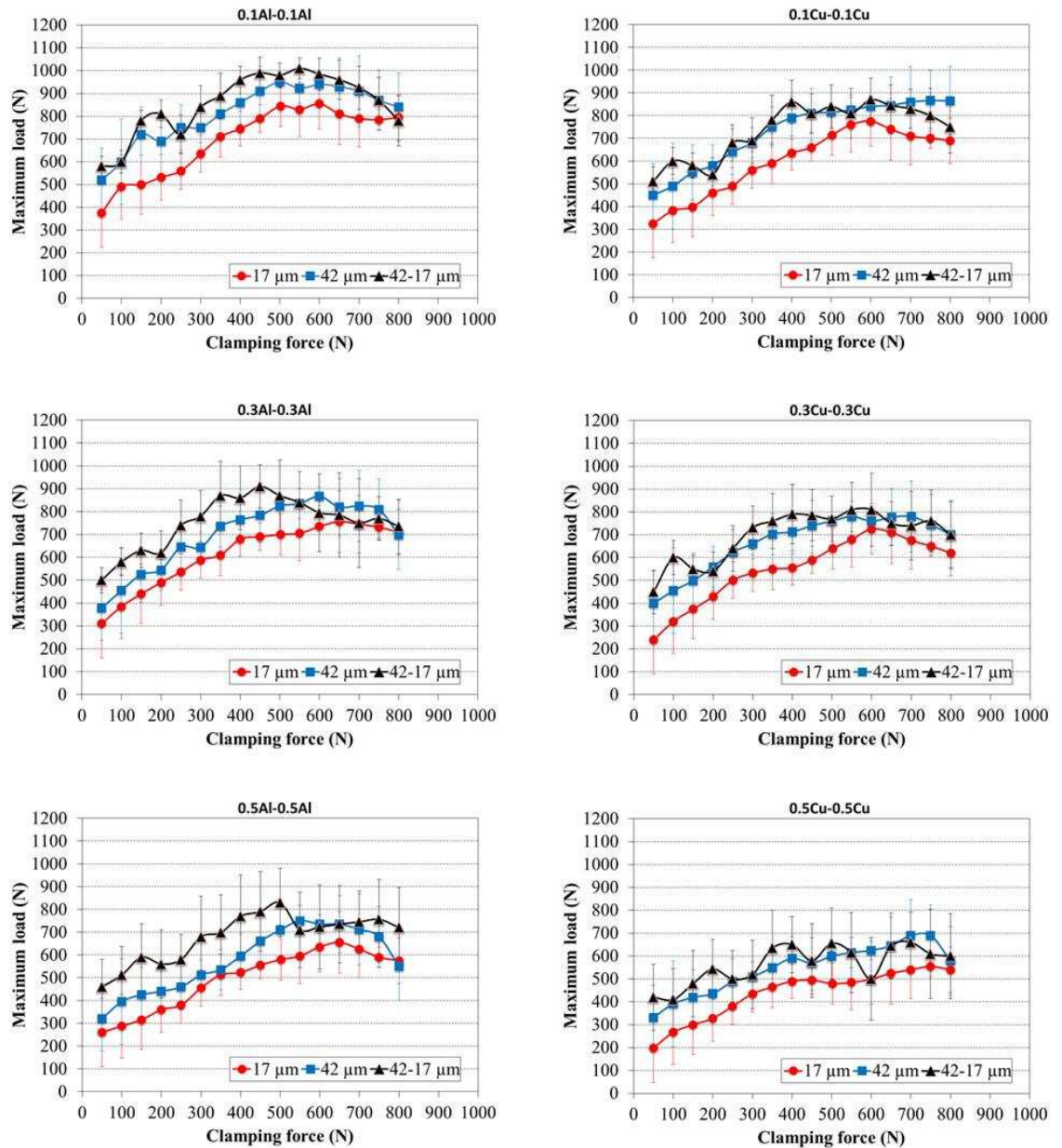


Figure 5-8 Welding Strength vs. clamping force for comparison between constant and amplitudes profiling in the welding of similar metals, for 17  $\mu\text{m}$ , 42  $\mu\text{m}$  constant and dropping 42-17  $\mu\text{m}$

In Figure 5-9, the amplitude profiling was adopted for the 0.1Al-0.1Cu and 0.1Cu-0.1Al weld coupons, it was shown to have a relatively low level of impact in terms of weld strength variation compared to those welds which were produced at a constant amplitude (for example 17 and 42  $\mu\text{m}$ ). Higher weld strengths were recorded to be around 990 N at a specific clamping force of 450 N. However, the maximum weld strength that was obtained using constant amplitude was approximately 900 N. For the tests involving the copper specimens placed on top near to the horn tip, in which the higher strength was fixed at 820 N relative to value of clamping force 450 N, it was shown that this weld strength magnitude was higher than that which was obtained by the constant amplitude approach, which was recorded as 750 N with a clamping force of 500 N. By increasing the thickness of the joints to 0.3 mm, the welding weld coupons of 0.3Al-0.3Cu and 0.3Cu-0.3Al exhibit a degree of difficulty in providing quality welds. Overall, this indicates that using the constant amplitude approach results in lower weld strength compared to amplitude profiling. For example, higher strengths were observed by amplitude profiling close to 900 N at a clamping force of 500 N for the welding of 0.3Al-0.3Cu, whilst for 0.3Cu-0.3Al, the strength remains around 790 N for a force of 350 N. It should be stated that the bondability began to decrease due to an increase in the thickness of the joined specimens and some difficulty in producing the weld also occurred at a higher force. Consequently, sticking and marking were found for this joining approach, and the resulting data indicate a high standard deviation for the strength variation. It was found that these unfavourable consequences were detected for the 0.5Al-0.5Cu and 0.5Cu-0.5Al weld coupons, in which the strengths were determined to be 770 N and 680 N respectively, with both being recorded as having a clamping force of 400 N. Overall, this shows that the strength remains high due to the influence of amplitude profiling, particularly up to 500 N clamping force, after which point the values drop.

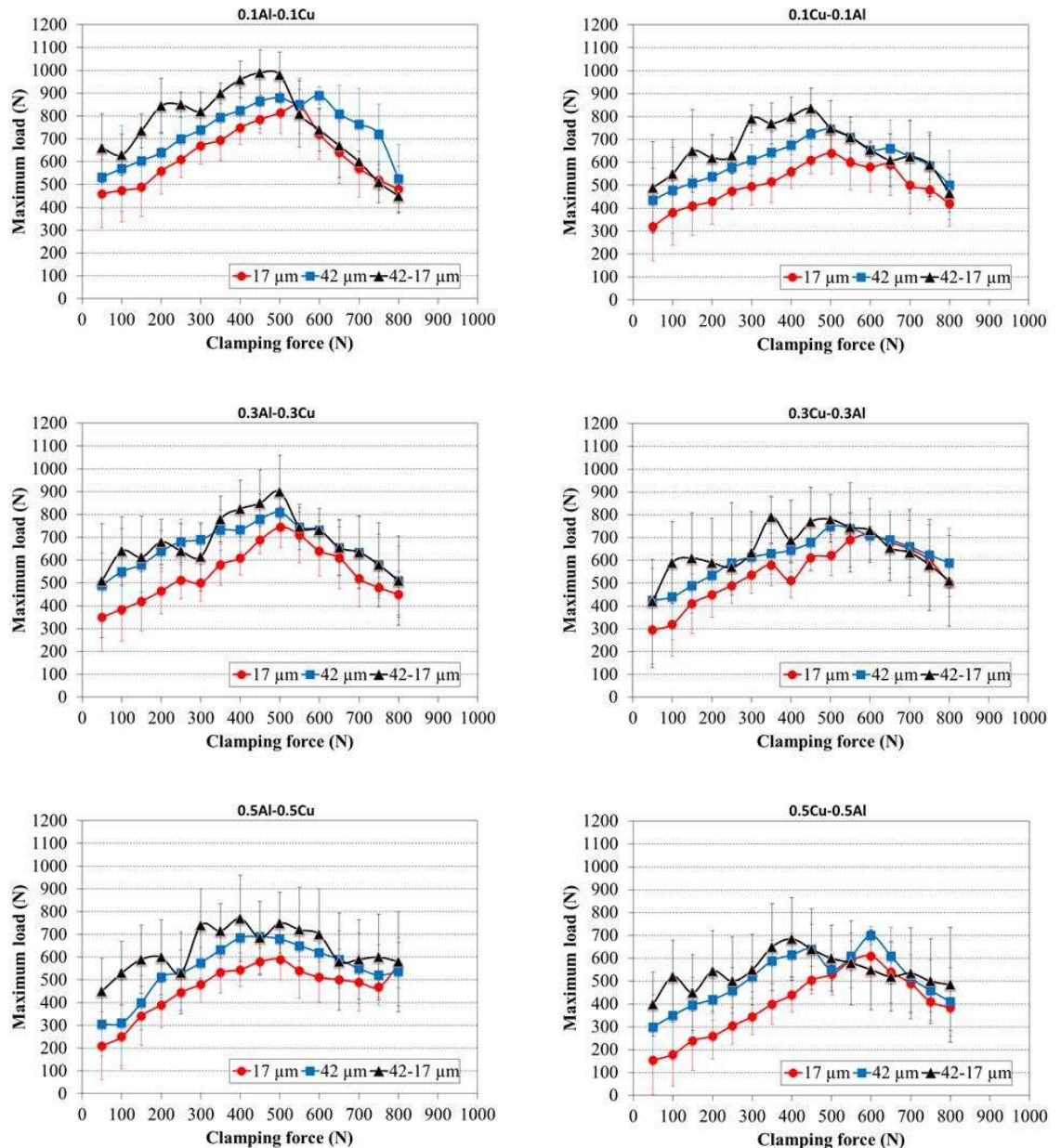


Figure 5-9 Welding Strength vs. clamping force for comparison between constant and amplitudes profiling in the welding of dissimilar metals, for 17  $\mu\text{m}$ , 42  $\mu\text{m}$  constant and dropping 42-17  $\mu\text{m}$

## 5.8 Extracting the curve for the joints of spot welding coupons

As explained in Chapter 4, the experimental results of the debonded welded coupons of similar and dissimilar metals were analysed using load-displacement diagrams. The analysis takes into account the different system settings which were used, as well as the metal parameters which were controlled in order to produce good weld strength and quality. The load (force) was extracted from the 2 kN load cell reading, and the elongation data was generated from the cross-head displacement of the Zwick tensile test machine

with a cross-head speed of 0.1 mm/min, until the debonding of all welded specimens was complete. To validate the experimental peak values of the weld strength for the debonded tests, FE models of the spot-welded joints were developed using Abaqus, where load-displacement curves were produced for all joint models in different welding conditions.

### **5.9 FE simulation of spot welding coupons**

A finite element analysis of the tensile test (lap shear test) for the spot welded specimens was conducted. The purpose of the finite element modelling was to provide a method of predicting the weld strength by incorporating the measured mechanical properties of the metals into the model and through validation against the shear test experimental data. The FE simulation code Abaqus was used to model the spot welding test specimens, where the test joints were modelled in full to accurately simulate the peak strength for different welding conditions which were produced by experiment. The values of the mechanical properties used for the aluminium and copper in these simulations are all taken from the data presented in Chapter 4, as shown in Table 4-6. An FE model was produced for each manufactured overlapped test coupon which was used in the experiments. The boundary conditions were set according to the conditions of the experimental tensile tests. It is noted here that all of the test coupons had a geometrically symmetric shape, but varied in thickness. The two specimens were overlapped, representing the area of spot welding, and matched to the surface area of the horn tip. The specimen was modelled as a deformable body. The material property definition, model section assignment, steps, mesh, contact condition, boundary conditions and loading conditions were all defined in the CAE environment. The assumptions which were set in this simulation were that the material model was isotropic, the spot welding was represented by a circular area for all models with a diameter equal to 4 mm and comprising 22 elements, and for the contact condition, the motion of the spot welding was constrained for all degrees of freedom. The mesh was applied over the weld coupons, which were modelled with solid elements.

The spot area was modelled and contacted to the overlapped specimens by defining the interactions between contact surfaces, both normal and tangential. C3D20R solid elements were used for all simulations. The boundary conditions were imposed on the model of the joint specimens to simulate the actual condition of grip. During modelling, one end of the welded coupon was constrained with an encastre boundary condition to restrict all degrees of freedom. The motion in the transverse direction of the load was restricted and the

rotational motion was omitted at the loading ends of the joint. The general metal-to-metal contact surfaces were defined with a friction formulation. Figure 5-10 shows the FE model for the simulated lap-shear test of the spot welding coupons, and shows a summary of the contact surfaces, loading and boundary conditions for the spot welding model. The FE simulations were performed using a quasi-static loading condition with the general and implicit Abaqus steps, and by applying the relevant material properties and boundary conditions to every weld model.

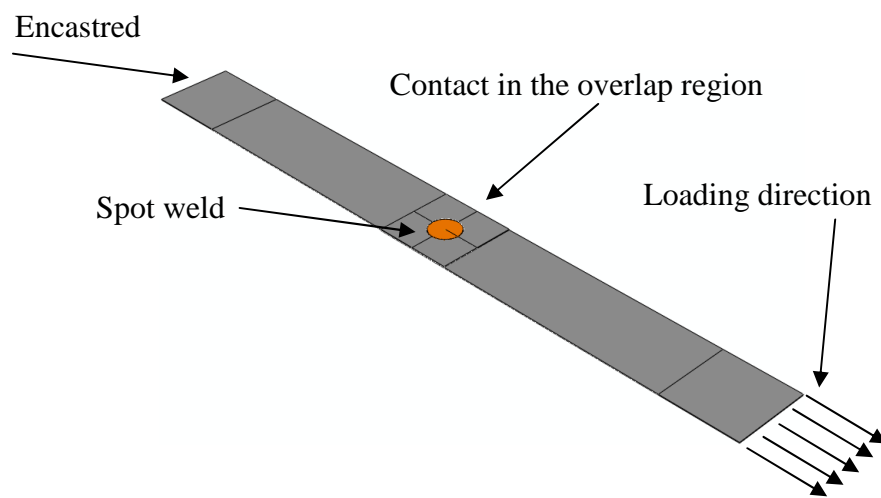


Figure 5-10 Lap shear spot welding model geometry and boundary conditions

The load-displacement data which were previously extracted from the tensile test machine was converted into engineering stress and engineering strain, to define material properties in the FE simulation. The deformed, undeformed and contour shapes of the lap shear spot welding test coupons are shown in Figure 5-11. The Von Mises stresses and displacement of the weld coupons are also shown. This simulation procedure was repeated using different thicknesses.

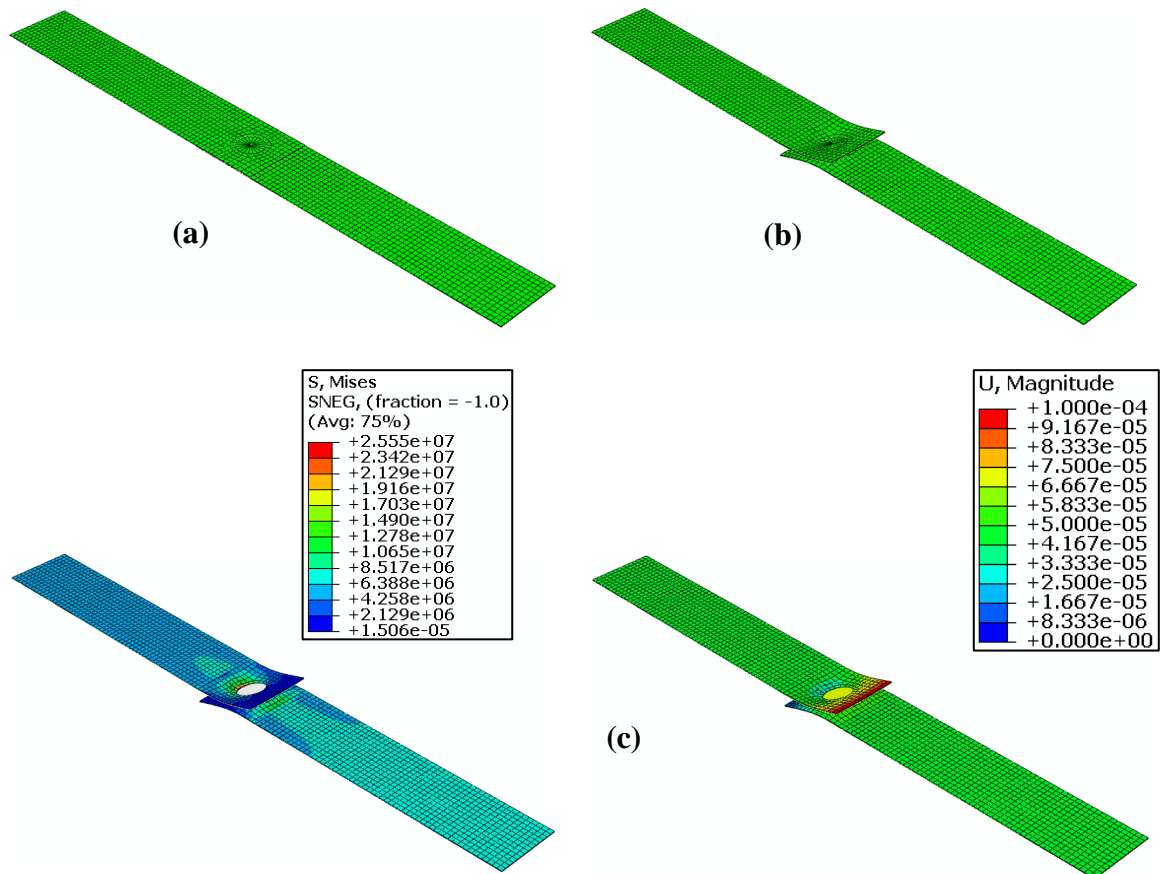


Figure 5-11 Mesh shapes for lap-shear spot welding test coupons: (a) undeformed (b) deformed (c) contours of stress and displacement

Figures 5-12, 5-13 and 5-14 show the complete load-displacement curves obtained from the FE models of the spot welded joints together with the corresponding experimental results from the debonded specimens. It is clearly shown that the process parameters such as clamping force (100 N and 500 N) and vibration amplitude (17 $\mu$ m and 42  $\mu$ m) significantly affect the load-displacement data, from which the maximum load of each test can be readily indicated by its peak point. From these figures, it is clear that there is an acceptable agreement in magnitudes of the peak points between the FE model and experimental results for the load-displacement curves, and that the magnitudes of maximum loads obtained from the modelling are close to the maximum loads which were obtained from the experimental tensile-shear tests. This confirms that the mechanical properties of aluminium and copper which were used as the input data to the FE modelling were extracted correctly, and that the definition of materials properties as required in the FE modelling was indeed conducted correctly. However, the curve profiles are slightly

different. Furthermore, the models of the specimen joints have not exhibited any fracture behaviour, as the failure criterion was excluded from this study.

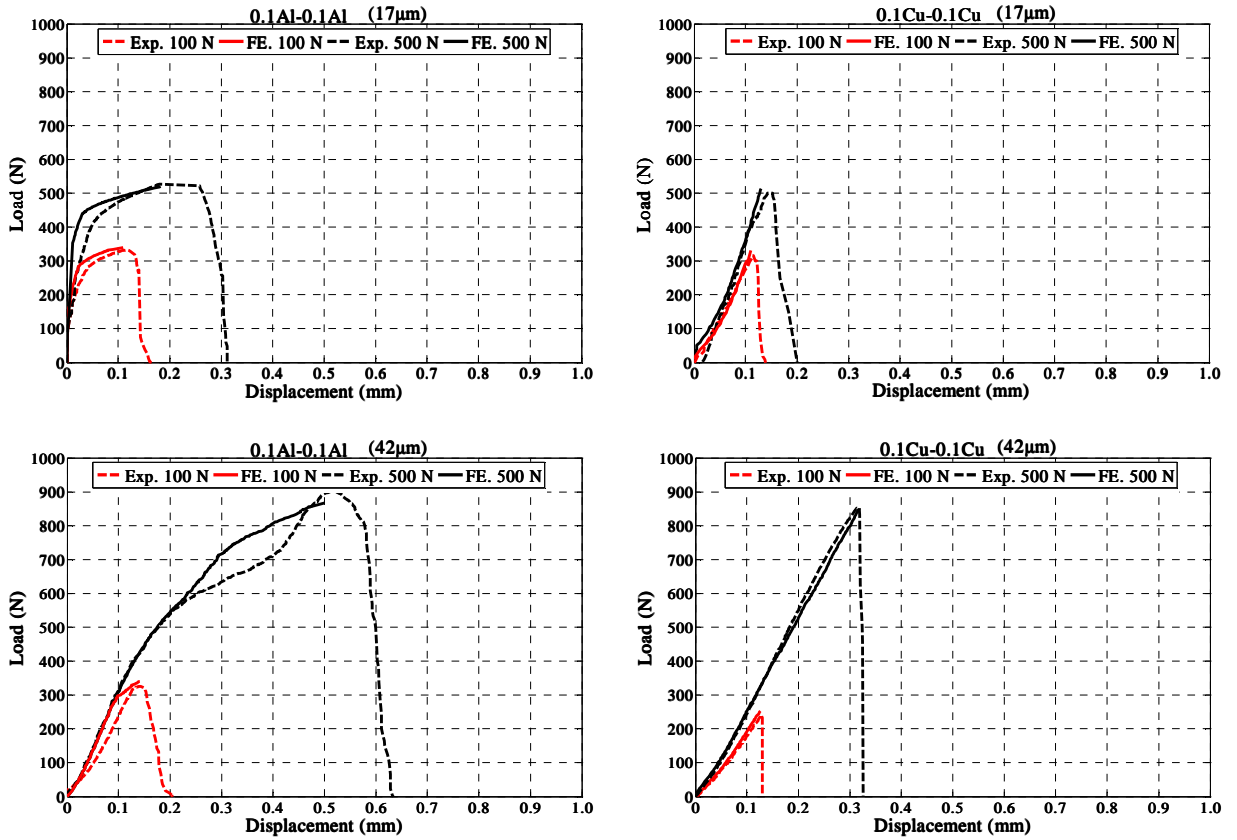


Figure 5-12 Comparison between experimental and FE results of lap shear spot welding test performed in a weld joint of aluminium and copper, thickness 0.1 mm

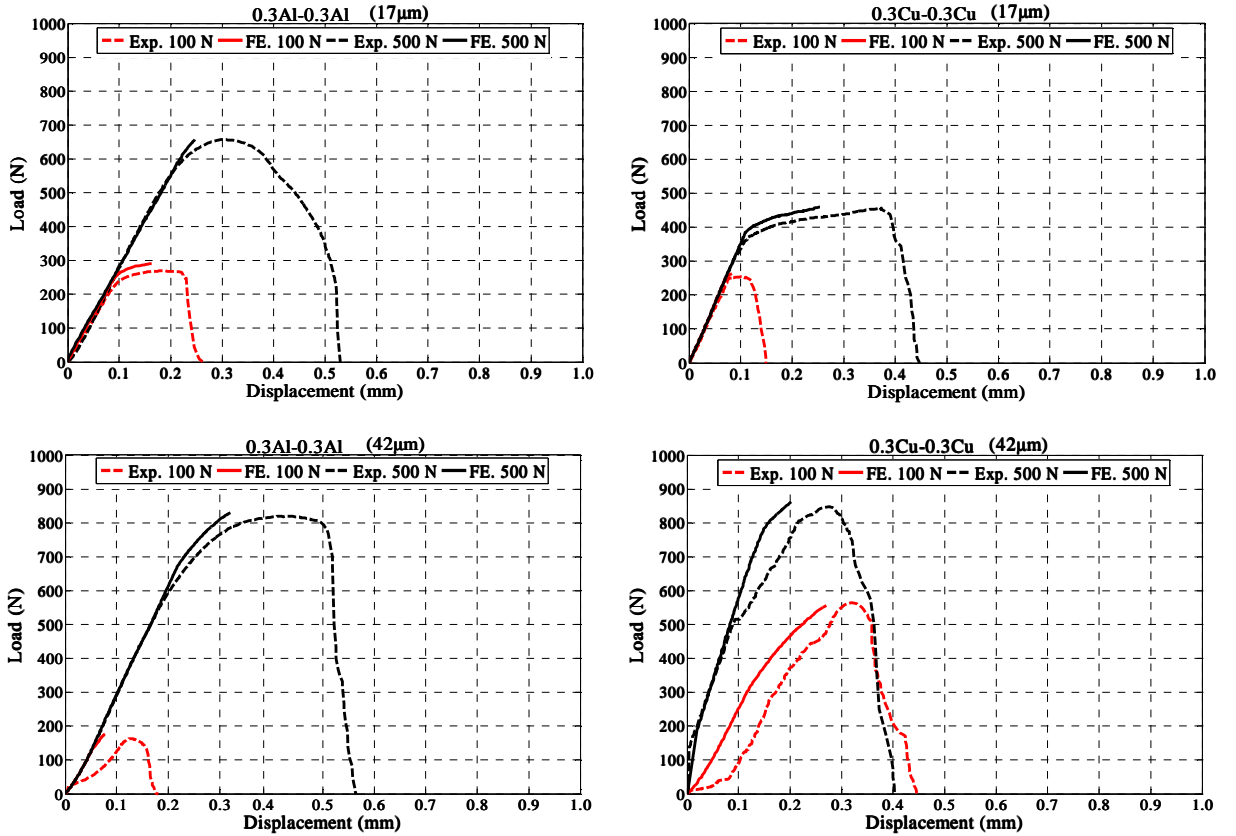


Figure 5-13 Comparison between experimental and FE results of lap shear spot welding test performed in a weld joint of aluminium and copper, thickness 0.3 mm

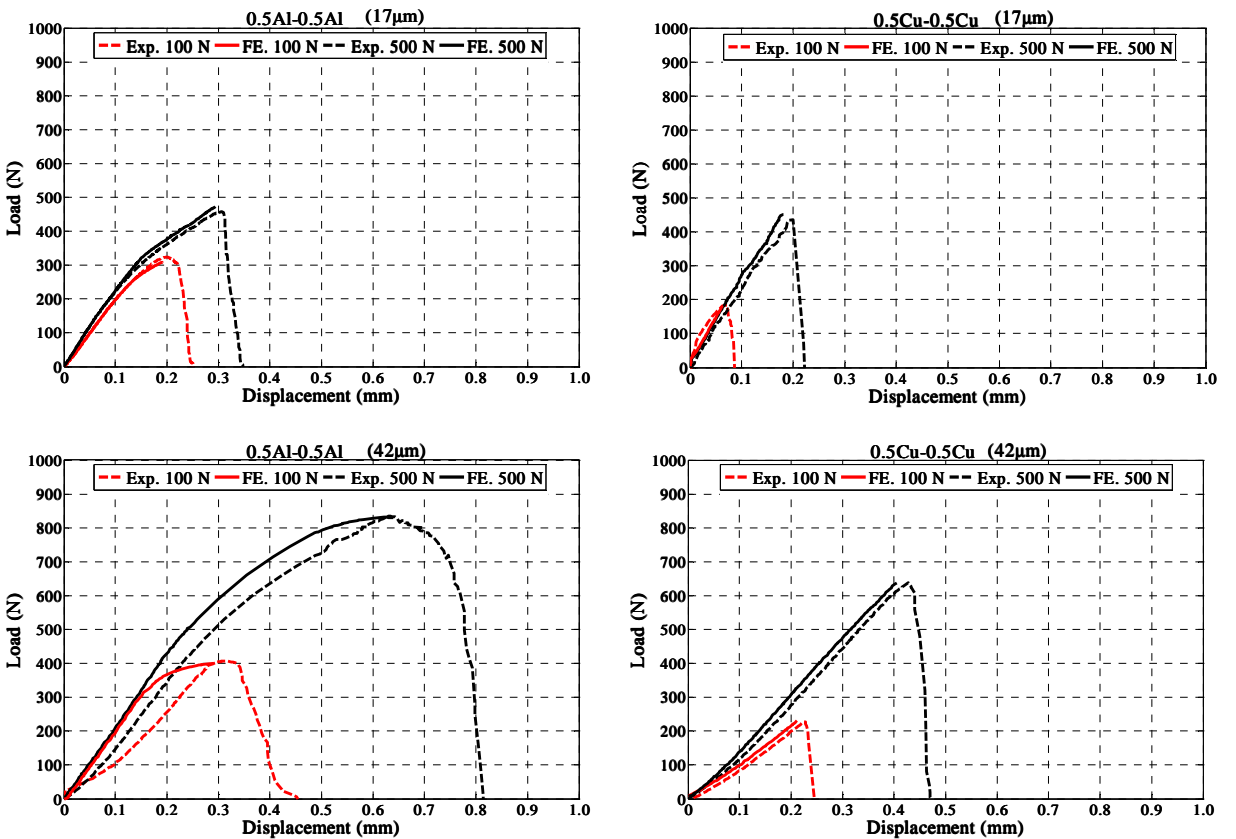


Figure 5-14 Comparison between experimental and FE results of lap shear spot welding test performed in a weld joint of aluminium and copper, thickness 0.5 mm

As seen from Figures 5-12, 5-13 and 5-14, the trends of the load-displacement responses are different for the different curve profiles. These are mainly due to the variations between the joints produced from the aluminium and copper specimens, for example because of the metal properties, hardness and surface conditions such as roughness and oxides. Furthermore, the load-displacement curves for each weld coupon exhibits a change in slope at different stages of applied load. In general, the load-displacement responses can be characterised by indicating that the deformations in the models take place in all of the elements which are located adjacent, both near and far, from the spot welding area. After that and during the applied loading condition, the load withstanding is referred to as the largest deformation in the model that is concentrated around the spot weld area only, which is the stage at which the maximum load that a spot weld can withstand is attained. Overall, the force response from the developed spot weld models is close to the experimental results. However, a number of trends offer clear variation from the force responses which were extracted experimentally. It was thought that the variations in the load-displacement curve profiles were because of a number of reasons including errors due to the sensitivity of the load cell testing machine, as very small forces were calculated from the Zwick machine during the experimental testing set up. Larger gripping forces are applied to the machine arms to pull the overlap-welded specimens, and this can create low bends in the specimens, which influence the development of the load-displacement profiles, especially for the specimens of 0.1 mm thickness. Furthermore, the differences between the force responses for specimens in the annealed condition compared to specimens in the half-hard conditions were clear, for both aluminium and copper. However, the FE models primarily exhibit close agreement with the experimental tests for the peak load values.

### **5.10 Summary**

The ultrasonic metal spot welding system was successfully designed and assembled in order to conduct a series of welding experiments on thin metal specimens. The properties of aluminium and copper specimens under different thicknesses comprising 0.1, 0.3 and 0.5 mm were extracted using tensile testing. The surface conditions of the different metals were important to consider, and vary between annealed and half-hard. The analysis and experimental results of the welding of debonded specimens conducted for different welded coupons (Al-Al, Cu-Cu, Al-Cu and Cu-Al) show how the relationships between process parameters such as clamping force, amplitude of vibration, ultrasonic power and welding time, and metal parameters comprising hardness and metal surface roughness and oxides,

influence the weld strength. Good contact between two metals was accomplished by maximising the interfacial slip at the intimate surface hence resulting in plastic deformation. This was established by a number of approaches, such as effective tool design, for example by the welding horn, providing sufficient power into the welding area, and ensuring that the proper setting of process parameters is implemented. The results suggest that the weld strength is most sensitive to relationships between clamping force and vibration amplitude, but also to relationships between clamping force and input power. The weld strength changes according to specimen thickness and metal properties such as oxides, hardness and surface roughness. Furthermore, the type of upper specimen that is placed in contact with the horn tip has an effect on the weld strength in relation to the consumed power. The relationship between weld time and weld amplitude was shown to have a much lower effect on weld strength, even for the tests that were conducted using a weld time greater than 1 second.

The results of the overall weld strength suggest that the Al-Al welds are stronger than the Cu-Cu welds and that the weld strength in both cases tend to increase with a rise in the magnitude of specific system parameters, such as clamping force and vibration amplitude. However, the alteration in strength approaches a critical value, above around 500 N, where the higher clamping forces restrict the lateral movements essential for welding. When dissimilar metals are considered, slightly stronger welds are obtained when the aluminium specimen is placed on top and in direct contact with the ultrasonic horn and, in general, there is a decrease in weld strength when clamping forces above approximately 600 N are applied. The analysis confirms that the clamping force must be sufficiently high to allow high-quality welds to be formed and to prevent sliding occurring between the horn tip and the upper surface of the top specimen. Also, the high excitation horn, matched with a high clamping force, can result in the suppression of the relative motion between intimate surfaces, and thereby lower strength as a consequence. Amplitude profiling between 42 and 17  $\mu\text{m}$  enables joining to become more effective, slightly increases the weld strength and also lowers standard deviations in comparison with those tests which used constant ultrasonic amplitude at either 17  $\mu\text{m}$  or 42  $\mu\text{m}$ . A higher stiffness was expected after joining similar and dissimilar metals, generally for those tests having a strong weld. However, the benefit from amplitude profiling has a more pronounced effect when the welding is performed on specimens with lower thicknesses. Even though the amplitude profiling did not reduce the horn tip/specimen adhesion and specimen marking, it could

still lower the variation in strength. The mechanical properties of aluminium and copper metals which were extracted in Chapter 4, in addition to the extracted elastic-plastic properties of the debonded specimens, were used as the input data for the definition of the FE model parameters for the specimen joints. The FE models of the aluminium and copper joints which were extracted from different process parameters, such as clamping force and vibration amplitude, under variable thicknesses of 0.1, 0.3 and 0.5 mm, show an acceptable agreement between modelling results and experimental results of the load-displacement curve profiles, and allow a satisfactory estimation of the order of magnitude of the peak load to be made, when comparing different joint geometries. However, the curve profiles are slightly different. From this work, it has been shown that the weld quality which is produced as a result of joining similar and dissimilar specimens for aluminium and copper under different welding conditions and variable arrangements is affected by the process parameter settings, and this is explained further in Chapter 6.

## **Chapter 6**

### **Weld quality**

#### **6.1 Introduction**

This chapter presents an analysis of the weld quality of joined metals by investigating the weld zone which is formed by ultrasonic spot metal welding, for different welding conditions. The quality of the weld is usually determined by the joint's operational conditions and the resistance to failure caused by fatigue. The effects of ultrasonic spot welding on different aluminium and copper specimens were studied using both optical microscopy and scanning electron microscopy (SEM). Different debonded specimens were investigated for a range of process and metal conditions, from which the examination of the surfaces was conducted. Similar and dissimilar specimens in a range of thicknesses were investigated. The weld quality was observed via a study of the process parameters, such as the impact of changes in clamping force and amplitude of vibration on different surface conditions, and also specimen thicknesses and metal conditions, such as hardness and surface roughness. A discussion of the characteristics of the observed deformed areas is provided. In addition, external morphology and chemical compositions of aluminium and copper surfaces are extracted, using x-ray diffraction analysis of the high-magnification images.

#### **6.2 Microscopic observation**

In this research, the Nikon Optical Nomarsky microscope (the ME600-L eclipse model) was employed to investigate the deformed surfaces of debonded welded specimens, as shown in Figure 6-1. A digital camera (type DXM 1200) was situated above the microscope and connected to the monitor to allow clear observation of the tested metals. The five-attachment objective lens was adopted for use with the microscope to allow for high magnification of the tested surface, where the magnification can be varied between x5, x10, x20, x50 and x100, whilst the Nomarsky mode, or differential interference contrast (DIC) with which the microscope is equipped, is directly employed as an illumination source to enhance the contrast in debonded specimens. The benefit of using the Nomarsky contrast is that it acquires important information regarding the optical path,

since the technique depends on the principle of interferometry, which aids in optimal feature observation [125].

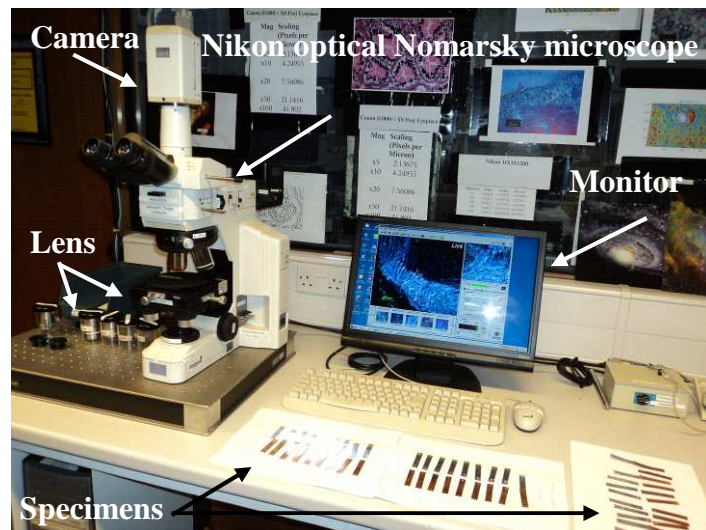


Figure 6-1 Nikon Nomarsky optical microscope

In order to gain an insight into the welding area, a number of debonded specimens which were produced by ultrasonic spot welding with different welding conditions and thicknesses were selected so that their deformation areas and the influence of system parameters on weld quality could be studied. To investigate the deformation surfaces of the debonded specimens which were extracted from welding of metals under different setting of process and metal parameters, the debonded specimens were separated into two groups which were in either similar or dissimilar configurations, as shown in Figure 6-2 and Figure 6-3. The specimens were selected from 0.1 mm, 0.3 mm and 0.5 mm welded coupons. The specimens which were used in ultrasonic spot welding differed in terms of metal conditions, as a number were annealed and the others were in the half-hard condition. The specimens were all prepared by mounting them in position and cleaning the welding area by using a concentrated Acetone solvent. However, the use of an etching agent on the deformation region prior to investigation was not required. Before testing weld quality, good and weak (or bad) weld quality are defined. Good weld quality is defined as two specimens welded together with no obvious signs of failure on the edge of the welding area and the tensile test results in a high maximum load. On the other hand, a weak weld is defined where the welding area can be easily debonded through applying a low force in the tensile test. In Figure 6-2 and Figure 6-3, the weld is categorised as ‘weak’, ‘good’ or ‘strong’.



Weak weld



Good weld

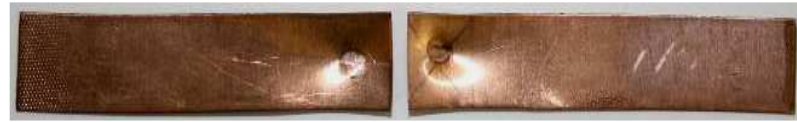


Strong weld

(a) Al-Al debonded specimens



Weak weld



Good weld



Strong weld

(b) Cu-Cu debonded specimens

Figure 6-2 Peeled specimens of similar metals, (a) Al-Al debonded specimens and (b) Cu-Cu debonded specimens



Weak weld



Good weld



Strong weld

(a) Al-Cu debonded specimens



Weak weld



Good weld



Strong weld

(b) Cu-Al debonded specimens

Figure 6-3 Peeled specimens of dissimilar metals, (a) Al-Cu and (b) Cu-Al

### 6.3 The influence of clamping force on weld quality

In order to study the effect of changes in clamping force on the weld area in joined specimens, two pairs of debonded specimens were selected, which were produced by being subjected to two different clamping forces of 100 N and 500 N. The horn amplitude was kept constant at 42  $\mu\text{m}$ , to allow for high relative motion between intimate surfaces. The duration of the process was kept constant at 1 second for all welding procedures. Also, 0.1 mm and 0.5 mm thick aluminium and copper specimens were selected for the weld quality investigations, because these thicknesses represented the limits of specimen thickness used in this study. Figures 6-4 and 6-5 show the Nomarsky microscopic photographs of debonded specimens of Al and Cu that were obtained from joining similar metals. The weld area is represented by the red dashed circles, whilst the green arrows indicate the direction of ultrasonic vibration.

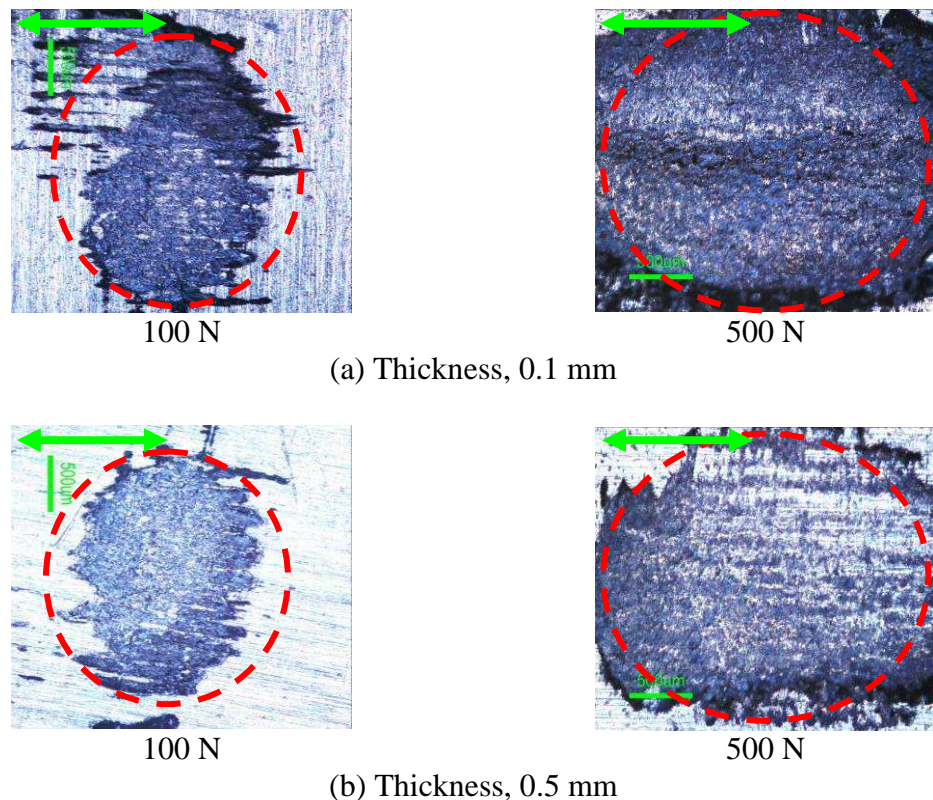


Figure 6-4 Photographs of peeled aluminium upper specimens, with double tipped arrows show direction of ultrasonic vibration, scale bar of 500  $\mu\text{m}$ , red dashed circle show weld area, amplitude of 42  $\mu\text{m}$  and thickness: (a) 0.1 mm, annealed (b) 0.5 mm, half-hard

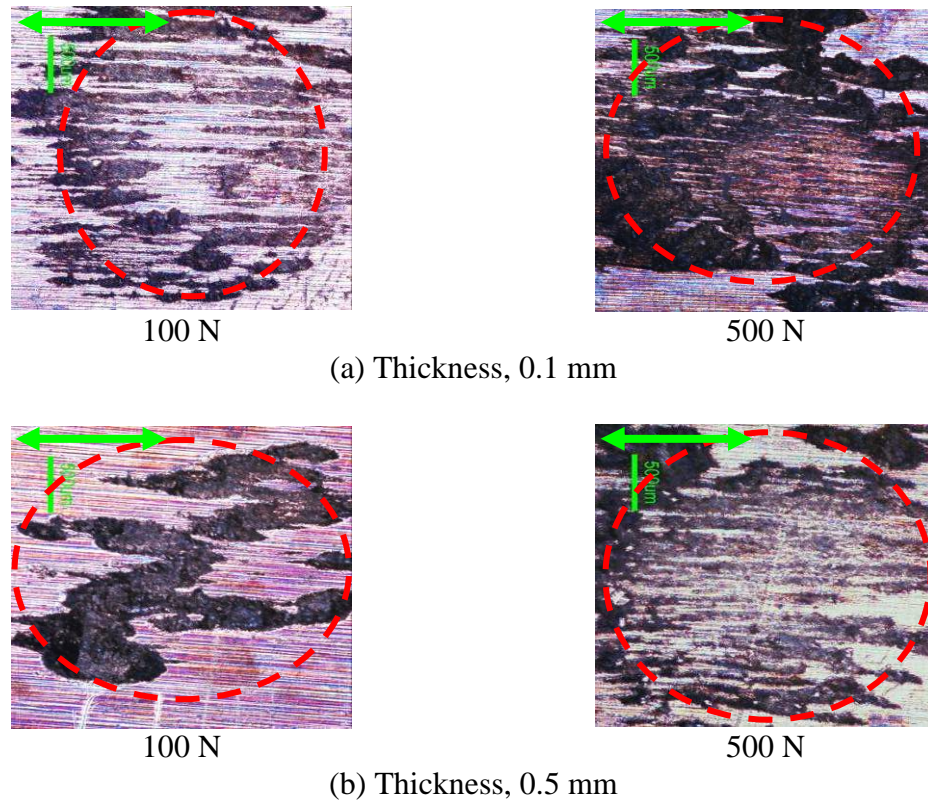


Figure 6-5 Photographs of peeled copper upper specimens, with double tipped arrows show direction of ultrasonic vibration, scale bar of 500  $\mu\text{m}$ , red dashed circle show weld area, amplitude of 42  $\mu\text{m}$  and thickness: (a) 0.1 mm, annealed (b) 0.5 mm, half-hard

In Figure 6-4, the photographs indicate that the dark regions are the areas where welding has occurred, in which the weld formation is clearly shown within the dashed circles. However, no welding areas were observed by the light regions. When welding is begun, weld formation between intimate surfaces is generated by producing small welded areas (microwelds). After that, the weld begins to grow due to the increase in time, in which the microwelds are distributed at random over the welded area, and their density is varied depending on the process parameter settings, such as clamping force and vibration amplitude. The investigations confirm that the length of the welded areas differs between aluminium and copper specimens, and the density of the formation areas depends not only on the process parameter settings, but also on the metal properties and surface conditions of the metals. For example, studies of the welded areas of annealed aluminium specimens with a thickness of 0.1 mm resulted in a weld length equal to 2.2 mm for an applied clamping force of 100 N. However, weld length was measured to be 4 mm under an applied force of 500 N. This indicates that higher diffusion of atoms occurs between the intimate surfaces, due to the good matching between clamping force and vibration

amplitude. Also, increasing the clamping force up to a certain point can result in an increase in the diffusion between intimate surfaces, which provides high weld area morphology. Within comparison, the weld area investigations of the half-hard aluminium specimens with a thickness of 0.5 mm showed that welded regions of similar size are produced. For a thickness of 0.1 mm and using a clamping force of 100 N, the length of the weld was measured to be 2.1 mm. For a clamping force of 500 N, it was observed to be 4 mm. However, the formation areas were of low weld density, as seen in Figure 6-4 for those surfaces of 0.5 mm thickness. Weld formation is affected by specimen thickness, hardness and surface roughness, of which high hardness (676) of the 0.5 mm aluminium surfaces suggests low density of the dark areas relative to the low hardness (273) of the 0.1 mm aluminium surfaces. Furthermore, the formation areas are affected by the surface roughness, as high roughness (3.2  $\mu\text{m}$ ) of the 0.5 mm aluminium produces low density in dark areas, compared with the low roughness (0.5  $\mu\text{m}$ ) of the 0.1 mm aluminium.

For the microscopic investigation of the debonded copper specimens, the conditions which were imposed were similar to those used for the investigation of aluminium specimens. The photographs of Figure 6-5 show the welded areas which are indicated by dark regions and enclosed with dashed circles, whilst the light regions show areas subjected to no welding. The photographs of copper specimens exhibited differences in terms of the formation of welded areas. This is likely due to the fact that the diffusion between atoms is lower than for aluminium specimens. This is related to the oxide and metal conditions such as hardness. Copper has high hardness that is equal to (517) and (863) for the annealed and half-hard conditions respectively, compared with low hardness of aluminium. Furthermore, the copper surfaces provided low weld formation, since more energy is required to remove oxide which influences the formation density. Comparing 0.1 mm and 0.5 mm thick specimens, the former provides a weld length of 3.4 mm for a clamping force of 100 N, and 3.8 mm for a clamping force of 500 N. However, the weld length was measured to be 3.7 mm and 3.9 mm for copper specimens with a clamping force of 100 N and 500 N respectively. A high density of the dark regions was indicated with specimens which were formed by applying a clamping force of 500 N. However, the light regions were found to be distributed over the welded areas formed using a clamping force of 100 N. The reason for this irregular weld is related to the surface condition of copper, as diffusion between intimate surfaces does not fully occur because of the remaining oxide, and also due to the effect of high hardness of the copper specimens. Overall, the results confirm that the

difference between weld lengths between aluminium and copper are not significantly large. However, the density of the formation areas is noticeable, which is indicated to be higher for annealed specimens compared to half-hard specimens. Furthermore, very low scattered weld regions were observed for the aluminium compared to the copper.

Figures 6-6 and 6-7 show the microscopic photographs of the debonded Al-Cu specimens for the selected thicknesses of 0.1 and 0.5 mm respectively, where again the welded areas are indicated by the dashed circles, and the direction of vibration is indicated by green arrow. In the case of the debonded Al-Cu specimens with a thickness of 0.1 mm, it was observed that the formation of weld begins to increase due to an increase in the clamping force, under a constant amplitude of 42  $\mu\text{m}$  and welding time of 1 second. For these conditions, the length of the weld was measured to be 2.6 mm for a clamping force of 100 N, and 3.75 mm for a clamping force of 500 N. Also, the formation area density was found to be higher when a clamping force of 500 N was applied, rather than 100 N. The reason for this is due to the diffusion of atoms between intimate surfaces, and situating the aluminium near to the horn tip results in a higher proportion of energy being transferred to the weld, as aluminium is softer than copper, and also its oxide layer is easier to remove than for copper. Furthermore, the low hardness and surface roughness of aluminium makes it more readily susceptible to plastic deformation than copper. With increase the thickness to 0.5 mm as with the debonded specimens of Al-Cu, the photographs display low levels of weld formation, compared to the specimen thicknesses of 0.1 mm, as shown in Figure 6-7. The photographs confirm that the welded area begins to increase due to increase in clamping force between 100 N and 500 N, for which the weld length was measured to be 2.8 mm for a clamping force of 100 N, and 3.65 mm at 500 N, as shown within the dashed circles. It was observed from photographs that the weld did form due to the application of the low force, resulting in an incomplete weld shape with slight scattering and irregularity in the formed areas. However, a uniform weld shape with no scattering was observed when using a high clamping force of 500 N.

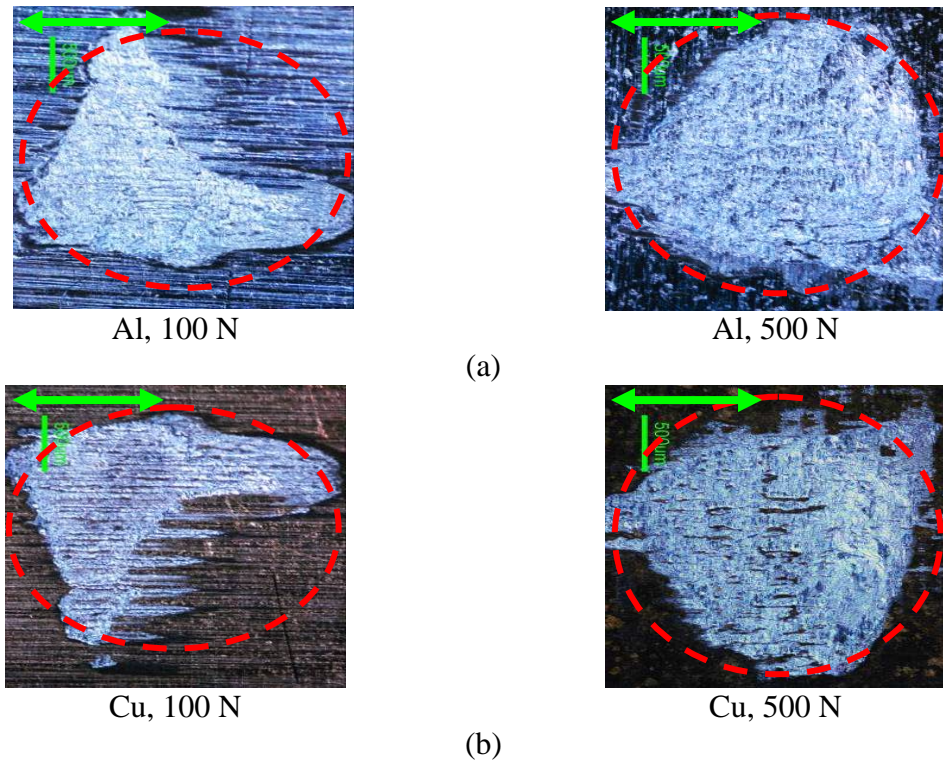


Figure 6-6 Photographs of peeled Al-Cu specimens, with double tipped arrows show direction of ultrasonic vibration, scale bar of 500  $\mu\text{m}$ , red dashed circle show weld area, amplitude of 42  $\mu\text{m}$  and thickness of 0.1 mm: (a) annealed aluminium (b) annealed copper

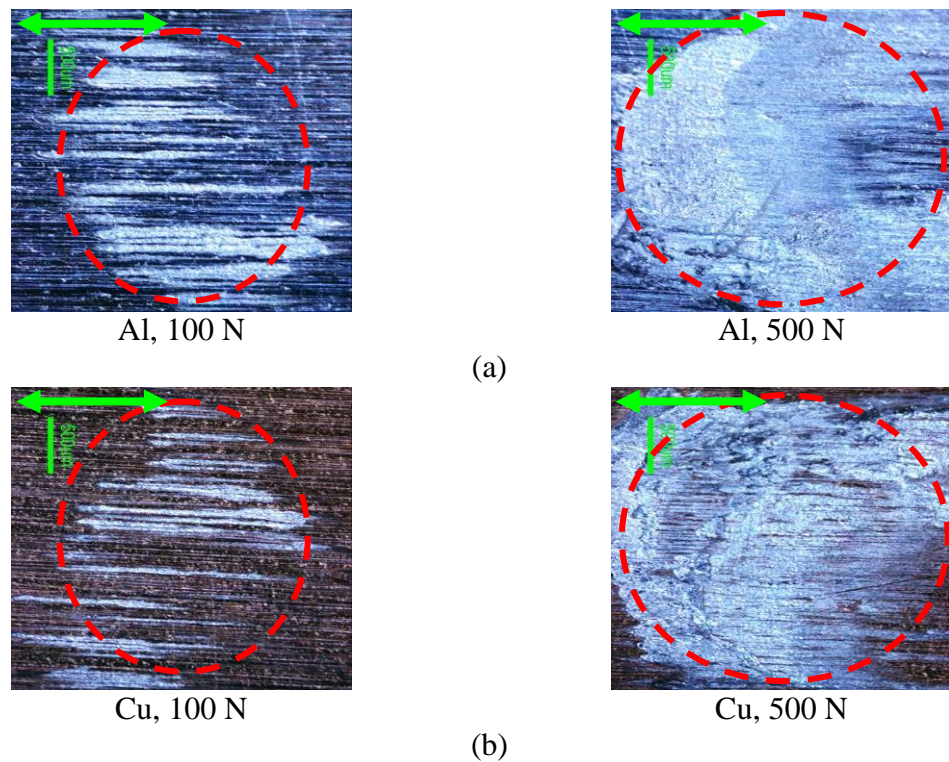


Figure 6-7 Photographs of peeled Al-Cu specimens, with double tipped arrows show direction of ultrasonic vibration, scale bar of 500  $\mu\text{m}$ , red dashed circle show weld area, amplitude of 42  $\mu\text{m}$  and thickness of 0.5 mm: (a) half-hard aluminium (b) half-hard copper

The investigation of the formed areas showed that metal conditions such as hardness and surface roughness, as well as thickness, significantly influence weld formation. High weld scattering with lined welds were observed from the photographs of the welded areas of the Al-Cu specimens which were formed under the application of a low force of 100 N. However, increasing the force to 500 N can overcome these lines by increasing the density of the weld formation. High force means that the two surfaces are under high compression, which enhances the mechanical interlocking between the surfaces to promote high diffusion of atoms according to the action of high relative motion between them. Overall, the weld formation can be marginally decreased by increasing the thickness, but the type and surface conditions of the metals are also very important factors. It is reasonable to always place the softer metal near to the horn tip to ensure that more energy is transferred to the weld with low dissipation, especially for metals with significant differences in surface conditions. It is important to state here that the photographs which were obtained from the microscope investigations have been cleared of variations in contrast colour of the welds, because these are related to the different compositions of the metals and also the variance of tempering metals. Furthermore, the use of the Nomarsky mode which can reflect different contrast colour in observing specimens that contain little or no optical. Because, the Nomarsky mode can increase the inspection of specimens and provide clear observation, through use interference contrast, which the features of surfaces can be standing out clearly under Nomarsky modes that are difficult to see under bright field illumination.

#### **6.4 The influence of vibration amplitude on weld quality**

In order to examine the influence of vibration amplitude on weld quality, two magnitudes of amplitude were chosen, comprising 17 and 42  $\mu\text{m}$ , which represent the limit of the ultrasonic generator used in this research. Understanding the influence of vibration amplitude on weld quality is not simple due to the complex relations between process parameters. For that reason, it was decided to select debonded aluminium and copper specimens in both similar and dissimilar combinations, welded under applied clamping forces of 500 N, with a constant welding time of 1 second. Figures 6-8 and 6-9 show the microscopic photographs of two types of debonded specimens, one being annealed and the other in the half-hard condition, with thicknesses of 0.1 and 0.5 mm respectively. The thicknesses represent the limits of the specimen thicknesses used in this study. The photographs show that the welded areas were increased due to increase in vibration

amplitude, in particular the increase in the scrubbing motion between intimate surfaces. In Figure 6-8, and for a 0.1 mm thickness, the length of the weld was measured to be 2.8 mm for an amplitude of 17  $\mu\text{m}$ , and 4 mm for an amplitude of 42  $\mu\text{m}$ , as indicated by the dashed circles. An increase in the scrubbing motion leads to an increase in atom diffusion, as seen from the high surface formation density acquired by applying an amplitude of 42  $\mu\text{m}$  with a 500 N clamping force, compared to applying an amplitude of 17  $\mu\text{m}$  with a 500 N clamping force. In comparison with the 0.1mm thick specimens, the welded areas on the 0.5 mm thick samples exhibit low formation, for which the weld length was measured to be 2.1 mm for 17  $\mu\text{m}$  amplitude, and 3.8 mm for 42  $\mu\text{m}$  amplitude.. However, low weld density was observed, as indicated by the light regions for the weld area in the 0.5 mm thick specimen, using an amplitude of 42  $\mu\text{m}$ . It has already been explained that the thickness and metal condition of hardness and surface roughness significantly influence the weld formation, as the annealed specimens have lower hardness and roughness than half-hard specimens, regardless of the specimen thickness.

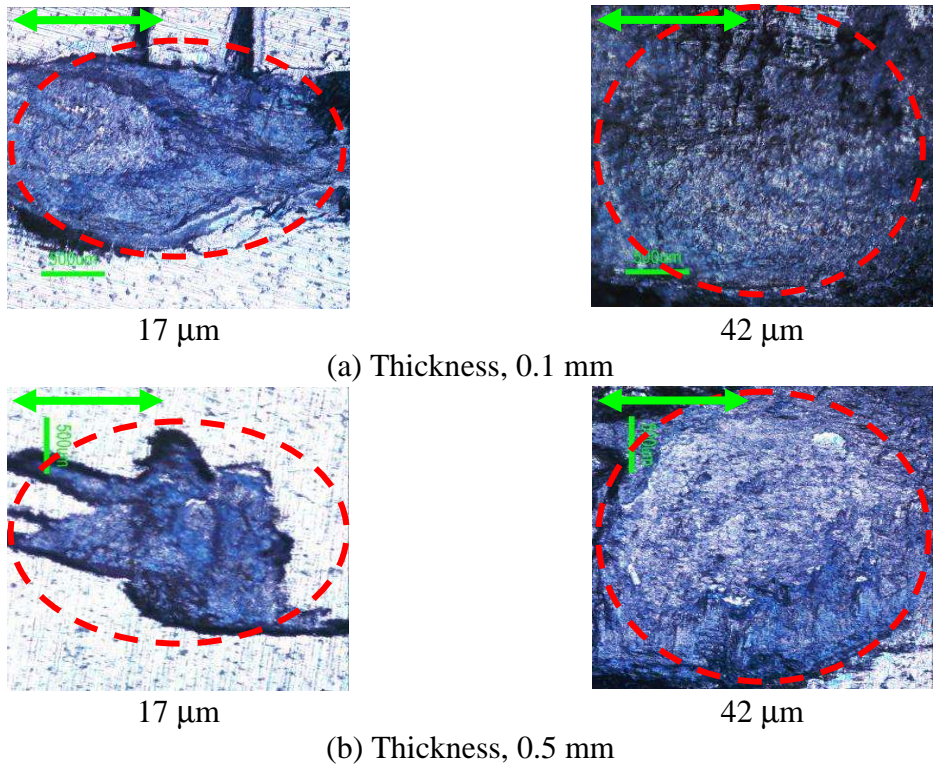


Figure 6-8 Photographs of peeled aluminium specimens, with double tipped arrows show direction of ultrasonic vibration, scale bar of 500  $\mu\text{m}$ , red dashed circle show weld area, clamping force of 500 N and thickness: (a) 0.1 mm, annealed (b) 0.5 mm, half-hard

Overall, this indicates that the weld quality was significantly affected by the increase in the amplitude of the exciting horn, but this does not mean that higher amplitude results in higher quality, because the quality of the weld can be undesirably affected by several parameters such as metal type, process parameters, surface conditions and selection of welding components. Figure 6-9 shows photographs of debonded copper specimens, which were taken for a similar welding condition to aluminium. The photographs indicate the welded area within dashed circles, for which the weld length for specimens of 0.1 mm thickness was measured to be 3.2 for an amplitude of 17  $\mu\text{m}$ , and 3.75 mm for an amplitude of 42  $\mu\text{m}$ . It was observed that although the weld length was measured to be significantly high, the forming areas are irregular, of which the density of the weld is low, with a low amplitude of 17  $\mu\text{m}$ . In addition, the welding procedure also results in high lined regions with no weld formation. However, increasing the amplitude to 42  $\mu\text{m}$  enables the formation areas to attain high weld density, but a higher weld density was observed in a thin specimen of 0.1 mm. This suggests that the high forming area occurs due to a matching between the clamping force and the vibration amplitude, whilst the metal condition significantly influences the formation area, in particular the diffusion of atoms. The annealed copper with low hardness and surface roughness allows for high diffusion, compared to the half-hard copper, regardless of specimen thicknesses. Furthermore, it appears that surface roughness of annealed copper (0.5  $\mu\text{m}$ ) and half-hard copper (3.2  $\mu\text{m}$ ) also influences the weld formation. The reason for this is most likely that mechanical interlocking of the rough contact areas hinders the relative motion between surfaces. However, this effect of surface roughness can be clearly reduced through an increase in vibration amplitude of the exciting horn, as seen in Figure 6-9.

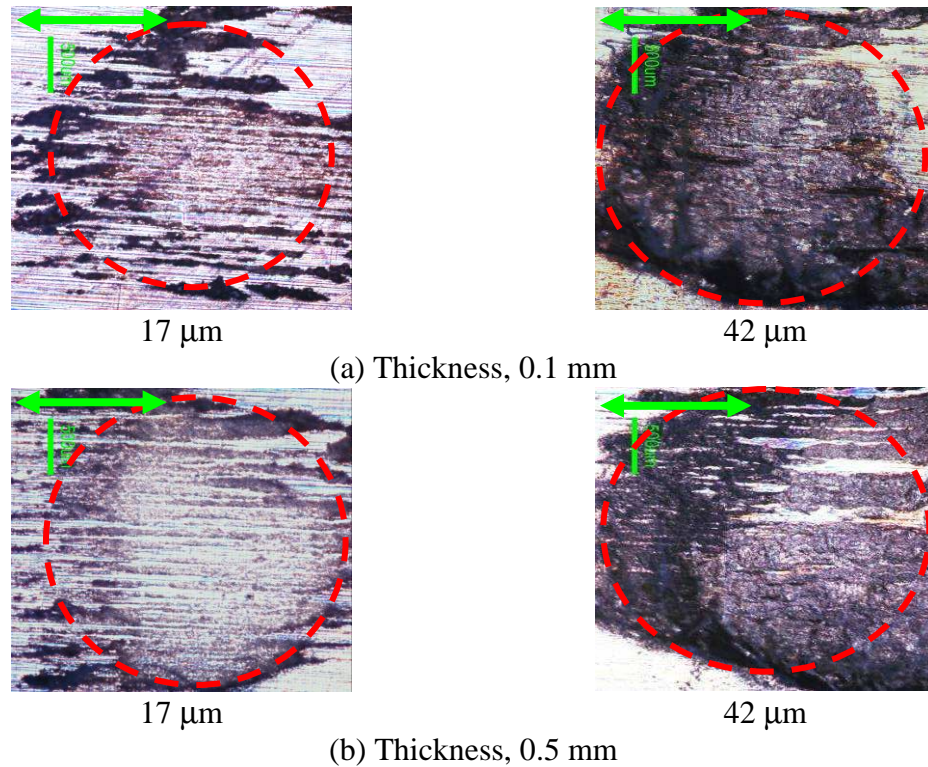


Figure 6-9 Photographs of peeled copper specimens, with double tipped arrows show direction of ultrasonic vibration, scale bar of  $500\ \mu\text{m}$ , red dashed circle show weld area, clamping force of 500 N and thickness: (a) 0.1 mm, annealed (b) 0.5 mm, half-hard

Figures 6-10 and 6-11 show the photographs of the formed welded areas for the welded dissimilar specimens of Al-Cu. The photographs are of the investigation of debonded specimens, which were welded under an applied clamping force of 500 N and welding time of 1 second, whilst the vibration amplitude was varied between  $17\ \mu\text{m}$  and  $42\ \mu\text{m}$ . In Figure 6-11, it was shown that the welded areas of 0.1 mm thickness with  $17\ \mu\text{m}$  amplitude have a uniformly distributed welded area, in which the density of weld covers most the surface, and the length of weld was measured to be 3.85 mm. However, higher weld density was observed with an increase in amplitude to  $42\ \mu\text{m}$ , and the length of weld was measured equal to 4 mm, as indicated by the dashed circles. Again, the metal condition and type of tempering metal significantly influenced the weld. Also, a high clamping force with high amplitude allows for high scrubbing motion between intimate surfaces, which results in a large welded area. It is clearly shown from the photographs that the aluminium surface offer higher susceptibility to plastic deformation than copper, as the aluminium is softer than copper, and also because aluminium is situated near to the horn tip, which receives more energy than copper, which is placed below.

In Figure 6-11, the photographs suggest an increase in the welded area in the specimens of 0.5 mm thickness, due to an increase in vibration amplitude, under a clamping force of 500 N and welding time fixed at 1 second. However, the weld density was observed to be lower than that observed for the 0.1 mm thickness specimen. The analyses of the forming areas confirm that the annealed specimens produce large weld areas relative to the half-hard specimens, where the weld length for the 0.5 mm thick, half-hard Al-Cu specimens was measured to be 3.4 mm for 17  $\mu\text{m}$  amplitude, and 3.8 mm for 42  $\mu\text{m}$  amplitude. Furthermore, the copper specimens exhibit a low weld density with significant light regions, and the reason for that was attributed to the difference between hardness and surface roughness for the aluminium and copper, meaning that the copper is harder than the aluminium and less susceptible to plastic deformation. Finally, it is important to state here that the photographs which were obtained from microscope investigations were different in contrast colour of the welds, because these photos were extracted from specimens of aluminium and copper with different compositions of metals as well as from different tempering. Furthermore, the use of the Nomarsky mode which can reflect different contrast colour in observing specimens that contain little or no optical. Because, the Nomarsky mode can increase the inspection of specimens and provide clear observation, through use interference contrast, which the features of surfaces can be standing out clearly under Nomarsky modes that are difficult to see under bright field illumination.

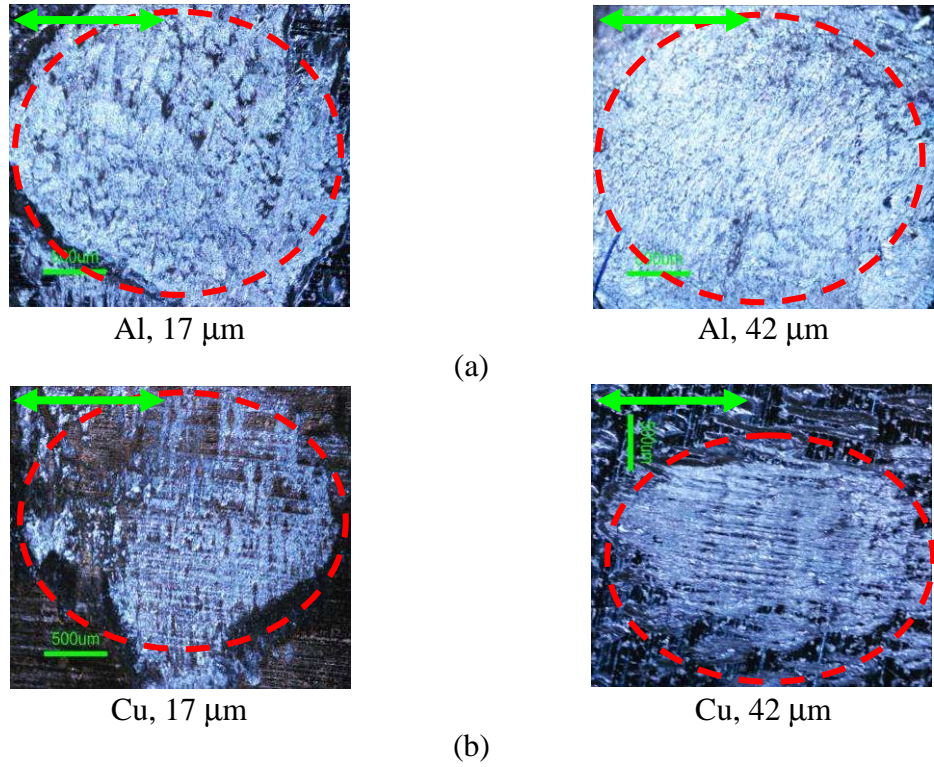


Figure 6-10 Photographs of peeled Al-Cu specimens, with double tipped arrows show direction of ultrasonic vibration, scale bar of 500 μm, red dashed circle show weld area, clamping force of 500 N and thickness of 0.1 mm annealed: (a) aluminium (b) copper

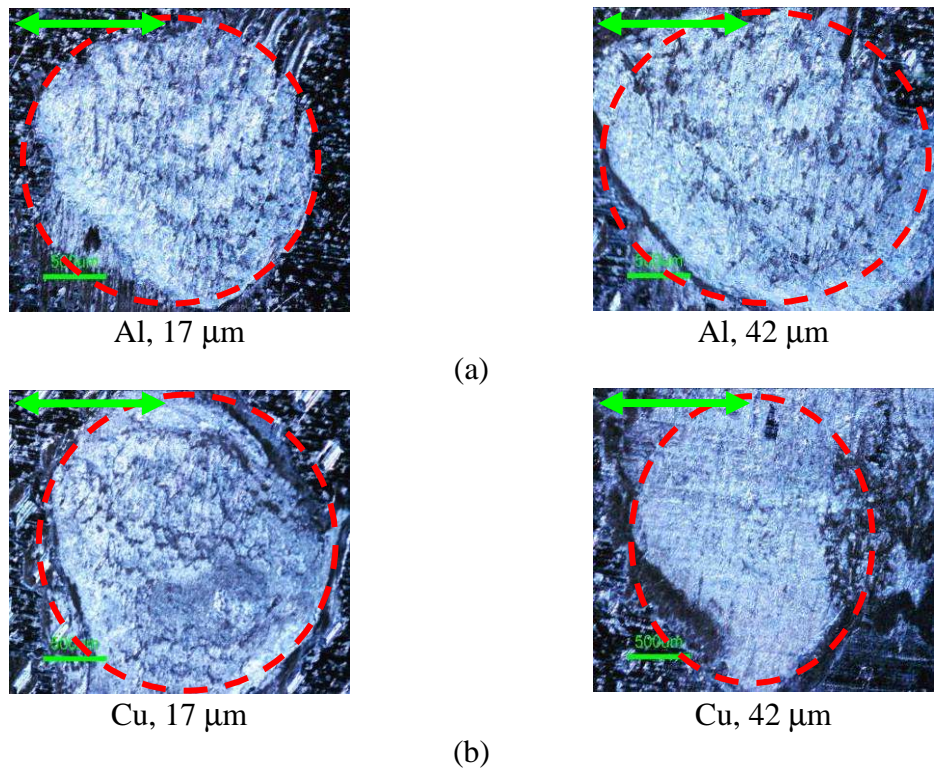


Figure 6-11 Photographs of peeled Al-Cu specimens, with double tipped arrows show direction of ultrasonic vibration, scale bar of 500 μm, red dashed circle show weld area, clamping force of 500 N and thickness of 0.5 mm half-hard: (a) aluminium (b) copper

## 6.5 Scanning electron microscopy (SEM) investigations

The microstructure of the deformed surfaces which are obtained from the debonded specimens that were welded under various process and metal parameters were investigated and analysed. The investigations were conducted using scanning electron microscope (SEM). The type of SEM which was used was a ZEISS-Sigma VP, as shown in Figure 6-12. The instrument operates by focusing high-energy electrons from the microscope to generate a signal at the deformed region of the specimen, which the microscope then examines at a very fine scale [126]. The signals which are produced from the electron sample interactions offer a significant amount of information about the tested surface, including chemical compositions, external morphology and crystalline information [127, 128].



Figure 6-12 Scanning electron microscopy (SEM)

In this research, the SEM was performed to study the external morphology and chemical compositions for testing surfaces which were selected from the combination of Al-Cu specimens. The investigations were performed on dissimilar configurations, produced under specified process parameter settings, for example a clamping force of 500 N and a vibration amplitude of 42  $\mu\text{m}$ . Also, two specimen thicknesses of 0.1 mm and 0.5 mm were chosen, in order to compare between the morphology of surfaces which were identified from joining due to the ultrasonic spot welding process. Prior to investigation, the debonded specimens were cleaned in an ultrasonic bath with acetone and methanol, and fixed inside the microscope chamber. After that, the prepared specimens were loaded into the SEM [27]. All images of the deformed surfaces were taken with a suitable resolution of

up to (100x) magnification. Images which were captured from the SEM were imported into Alicona Mex software [129], to analyse the welded areas. The Alicona software is used to process the experimentally-acquired SEM images of the aluminium and copper specimens, which are categorised as either fully annealed for specimens of 0.1 mm thickness, or half-hard for specimens of 0.5 mm thickness, as shown in Figure 6-14. The observations were conducted using an SEM DEM (Digital Elevation Model) with a (50 x) magnification, and were used to investigate the deformed surfaces produced from welds using process parameters settings such as a clamping force of 500 N, and vibration amplitude of 42  $\mu\text{m}$ . The measurements of the deformation surfaces were drawn across the horizontal path (indicated by the red line) as shown in Figure 6-13, which the path is represented the actual length of the weld (up to 4 mm).

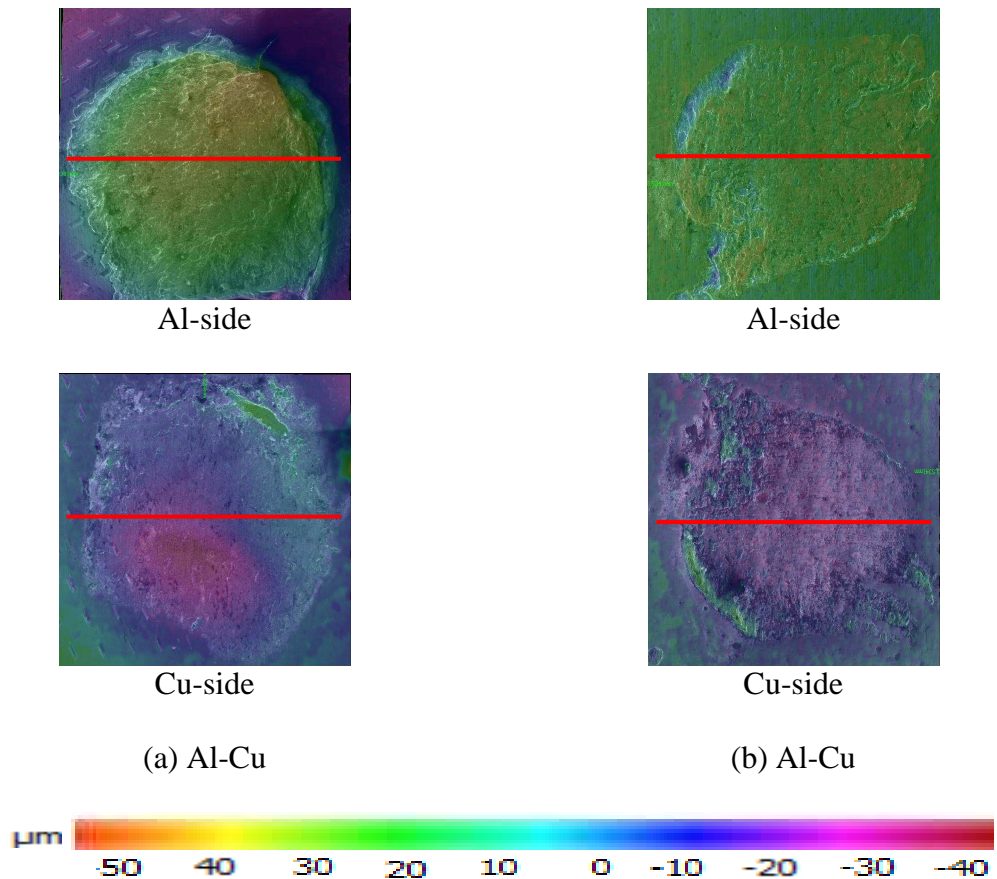


Figure 6-13 SEM images of Al-Cu specimens, magnified at 50 x, thickness: (a) 0.1 mm annealed, (b) 0.5 mm half-hard. the lower image shows the mating surface to the upper image

From Figure 6-13, it can be seen that these process parameters clearly affect the deformation areas, where the differences can be identified by the contours which indicate

the levels of morphology, measured in microns. The anaglyph viewer is a mode available in the Alicona software which contains the basic features of the image viewer and enables 3D measurements to be conducted without requiring a DEM. The anaglyph is necessary to make measurements because it allows the disparities between the images to be analysed, by magnification of the tested surfaces. For better observation of the deformed surfaces (shown in Figure 6-13), an adjustment was made by the appropriate scaling of the z-position of the visualised DEM images. Figure 6-14 shows the 3D topography scaling of the aluminium and copper deformation surfaces respectively. The topography indicates the disparities in the deformed surfaces, for which the regions were coloured relative to the percentage of deformation, measured in microns. It is very important to state that the adjustment of the z-position does not have an influence on the actual surfaces computed for the DEM, as the magnification of the adjustment only affects the visualisation of the DEM images.

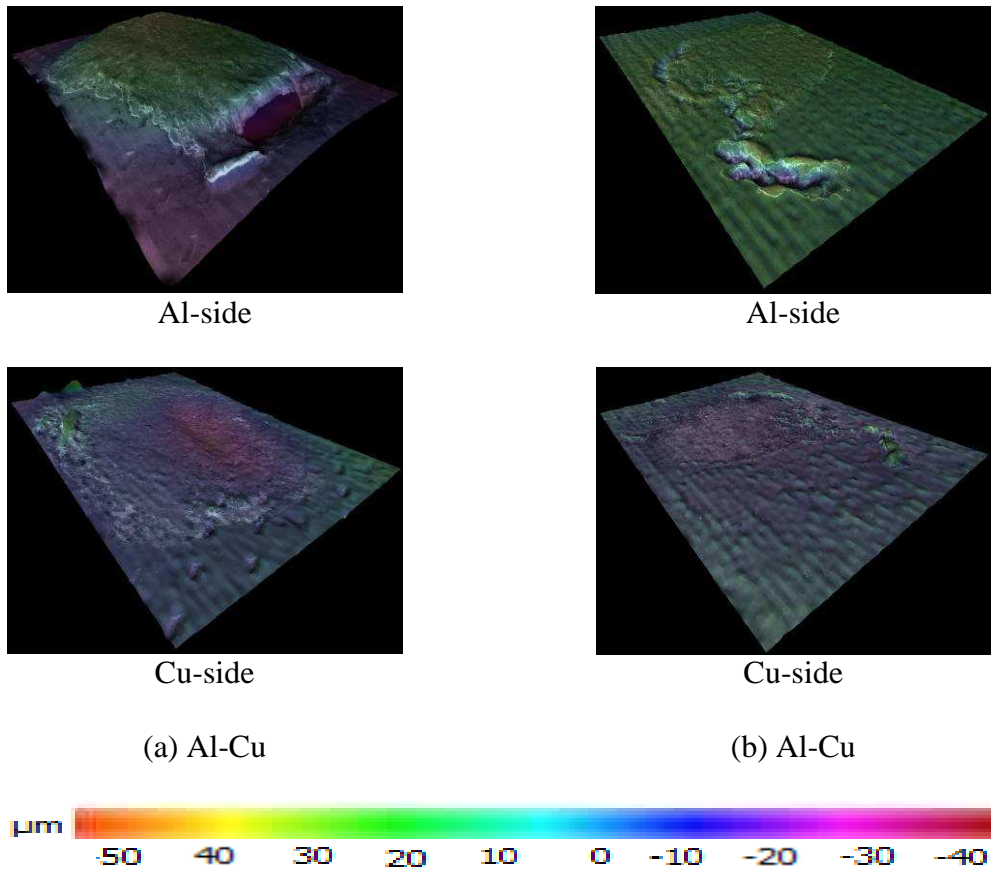
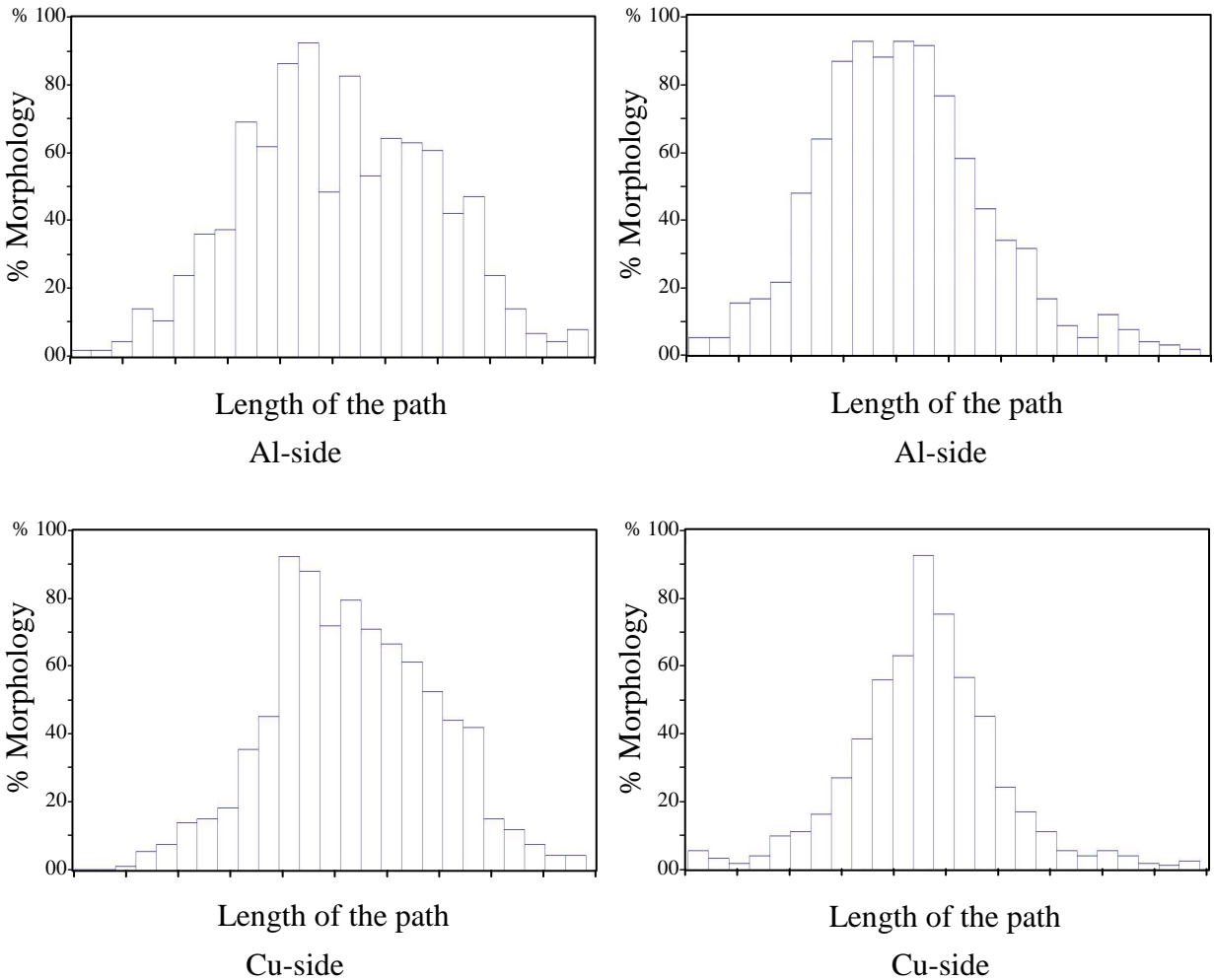


Figure 6-14 Anaglyph z-position images of Al-Cu specimens, magnified at 50x, thickness: (a) 0.1 mm annealed, (b) 0.5 mm half-hard, showing the same specimens as in Figure 6-13

The analyses of the results were extracted from the Anaglyph images of the SEM, and are shown in Figure 6-15. It was shown that the percentage of morphology surfaces is greater when welding Al-Cu with 0.1 mm thickness, compared to Al-Cu with 0.5 mm thickness, which indicates that more energy was received by the welded areas, due to the low hardness of aluminium (273) and copper (517), with 0.1 mm thickness, compared to the hardness of aluminium (676) and copper (863), with 0.5 mm thickness. However, thickness and surface roughness were also considered as an important factor that influenced the morphology of the welded areas. Furthermore, the Anaglyph indicates how the thickness and metal surface conditions can affect welded areas, due to the reactivity of clamping force at 500 N and vibration amplitude at 42  $\mu\text{m}$ , to allow sufficient energy transfer to welded areas. The images indicate that the Al-Cu with 0.1 mm thickness allows marginally greater morphology than images of Al-Cu with 0.5 mm thickness. From these analyses, it can be concluded that higher morphology of the surfaces were generally shown with surfaces with low hardness and surface roughness, regardless of the thickness.



(a) Al-Cu

(b) Al-Cu

Figure 6-15 Deformation of (Al-Cu), clamping force 500 N, amplitude 42  $\mu\text{m}$ , length of the path 4 mm, (a) 0.1 mm annealed, (b) 0.5 mm half-hard

An SEM investigation was also performed to examine the weld quality of a Al-Cu welded configuration, by providing detailed high resolution images of the specimens by using an energy dispersive x-ray analyser technique (EDAX). The technique is used to provide elemental identification and quantitative compositional information. The studies were conducted on a configuration which was produced under the process parameter settings of a clamping force of 500 N, vibration amplitude of 42  $\mu\text{m}$ , specimen thickness of 0.1 mm in the annealed condition, represented by the symbols (1) and (2), and a specimen thickness of 0.5 mm in the half-hard condition, represented by the symbols (3) and (4) respectively, as shown in Figure 6-16. The reason for this was to investigate the deformation surfaces by indicating the reactivity of diffusion between aluminium and copper deformed surfaces, through extraction of the chemical compositions between intimate surfaces. Figure 6-17 and Figure 6-18 show higher magnifications for the locations 1, 2, 3 and 4 for the aluminium and copper deformed surfaces which are indicated in Figure 6-16 by white circles, using SEM EDAX investigations.

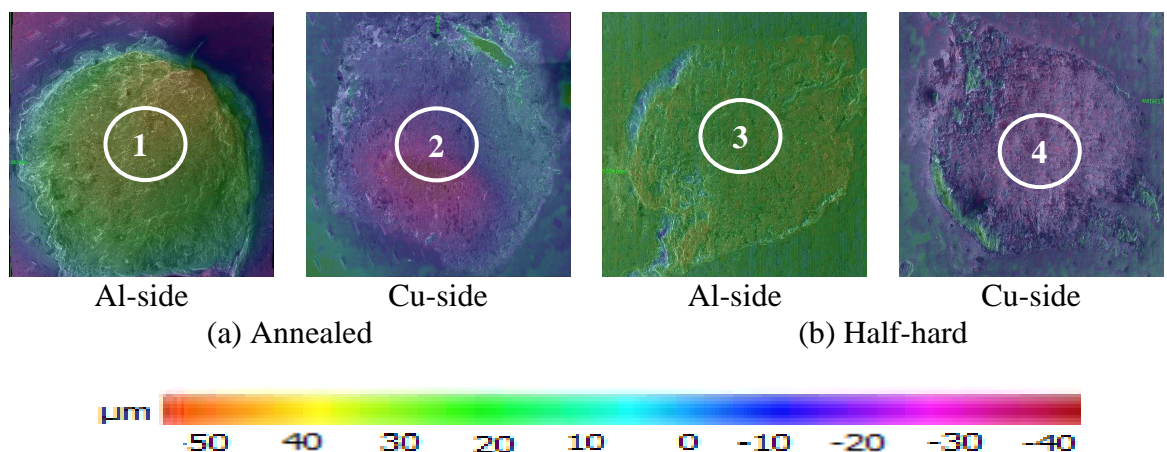


Figure 6-16 SEM images of (Al-Cu) specimens, magnified at 50 x, clamping force 500 N, amplitude 42  $\mu\text{m}$ , (a) 0.1 mm annealed, (b) 0.5 mm half-hard. Regions 1-4 show the regions examined by SEM in Figures 6-17 and 6-18

From Figure 6-17 and Figure 6-18, the x-ray diffraction reveals a chemical composition for the different tempering conditions of aluminium and copper deformation surfaces, where

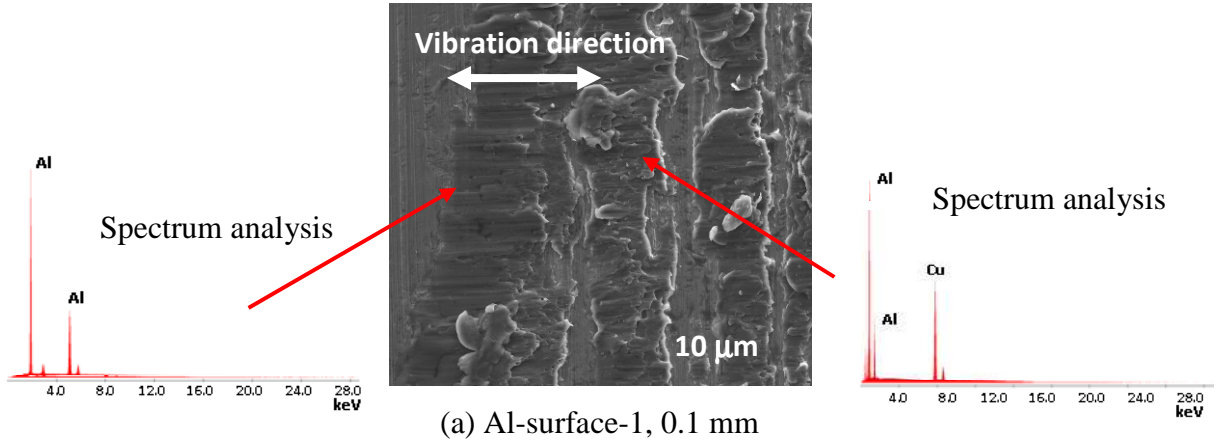
the x-ray diffraction spectrum indicates the deposition percentage for each testing metal. For example, the x-ray diffraction records a chemical composition for Cu of 38.69 (wt %), which indicates low deposition of Cu on the Al surface, as shown in Figure 6-18 at location-1. However, high deposition of Al was identified on the Cu surface, since the spectrum analysis of reaction surface records a chemical composition for Al of 79.43 (wt %), as shown in Figure 6-17 at location-2. The results suggest that the Al is more susceptible to plastic deformation than Cu, although the two metals share the same tempering condition (annealed). The percentage of chemical compositions was observed to be different when the investigation of the aluminium and copper surfaces was carried out on the half-hard condition samples. Figure 6-18 and at location-3, suggests a lower composition of Cu is identified on the Al surface, which is equal to 14.55 (wt %), relative to the Cu composition that is indicated with the annealed specimens, whilst the Al shows a high percentage of chemical composition on the Cu surface, where the spectrum analysis of the reaction surface records the composition for Al equal to 69.05 (wt %) and 30.95 (wt %) for Cu, as seen with location-4. However, the higher depositions of Al in the case of half-hard specimens are still lower than Al for the annealed specimens.

EDAX ZAF Quantification (Standard less)  
Element Normalized

Elem	Wt %	At %	K-Ratio	Z	A	F
AlK	100.00	100.00	1.00	1.00	1.00	1.00
Total	100.00	100.00				

EDAX ZAF Quantification (Standard less)  
Element Normalized

Elem	Wt %	At %	K-Ratio	Z	A	F
AlK	61.31	18.33	0.0351	1.0744	0.2895	1.00
CuK	38.69	54.25	0.7567	0.9599	1.0018	1.00
Total	100.00	100.00				



EDAX ZAF Quantification (Standard less)  
Element Normalized

Elem	Wt %	At %	K-Ratio	Z	A	F
AlK	69.05	90.09	0.5309	1.0195	0.6556	1.00
CuK	30.95	9.91	0.1850	0.8991	1.0004	1.00
Total	100.00	100.00				

EDAX ZAF Quantification (Standard less)  
Element Normalized

Elem	Wt %	At %	K-Ratio	Z	A	F
CuK	100.00	100.00	1.00	1.0000	1.00	1.00
Total	100.00	100.00				

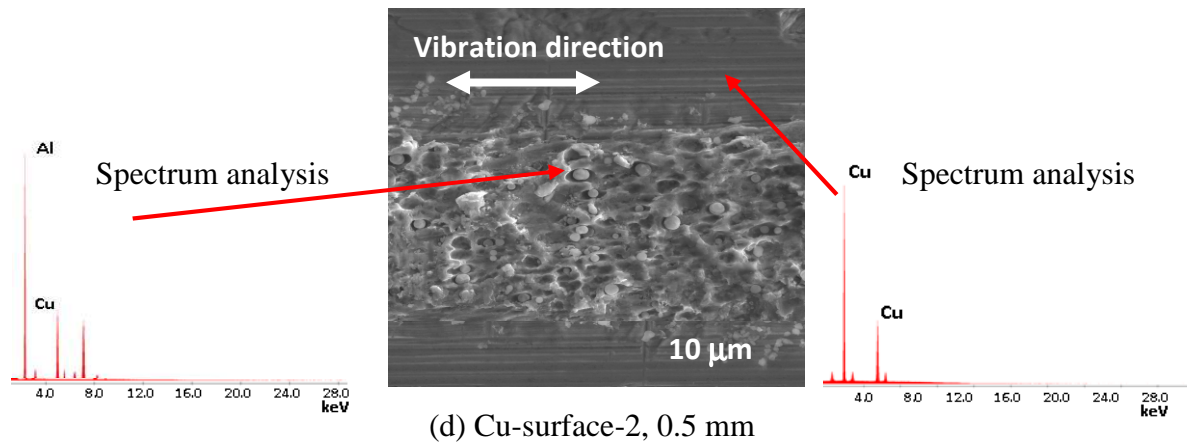


Figure 6-17 SEM EDAX images of 0.1 mm annealed surfaces for Al-surface-1 (a) and Cu-surfaces-2 (b), show as regions 1 and 2 in Figure 6-16

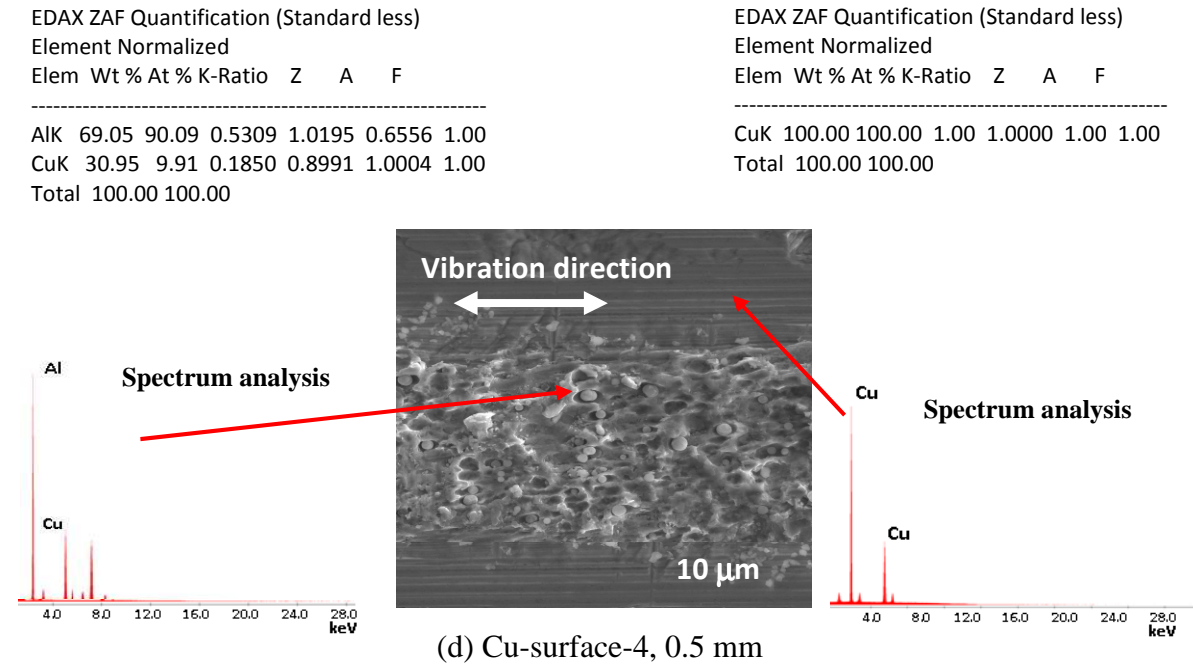
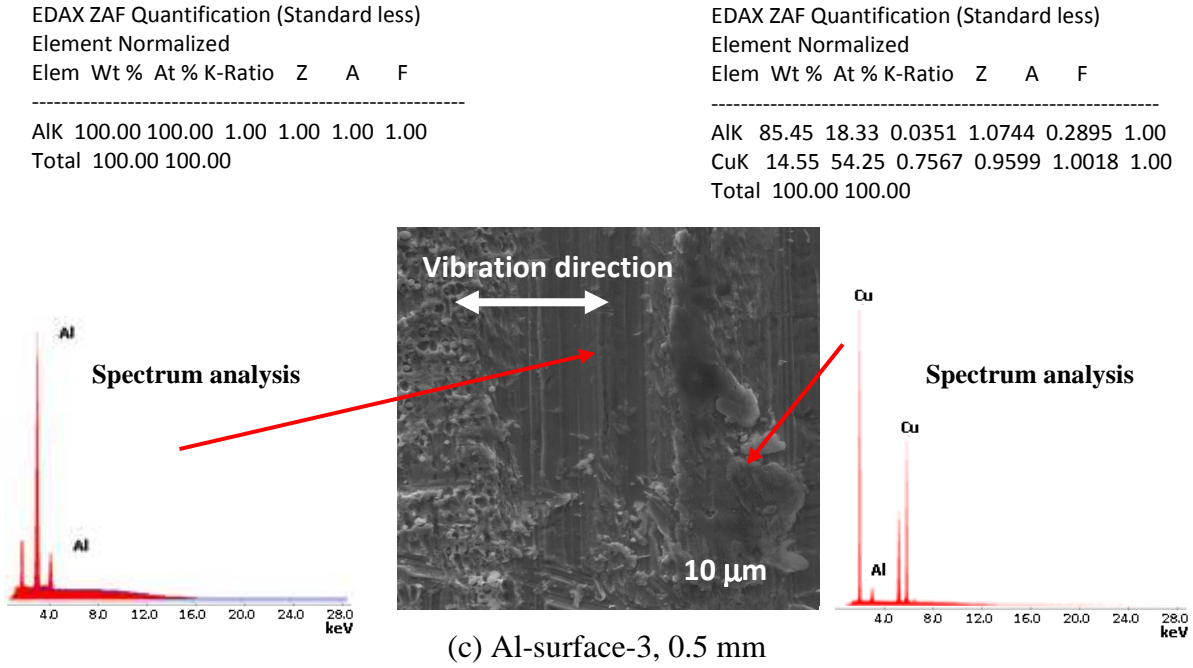


Figure 6-18 SEM EDAX images of 0.5 mm half-hard surfaces for Al-surface-3 (c) and Cu-surfaces (d), show as regions 3 and 4 in Figure 6-16

The results suggest that the susceptibility of the weld coupon metal to plastic deformation under ultrasonic vibration and clamping force is related to the hardness and metal surface condition such as roughness and oxides. Al is a softer metal than copper and can be more readily deformed plastically during ultrasonic welding, for which high deposition of Al

atoms was observed on the Cu surface, and the x-ray diffraction confirmed that through providing high percentage of chemical composition for Al, relative to Cu. Hardness, roughness and oxides significantly affect the reactivity between intimate surfaces, through providing low deposition of metal atoms that influence weld quality.

## 6.6 Summary

An analysis of the weld quality of the deformation surfaces produced by ultrasonic spot welding has been performed. The deformation areas of specimens were investigated for a range of welding conditions. The data was extracted for similar and dissimilar configurations of aluminium and copper specimens with thicknesses of 0.1 mm and 0.5 mm. The investigation of the testing surfaces was successfully conducted by utilising both the optical microscope and the scanning electron microscopy system. The microscope investigations show the difference in deformation condition between the Al and Cu surfaces in debonded specimens of Al-Al, Cu-Cu, and Al-Cu. Higher weld area density was recorded with the softer metals, which are characterised by low hardness and surface roughness in comparison with the harder metals. The thickness of the specimens, in addition to the metal tempering, provides clear variations in the deformations of examined surfaces. The results agreed that the difference between weld lengths is not so large between aluminium and copper. However, the density of formation areas is noticeable, which is indicated to be higher with annealed specimens rather than half-hard specimens. Also, very low weld scattering regions were shown with aluminium compared to the copper. Good weldability of configurations comprising similar specimens result in the generation of good quality welds, however more energy is required to improve the resultant weld quality for dissimilar metal configurations. Furthermore, weld quality can be enhanced by joining thinner specimens, regardless of the metal surface properties.

The SEM investigations of welded surfaces show that oxide layers on the metal surfaces can be removed using high intensity ultrasonic vibration, such as an amplitude of 42  $\mu\text{m}$ , combined with a suitable clamping force, for example 500 N, allowing the welding of newly formed surfaces to take place, through providing high morphology which enhances weld quality, such as for annealed specimens. However, half-hard specimens exhibit significant severity with the same process parameters, which can provide acceptable welds with low deformation, and consequently lower quality. The SEM mode 'Anaglyph' showed that no mixing of the metallic components occurred by the diffusion between

intimate surfaces. Thus, it can be concluded that adhesion and cohesion are the main mechanisms responsible for the ultrasonic welding of metals. However, the SEM measurements of deformed surfaces can reveal the percentage of morphology, which indicate that higher deformations are prevalent over those specimens that are softer and lower in hardness and surface roughness. In addition, low thicknesses, such as 0.1 mm, offer a high density of the welded areas, compared with thicker specimens. High magnification SEM results suggest Al is a softer metal than copper and can be more readily plastically deformed during ultrasonic welding, on which high deposition of Al atoms was observed on the Cu surface. The x-ray diffraction analyses record the percentages of chemical compositions for Al and Cu, due to hardness, roughness and oxides, as well as due to different metal tempering. Hardness, roughness and oxides significantly affect the reactivity between intimate surfaces, by providing low metal atom deposition that influences weld quality. Finally, it can be concluded that the weld quality can be affected by several factors such as standard of tooling design, amount of energy delivered to the welding area, and the level of knowledge of the best combinations of welding process parameters for the desired metal joining configuration.

## Chapter 7

### Discussion, conclusions and suggestions for future work

#### 7.1 Discussion

The work presented in this thesis outlines the study of the ultrasonic welding of metals. The work is based around the fact that the welding system will be tuned at an operating frequency of 20.81 kHz, which is very close to the operating frequency of the ultrasonic transducer. The first part of this study focuses on the design of the welding horn. This is a very important procedure, because the device is responsible for several vital functions, including the transfer of ultrasonic energy to the welding zone, prevention of specimens sliding during the joining process, and the application of the proper clamping force which is recommended for acceptable bonding. It also supports the welding stack, which is the horn connected with the transducer, on the driving machine by fixing it at the nodal plane. The development of the welding horn was split into two stages. The first stage begins with mathematical modelling, including the development of both an analytical model and a finite element model (FE). The analytical model is produced by deriving the equation of motion, based on the assumption that the horn vibrates according to a half-wave length ( $\lambda/2$ ), an assumption on which the model was created, modelled and predicted. The FE program Abaqus was employed to design the final configuration of the welding horn. The benefit of modelling is to reduce the number of design iterations and optimise the solution, thereby reducing the time and costs involved for the horn manufacturer.

The FE modelling approach results in the development of the welding horn through the enhancement of the understanding in the vibrational and dynamic characteristics, and the examination of many criteria which indicate the performance of the working horn. For example, matching the horn excitation frequency to the operating frequency of the transducer ensures that the horn will be vibrated longitudinally at 20.81 kHz, allowing a good separation of the longitudinal frequency mode through the isolation of the tuning mode from other non-tuned modes, guaranteeing uniformity of the vibration amplitude at the horn working surface, high gain factor and the avoidance of any stress which may initiate at the points between connecting components. The identification of these criteria is essential to model the excitation horn at the desired vibration mode of 20.81 kHz, and to

ensure the high transmission of ultrasonic energy to the welding specimens with minimum dissipation. The experimental techniques which have been adopted in this work consist of experimental modal analysis (EMA), and harmonic response analysis, and are used to characterise the fabricated models and to validate and update the mathematical models. The analyses of the steel horn result in a good validation between modal analysis and harmonic analysis. For example, the frequency of the horn was longitudinally analysed and recorded at 20.81 kHz for FEA and 20.77 kHz for EMA, which indicates a low percentage of error of 0.19 %. Analyses of the non-tuned modes were also undertaken, because the amplitude uniformity of the welding tip significantly influences the weld quality. Acceptable variations of vibration modes were measured using both FEA and EMA, which recorded variations of over 1 kHz between longitudinal and torsional modes, and even higher between longitudinal and flexural modes. Different horn shapes were modelled, and it was found that the horn with a catenoidal profile and integrated flange coupling and welding tips provides a good vibration response, offering a high amplitude magnification which is characterised by a gain factor of 4.108. The accurate design of an integrated spot welding horn tip with flange coupling located at the nodal plane shows that the shifting of maximum stress can be achieved, and directed to be concentrated near to the nodal plane. The final design of the spot welding horn was manufactured using a CAD-CAM technique, for which the experimental analysis verifies the vibrational response of the welding horn. Welding components were also designed, such as a rigid anvil, welding stack holder, rigid bed and fixing tools, which form the complete welding system. The size and dimensions of the welding components were set to match the lateral-drive system configuration which is suitable for joining thin gauges such as light plates, sheets and foils. Verification from the spot-welding system is identified by experimentally joining metals. The welding stack was mounted to the driving machine by means of a stack holder. A stationary anvil, welding bed and fixtures were also installed to ensure the system was prepared for welding.

An experimental study of welding conditions was undertaken, by investigating the relations of a number of process and metal parameters, and many tests were conducted. Aluminium and copper were selected for the welding tests, and the overlap position of the specimens to be joined was identified to match the spot-welding condition. The geometry of the specimens were prepared according to the standard required for the welding of thin specimens, whilst the mechanical data was extracted using high precision techniques such as uniaxial tensile testing to determine Young's modulus, yield tensile strength, ultimate

tensile strength, and elongation after test completion. Other techniques, such as extensometry, were adapted to measure actual elongation in the test specimens. A series of weld coupons were studied, comprising the welding of similar metal specimens in the form of Al-Al and Cu-Cu, and for dissimilar metal specimens, including Al-Cu and Cu-Al. The weld coupons were 0.1, 0.3 and 0.5 mm thick and either in the annealed or half-hard metal condition. The different metal surface conditions of aluminium and copper were also investigated, such as hardness and surface roughness, because these parameters significantly affect both bond strength and weld quality.

Good welds were obtained for tests involving variations in both process and metal parameters, and the results were successfully collected using the computerised program of the 2 kN load cell machine. Study the relations of process parameters such as clamping force, amplitude of vibration, welding time and ultrasonic power, as well as metal parameters such as oxides, hardness and surface roughness, was successfully undertaken on the debonded specimens from the tensile test machine. Although there have been numerous studies into weld strength and weld quality, and that the fundamentals have been known for long time, they have not received proper attention. In this study, the results suggest that the bond strength is most sensitive to the relationships between clamping force and vibration amplitude, and also to a lesser extent, the relationships between clamping force and input power. However, the relationships between weld time and vibration amplitude have a much lower effect on strength. Overall, the weld strength results suggest that the Al-Al welds are stronger and more consistent with the weldability than the Cu-Cu welds, and the average weld strengths are higher, above 500 N, where excessive force restricts the lateral movements which are essential for welding. Good levels of bondability in aluminium and copper joints were obtained by welding thin specimens, such as those of 0.1 mm in thickness, compared to those with thicknesses of 0.3 mm and 0.5 mm. In the welding of dissimilar metals, stronger welds are produced when the aluminium specimen is placed on top and in contact with the ultrasonic horn tip, rather than the copper. Experimental evidence has shown that joining dissimilar metals either in configurations of Al-Cu or Cu-Al, the increase in energy level and time was necessary to generate an acceptable bond. For most weld configurations, prolonged welding times will affect the bonds by creating fatigue damage. However, very short welding durations result in incomplete welds. The welding tests showed that good welds are those which are characterised by matching between clamping force and vibration amplitude, because

insufficient clamping force results in sliding between the horn tip and the upper surface of the top specimen, whilst a very high force can reduce the weldability. From a different perspective, the high amplitude of the exciting horn matched with a high clamping force can result in the suppression of the relative motion between intimate surfaces, and hence lowers the weld strength and reduces weld quality, whereas excessive vibration can lead to a dislocation of the bonding between atoms at intimate surfaces, particularly at the end phase of weld, resulting in a reduction in weld consistency. Also, high noise and specimen marking were observed for these conditions, especially with the harder metal, such as the specimens in the half-hard condition. During the weld strength investigations under different welding conditions, it was observed for some tests that the welds were damaged in the deformation area was identified. Amplitude profiling from 42  $\mu\text{m}$  to 17  $\mu\text{m}$  resulted in a more pronounced increase in weld strength and raised consistency and reduced damage in the welds. Furthermore, in addition to the elevation in weld strength, a significant enhancement in weldability was observed. However, horn tip/specimen adhesion and specimen marking did not abate, but low variations of weld strength were observed for high-stiffness specimens. The FE models were used to investigate numerically the metal properties that extracted from the experimental tests. The numerical model was adjusted at each setting of process parameters to define the boundary conditions of spot welded specimens. The results of the FE model and experimental tensile test machine, for the load-displacement curves profiles, allow for good estimation to the order of magnitude of the peak load. The numerical results of the FE model of joining tests were matched with the experimental results that were obtained from the tensile shear tests.

It can be concluded that melting does not occur as a mechanism of welding, irrespective of the configuration which has been adopted, and that the bonded interface is generated in a solid-state form. The deformed area of the welded specimens was successfully investigated, using Nomarsky optical microscopy. A range of deformation conditions were studied and observed for different weld coupons, such as Al-Al, Cu-Cu, Al-Cu and Cu-Al. Areas with higher deformation levels were recorded in softer metals, such as those which were in the annealed state. This is because sufficient energy has been transferred into the welding area. Specimen thickness and metal properties and conditions of the metal surface, such as hardness and roughness, also affect the deformation level significantly more compared to harder metals. If good matches of process parameters are guaranteed, and if the weldability is fine, then the weld quality which is produced will be satisfy, such as for

those configurations which contain specimens of similar metals, whilst in dissimilar metal configurations, higher energy and durations are recommended in order to achieve good quality. A number of the results shown in this thesis illustrate that good quality welds can be developed by joining thin specimens, regardless of the surface conditions of the metal.

The SEM observations made at the welding interface for the deformed surface areas of both aluminium and copper show that the surface oxide layer can be removed by applying high intensity ultrasonic vibration with amplitude of 42  $\mu\text{m}$  along with a proper clamping force, for example 500 N, allowing the welding of newly formed surfaces to take place. The SEM Anaglyph viewer showed that no mixing occurred by melting between intimate surfaces, which indicates that USMW occurs due to adhesion and cohesion mechanisms. Furthermore, a high concentration of weld activity is exhibited in the topography of the deformed surfaces for those specimens with a low thickness, such as 0.1 mm (annealed) for both aluminium and copper, compared to the thicker specimens, such as 0.5 mm (half-hard). Also, the x-ray diffraction analyses indicate the percentage of chemical compositions for Al and Cu, which extracted from the high magnification images. The spectrum analyses confirm that high deposition of Al atoms seen on Cu surface.

## **7.2 Conclusions**

This study has provided details on the design, characterisation and testing of a lateral-drive ultrasonic metal spot welding system. The welding system is able to join relatively thin metals, such as sheets, plates, foils and wires. The system configuration which should be adopted for the intended metal welding is dependent on the force and vibration levels which are required. An ultrasonic metal welding horn has been modelled and fabricated with high precision to ensure that a high level of ultrasonic energy is transferred to the welding zone, through intensive engineering design and manufacture. Furthermore, the horn design overcomes many issues which encountered by industrial fields and manufacturing process. The welding system, represented by the welding stack (the horn connected to the transducer) and the respective rigid anvil and fixtures are precisely mounted on driving machine. The device is capable of controlling process parameters, which provides good weldability under the application of different welding conditions. Furthermore, the system is suitable for the study of weld strength and quality, and their dependencies on the relations of process parameters such as clamping force, amplitude of vibration, welding time and input power. This can overcome conventional welding

machines which have limitations in terms of delivering energy to the weld and also in the control of process parameters. Furthermore, the study provided an inexpensive welding machine, compared with other commercial welding machines. It was observed that the welding performance of an ultrasonic metal spot welding system depends on the design of the acoustic horn, efficiency of the transducer and capacity of supplying power from the generator. Consistency of the joint and enhancement of the weld strength and quality is obtained in this study through employing both constant and stepped amplitude profiling. Finally, the study provides the foundation for ultrasonic metal welding, by contributing an effective tool design to enable a high level of performance which can result in the welding together of any thin metals.

### **7.3 Future works**

The current work has provided an integrated design of an ultrasonic spot welding system which is suitable for joining thin metal specimens. Several distinct welding configurations have been analysed, providing good study of weld strength and quality with respect to the relations between process and metal parameters. Despite the success of the welding system, there are several avenues of research which would be of interest in the future which would improve the welding procedure and weld quality even further, and these are outlined below.

1. For further enhancement of ultrasonic metal spot welding, the process should be more integrated, through the establishment of a suitable ultrasonic tooling system. It may be necessary to develop an improved methodology for measuring the electrical impedance at the terminal surface of the ultrasonic transducer, as the electrical impedance is dependent on the mechanical impedance, among a number of other quantities, by which the adjustment of the clamping force to a specific level can lead to the matching of the electrical impedance to the horn.
2. To better demonstrate the feasibility of ultrasonic metal spot welding of high ultrasonic vibration amplitude and proper clamping force on specimens to be joined, it is recommended that ultrasonic metal spot welding should be performed using a high capacity of power supply, for example greater than 1 kW, to allow the system to be more versatile and applicable, not only for joining small-scale specimens together, but also

large-scale. A high ultrasonic energy would produce strong welds for thicker specimens than are presently used.

3. Further research should investigate amplitude profiling, not only for joining ductile metals, but also extended to other metals such as those which are brittle. The ability to join specimens together should be examined by using a stepped amplitude input to improve the weld consistency and reduce adverse issues which can be encountered in welding, such as specimen adhesion and marking.

4. The enhancement of the weld quality should be analysed in greater depth. From this work, it is clear that the weld quality can be improved by matching between process and metal parameters. Therefore, it would be of interest to evaluate an alternative method of improving both weld strength and quality, using approaches such as metal strip insertion, buffer sheet composition, and horn tip coating vibration mode coupling for the tool excitation.

## References

1. N. Ahmed, *New Developments in Advanced Welding*, Woodhead/publishing, Place Published, 2005.
2. G. D. Janaki Ram, C. Robinson, Y. Yang, and B. E. Stucker, "Use of Ultrasonic Consolidation for Fabrication of Multi-Material Structures," *Rapid Prototyping Journal*, vol. 13, no. 4, pp. 226-235, 2007.
3. <http://www.techsonicultrasonic.com/index.php?option=com>, Accessed on 10<sup>th</sup> November 2012.
4. J. Mackerle, "Finite Element Analysis and Simulation of Welding - An Addendum: A Bibliography (1996-2001)," *Modelling and Simulation in Materials Science and Engineering*, vol. 10, no. 3, pp. 295-318, 2002.
5. M. Vlad, *Ultrasonic Welding of Aluminum: A Practical Study in Consistency, Part marking and Control Modes*, PhD Thesis, University of Iowa, 2008.
6. R. L. O'Brien, *Welding Handbook: Welding Processes*, American Welding Society, 1997.
7. D. Bakavos and P. B. Prangnell, "Mechanisms of Joint and Microstructure Formation in High Power Ultrasonic Spot Welding 6111 Aluminium Automotive Sheet," *Materials Science and Engineering*, vol. 527, no. 23, pp. 6320-6334, 2010.
8. F. Haddadi, D. Strong, and P. B. Prangnell, "Effect of Zinc Coatings on Joint Properties and Interfacial Reactions in Aluminum to Steel Ultrasonic Spot Welding," *Journal of the Minerals, Metals and Materials Society*, vol. 64, no. 3, pp. 407-413, 2012.
9. H. P. C. Daniels, "Ultrasonic Welding," *Ultrasonics*, vol. 3, no. 4, pp. 190-196, 1965.
10. S. Elangovan, S. Semeer, and K. Prakasan, "Temperature and Stress Distribution in Ultrasonic Metal Welding-An FEA-Based Study," *Journal of Materials Processing Technology*, vol. 209, no. 3, pp. 1143-1150, 2009.
11. E. T. Hetrick, J. R. Baer, W. Zhu, L.V. Reatherford, A.J. Grima, D.J. Scholl, D. E. Wilkoszd, S. Fatima, and S. M. Ward, "Ultrasonic Metal Welding Process Robustness in Aluminum Automotive Body Construction Applications," *Welding Journal*, vol. 88, no. 7, pp. 149-158, 2009.
12. <http://www.assemblymag.com/>, Accessed on 1<sup>st</sup> August 2003.
13. L. L. Silin, G. F. Balandin, and M. G. Kogan, "Ul'trazvukovaia Svarka," *Moscow*, 1962.
14. <http://www.thefabricator.com/article/arcwelding/understanding-ultrasonic-welding>, Accessed on 30<sup>th</sup> September 2008.
15. [http://www.emersonindustrial.com/en-US/documentcenter/BransonUltrasonics/Metal\\_Welding/165019\\_MetalWeldingBro\\_Final.pdf](http://www.emersonindustrial.com/en-US/documentcenter/BransonUltrasonics/Metal_Welding/165019_MetalWeldingBro_Final.pdf), Accessed on 1<sup>st</sup> June 2012.
16. <http://www.twi.co.uk/content/Ksrjip002.html>, Accessed on 19<sup>th</sup> June 2011.

17. J. L. Harthoorn, *Ultrasonic Metal Welding*, PhD Thesis, Eindhoven University of Technology, 1978.
18. J. G. Kura and H. W. Mishler, "Literature Survey on the Effect of Sonic and Ultrasonic Vibrations in Controlling Grain Size During Solidification of Steel Ingots and Weldments. Part 1 - Steel Ingots," *Battelle Memorial Institution Columbus of Defence Metals information center*, 1963.
19. J. C. Tucker, *Ultrasonic Welding of Copper to Laminate Circuit Board*, Faculty of the Worcester Polytechnic Institute, 2002.
20. <http://www.weldmyworld.com/blog/2012/01/the-process-of-ultrasonic-welding.html>, Accessed on 1<sup>st</sup> February 2012.
21. <http://www.thermosole.com/products/Ultrasonic%20Welding.pdf>, Accessed on 10<sup>th</sup> April 2012.
22. R. Goldman, *Ultrasonic Technology*, Reunhold Publishing Corporation, 1962.
23. P. B. Nagy, *Introduction to Ultrasonics*, 2001.
24. G. L. Timothy, "Review What is Ultrasound," *Biophysics and Molecular Biology*, vol. 93, pp. 3-83, 2006.
25. E. McCulloch, *Experimental and Finite Element Modelling of Ultrasonic Cutting of Food*, PhD Thesis, University of Glasgow, UK, 2008.
26. [http://www.guided-nde.com/\\_mgxroot/lle-volni-eng.html](http://www.guided-nde.com/_mgxroot/lle-volni-eng.html), Accessed on 2<sup>nd</sup> July 2010.
27. M. Bloss, *Ultrasonic Metal Welding: The Weldability of Stainless Steel, Titanium and Nickel-Based Super Alloys*, PhD Thesis, University of Ohio, 2008.
28. E. de Vries, *Mechanics and Mechanisms of Ultrasonic Metal Welding*, PhD Thesis, University of Ohio, 2004.
29. <http://www.sonobondultrasonic.com/welders-bonders-metals.asp>, Accessed on 5<sup>th</sup> June 2012.
30. [http://www.typesofwelding.net/ultrasonic\\_welding.html](http://www.typesofwelding.net/ultrasonic_welding.html), Accessed on 10<sup>th</sup> August 2011.
31. P. L. Derks, *The Design of Ultrasonic Resonators with Wide Output Cross-Sections* Eindhoven University of Technology, 1984.
32. S. Matsuoka and H. Imai, "Direct Welding of Different Metals Used Ultrasonic Vibration," *Journal of Materials Processing Technology*, vol. 209, no. 2, pp. 954-960, 2009.
33. J. P. Curie and P. Curie, *Translated in Lindsay, (1973), Academie des Sciences, Paris*, vol. 91, p. 294, 1880.
34. Lin, S., "Study on the Multifrequency Langevin Ultrasonic Transducer," *Ultrasonics*, vol. 33, no. 6, pp. 445-448, 1995.
35. Lin, S., "Sandwiched Piezoelectric Ultrasonic Transducers of Longitudinal-Torsional Compound Vibrational Modes," *Ultrasonics, Ferroelectrics and Frequency Control, IEEE Transactions on*, vol. 44, no. 6, pp. 1189-1197, 1997.

36. G. W. Pierce, *To Atherton Noyes, Jr.*, 1933.
37. M. Lucas, A. Cardoni, E. McCulloch, G. Hunter, and A. MacBeath, "Applications of Power Ultrasonics in Engineering," *Applied Mechanics and Materials*, vol. 13-14, pp. 11-20, 2008.
38. L. G. Merkulov, "Design of Ultrasonic Concentrations," *Soviet Physical Acoustics*, vol. 3, pp. 230-238, 1957.
39. D. Ensminger, "Solid Cone in Longitudinal Half-Wave Resonance," *The Journal of the Acoustical Society of America*, vol. 32, no. 2, pp. 194-196, 1960.
40. E. A. Neppiras, "Ultrasonic Welding of Metals," *Ultrasonics*, vol. 3, no. 3, pp. 128-135, 1965.
41. J. F. Belford, *The Stepped Horn*, Morgan Electro Ceramics, 2011.
42. G. Amza and D. Drimer, "The Design and Construction of Solid Concentrators for Ultrasonic Energy," *Ultrasonics*, vol. 14, no. 5, pp. 223-226, 1976.
43. A. Satyanarayana and R.B.G. Krishna, "Design of Velocity Transformers for Ultrasonic Machining," *Electrical India*, pp. 11-20, 1984.
44. A. Nanu, N. Marinescu, and D. Ghiculescu, "Study on Ultrasonic Stepped Horn Geometry Design and FEM Simulation," *Nonconventional Technology review*, vol. 4, no. 4, pp. 25-30, 2011.
45. K. Shu, H. Hsiang, and C. Chen, "The Design of Acoustic Horns for Ultrasonic Insertion," *Journal of the Chinese Society of Mechanical Engineers*, pp. 338-342, 2010.
46. S. S. Muhlen, "Design of an Optimized High-Power Ultrasonic Transducer," *Ultrasonics Symposium, 1990. Proceedings., IEEE 1990*, vol. 3, pp. 1631-1634, 1990.
47. K. Adachi, S. Ueha, and E. Mori, "Model Vibration Analysis of Ultrasonic Plastic Welding Tools Using the Finite Element Method," *The Proceeding of Ultrasonics International*, vol. 85, p. 727, 1986.
48. Kevin. O'Shea, "Enhanced Vibration Control of Ultrasonic Tooling Using Finite Element Analysis," *Vibration Analysis - Analytical and Computational, ASME*, vol. 37, pp. 259-265, 1991.
49. J. Woo, Y. Roh, K. Kang, and S. Lee, "Design and Construction of an Acoustic Horn for High Power Ultrasonic Transducers," *Ultrasonics Symposium, 2006. IEEE*, pp. 1922-1925, 2006.
50. J. B. da Silva, N. N. Franceschetti, and J. C. Adamowski, "Numerical Analysis of a High Power Piezoelectric Transducer Used in the Cutting and Welding of Thermoplastic Textiles," *ABCM Symposium Series in Mechatronics*, vol. 2, pp. 142-149, 2006.
51. G. Amza, Z. Apostolescu, and D. Nito, "Ultrasonic Welding of Composite Materials. Ultrasonic Booster Design and FEM Simulation," *Fascicle of Management and Technological Engineering*, vol. 6, no. 16, pp. 1181-1190, 2007.

52. J. B. Jones and J. J. Powers, "Ultrasonic Welding," *Welding Journal*, vol. 35, pp. 761-766, 1956.
53. J. N. Antonevich, "Ultrasonic Welding Equipment," *IRE Transaction on ultrasonics engineer*, 1959.
54. R. F. Tylecote, *The Solid Phase Welding of Metals*, Edward Arnold, 1968.
55. U. I. Chang and J. Frisch, "On Optimization of Some Parameters in Ultrasonic Metal Welding," *Welding Journal*, vol. 53, no. 1, pp. 24-35, 1974.
56. Heymann, E. and G. Pusch, "Contribution to the Study of the Role of Recrystallisation in the Formation of the Joint in Ultrasonic Welding," *Schweisstechnik*, vol. 19, no. 12, pp. 542-545, 1969.
57. M. Okada, S. Shin, M. Miyagi, and H. Matsuda, "Joint Mechanics of Ultrasonic Welding," *Journal of Japan Institute of Metals*, vol. 4, no. 4, pp. 250-256, 1962.
58. T. H. Hazlett and S. M. Ambekar, "Additional Studies on Interface Temperatures and Bonding Mechanisms of Ultrasonic Welds," *Welding Journal*, vol. 49, no. 5, pp. 196-200, May 1970.
59. P.L.L.M. DERKS, "Parameters That Influence the Ultrasonic Bond Quality," *Electro Component Science and Technology*, vol. 10, no. 4, pp. 269-275, 1982.
60. S. Elangovan, K. Prakasan, and V. Jaiganesh, "Optimization of Ultrasonic Welding Parameters for Copper to Copper Joints Using Design of Experiments," *The International Journal of Advanced Manufacturing Technology*, vol. 51, no. 1, pp. 163-171, 2010.
61. S. Elangovan, K. Anand, and K. Prakasan, "Parametric Optimization of Ultrasonic Metal Welding Using Response Surface Methodology and Genetic Algorithm," *The International Journal of Advanced Manufacturing Technology*, vol. 63, no. 5, pp. 561-572, 2012.
62. S. Elangovan, H. Shenton, and K. Prakasan, "Experimental Studies on Optimization of Process Parameters and Finite Element Analysis of Temperature and Stress Distribution on Joining of Al-Al and Al-Al<sub>2</sub>O<sub>3</sub> Using Ultrasonic Welding," *The International Journal of Advanced Manufacturing Technology*, vol. 55, no. 5, pp. 631-640, 2011.
63. S. Elangovan, S. Venkateshwaran, and K. Prakasan, "Experimental Investigations on Optimization of Ultrasonic Welding Parameters for Copper to Brass Joints Using Response Surface Method and Genetic Algorithm," *International Journal of Advanced Engineering Research and Studies*, vol. 1, no. 3, pp. 1-6, 2012.
64. S. Matsuoka, "Ultrasonic Welding of Ceramic/Metal," *Journal of Materials Processing Technology*, vol. 47, pp. 185-196, 1994.
65. T. Ishikuro and S. Matsuoka, "Ultrasonic Welding of Thin Alumina and Aluminum Using Inserts," *JSME Int Journal. Ser A. Solid Mech Material* vol. 48, no. 4, pp. 317-321, 2005.

66. H. Imai and S. I. Matsuoka, "Direct Welding of Metals and Ceramics By Ultrasonic Vibration," *Jsm International Journal Series a-Solid Mechanics and Material Engineering*, vol. 49, no. 3, pp. 444-450, 2006.
67. H. Imai and S. Matsuoka, "Finding the Optimum Parameters for Ultrasonic Welding of Aluminum Alloys," *Jsm International Journal Series a-Solid Mechanics and Material Engineering*, vol. 48, no. 4, pp. 311-316, 2005.
68. M. Kodama, "Ultrasonic Welding of Non-Ferrous Metals," *Welding International*, vol. 3, no. 10, pp. 853-860, 2010.
69. A. P. Hulst, "Macrosionics in Industry 2: Ultrasonic Welding of Metals," *Ultrasonics*, vol. 10, no. 6, pp. 252-261, 1972.
70. T. Watanabe, A. Yanagisawa, S. Konuma, A. Yoneda, and O. Ohashi, "Ultrasonic Welding of Al-Cu and Al-SUS304. Study of Ultrasonic Welding of Dissimilar Metals," *Welding International*, vol. 13, no. 11, pp. 875-886, 1999.
71. T. Watanabe, H. Sakuyama, and A. Yanagisawa, "Ultrasonic Welding Between Mild Steel Sheet and Al-Mg Alloy Sheet," *Journal of Materials Processing Technology*, vol. 209, no. 15-16, pp. 5475-5480, 2009.
72. M. Bloss and K. Graff, "Ultrasonic Metal Welding of Advanced Alloys: The Weldability of Stainless Steel, Titanium, and Nickel-Based Superalloys," *Trends in Welding Research, Proceedings of the 8th International conference* pp. 348-353, 2009.
73. N. W. Wright, J. D. Robson, and P. B. Prangnell, "Effects of Thickness Combinations on Joint Properties and Process Windows in Ultrasonic Metal Welding," *SAE International*, 2009.
74. M. Annoni and M. Carboni, "Ultrasonic Metal Welding of AA6022-T4 Lap Joints: Part I - Technological Characterisation and Static Mechanical Behaviour," *Science and Technology of Welding & Joining*, vol. 16, pp. 107-115, 2011.
75. Z. Zhu, K. Lee, and X. Wang, "Ultrasonic Welding of Dissimilar Metals, AA6061 and Ti6Al4V," *The International Journal of Advanced Manufacturing Technology*, vol. 59, no. 5, pp. 569-574, 2012.
76. T. H. Kim, J. Yum, S. J. Hu, J. P. Spicer, and J. A. Abell, "Process Robustness of Single Lap Ultrasonic Welding of Thin, Dissimilar Materials," *CIRP Annals - Manufacturing Technology*, vol. 60, no. 1, pp. 17-20, 2011.
77. M. Baboi and D. Grewell, "Evaluation of Amplitude Stepping in Ultrasonic Welding," *Welding Journal, Sponsored by the American Welding Society and the Welding Research Council*, 2010.
78. M. Baboi and D. Grewell, "Effect of Buffer Sheets on the Shear Strength of Ultrasonic Welded Aluminum Joints," *Welding Journal, Sponsored by the American Welding Society and the Welding Research Council*, pp. 86-91, 2009.

79. A. R. Pfluger and X. N. Sideris, "New Developments in Ultrasonic Welding," *Sampe Quarterly*, vol. 7, pp. 9-19, 1975.
80. J. Wodara, "Joint Formation in the Ultrasonic Welding of Metallic Substances " *ZIS Mitteilungen*, vol. 28, no. 1, pp. 102-108, 1986.
81. P. Kwanghyun, *Development and Analysis of Ultrasonic Assisted Friction Stir Welding Process*, PhD Thesis, University of Michigan, 2009.
82. G. Harman and J. Albers, "The Ultrasonic Welding Mechanism as Applied to Aluminum- and Gold-Wire Bonding in Microelectronics," *IEEE Transactions on Parts, Hybrid and Packaging* vol. 13, no. 4, pp. 406-412, 1977.
83. <http://www.ultrasonicwelding.org/horns.htm>, Accessed on 13<sup>th</sup> March 2012.
84. <http://jascoes.com/datasheets/WhatIsAnUltrasonicWeld.pdf>, Accessed on 5<sup>th</sup> May 2012.
85. <http://www.dukane.com/us/Documents/DesignGuides/Ti-MaterialCompatibility.pdf>, Accessed on 1<sup>st</sup> September 2009.
86. <http://en.wikipedia.org/wiki/Weldability>, Accessed on 7<sup>th</sup> April 2011
87. C. K. Fung, *Ultrasonic Transducer Equipped With a Magnetolectric Sensor for Weld Quality Monitoring*, MSc. Thesis, Hong Kong, Polytechnic University, 2009.
88. L. G. Merkulov and L. A. Yakovlev, "Propagation and Reflection of Ultrasonic Beams in Crystal," *Soviet Physics Acoustics*, vol. 8, no. 1, pp. 72-77, 1962.
89. L. G. Merkulov and A. V. Kharitonov, "Theory and Analysis of Sectional Concentrators," *Soviet Physical Acoustics*, vol. 5, pp. 183-190, 1960.
90. A. Cardoni, *Characterising the Dynamic Response of Ultrasonic Cutting Devices*, PhD Thesis, University of Glasgow, 2003.
91. <http://www.plasticsdecorating.com/articlesdisplay.asp?ID=102>, Accessed on 5<sup>th</sup> June 2012.
92. <http://www.nenastran.com/NewtoFEA/>, Accessed on 11<sup>th</sup> March 2012.
93. Hibbitt, K.a.S., Inc., ABAQUS User's Manual Version 6.10, 2011.
94. Experimental Modal Analysis, University of Cincinnati, CN-20-263-663/664, June 7, 1999.
95. P. Avitabile, "Experimental Modal Analysis: A Simple Non-Mathematical Presentation," *Modal Analysis and Control Laboratory*, 2010.
96. [http://en.wikipedia.org/wiki/Function\\_generator](http://en.wikipedia.org/wiki/Function_generator), Accessed on 18<sup>th</sup> May 2012.
97. D. K. Maslen and D. N. Rockmore, "The Cooley–Tukey FFT and Group Theory," *Modern Signal Processing, MSRI Publications*, vol. 46, pp. 281-300, 2003.
98. A. C. Mathieson, *Nonlinear Characterisation of Power Ultrasonic Devices Used in Bone Surgery*, PhD Thesis, University of Glasgow, 2012.
99. M. J. Troughton, *Handbook of Plastics Joining: A Practical guide*, William Andrew Inc., 2008.
100. [http://en.wikipedia.org/wiki/Ultrasonic\\_horn](http://en.wikipedia.org/wiki/Ultrasonic_horn), Accessed on 22<sup>nd</sup> May 2012.

101. A. Shoh, "Welding of Thermoplastics by Ultrasound," *Ultrasonics*, vol. 14, no. 5, pp. 209-217, 1976.
102. <http://www.matweb.com/>, Accessed on 24<sup>th</sup> June 2011.
103. K. Nishihara, T. Watanabe, and T. Sasaki, "Effect of Weld Tip Geometry on Ultrasonic Welding between Steel and Aluminum Alloy," *Advanced Materials Research*, vol. 89-91, pp. 419-424, January, 2010.
104. R. C. Hibbeler, *Mechanics of Materials*, Prentice Hall, 2011.
105. Y. Qiu, Z. Huang, A. Slade, and G. Thomson, *Optimization of Ultrasonic Tool Performance in Surgery*, Edited by J. Sloten, et al., Springer Berlin Heidelberg, Place Published, 2009.
106. Y. Ming, L. S. Fu, and S. Zheng, A New Optimization Method for Horn Designs in Ultrasonic Welding Systems, 2002.
107. G. Hunter, M. Lucas, I. Watson, and R. Parton, "A Radial Mode Ultrasonic Horn for the Inactivation of Escherichia Coli K12," *Ultrasonics Sonochemistry*, vol. 15, no. 2, pp. 101-109, 2008.
108. Signal Calc. 240V, 4.2.207, User's manual, Data Physics Corporation, 2007.
109. <http://en.wikipedia.org/wiki/Amplifier>, Accessed on 5<sup>th</sup> June 2012.
110. S.R. Kim, J. H. Lee, C. D. Yoo, J. Y. Song, and S. S. Lee, "Design of Highly Uniform Spool and Bar Horns for Ultrasonic Bonding," *IEEE Transactions on Ultrasonics, Ferroelectrics and Frequency Control*, vol. 58, no. 10, pp. 2194-2201, 2011.
111. <http://www.goodfellow.com/>, Accessed on 12<sup>th</sup> May 2010.
112. <http://mee-inc.com/tensile-testing.html>, Accessed on 20<sup>th</sup> June 2012.
113. Methods For Calibration and Grading of Extensometers for Testing of Metals, London, 1985.
114. <http://www.epsilontech.com/3542.htm>, Accessed on 13<sup>th</sup> June 2012.
115. Standard Test Methods for Tension Testing of Metallic Materials, ASTM International, 2009.
116. Aluminium and Aluminium Alloys-Foil, British Standard, 2006.
117. Test Pieces and Test Methods for Metallic Materials for Aircraft, British Standard, 2009.
118. D. Roylance, "Introduction to Fracture Mechanics," *MIT Open Course Ware*, pp. 1-17, June 14, 2001.
119. <http://www.jwnc.gla.ac.uk/metrology.html>, Accessed on 27<sup>th</sup> June 2012.
120. [http://www.instron.us/wa/applications/test\\_types/hardness/vickers.aspx](http://www.instron.us/wa/applications/test_types/hardness/vickers.aspx), Accessed on 28<sup>th</sup> June 2012.
121. F. Balle, G. Wagner, and D. Eifler, "Ultrasonic Metal Welding of Aluminium Sheets to Carbon Fibre Reinforced Thermoplastic Composites," *Advanced Engineering Materials*, vol. 11, no. 1-2, pp. 35-39, 2009.

122. E. Goold, "The Feasibility of Ultrasonically Bonding Surface Mount Components to Printed Circuit Boards," vol. 15, no. 3, pp. 33-39, 1989.
123. Z. Al-Sarraf and M. Lucas, "A Study of Weld Quality in Ultrasonic Spot Welding of Similar and Dissimilar Metals," *Journal of Physics: Conference Series*, vol. 382, no. 1, pp. 1-6, 2012.
124. M. Baboi and D. Grewell, "Comparison of Control Algorithms for Ultrasonic Welding of Aluminum," *Welding Journal*, vol. 89, pp. 243-248, 2010.
125. D. Murphy, *Differential Interference Contrast (DIC) Microscopy and Modulation Contrast Microscopy*, in *Fundamentals of Light Microscopy and Digital imaging*, Edited by Wiley-Liss, Place Published, 2001.
126. <http://web.utk.edu/~prack/MSE%20300/SEM.pdf>, Accessed on 1<sup>st</sup> October 2012.
127. [http://serc.carleton.edu/research\\_education/geochemsheets/techniques/SEM.html](http://serc.carleton.edu/research_education/geochemsheets/techniques/SEM.html), Accessed on 4<sup>th</sup> September 2012.
128. R. B. Pearce, "Scanning Electron Microscopy and X-Ray Microanalysis," *Geological Magazine*, vol. 140, no. 6, pp. 728-729, Nov. 2003.
129. Lime Tree House, *Alicona Imaging Mex, 5.0.H1*, Lime Tree House, 2006.

## Appendix I: Publications

1. Z. Al-Sarraf and M. Lucas, (2012), “A study of weld quality in ultrasonic spot welding of similar and dissimilar metals”, *Modern Practice in Stress and Vibration Analysis, Journal of Physics Conference series*, Vol. 382, Article No. 012013, doi: 10.1088/1742-6596/382/1/012013
2. Z. Al-Sarraf, M. Lucas and P. Harkness, (2012), “A numerical and experimental study of ultrasonic metal welding”, *International Symposium On Ultrasound in the Control of Industrial Processes*, IOP Conference series-Materials Science and Engineering, Vol. 42, Article No. 012015, doi: 10.1088/1757-899X/42/1/012015